Thermo-mechanical analysis of GTA welding of Modified 9Cr-1Mo steel considering the effects of phase transformation, Pre heating and Post heating

By

MOHAMMED ZUBAIRUDDIN
ENGG06201104002

Institute for Plasma Research Gandhinagar

A thesis submitted to the
Board of Studies in Engineering Sciences

In partial fulfillment of requirements
for the Degree of
DOCTOR OF PHILOSOPHY
of
HOMI BHABHA NATIONAL INSTITUTE

October, 2018

Homi Bhabha National Institute

Recommendations of the Viva Voce Committee

As members of the Viva Voce Committee, we certify that we have read the dissertation prepared by Mohammed Zubairuddin entitled "Thermo-mechanical analysis of GTA welding of Mod. 9Cr-1Mo steel considering the effects of phase transformation, Pre heating and Post heating" and recommend that it may be accepted as fulfilling the thesis requirement for the award of Degree of Doctor of Philosophy.

Chairman – Dr. B. K. Dutta		Date: 16 Jan 21
Guide / Convener – Dr. S. K. Albert		Date: 16 Jan 21
Co-guide - Dr M. Vasudevan		Date: 16 Jan 21
Examiner - Dr. M. M. Mahapatra		Date: 16 Jan 21
Member 1- Dr. J.Chattopadhyay		Date: 16 Jan 21
Member 2- Dr. T. A. Dwarakanath		Date: 16 Jan 21
Member 3- Dr. R. Balasubramaniam		Date: 16 Jan 21
Member 4- Dr. I. A. Khan		Date: 16 Jan 21

Final approval and acceptance of this thesis is contingent upon the candidate's submission of the final copies of the thesis to HBNI.

We hereby certify that we have read this thesis prepared under our direction and recommend that it may be accepted as fulfilling the thesis requirement.

Date: 16 Jan 21
Place: Kalpkkam

Signature
Co-guide (if any)

Signature
Guide

STATEMENT BY AUTHOR

This dissertation has been submitted in partial fulfillment of requirements for an advanced degree at Homi Bhabha National Institute (HBNI) and is deposited in the Library to be made available to borrowers under rules of the HBNI.

Brief quotations from this dissertation are allowable without special permission, provided that accurate acknowledgement of source is made. Requests for permission for extended quotation from or reproduction of this manuscript in whole or in part may be granted by the Competent Authority of HBNI when in his or her judgment the proposed use of the material is in the interests of scholarship. In all other instances, however, permission must be obtained from the author.

Mohammed Zubairuddin

Name & Signature of the student

DECLARATION

I, hereby declare that the investigation presented in the thesis has been carried out by me. The work is original and has not been submitted earlier as a whole or in part for a degree / diploma at this or any other Institution / University.

Mohammed Zubairuddin

Name & Signature of the student

CERTIFICATION ON ACADEMIC INTEGRITY

1. I, Mohammed Zubairuddin, HBNI Enrollment No. ENGG06201104002 hereby undertake that, the Thesis titled "***Thermo-mechanical analysis of GTA welding of Mod. 9Cr-1Mo steel considering the effect of phase transformation, Pre-heating and Post-heating***" is prepared by me and is the original work undertaken by me and free of any plagiarism. That the document has been duly checked through a plagiarism detection tool and document is plagiarism free.

2. I am aware and undertake that if plagiarism is detected in my thesis at any stage in future, suitable penalty will be imposed as per the applicable guidelines of the institute/UGC.

Signature of student

Endorsed by the thesis Supervisor:

I certify that the work done by the Researcher is plagiarism free

Signature

List of Publications arising from the thesis

<u>Refereed International Journals:</u>

<u>Accepted papers</u>

1. M. Zubairuddin, S. K. Albert, S. Mahadevan, M. Vasudevan, V. Chaudhari, V. K. Suri, "Experimental and Finite Element Analysis of Residual stress and Distortion in GTA Welding of Modified 9Cr-1Mo Steel". Journal for Mechanical science and Technology, 2014, Vol. 28, Issue12, 5095-5105.
2. M. Zubairuddin, S. K. Albert, M. Vasudevan, V. Chaudhari, V. K. Suri, "Finite Element Simulation of Weld Bead Geometry and Temperature Distribution during GTA Welding of Modified 9Cr-1Mo Steel and Experimental Validation". Journal for Manufacturing science and Production, 2014, Vol. 14, Issue 4, 195–207.
3. M. Zubairuddin, S. K. Albert, V. Chaudhari, V. K. Suri, "Influence of Phase Transformation on Thermo-mechanical Analysis of Modified 9Cr-1Mo steel". Material Procedia, 2014, Vol. 5, 832-840.
4. M. Zubairuddin, S. K. Albert, M. Vasudevan, S. Mahadevan, V. Chaudhari, V. K. Suri, "Thermo-mechanical Analysis of the Preheat effect on Grade P91 Steel during GTA Welding". Material and Manufacturing processes. 2015, Vol.31 Issue.3, 366-371.
5. M. Zubairuddin, S. K. Albert, M. Vasudevan, S. Mahadevan, V. Chaudhari, V. K. Suri, "Numerical simulation of multi-pass GTA welding of grade 91 steel". Journal of Manufacturing Processes, 2017, Vol.27, 2017, 87-97.

<u>Paper under communication</u>

6. M. Zubairuddin, S. K. Albert, M. Vasudevan, S. Mahadevan, V. Chaudhari, "Effect of Post Heating on Residual Stresses and Distortion of Grade 91 Steel GTA Welding". Achieves of Civil and Mechanical Engineering.

Other Papers

7. A. R. Pavan, **M. Zubairuddin**, B. Arivazhagan, S. Mahadevan, M. Vasudevan "Thermo-mechanical Analysis of A-TIG and MP-TIG Welding of 2.25Cr-1Mo Steel", Journal of Materials Engineering and Performance, Journal of Materials Engineering and Performance volume 28, pages4903–4917(2019).
8. G. Chakraborty, Rejeesh, **M. Zubairuddin**, S. K. Albert "Effect of preheating and post heating in reducing diffusible hydrogen content and hydrogen assisted cracking susceptibility of modified 9Cr-1Mo steel" Science and Technology of Welding and Joining, Accepted Taylor and Francis.

Chapters in books and lectures notes

1. M. Zubairuddin, S. K. Albert, M. Vasudevan, S. Mahadevan, V. Chaudhari, V. K. Suri, "Thermo-mechanical analysis of residual stress and distortion of Grade P91 steel during GTA welding".11th International Seminar "Numerical Analysis of Weldability 27-30 September 2015, Graz Institute of Technology, GRAZ, Austria.

Conferences

1. M. Zubairuddin, S. K. Albert, V. Chaudhari, V. K. Suri "Influence of Phase Transformation on Thermo-mechanical Analysis of Modified 9Cr-1Mo steel", ICAMME 2013 NIT Surathkal.
2. M. Zubairuddin, S. K. Albert, V. Chaudhari, "Effect of heat input parameters on modified 9Cr-1Mo bead-on-plates and its finite element analysis by SYSWELD" IIW-ADWEST 2013, Puducherry, May 3-4, 2013.
3. M. Zubairuddin, S. K. Albert, V. Chaudhari, "Effect of heat input on weld analysis of Grade 91 steel" ICON 2014, IGCAR, Kalpakkam.
4. M. Zubairuddin, S. K. Albert, M. Vasudevan, S. Mahadevan, V. Chaudhari, V. K. Suri, "Thermo-mechanical analysis of residual stress and distortion of Grade P91 steel during

GTA welding".11th International Seminar "Numerical Analysis of Weldability 27-30 September 2015, Graz Institute of Technology, GRAZ, Austria.

Dedicated to

To my Family

ACKNOWLEDGEMENTS

At first, I would like to express my deepest gratitude to my research guide, Dr. Shaju K. Albert, (Associate Director, MMG, IGCAR) for his magnanimity in expending his valuable time and restless effort with his invaluable guidance, constant encouragement, unstinted inspiration and keen interest throughout my research work and in preparing this thesis. He has been a dream guide for me. I am grateful to Dr. M. Vasudevan (MMD, IGCAR) for making me motivated to take up this project. I am grateful to Vilas Chaudhari IPR Gandhinagar for extending his support and good wishes throughout my research work.

It's my pleasure to thank my doctoral committee, Dr. B. K. Dutta (Chairman), Dr. J. Chattopadhyay (Member), Dr. T. A. Dwarakanath (Member), Dr. R. Balasubramaniam (Member) and Dr. Imran Ali Khan (Member) for their meticulous evaluation of my work and their valuable suggestions. I thank Dr. V. K. Suri Professor of HBNI for constant encouragement during my PhD.

I am privileged to thank Dr. Subroto Mukherjee and Dr. Sudip Sengupta (Dean Academic IPR), Dr. Shashank Chaturvedi (Director, IPR) for their trust and support on me. Furthermore, I sincerely thank the Department of Atomic Energy (DAE), India for providing the necessary financial support.

I would like to thank Mr. D. Manokaran for preparing weld specimens and to Mr. Arun kumar and Dr. M. Mahadevan, for helping in measuring residual stress using XRD Technique.

CONTENTS

LIST OF TABLES

Table No. Title Page No.

LIST OF FIGURES

List of Symbols

Symbol	Description
A_1	Ferrite to austenite start temperature in steel
A_3	Ferrite to austenite finish temperature in steel
Ac	Transformation temperatures in steel during heating at a finite rate
Ac_1	Ferrite to austenite start temperature during heating of steel
Ac_3	Ferrite to austenite finish temperature during heating of steel
Ae	Equilibrium transformation temperatures in steel
α	Ferrite, a body centered cubic form of iron and steel below A_1 temperature
γ	Austenite, a face centered cubic form of iron and steel
δ-ferrite	A high temperature a body centered cubic form of iron and steel
λ	Wavelength
d	Inter-planer spacing of crystallographic planes
do	Interplaner spacing of crystallographic planes in stress-free condition
ε	Strain
ζ	Stress
E	Young‘s Modulus
ν	Poisson‘s ratio
(hkl)	Miller index of a crystallographic plane
k	Thermal conductivity
c, c_p	Heat capacity
K	Coefficient of linear expansion
q	Heat density (energy per unit volume)

r_O	radius of the spherical heat source
z	Height of the truncated conical heat source
b	Weld width of double ellipsoidal heat source
a_f	Front weld length
a_r	Rear weld length
c	Depth of penetration
ρ	Density
T	Temperature
h	Heat transfer coefficient
s	Stefan's constant
e	Emissivity
T_O	Temperature of ambient
P(T)	Phase fraction at temperature T
Peq	Equilibrium phase fraction
t	Time
τ	Delay time or time lag
P	Laser power
d	Depth of penetration
v	Welding speed

List of Abbreviations

Abbreviation	Description
FMS	Ferritic / martensitic steel
RAFMS	Reduced activation ferritic / martensitic steel
CLAM	Chinese low activation martensitic steel
In-RAFMS	Indian reduced activation ferritic / martensitic steel
N&T	Normalized and tempered
CCT	Continuous cooling transformation
MMAW	Manual metal arc welding
SMAW	Shielded metal arc welding
GTAW	Gas tungsten arc welding
A-TIG	Activated tungsten inert gas
NG-TIG	Narrow gap tungsten inert gas
GMAW	Gas metal arc welding
MIG	Metal inert gas
FCAW	Flux cored arc welding
SAW	Submerged arc welding
EBW	Electron beam welding
PWHT	Post weld heat treatment
FZ	Fusion zone
HAZ	Heat affected zone
PMZ	Partially melted zone
CGHAZ	Coarse grained heat affected zone
FGHAZ	Fine grained heat affected zone

ICHAZ	Inter-critical heat affected zone
SCHAZ	Subcritical heat affected zone
PM	Parent Material
TM	Tempered martensite
M	Martensite
A	Austenite
YS	Yield strength
UTS	Ultimate tensile strength
EDS	Electron dispersive spectroscopy
TBM	Test blanket module
ITER	International thermonuclear experimental reactor
HPDL	High power diode laser
Nd-YAG	Neodymium-yttrium aluminum garnet
CNC	Computer numerical control
HAC	Hydrogen Assisted cracking
2D	Two dimensional
3D	Three dimensional
RT	Room temperature
SSPT	Solid state phase transformation

CHAPTER 6

SUMMARY AND CONCLUSIONS

Summary of the results and major conclusions derived from these results are given in this chapter. It is given separately for each of the sections identified in Chapter 5: (1) Heat source fitting and material property data generation, (2) thermo-mechanical analysis of the autogenous welds of 3 mm thick plate welds, (3) thermo-mechanical analysis of 6 mm thick plate multi-pass welds, (4) thermo-mechanical analysis of welds prepared with preheating, (5) thermo-mechanical analysis of welds prepared with both preheating and post heating and (6) effect of preheating and post heating and residual stress and distortion of the weld joints

6.1. Material data base creation and Bead-on-plate weld

1. Using the weld bead dimensions obtained from bead-on-plate welds made with different heat input, heat source fitting for double ellipsoidal model was successfully carried out
2. Material data base for modified 9Cr-1Mo steel, which considers phase transformation in the steel was generated and provided as material data input file for SYSWELD for thermo-mechnical analysis.

6.2. Thermo-Mechanical Analysis of Autogenous welding

1. A numerical model which can predict weld thermal cycles, residual stress and distortion in the autogeneous welds of modified 9Cr-1Mo steel plate was developed. Material data base generated for this steel and double ellipsoid heat source model with its parameters adjusted to match the experimentally measured bead parameters were used as input for this model.
2. Results of prediction from this model was compared with weld thermal cycles

experienced, residual stress present and distortion that took place in actual weld and it is demonstrated that the predictions are reasonably accurate.

3. For accurate prediction of residual stress distribution, phase-transformation that takes place in the material during weld thermal cycle should be considered in the material data base. It is shown that 'M' shaped distribution of the longitudinal residual stress in the transverse direction of the weld is a direct consequence of solid-state phase transformations (ferrite to austenite during heating part and austenite to martensite during cooling part) that occur during weld thermal cycle.
4. Distortion analysis using two different theories (large and small displacement) showed that distortion is predicted correctly only for models that considers large displacement theory.

6.3. Thermo-Mechanical Analysis of Multi-pass welding

1. The numerical model developed to simulate the thermo-mechanical behavior of autogenous weld was suitably modified for multi-pass welding involving V groove geometry and filler addition. Heat source fitting was also modified to match the multi-pass weld based on bead-geometries.
2. Predictions of weld thermal cycles, residual stress distribution and distortion made using this model matched reasonably well with those obtained from experiments.
3. It is shown that prediction of residual stress and distortion that match the experimental results is obtained only when 3D model with fine mesh is employed. Deviations for the results obtained for the predictions based on 2D model from that measured experimentally is high; 2D model predicts lower displacements than actually measured values.
4. Results of the distortion estimation both from modeling and measurements on multi-pass welds reveal that solid state phase transformations that occur during

weld thermal cycle influences not only the residual stress distribution but also the distortion of the weld joint. This was not revealed in the study carried out on autogenous welds.

6.4. Thermo-Mechanical Analysis of Modified 9Cr-1Mo steel GTA welding with pre heating

1. The numerical models developed for autogenous welds and multi-pass welds were modified by incorporating preheating of the joint prior to welding. A disk shaped heat source with gaussian distribution was used for simulating the effect of preheating.
2. The developed models were able to predict the effect of pre heating on residual stress and distortion with reasonable accuracy. The analysis showed that pre heating before welding reduced the peak tensile residual stress value, caused wider distribution of residual stresses as compared to those without pre heating weld plate in both cases. There was good agreement between the simulated and measured values.
3. Predicted vertical displacements in both transverse and longitudinal direction were validated with experimental measured values. There was a good agreement between predicted and experimental measured displacement values. In case of autogenous welds maximum vertical displacement reduced to 12% from that obtained for weld without preheating. Similarly, in case of longitudinal direction peak value of vertical displacement was reduced by 41%.
4. In case of 6 mm thick multi-pass welding of modified 9Cr-1Mo steel peak value of predicted verticle displcament in transverse direction was redcued 23%, where as in longitudinal direction this reduction was 24%.

6.5. Thermo-Mechanical Analysis of Modified 9Cr-1Mo steel GTA welding with combined pre heating and post heating

1. The numerical models for autogenous and multi-pass welds with preheating was further modified to incorporate post heating of the weld joint after welding. However, this model does not cover cooling of the weld from post heating temperature to ambient temperature i.e. model considers post heating temperature as ambient temperature during cooling part of the weld thermal cycle.
2. Predicted longitudinal residual stress at the weld centerline using this model for autogenous weld is slightly lower than actually measured, though in other location the values are comparable. Similarly, for multi-pass welds, predicted residual stress values are slightly higher than actually measured in most of the cases. These differences are attributed to limitation of the model to consider cooling down of the weld joint down to ambient temperatures.

6.6. Effect of pre heating and combined pre heating & post heating on residual stress and distortion

Residual stresses in a weld plate generated due to localized heating and fast cooling causing generation of differential expansion and contraction at different location of weld joint. Due to pre and post heating, the heating becomes more distributed, it reduces the temperature gradient and it decreases the cooling rate this indirectly reduces thermal expansion and contraction, which reduces the residual stresses. A comparison of both the predicted and experimentally estimated values of residual stress and distortion in the welds made without any preheating, with preheating and with combined preheating and post heating reveals that preheating + post heating significantly bring down residual stress levels in the weld joints as well as distortion from those reported for welds made without any preheating or post heating. In the case of autogenous welds, the reduction in the peak residual stresses is ~30% while in the case of multi-pass welds it is ~50%. Reduction in peak vertical displacement for the weld joints of autogenous and multi-pass welds made with both preheating and post heating are 45 and 39 % respectively from that of the weld made without any preheating and post heating. Corresponding reduction for the welds made only with preheating are 35 and 16% only. Based on this study it can be concluded pre heating and post heating is more beneficial than only pre heating to bring down residual and distortion for modified 9Cr-1Mo steel welds.

Overall, the results from the present study offer a FE based numerical model for predicting residual stress and distortion in the plate butt welds of modified 9Cr-1Mo steels. This model incorporates the material data base for this steel, uses heat source parameters optimized from experimental trials, considers solid state transformations that material undergoes during welding, chooses large displacement theory for prediction of displacement, select 3D fine meshing for multi-pass weld joints and proposes disk shaped heat source for modeling preheating.

6.7. Scope for future work

1. At present the numerical model developed is validated up to 6 mm thick weld joint with 'V' groove weld geometry with single pass for each layer of weld deposition. Model can be validated for large thickness plates and multi-pass welds with multiples passes for the same layer.
2. Numerical model can be developed for tube and pipe weld joints. It may be noted that modified 9Cr-1Mo steels are used extensively in these product forms.
3. The present model can be modified to cover different arc (SMAW, GMAW, SAW etc.) and beam (laser and electron) welding processes. Similar modifications can be attempted for Narrow Gap-Tungsten Inert Gas (NG-TIG) process for which modification in heat source may be required.

4. In the present model that considers post heating, it is not possible to incorporate cooling of the weld joint from the post heat temperature to ambient. This seems to affect the accuracy of the predictions from the model. Hence, modification is needed in the model to overcome this limitation.
5. The present model considers only conductive heat transfer; convective and radiation losses from the molten pool have been neglected. Similarly effect of electromagnetic, buoyancy forces on molten pool is also neglected. Hence, the present model can be modified to include these aspects so that accuracy of prediction can be improved.

Abstract

Grade 91 steel weld joints are prone to Hydrogen Assisted Cracking (HAC). It is a normal practice to carry out pre heating and post heating to minimize the risk of cracking. The three essential requirements for HAC to take place in welds are sufficient diffusible hydrogen, crack susceptible microstructure (e.g. martensite) and tensile residual stress present in the weld. If one or more of these are removed or reduced to low levels, then HAC can be prevented. In general, martensitic microstructure is the most susceptible and ferritic is the least. In low carbon and C–Mn steels, by choosing appropriate welding parameters, it is possible to control martensitic formation; however, for alloyed steels like P91 steel, martenisitic are formed in their welds irrespective of the welding parameters chosen. For HAC second requirement is hydrogen content which depends upon consumables, preheating and post heating employed, surface contamination on the weld surfaces etc.

Increasing demand worldwide for energy production has accelerated the research and development in high temperature materials. For enhancing the life of high temperature structural components of power plants, Ferritic-Martensitic stainless steels are becoming the primary choice due to their good high temperature mechanical properties and resistance to stress corrosion cracking etc. The modified 9Cr–1Mo steel containing small amount of V and Nb, has been of much interest because of its superior creep rupture properties in applications up to about 650 °C. Modified 9Cr-1Mo steel depending upon the product term is referred as T91 (Tube), P91 (Pipe), F91 (Forging) or Grade 91 steel. The material is being used in the steam generator of the Indian Prototype Fast Breeder Reactor (PFBR) at Kalpakkam. Reduced Activation Ferritic Martensitic Steel (RAFMS) is a modified version of Grade 91 steel developed for fusion reactor application with an objective to reduce the induced radioactivity and to facilitate easy disposal

after service. RAFM steel is used for Test Blanket Module (TBM) of Indian Lead Lithium Ceramic Breeder (LLCB), to be installed in (upcoming fusion reactor) ITER. However, for mock up trails envisaged before the actual fabrication of TBM, Grade 91 steel would be used as a surrogate material. Thickness of the plates used for these fabrication trials range from 1 mm to 15 mm.

Hence, numerical modelling using FEM is widely followed for estimation of residual stresses in the weld joints,. For this purpose, software packages like ANSYS, ABAQUS and SYSWELD are popular. ANSYS and ABAQUS require complex subroutines programming, whereas SYSWELD is specially designed for heat treatment and welding process simulation. However, there is only limited literature available on thermo-mechanical analysis of GTA welding of Grade 91 steel welding for Autogenous and multi-pass welding.

The objective of PhD work is to develop numerical models capable of predicting thermal cycles, residual stress and distortion in both Autogenous and multi-pass GTA welding of mod. 9Cr-1Mo steel plates of 3 and 6 mm thicknesses taking into account the effects of phase transforamtion, pre and post heating during welding and experimental validation of the predicted results. In the present work, it is proposed to develop numerical models for predicting residual stress and distortion in modified 9Cr-1Mo steel plate weld joints by considering phase transformation effects for autogenous and multi-pass GTA welding. The beneficial effects of combined preheating and post heating on the residual stresses and distortion need to be quantified. Hence the effect of preheating before welding and the combined effect of pre heating and post heating on the residual stresses and displacements is proposed to be studied in detail using simulation. Validation of the simulated results on the residual stresses and displacements employing suitable experimental tools such as XRD technique and height gauge respectively is envisaged. Two different thicknesses of plates 3 mm and 6 mm were preheated at 200°C and after welding; the joint was post heated at 200°C for 30 minutes. Thermo-mechanical analysis of GTA welding was carried out using SYSWELD software. Predicted and measured values are compared for the joints fabricated employing combined pre heating and post heating.

Following are the scope of the work to achieve this objective.

1. To create database of thermal and mechanical properties required for simulation for mod. 9Cr-1Mo steel by considering effect of phase transformation.
2. To calibrate the double ellipsoidal heat source from bead-on-plate experiments for various heat input conditions.
3. To carry out thermo-mechanical analysis of 3 mm thick mod. 9Cr-1Mo steel plates fabricated by autogenous TIG welding and 6 mm thick plates fabricated by multi-pass TIG welding considering the effect of phase transformation. Experimental validation of simulated thermal cycles, residual stresses and distortion.
4. To study the effect of preheating by choosing a suitable heat source followed by thermo-mechanical analysis of 3 mm thick and 6 mm thick mod. 9Cr-1Mo steel welding and experimental validation.
5. To study the combined effect of pre and post heating on the thermo-mechanical behavior of mod. 9Cr-1Mo steel weld joints of 3 mm thick and 6 mm thick plates.
6. To compare the effects of with and without pre and post heating on the residual stresses and distortion in Grade 91 steel weld joints of 3 mm and 6 mm thick plates.

CHAPTER-1

INTRODUCTION

Modified 9Cr-1Mo steel is ferritic martensitic steel extensively used for high temperature applications in fossil and nuclear power plants and petrochemical industries. This steel is developed by modifying the composition of 9Cr-1Mo steel by the addition of V, Nb and N to enhance the creep rupture strength. This steel designated as Grade 91 or modified 9Cr-1Mo steel included in the ASTM standard as A335P91/A235 T91 steels. Depending upon the product type it is referred as T91 (Tube), P91 (Pipe), F91 (Forging) or Grade 91 steel. This steel is used in normalized and tempered (N&T) condition [1-2].

In nuclear power plants, this material is considered for steam generators of Fast Breeder Reactors (FBRs) is currently used for fabrication of the steam generator of the Indian Prototype Fast Breeder Reactor (PFBR), at Kalpakkam. Reduced Activation Ferritic Martensitic Steel (RAFMS) is an improved version of modified 9Cr-1Mo steel developed with an objective to reduce the induced radioactivity after being used in a radioactive environment in fission or fusion reactors. RAFM steel is being proposed for Test Blanket Module (TBM) of Indian Lead Lithium Ceramic Breeder (LLCB), to be installed in ITER. However, for mock up trails envisaged before the actual fabrication of TBM, modified 9Cr-1Mo steel would be used as a surrogate material. Thickness of the plates used for these fabrication ranges from 1 to 15 mm [3].

Welding is an important process employed for fabrication of many components using Modified 9Cr-1Mo steel. Different processes like Manual Metal Arc Welding (MMAW), Flux Cored Arc Welding (FCAW), Gas Tungsten Arc Welding (GTAW), Gas Metal Arc Welding (GMAW), Submerged Arc Welding (SAW), Activated Tungsten Inert Gas (A-TIG) welding and Narrow Gap Tungsten Inert Gas (NG-TIG) welding, Laser Beam Welding, Electron Beam

Welding etc [4-9] can be used for welding of this steel. Joining of this steel using conventional welding processes, requires preparation of suitable joint design V, J, U-groove etc. and filling the groove with weld metal by melting the filler wire/rod using the heat from the arc in multiple passes.

Generation of residual stresses and distortion is a major concern in any fusion welding operation. Another specific concern of high alloyed steels like modified 9Cr-1Mo steel is the martensitic microstructure of the weld metal and heat affected zone (HAZ) which make these zones hard and brittle. As result, weld joints are given a suitable Post Weld Heat Treatment (PWHT) to bring down the hardness and improve the toughness and ductility. The as-welded martensitic microstructure also makes the weld highly prone to Hydrogen Assisted Cracking (HAC) [10-13]. In addition to a susceptible microstructure, high residual stress and presence of diffusible hydrogen in the weld are prerequisite for HAC to occur. Source of hydrogen is the moisture in welding consumables, organic contamination on the steel surface, moisture and hydrocarbon impurities in the shielding gas etc. Preheating (before welding) and post heating (after welding) are two techniques adopted to remove hydrogen from the weld and avoid cracking.

Though it is well known that presence of tensile residual stresses in the weld joints can make it susceptible to cracking, adversely affect its fatigue and corrosion properties in service and make it prone to brittle fracture under low temperature service of high strain rate loading, measurement of residual stresses present in a welded component is not easy. Techniques available for measurement of residual stresses are either destructive or semi-destructive or can be applied only to relatively small components. Hence, there is a need for predicting the residual stresses in the weld joints by proper numerical modeling.

In the case of distortion of welds also, there is a need to predict the distortion using the welding parameters employed and material properties available. Removing distortion after welding could be expensive and time consuming. It can also lead to degradation of the properties. Hence, once a reliable method of prediction is available, an appropriate welding sequence that would bring down distortion can be adopted so that net distortion in the final components is minimized.

In the case of modified 9Cr-1Mo steel welds, residual stress in the weld joint is not a serious concern as far as the performance of the component in service is concerned because the PWHT given to weld joint would bring down the residual stresses. However, HAC soon after welding is a concern and further, there could be long time gap between welding and PWHT especially in the case of fabrication of large components and the weld may remain in the as-welded condition during this period making it susceptible to hydrogen embrittlement or stress corrosion cracking.

Because of the relatively low thermal expansion coefficient and high thermal conductivity of the ferritic steels (compared to austenitic stainless steels), distortion in the components fabricated from modified 9Cr-Mo steels is expected to be low. However, information on distortion prior to welding can help to adopt techniques that would control distortion during fabrication.

Hence, there is a need to develop a reliable numerical model to predict residual stress and distortion in the welds of modified 9Cr-1Mo steel. This model should consider the solid-state phase transformation that occur during weld thermal cycle and effect of preheating and post heating to which the welds are subjected to during welding. Model should also consider multi-pass welding which include joint groove design (single 'V' and double 'V' etc) and filler metal deposition to the groove.

In the present thesis work, it is proposed to develop numerical models for predicting residual stress and distortion in modified 9Cr-1Mo steel plate weld joints by considering phase transformation effects for autogenous and multi-pass GTA welding. The beneficial effects of combined preheating and post heating on the residual stresses and distortion need to be quantified. Hence the effect of preheating before welding and the combined effect of pre heating and post heating on the residual stresses and displacements is proposed to be studied in detail using simulation. Validation of the simulated results on the residual stresses and displacements employing suitable experimental tools such as XRD technique and height gauge respectively is envisaged.

The thesis has been organized as below having six chapters including

Chapter 1 *Introduction* - In this chapter introduction of modified 9Cr-1Mo steel welding is discussed.

Chapter 2 *Literature survey* –This chapter discuss the details of the work done by various researchers in the field of welding of Modified 9Cr-1Mo steel, welding simulation, residual stress and distortion analysis and thermo-mechanical analysis of welding, specially modified 9Cr-1Mo steel welding. The experimental and numerical analyses performed so far with their significant contribution and importance for the development of various models is discussed here.

Chapter 3 *Research Methodology* - In this chapter detailed study of different heat source models based on different equations and boundary conditions is presented. Steps for thermo-mechanical analysis of Modified 9Cr-1Mo Steel welding are discussed in detail.

Chapter 4 *Experimental work* - In this chapter bead-on-plate, autogenous and multi-pass welding carried out on modified 9Cr-1Mo steel is discussed in detail. Three different cases of welding plates were carried out like welding without pre heating, welding with pre heating and welding with combined pre heating and post heating. Pre heating and post heating are carried out using Oxy-Acetylene flame heating on selected area only. Determination of thermal cycles estimation of residual stress and measurement of displacements leading to distortion are discussed in detail.

Chapter 5 *Results and discussion* - In this chapter thermal analysis of bead-on-plate welding and thermo-mechanical analysis of autogenous and multi-pass welding considering effect of pre-heating and post-heating are discussed in detail in different sections.

Section 5.1 In this section, creation of modified 9Cr-1Mo steel material data base and various assumptions considered for creation of this data base are discussed. Heat source model was developed and accuracy, consistency and validations of this model are demonstrated using measurements carried out on 16 bead-on-plate welds of different heat inputs..

Section 5.2 In this section, thermo-mechanical analysis of autogenous welding of 3 mm thick modified 9Cr-1Mo steel plate welding considering the effect of phase transformations in material data base is discussed. Comparison of residual stress values for two different data base one considering with and without phase transformation is discussed and it is shown the phase transformation during welding thermal cycle should be considered for predication of residual stresses in the weld joint with reasonable accuracy. Predicted distortions in different direction are also validated with experimental results.

Section 5.3 In this section, thermo-mechanical analysis of multi-pass welding of 6 mm thick modified 9Cr-1Mo steel plate is studied using different meshed models. Effect of phase transformation on distortion is also studied.

Section 5.4 In this section, numerical modelling of effect of pre-heating on two different thickness of plate 3 mm and 6 mm plate is carried using combined disk-shaped heat source and double ellipsoidal model. Predicted residual stress and distortion validated with experimental values.

Section 5.5 In this section, thermo-mechanical analysis of effect of combined pre-heating and post heating on two different thicknesses of plates 3 mm and 6 mm plate is carried by considering different assumptions in FEM model. Predicted distortion in both thickness of weld plates in different direction validated with experimental values.

Section 5.6 In this section, effect of pre-heating and combined effect pre heating and post heating are compared for the welds of both 3 mm (autogenous weld) and 6 mm (multi-pass welds) plates. This comparison was done for results obtained from the experiments as well as those predicted by modelling. It is demonstrated that welding with preheating combined with post heating can reduce both peak tensile residual stresses and distortion in the weld joints of this steel.

Chapter 6 *Summary and conclusion* – This chapter focuses on summary, conclusion and scope for future work is also discussed.

References

1. J. Hilkes, V. Gross, "Welding Cr-Mo steels for power generation and petrochemical applications-past, present and future" Institute of Welding Bulletin, 2013, Vol. 2, 11.
2. R. W. Swindeman, M. L. Santella, P. J. Maziasz, B. W. Robert, K. Colermen, "Issues in replacing Cr–Mo steels and stainless steels with 9Cr–1Mo–V steel", International journal of pressure vessels and piping, 2004, Vol. 81, 507-512.
3. E. Rajendra, T, Jayakumar, A. K. Suri, "Overview of TBM R&D activities in India", Fusion Engineering and Design, 2012, Vol. 84, Issue 5-6, 461–465.
4. M. Vasudevan, V. Arunkumar, N. Chandrasekhar, V. Maduraimuthu, "Genetic algorithm for optimisation of A-TIG welding process for modified 9Cr–1Mo steel", Science and Technology of Welding and Joining, 2010, Vol. 15, Issue 2, 117-123.
5. S. Kumar, R. Awasthi, C. K. Vishwanadham, K. Bhuanumurthy, G. K. Dey, "Thermo-metallurgical and thermo-mechanical computations for laser welded joint in 9Cr–1Mo (V, Nb) Ferritic-martensitic steel", Materials and Design, 2014, Vol. 59, 211-220.
6. S. Paddea, J. A. Francis, A. M. Paradowska, P. J. Bouchard, I. A. Shibli, "Residual stress distribution in a P91 steel-pipe girth weld before and after post weld heat treatment", Material Science and Engineering, A, 2012, Vol.534, 663-672.
7. C. Pandey, M. M. Mahapatra, P. Kumar, N. Saini, "Some studies on P91 steel and their weldments", Journal of Alloys and compounds, 2018, Vol. 743, 332-364.
8. B. Arivazhagan, M. Kamaraj, "Metal-cored arc welding process for joining of modified 9Cr-1Mo (P91) steel" Journal of Manufacturing Processes, 2013, Vol. 15, Issue 4, 542-548.
9. B. Arivazhagan, S. Sundaresan, M. Kamaraj, "A study on influence of shielding gas composition on toughness of flux-cored arc weld of modified 9Cr–1Mo (P91) steel" Journal of Materials Processing Technology, 2009, Vol. 209, Issue 12-13, 5245-5253.

10. G. K. Padhy, V. Ramasubbu, N. Murugesan, C. Ramesh, S. K. Albert, “Effect of preheat and post heating on the diffusible hydrogen content of welds”, Science and Technology of Welding and Joining, 2012, Vol.17, Issue5, 408-413.

11. G. K. Padhy, V. Ramasubbu, N. Murugesan, C. Ramesh, S. K. Albert, “Diffusible hydrogen measurement in steel welds using an electrochemical hydrogen sensor”, Indian Welding Journal,2012, Vol.45, Issue 1,35-46.

12. R. Mythili, P. V. Thomas, S. Saroja, M. Vijayalakshmi, V. S. Raghunathan, "Microstructural modification due to reheating in multi-pass manual metal arc welds of 9Cr-1Mo steel", Journal of Nuclear Materials, 2003, Vol. 312, Issue 2-3, 199-206.

13. P. K. Ghosh, U. Singh, "Influence of pre and post weld heating on weldability of modified 9Cr-1Mo (V-Nb) steel pipe under shielded metal arc and tungsten inert gas welding process”, Science and Technology of Welding and Joining, 2004, Vol. 9, Issue 3, 229-236.

CHAPTER-2

LITERATURE SURVEY

In this chapter a detailed literature review on welding of modified 9Cr-1Mo steel using different processes, problem associated with the welding of modified 9Cr-1Mo steel, thermo-mechanical analysis of modified 9Cr-1Mo steel welding is presented. The literature survey is given in different sections such as properties of modified 9Cr-1Mo steel, welding of modified 9Cr-1Mo steel, Finite Element (FE) simulation of welding, various heat source models, residual stresses and distortion analysis of various steels and thermo-mechanical analysis of modified 9Cr-1Mo steel based on the work carried out by different researchers. At the end of literature survey, research gaps in the numerical simulation of welding of modified 9Ccr-1Mo steel are identified.

2.1. Introduction

Energy saving and environmental protection in power generation require further improvements in efficiency, one way in which these can be achieved is by increasing the temperature and pressure of the steam, as illustrated in Fig. 2.1 [1-2].

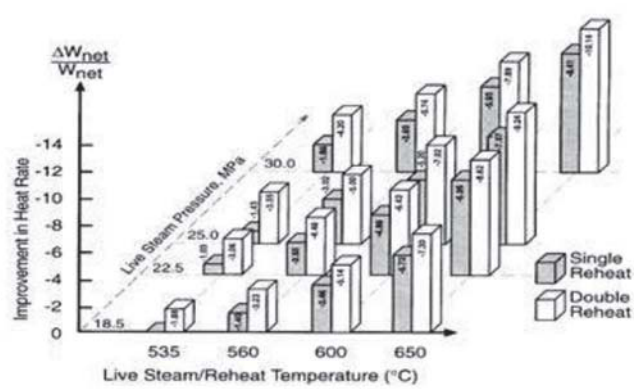

Fig.2.1. Improvement in heat rate [2]

Fig. 2.1 shows the improvements in heat rate (efficiency) achieved in thermal power plants by increasing steam temperature and pressure using single and double reheat cycles compared to the base case of 535ºC/18.5 MPa. For example, a 6% increase in efficiency can be achieved by changing the steam conditions from 538ºC/18.5 MPa to about 593ºC/30 MPa. Higher temperatures and pressure up to about 650ºC/34.5 MPa are currently being pursued for improving the efficiency. The main technology enabling the increase of temperature and pressure of steam is the development of improved materials capable of operating under high stresses at high temperatures [3-5]. Materials with ferritic-martensite microstructures are preferred to austenitic stainless steels in fossil power plants because of their favourable thermo physical properties, such as good thermal conductivity and low coefficient of thermal expansion, coupled with a high resistance to thermal shock [6]. The historical development of the steels for power plant application is shown in Fig. 2.2 [9]. It can be seen that the development of the ferritic steels has taken place over four generations, which is also indicated in Table 2.1.

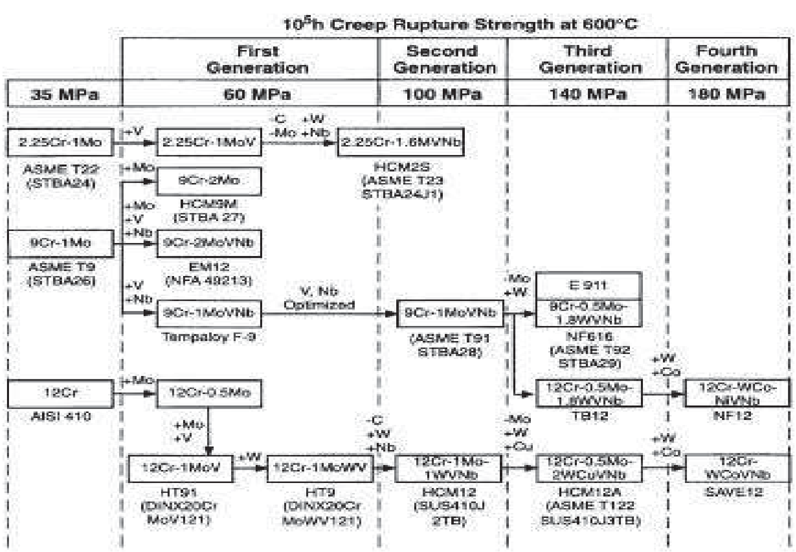

Fig.2.2. Development progresses of ferritic steels for boiler [9].

In the early 20th century Carbon and Carbon–Manganese steels were put in service for high temperature applications up to 400°C. The first-generation low alloy creep resisting steels contain 0.5% Mo which is limited to 450°C because of its low creep ductility and tendency towards graphitisation. Then 1% Cr was added to the 0.5% Mo steel which was designated as P11/T11 having the service temperature in the range of 500–520°C. Further addition of chromium improved the creep strength and ductility and also retarded the graphitisation formation. The Cr content in the P11 steels was increased from 1% to 2.25% and the Mo to 1% to develop 2.2Cr-1Mo steels designated as P22/T22, this class of steels is used in service in Normalised and Tempered condition (N&T). The higher Cr content improves the Oxidation resistance and the also neutralises the embrittling tendency [7]. High alloyed steels like Cr content higher than P22 were developed because of the demand for materials operates at a temperature more than 550°C (or) in a corrosive environment.

9Cr–1Mo steels are one of the widely used high alloy steels for high temperature oxidation resistance, designated as P9/T9 Steels, but creep rupture strength of this steel is not better than that of P22 type steels [8]. Addition of small quantities of V, Nb and N improves the creep rupture strength of P9 steels and this led to the development of modified 9Cr-1Mo steel, designated as P91/T91 steel. This steel is now included in ASTM standards of A335 /A213. Designation P indicates the pipe and T stands for tubes. Further modification of this steel by partial replacement of Mo with W led to the development of P92 /T92 steels [9].

Table.2.1. Changes in steel [9]

Generation	Year	Alloy modification	Strength 10^5hr creep rupture at 600°C	Example alloy	Max. Metal temp. °C
1	1960-1970	Addition of Mo (or) Nb,V to simple 12 Cr or 9Cr steels	60	EM12, HCM9M, HT9, Tempaloy, F9, HT91	565

2	1970-1985	Optimization of C,Nb,V	100	HCM12, T91, HCM2S	593
3	1985-1995	Partial substitution of W for Mo	140	P-92, P-122, (HCM12A, NF616)	620
4	Emerging	Increase of W and addition of Co	180	NF12, SAVE12	650

2.2. Modified 9Cr-1Mo steel

The modified 9Cr–1Mo steel known as Grade 91 steel, P91/T91 (or) as X10CrMoVNb9–1 in Europe has been successfully accepted world–wide since the late 80's for header and steam piping in power industries due to its excellent elevated temperature strength. In modern fossil fired power plant, the application of Grade 91 steels allows higher operating temperatures and pressures, and therefore higher efficiencies. Based on European experience, Grade 91 steels can be used inside the boiler (super-heaters and re-heaters) for steam temperatures up to 560ºC (maximum metal temperatures around 600ºC), and outside the boiler for pipe and headers up to about 610ºC [10]. Chemical composition of Grade 91 specified by ASTM standards and listed in Table 2.2.

Table 2.2 Chemical composition of Grade 91 steel (Wt %) with range

	C	Mn	P	S	Si	Cr	Mo	V	Nb	N	Al	Ni	Fe
Min	0.08	0.3	-	-	0.20	8.00	0.85	0.18	0.06	0.030	-	-	Bal
Max	0.12	0.6	0.020	0.01	0.50	9.50	1.05	1.05	0.10	0.070	0.040	0.40	Bal

2.3. Welding process for modified 9Cr-1Mo steel

Welding is a joining process in which two similar or dissimilar materials are joined with the application of heat or pressure or with the help of both. As a result, metallurgical bonding is established between them. Fusion welding is a welding process where fusion is employed to complete the weld. The weld joints are made by fusing together adjacent edges or surfaces. It involves a heat source and the use of a filler material such as a consumable electrode or a wire fed into the weld pool. A protective layer is also used between the atmosphere and the molten metal, either in the form of gas shielding or a flux which melts to give a viscous slag on the weld metal that eventually can be removed. In terms of heat source, fusion welding is often classified as gas welding, arc welding, resistance welding, electron and laser beam welding etc. For power plant applications, P91 steel welding is carried out using one of the arc welding processes such as GTAW, SAW, Shielded Metal Arc Welding (SMAW) (or) Manual Metal Arc Welding (MMAW). Prior to welding preheating between 200°C and 350°C is given to the steel [11-12]. Welds are also subjected to post weld heat treatment (PWHT) in the range of temperatures 730- 780°C and the duration is determined by the thickness of the components at the weld location.

2.4. Microstructural features of welds

In welding, the intense heat source interacts with the materials in a localized zone and as result, different thermal profiles are experienced in the materials from region to region, giving unique microstructure features in different regions of the weld. The classical definition of a welded structure includes three regions, these are the unaffected parent metal (PM), the heat-affected zone (HAZ) and the fusion zone, namely the weld metal (WM) [13-15]. However, microstructure examination at finer scales shows the HAZ consists of at least three distinct zones, Coarse Grain HAZ (CGHAZ), Fine Grained HAZ (CGHAZ) and Inter-critical HAZ

(ICHAZ) depending on the size of the prior austenite grains and the peak temperatures experienced by these zones during weld thermal cycles. The schematic diagram of the weld microstructures is shown in Fig. 2.3.

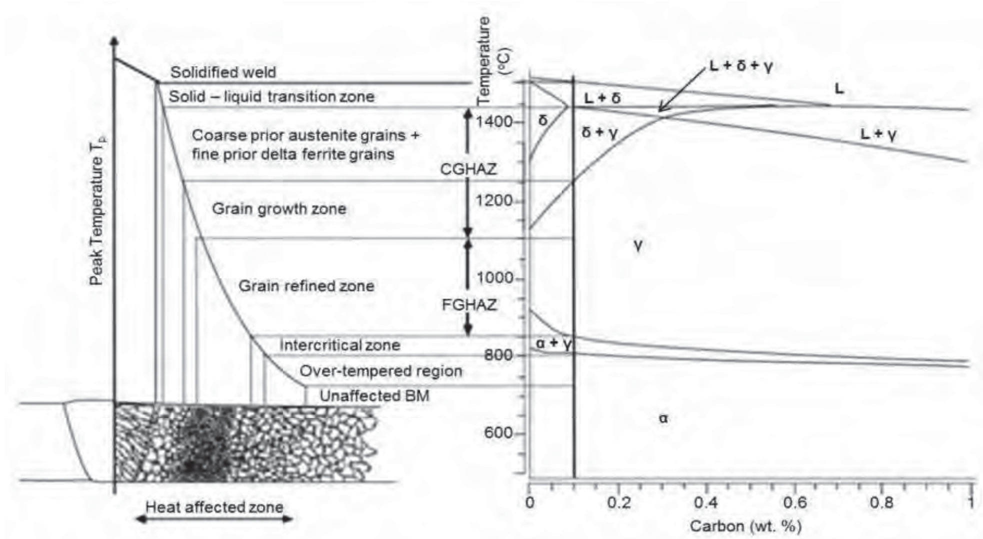

Fig.2.3. Schematic diagram of micro-structural variation across weld joint in P91 steel [15]

2.4.1. Heat-Affected Zone (HAZ)

Heat affected zone (HAZ) is the area of base metal, which has had its microstructure and properties significantly altered by the thermal cycle associated with welding. Depending on the thermal history different microstructures appear in the HAZ of a P91 fusion weld, which can be divided into two distinct regions the high temperature region and the low temperature region. The former region is mainly the coarse-grained heat affected zone (CGHAZ), while the latter consists of the fine-grained heat affected zone (FGHAZ) and the inter-critical heat affected zone (ICHAZ). The distributions of these different regions are shown in Fig. 2.3. During the welding process, the CGHAZ is just adjacent to the hot, molten weld deposit. It experiences very high peak temperature, which is much higher than α to γ transformation temperature Ac_3, completely re-austenising the microstructure. Due to high temperature experienced at this region, austenite grains grow large resulting in the coarse-grained microstructure. The number of grain boundary precipitates in the CGHAZ is quite low, due to the high temperature experienced which is enough to dissolve previously existing particles, and the rapid cooling which does not give enough time of temperature to form new precipitates. The FGHAZ experiences a lower peak temperature, but above the Ac_3. It allows complete transformation to austenite but not the growth of the austenite grains, yielding a fine grain structure. Pre-existing precipitates do not dissolve completely. The ICHAZ experiences an even lower peak temperature during welding, above the eutectoid Ac_1 temperature, but below that of Ac_3. The microstructure in this region is a mixture of grains that has undergone transformation and those that has not transformed during weld thermal cycle. [15-17].

2.4.2. Weld metal (WM)

Weld metal is the portion of the weldment which experienced melting and re-solidification during the welding process. Filler metal and parent metal are melted together and well mixed. The weld metal in single-pass weldment exhibits a coarse columnar microstructure. The weld metal in multi-pass weldments is normally made up of a large number of overlapping weld beads where a heating and cooling thermal cycle of each bead was repeated and has affected previously deposited beads.

Multi-pass welding processes introduce non-uniformity in the fusion zone microstructure as the heat from the succeeding passes leads to formation of a graded HAZ, consisting of various microstructural zones, in the weld metal deposited by the previous passes and also cause tempering of the same. Thus, fusion zone of a multi-pass weld joint in ferritic steels is essentially a mixture of virgin fusion zone (unaffected by the thermally cycles of the subsequent passes), remelted zone, fusion zone HAZ and tempered fusion zone [18-21].

Reed et al. have presented a model for multi-pass weld joints in steels. Different metallurgical regions in fusion zone and HAZ resulting from a typical multi-pass welding process in ferritic steel are shown in Fig. 2.4. It can be seen that the fusion zone and the HAZ consists of a mixture of different metallurgical regions, resulting from the heat input of multiple passes. This kind of micro-structural heterogeneity is always present in the fusion zone and HAZ of a multi-pass weld joints in Grade 91 steel. This micro-structural heterogeneity is one of the prominent contributing factors for the weld joint failure in service, often referred as Type I and Type II cracking [21, 33].

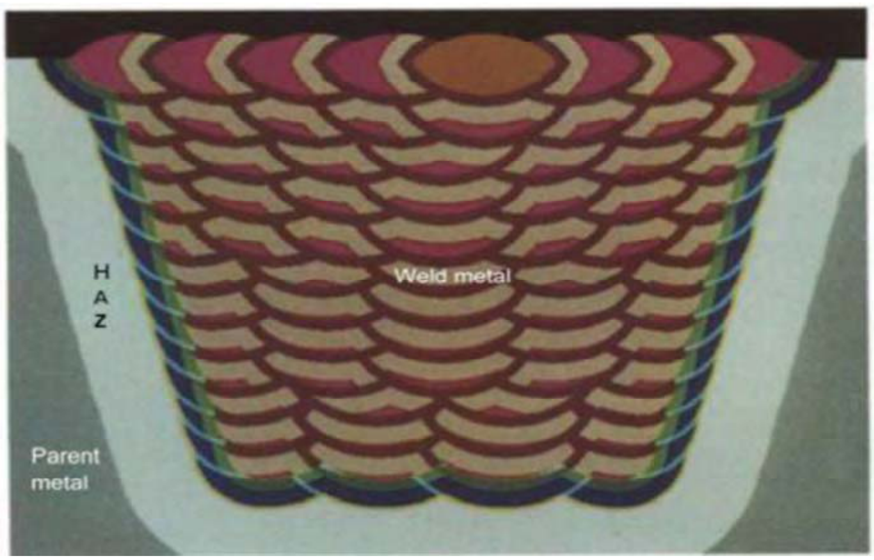

Fig.2.4. Multilayer welds of E911 base material with matching filler material [17]

2.5. Studies on the weld joints of modified 9Cr-1Mo steel

Ferritic/Martensitic steels including 9Cr-1Mo (V, Nb) steels are welded by different welding processes like SMAW, GTAW, Flux Cored Arc Welding (FCAW), GMAW and SAW or combination of these processes [19-34].

Laha et al. [20] have reported a detailed micro-structural and creep study on weld joints in modified 9Cr-1Mo steel and also on simulated HAZ specimens. These weld joints were made between 12 mm thick plates of modified 9Cr-1Mo steel by SMAW process. The study focused on the micro-structural variation across the HAZ and its role on inter-critical softening and loss of creep rupture strength due to Type – IV cracking.

Mythili et al. [21] have reported micro-structural modification due to reheating in multi-pass SMA welds of 9Cr–1Mo steel. Presence of a repetitive microstructure consisting of columnar grain, coarse grained austenite, fine grained austenite and unaffected structure within the weld zone was reported in this study, confirming a significant modification of microstructure due to multiple passes. Significant coarsening of laths, decrease in defect density and extensive precipitation with Cr enrichment in the carbides along the weld centre line from top to root was also reported in this study.

Shiue et al. [22] have reported effect of tempering temperature on fracture toughness and stability of retained austenite in the weld joints in modified 9Cr-1Mo FMS. The welds were made by multi-pass arc welding (GTAW for root pass and SMAW for filling passes) between 6.4 mm thick plates. The fusion zone produced by SMAW showed profound slag inclusions. Significant drop in the fracture toughness and increase in the hardness for the weld joints tempered in 450°C–610°C temperature range with lowest fracture toughness for the welds tempered at 540°C was reported in this study. However, there was significant improvement in the fracture toughness for the tempering temperatures higher than 680°C. However, acceptable fracture toughness and hardness was obtained for the welds tempered at 750°C for 1 hour and these welds fractured in ductile manner with dimpled fracture surface. Results from this study is mostly of academic interest only as the PWHT temperature range reported here does not match with the PWHT temperature range recommended in various fabrication codes for this steel.

Arivazhagan et al. [23] have reported the effect of surface re-melting using GTAW arc on the toughness of SMAW welds in P91 steel. SMAW process was reported to introduce micro inclusions in the weld metal which has adverse effect on fracture toughness of these weld joints. It was reported that surface re-melting of the SMAW welds by GTAW arc resulted in refinement of the coarse (> 5 μm) inclusions and improvements in the fracture toughness of the weld joints from 40 J for SMAW welds to 72 J for the GTAW arc re-melted SMAW welds.

Ghosh et al. [24] have reported influence of pre- and post-weld heat treatment temperatures on weldability of modified 9Cr-1Mo (V-Nb) steel pipe, produced using SMAW and GTAW. In this study, the preheating temperatures and PWHT temperatures were respectively varied in 200°C–300°C and 650°C–850°C range. They have not explained the reason for the selection of a PWHT temperature of 850°C, much higher than the code specified values (730°C–780°C range) and also, where this PWHT temperature stands in relation to the Ac1 temperature of the material, they have used. No appreciable reduction in the hardness of the weldment was reported as a result of PWHT at any temperature, they have used. The results reported in this study does not confirm to the existing and well accepted knowledge about characteristics of the welds in this steel. The reason for such a result could be insufficient time for PWHT, which is not reported in this paper.

Watanabe et al. [25] have reported evaluation of creep damage of 9Cr-Mo-V-Nb steel welded joints by conducting experiments over a temperature range of 550°C–650°C and stress range of 40–230 MPa range. A shift in the rupture location from weldment region at high stress low temperature condition to the FGHAZ region at low stress high temperature condition was reported in this study. They observed accelerated coarsening of carbides and recovery of the dislocation structure in the FGHAZ region, which led to preferential accumulation of creep damage in this region causing creep void formation and Type IV cracking. Hongo et al. [26] have also reported similar results for weld joints, in 25 mm thick Grade 91 steel plates.

Kumar [27] has reported welding of P91 steel by autogenous and cold- and hot wire GTAW processes for fabrication of steam generators of the 500 MWe Prototype Fast Breeder Reactor. The steam generators are designed to operate at high steam outlet temperature and pressure of 493°C and 172 bar respectively. A preheating temperature in 200°C–250°C range and PWHT at 760±10C was used in these welding. It was reported that hot wire GTAW not only increases the weld deposition rate, but also associated lower heat input, lower distortion and a significant reduction in the porosity as joule heating removes any volatile matter from the filler wire. Barthoux [28] has also reported similar benefits for welding of heavy wall thickness materials by narrow gap welding for nuclear application.

Arivazhagan et al. [29] have reported effect of variation in heat input on the microstructure of reduced activation ferritic martensitic steel weld metal produced by GTAW process. In the weld metal, δ-ferrite was observed, volume fraction of which increased with increasing heat input. They inferred that slower cooling rate associated with high heat input was the facilitating factor for formation of δ-ferrite in the weldment.

A detailed study on structure and properties of the actual as well as Gleeble simulated heat affected zone of P91 steel has been subject of doctoral study of Sulaiman [30]. He reported very good agreement between the actual and the Gleeble simulated HAZ in terms of structure and properties. Dilatometric studies showed that simulated normalizing did not result in complete dissolution of the carbides affecting hardness and transformation temperatures of the resulting austenite and the M_s Temperature.

Arivazhagan et al. [31] have reported influence of shielding gas composition and gas tungsten arc re-melting on toughness of flux-cored arc weld of P91 steel. They found that Ar+5%CO2 mixture resulted in minimal slag inclusion and superior toughness of the weld metal. Increasing the proportion of CO_2 led to inclusion of coarse slag particles and associated deterioration in the weld toughness. This deterioration in the toughness of the weld due to slag inclusions could be rectified by gas tungsten arc re-melting of the welds, which led to formation of fine inclusion particles at the expense of coarse particles. However, the researchers have not provided any rationale for this study on variation of the shielding gas composition and also why this variation affected the inclusion content of the welds.

Paddea et al. [32] have reported residual stress distributions in a P91 steel-pipe girth weld before and after PWHT. It was reported that highest residual stress was found towards the outer HAZ region and the root region in as welded and also in PWHT condition.

Parker [33] has reported his investigation on the factors affecting Type IV creep damage in Grade 91 steel welds. Through microstructural and creep studies on welds made in P91 steel pipes and Grade 91 steel plates by SMAW process, he concluded that in the outer HAZ region, which forms FGHAZ and ICHAZ, martensitic transformation is not likely to occur because for the fine-grained austenite the ability to undergo martensitic transformation may be limited. This region is susceptible for accelerated softening of the matrix and accelerated coarsening of the precipitates leading to localization of the creep damage, creep cavitation and Type IV cracking.

Xu [34] has reported laser welding of pipe with 3.34 mm wall thickness using a pulsed Nd-YAG laser of 1.6 kW nominal powers. He has reported the effect of process parameters on the various attributes like depth and lateral spread of fusion zone and the HAZ. A narrow fusion zone and HAZ with much higher hardness (~420 – 500 VHN) was reported by him. In post weld heat treated condition, cross-weld hardness profile did not show any soft zone, which is always associated with a multi-pass weld joint in the HAZ. PM interface region and attributed for failure by Type-IV cracking under creep condition.

Shanmugarajan et al. [35] have reported laser welding studies for 6 mm thick plate of P91 steel using continuous wave CO2 laser (Power 3.5 kW). They have studied weld beads and square butt weld joint produced by varying heat input in 168 J/mm to 1500 J/mm. They have reported increase in width of the fusion zone and the HAZ with increasing heat input. Further, at lower heat input up to 420 J/mm, they did not observe any soft inter-critical region; which was observed at heat inputs exceeding 700 J/mm. At lower heat input (up to 420 J/mm) they did not observe any δ-ferrite in the fusion zone, which was present in the fusion zone of the joints made at heat inputs exceeding 700 J/mm. Besides, they have reported superior impact toughness for the weld joints than that of the parent metal, which is in contrast to that reported by Lee et al. [36].

Harinath et al. [37] have reported their work on laser welding of fuel clad tube – end cap, both made of 9Cr-1Mo (V, Nb) FMS, for potential application in Indian fast breeder reactors. They have reported their work on process parameter optimization and preliminary microstructural examination on the weld joint cross-section. They have reported presence of δ-ferrite in the fusion zone, which comprised predominantly of as transformed martensitic microstructure. They have also reported considerable grain refining in the narrow HAZ region adjacent to the fusion zone. They have attributed the presence of δ-ferrite to incomplete δ-ferrite to γ (austenite) transformation, during cool down of the weld joint.

2.6. Weldability of Modified 9Cr-1Mo Steel

A major concern in welding of this class of steels is their high susceptibility to hydrogen assisted cracking; also known delayed cracking or cold cracking. This is a form of hydrogen embrittlement that occurs at temperatures in the range of -50°C to 150°C when hydrogen in steel is accompanied with favorable conditions such as crack susceptible martensitic microstructure and sufficient tensile stress [38-41]. Hydrogen is absorbed in steel during its processing, fabrication and also while in service. The fact that HAC occurs several hours or days after absorption of hydrogen often results in unexpected catastrophic failure while components are in service or storage. The delay in hydrogen cracking is due to the time required for hydrogen to be accumulated to a critical level at potential crack sites (such as the regions of high triaxial stress) in the steel microstructure. This accumulation takes place by diffusion of hydrogen through the lattice. Critical size of the site (where hydrogen is accumulated) which can cause cracking varies with steel microstructure. Similarly, concentration of hydrogen required to cause cracking also depends on microstructures as shown in Fig. 2.5 [42]. From this figure, it is clear that critical concentration of hydrogen that can cause cracking in steel is lower for martensitic microstructure. Hence, martensitic microstructure is highly susceptible to HAC. With increasing strength of the martensite, critical concentration of hydrogen required to cause HAC still decreases.

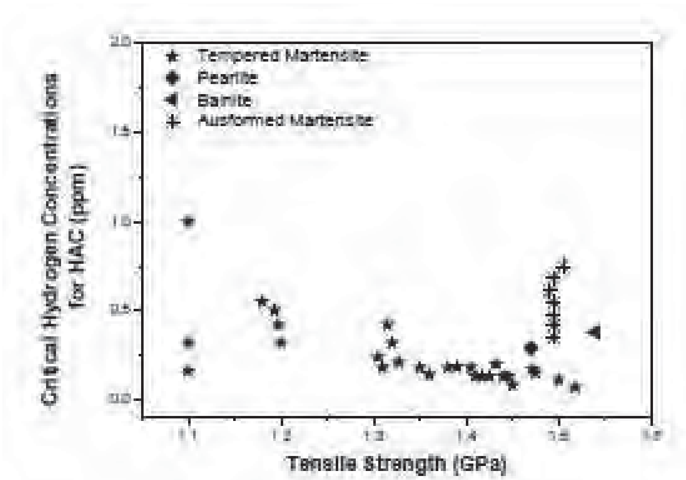

Fig.2.5. Critical hydrogen concentration causing HAC in steel microstructures [42]

Three essential requirements for HAC to take place in welds are sufficient diffusible hydrogen in weld, crack susceptible microstructure (e.g. martensite) and tensile stress. If one or more of these are removed or reduced to low levels then HAC can be prevented, like in case of low carbon steel with controlled heat input parameters and cooling rate, ferrite phase can obtain at weld and Heat Affected Zone (HAZ) that prevents HAC. However, in case of Grade 91 steel which is having final structure as martensitic only irrespective to any controlled weld heat input or cooling rate. Thus, in case of Grade 91 steel HAC can be controlled by either reducing hydrogen to low level or controlling the residual stress in weldment. An effective way of preventing the HAC in Grade 91 steel is by pre-heating, inter-pass temperature control, pre-post heating and post weld heat treatment or using low hydrogen filler wire [43-45]. With post weld heat treatment, chances of HAC due to residual stress can be completely minimized but post weld heat treatment is not always carried out immediately after welding. There may be delay in carrying out post weld heat treatment; this delay may cause HAC in weld joints. Hence some intermediate heat treatment referred as dehydrogenation heat treatment as a pre and post heating is generally recommended for avoiding or minimizing HAC cracking [46].

2.7. Welding Simulation

Arc welding is a complex process in which electrical energy is converted into thermal energy causing melting and solidification of the parts to be joint. This involves physical, chemical, metallurgical and structural changes in the material. At the end of welding cycle, due to rapid and localized heating and cooling, residual stress and distortion are also introduced in the parts to be joined by welding. Hence, modeling and simulation of the entire welding process is very challenging. Finite element method (FEM) is very useful and widely used method for this purpose.

The starting point can be interaction of the energy source flame, arc, beam etc., with the material leading to generation of heat in the solid. This is a very complex problem to model, in itself. The heat source resulting from the interaction of the energy source can be of different spatial (point, line, area, volume with different kind of intensity distributions) and temporal profile (continuous, pulsed, modulated etc). Computation of the thermal profile (the heating and cooling rates) resulting from a heat source requires simultaneous solution of the heat diffusion equation in the solid, in conjugation with cooling of the solid by convection and radiation. Since fusion welding involve melting and solidification, modeling of solid to liquid transition and convection in the melt, driven by surface tension and density gradients, becomes necessary to accurately predict weld pool morphology and temperature profile in the weld pool. One can go on counting many phenomena that need to be considered simultaneously, for accurate modeling of any welding process. However, it is not possible to include all of these in a single model. Therefore, only the phenomena of interest and relevance for the outcomes of interest are included in a model. The outcomes of interest can be the temperature profiles, the

FZ and HAZ profiles, the heating and the cooling rates, distortion of the joint, residual stress profiles etc.

2.7.1. Welding analysis using different heat source

In arc welding, energy required for welding is generated by electrical arc. However, modeling electric arc with electromagnetic forces in the arc, generation of plasma and the transfer of heat from the arc to the job is too complex to be covered in simple model. Similar is the situation for simulation of beam welding processes like electron beam and laser welding. Hence, what is usually done is that the electrical arc or beam is replaced by a heat source in such a way that the energy content in the heat source and dimensions of the heat source simulate a molten weld pool which has dimensions that match with the actual weld pool. Actual weld pool dimensions for a given heat input can be estimated experimentally from the measurements carried out on weld bead and its cross section. Different types of heat source models have been employed by various researchers for their studies to accurate prediction of weld induced effects. The movement of heat source through time and space is another aspect that should be considered in modeling.

Rosenthal et al. reported analytical point source model. Though surface melt runs relating to conduction welding were able to be simulated, it could not properly simulate the region where the point heat source is striking and transferring the heat. [47].

Pavelic et al. proposed the heat flux applied on the surface of the plate followed by the Gaussian surface distribution. The moving heat input was given as in the form of circular shape in Pavelic Disc model [48].

Hook et al. modified the Rosenthal's model for beam welding processes and predicted the proportion of power needed to cause melting. Author considered the moving heat source and estimated the weld dimensions as a function of laser power and beam velocity relative to the workpiece [49].

Dowden et al. reported a mathematical model for the weld pool simulation for laser beam welding. Author investigated the influence of the fluid dynamics fusion zone on the local temperature distribution. Results of weld showed that deep penetration using three dimensional models [50].

Goldak et al. proposed the non-axis symmetric three-dimensional double ellipsoidal model for welding heat input source to simulate the welding heat effects. This model combines two different size ellipsoids for predicting heat source distribution. This model is suited for both shallow and deep penetration for different arc welding [51]. Goldak et al. gave a complete account of various generations of heat source models used by many researchers over the years [52].

Steen et al. combined both point and line heat source model for predicting key hole effect that occurs in beam welding processes [53]. Frewin et al. developed a 3D heat source model for calculating transient temperature profiles and the weld bead dimensions. Author reported temperature profiles and the weld dimensions are strong functions of absorptivity and energy distribution of laser beam [54]. Brockmann et al. proposed a mathematical model for predicting thermal history over a thin sheet heated by laser [55].

Ravichandran et al. modeled the thermal analysis of circumferential welding in cylindrical and spherical components using FE method. Temperature-dependent material properties, Gaussian distributed heat source, heat transfer losses and latent heat were included for the model. The authors reported that the proper selection of arc distance and welding heat input of rear arc were effectively reducing the angular distortion [56].

Dong et al. investigated the ramp heat input and double ellipsoidal moving heat input models. The thermal characteristics of the welding process were predicted by these two models. The mechanical analyses were carried out using previously predicted thermal histories given as an input. Similar distribution of longitudinal residual stress was predicted [57].

Fassani et al. presented the new analytical solution to estimate temperature fields in multi-pass welding, as generated by Gaussian heat sources. The thermal histories obtained from analytical models regarding point (concentrated) and Gaussian (distributed) heat sources. The thermal cycles obtained from the distributed heat source model are more reliable than those obtained from the concentrated heat source model [58].

Deng et al. developed numerical procedure to determine the deformation induced by the fillet welding. The effect of flange thickness on deformation was investigated experimentally and numerically. The ABAQUS code was used to simulate the welding process. The combined Gaussian surface and volumetric heat source model was used to simulate the weld heat input. It was concluded that the transverse shrinkage and the flange thickness were inversely proportional [59].

Tsoukantas et al. theoretically studied the remote welding process. The laser beam welding was employed in lap joined on AISI 304 sheets. The ANSYS FE code was utilized, and respective mesh models had been generated. The surface and volume heat sources were modeled by Gaussian distribution [60].

Kazemi et al. developed heat source by combined surface and line heat source. The circular surface with Gaussian distribution was applied on the top surface, and line source was applied in thickness direction. It was reported that the shape of the weld zone was strongly influenced by Peclet number and conductivity of the material [61].

H Zhang et al. investigated the effect of arc distance and heat input on welding deformation using asymmetrical double-sided double arc welding method. The heat input assumed the volumetric double ellipsoidal heat distributed model. The FE-based thermal elastic plastic model was developed for this welding process [62].

Sattari-Far et al. investigated the influence of welding sequence on deformation in stainless steel pipe joints. GTAW process was used to make the welding with V-joint geometry.

The FE numerical results were compared with experimental data. FE simulation of this process was performed using ANSYS FE code. The double ellipsoidal heat source distribution proposed by Goldak was used. It was reported that more distortion was induced by the welding with four segments than welding with one or two segments [63].

H. M. Asl et al. developed a suitable numerical model to predict the inception of the failure of a pipeline wall during in-service welding process. The volumetric heat source with semi-ellipsoid shape was used to model the heat input from the welding arc. The thermal distribution across the pipe wall and thermo-mechanical stresses had been calculated. The predicted residual stress values were compared with the yield strength of the material [64].

Chukan et al. investigated the thermo-mechanical analysis of 316L steel plate Laser welding using SYSWELD Software. The author used 3D conical, conical with double ellipsoidal and conical with cylindrical shell model. Predicted thermal cycles, residual stress and distortion in weld plate validated with experimental values. It is concluded that 3D Conical model combine with cylindrical shell predicted more accurate results [65].

2.7.2. Filler material addition

In FE analysis of welding process, the role of filler material deposition is very important. The FE model of weld joint consists of base metal and filler material in a single mesh. Based on literature it is observed that to simulate the filler material deposition, the element birth and death technique is used in ANSYS and ABAQUS software, where as in SYSWELD software (using FORTRAN coding) chewing Technique is used. Initially, all the elements in the bead or groove in V joint are killed and empty groove is obtained. Subsequently, the elements located at the bead or groove is activated segment by segment with time to reproduce the weld bead formation by the filler material.

Andrea et al. used the same technique in laser welding and GTA welding processes. The elements describing the molten metal were kept alive during the thermal analysis because they absorbed the heat energy. The ANSYS birth and death technique was applied for their study [66].

Mollicone et al. utilize the element activation and deactivation to simulate the incremental weld metal deposition for both 2D and 3D analyses. In their study, simulation process was carried out in ANSYS FE program [67].

Del Coz Díaz et al. used a similar technique in thermal stress analysis of GTA welding process of two different stainless steels. The element loads connected with deactivated elements were zeroed out of the load vector. The heat generation was applied as a load in the thermal analysis and predicted the thermal strains for the newly activated elements based on the current load step temperature [68].

B. Q. Chen et al. investigated the effect of element birth and death (EBD) technique, and two indistinguishable FE models were developed for single pass GTAW process. One of them was analyzed using EBD, whereas the other one did not consider EBD. The residual stress and deformation of the welded plates were studied. The simulation studies on the effect of FE mesh size and convection coefficient were made. They reported that the magnitude of the temperature in the EBD model was higher than the other. It was also, recorded that convection heat transfer coefficient had poor effect on peak temperature [69].

Abdulkareem Aloraier et al. discussed the 3D FE simulations of flux cored arc welding process in a single bead on plate weld using SYSWELD code. FE transient thermal analysis results were validated with thermocouple measurements. The simulated residual stresses were compared with experimental results. The residual stress hole drilling method was used for the measurement of residual stresses experimentally [70].

Mato Peric´ et al. numerically and experimentally studied the weld induced residual stresses and distortion in T-joint. Kinematic hardening rule was employed in mechanical analysis. Three-dimensional image correlation systems were used to measure the displacement of the plates experimentally [71].

M. Hadi et al. analyzed the single pass multi-welded aluminum plates. The predicted residual stresses predicted by the FE were verified through experimental measurements. The FE analysis was carried out in ABAQUS. The moving heat load was modeled by the Gaussian surface heat source model. It was reported that the element interaction technique revealed applicability and flexibility in filler metal reposition modeling [72].

X. Shan et al. described three-dimensional thermo-mechanical FE analysis of a single weld bead-on-plate of austenitic stainless steel. For the thermal analysis, two approaches had been adopted to simulate the process. One approach was the weld bead's elements were sequentially deposited, while in the other, the whole bead was deposited simultaneously. Goldak's ellipsoidal heat source model was employed for the modeling of weld heat input. The FE analysis had been carried out in ABAQUS [73].

A. Kermanpur et al. simulated the multi-pass GTAW process of Inconel 800 pipes using FE analysis. The GTA torch movement was assumed in a discontinuous fashion with a constant welding speed. The arc heat input was modeled by surface, volumetric and combined heat flux distribution functions [74].

Yaghi et al. investigated the effect of pipe diameter on residual stresses. FE method was used to analyze the residual stresses in a multi pass butt welded steel pipe. ABAQUS FE program was used to conduct the sequentially coupled thermal stress analysis. Filler addition in V- butt welded joint was modeled by element birth technique. The constant distributed volumetric heat flux was applied to elements of the model. The temperature-dependent heat transfer coefficient was employed in FE analysis [75].

Narang et al. predicted the shape profiles and characteristic of submerged arc weldment zones by statistical methods. A full factorial design matrix was used for bead plate welds to study the effect of welding process parameters [76].

N. Yadaiah et al proposed egg-configuration heat source model for autogenous welding of GTA and Laser welding process. Author concluded that computation of cooling rate is directly influenced by the shape and size of proposed heat source model and the developed heat source model is flexible enough to accommodate different type of fusion welding process [77].

2.7.3. Residual stress analysis

The residual stresses in weld joints are generated due to uneven heating and cooling during welding. Measurement of stress at specific location requires sophisticated equipments and different destructive type and non-destructive testing (hole drilling and XRD techniques). FE modeling is conveniently employed to evaluate the residual stress over the entire plate geometry. The accuracy of prediction requires reliable thermal cycles experienced by weld, availability of suitable temperature dependent material properties and selection of appropriate boundary conditions. Further, residual stresses generated are always accompanied deformation, appropriate theories of strain hardening (kinematics, isotropic and mixed) also need to be considered. For predicting residual stresses, two dimensional and three-dimensional meshing models have been considered by different authors; the former is less time consuming than the latter; but accuracy is better for the simulation based on 3D meshing.

H. Purmohamad et al. modeled multi pass circumferential butt welding of pipes with FE analysis. GTAW process was used to make the joints of Inconel 800H pipes. Goldak double ellipsoidal model was used to simulate the arc heat input. Transient thermal analysis was performed for the prediction temperature distribution and shape of weld zone. It was reported that the increasing welding heat input contributed to wider weld zone and higher peak temperature in heat affected zone [78].

Shan et al. modeled a European network single-bead-on- plate test specimen using FE method. The ABAQUS FE program was used to predict the final residual stresses. Due to the complexity of the three- dimensional analyses, a two-dimensional FE analysis was carried out for the sensitivity tests [79].

C. Lee et al. used volumetric heat source model to identify temperature field and residual stress distributions in dissimilar steel butt welds. The weld induced residual stresses were predicted in dissimilar steel butt-welded joints connecting stainless steels and carbon steels. The FE predicted welding residual stresses in the butt welds were by no means of the same magnitude or direction as those in corresponding similar steel butt welds [80].

Xu et al. investigated the effect of hardening models such as isotropic hardening, kinematic hardening and mixed isotropic-kinematic hardening on residual stresses. It was reported that the mixed isotropic-kinematic hardening model results showed very close agreement with the experimental measurements. The effect of restraints was also studied, and it was concluded that the restraint clamping condition has a slight effect on residual stress. The arc heat input was modeled by two offset double ellipsoid heat source models [81].

Heinze et al. studied the residual stress development in multi pass gas metal arc welding under high restraint conditions. It was reported that the longitudinal residual stresses were not considerably influenced by the transverse shrinkage restraint. The transverse residual stress near the weld center line up to 400MPa was due to the restriction of the plate in the transverse direction [82].

K.H. Chang et al. studied the description of residual stresses in T-joint fillet weld made from dissimilar materials. The combination of Gaussian surface and volumetric heat distribution functions was used to model the welding heat input from the arc. The weld metal deposition was simulated by element birth and death technique. Linear kinematic hardening rule had been employed in stress analysis [83].

Adak et al. investigated the influence of restraint conditions on residual stresses and deformations induced by butt joint welding. In addition to this, effects of plate thickness and plate width on residual stresses were also studied. Mechanical analysis was carried out with the aid of bilinear isotropic hardening rule with von-misses yield criteria. The element birth and death feature were employed to simulate the filler material addition in ANSYS. It was reported that the thickness of the plate was directly proportional to the residual stresses and mesh sizes that influenced the residual stresses [84].

Dean Deng et al. presented the numerical procedure for studying temperature distribution and residual stresses induced by multi pass welds in 304 stainless steel pipes. The uncoupled three-dimensional and two-dimensional FE models were developed. The double ellipsoidal volumetric heat source was used for temperature analysis. The combined convection and radiation heat transfer losses were employed in the FE modes. The linear kinematic hardening rule was employed in stress analysis. It was reported that the large amount of computational time had been saved with two-dimensional axis-symmetric models [85]. In other study 2.25Cr-1Mo steel pipe numerical analysis was carried out. The joining of pipes was made by multi-pass GMA welding process. Prediction of residual stress was carried by sequentially coupled thermal mechanical FE procedure in ABAQUS program. It was reported that the phase transformation affected the outer surface hoop tensile stress [86]. They have also modeled the effect of solid stage phase transformation during weld thermal cycle on residual stresses developed in the welds made from low carbon and medium carbon steels. It is shown that effect of phase transformation on residual stress is significant in the welds of medium carbon steels [87]. In other investigation same author investigated the residual stress induced in SUS304 pipe. The effect of yield strength of the weld metal on residual stress was numerically studied. The numerical simulation carried out using ABAQUS FE by adopting sequentially coupled thermo-mechanical analysis. It was reported that the yield strength of the weld metal at higher temperature occurred in weld zone [88].

Sattari-Far et al. studied the influence of the weld groove and number of passes on residual stresses in pipe made by GTA welding process using AISI 304 stainless steel. FE thermo-mechanical process was used to simulate the entire process. The heat input of moving welding arc was modeled by Goldak's double ellipsoidal volumetric heat source distribution. It was concluded that the weld groove shape had no effect on residual stress distribution in 6 mm thick plate. The hoop residual stresses significantly decreased when the number of passes increased [89].

Moraitis et al. developed the numerical simulation model of Laser beam welding (LBW) process for the prediction of residual stress and distortion fields. The efficient keyhole model with empirical parameter was introduced to calculate the keyhole size and shape using ANSYS FE code. The model was validated in butt joint welding of DH-36 steel plates, and the efficiency of the process was demonstrated for the lap joint welding of aluminium 6061-T6 plates [90].

Z. Barsoum et al. studied T-joint fillet weld with the thickness of 8 and 20mm. 2D and 3D FE simulations were carried out for their study. Experimental measured residual stresses using X- ray diffraction on T- Joint structure were compared with predicted results. There was a good agreement between predicted and experimental values [91].

Y. Javadi et al. investigated the sub-surface residual stress and deformations induced by GTA welding process using ultrasonic stress measurement and FE simulation. The two type's plates were welded with and without the use of clamp for their investigation. The effect of clamping on residual stress and distortion was studied. It was reported that the clamping effect had significantly influenced the magnitude and distribution of longitudinal residual stress [92].

Ficquet et al. measured residual stresses in thickness direction using deep hole drilling technique and near surface using incremental centre hole drilling method. The experimental measured results were compared with predictions made using FE analysis by considering non-linear kinematic hardening rule [93].

Hilson et al. measured the residual stress using X-ray diffraction method (XRD), incremental centre-hole drilling method (ICHD) and deep-hole drilling method. XRD method was used to measure the stresses at <10 μm from the surface of the pipes whereas deep hole drilling method was used to measure through wall section of the pipes [94].

Keivani et al. (2014) carried out 3D thermo-mechanical FE analysis to model and study the effect of welding sequence on residual stresses and distortion in T-joints. The volumetric double ellipsoidal distributed heat source was employed for the modeling of moving welding arc. Newton's law and Stefan-Boltzmann law were used to estimate the convection and radiation heat losses respectively. It was reported that the peak residual stresses at mid span of the weld line was influenced by the welding sequences [95].

Singh et al. (2014) used finite element based numerical model to simulate the weld induced stresses. Adoptive volumetric heat source distributed model was used to simulate the thermal model and predict the temperature distribution. The residual stresses induced by three different fusion processes were studied. The behavior of the material during the welding process was assumed as elastic plastic in nature [96].

Afshari et al. (2013) studied electro thermal structural coupled FE model to simulate the spot-welded aluminum alloys joint. The residual stresses were measured experimentally by X-ray diffraction technique. The temperature-dependent material properties were incorporated to improve the accuracy of the FE model [97].

S. A. A. Mousavi et al. analyzed the residual stress induced in the GTA welding process. The 2D and 3D FE analyses were used in their study. The X-ray diffraction technique was used to measure the residual stress experimentally. The FE simulated results were compared with the measured results, and the effects of geometry configurations on residual stresses were studied. The material properties were used in the FE analyses was assumed to be temperature dependent. The authors reported that less distortion had been produced when the structure had constrained rather than unconstrained structure [98].

A. A. Bhatti et al. implemented three different FE approaches on a large bogie beam structure. The welding stresses were predicted by using sequentially coupled thermo-mechanical analysis. The ANSYS FE program was used to model and simulate the bogie beam three dimensionally. The heat source was modeled by uniform surface and volumetric heat source models. The authors concluded that the residual stresses induced by rapid dumping approach showed very good agreement with the X-ray diffraction measurements [99].

Price et al. have reported comparison of the residual stress in welds computed using SYSWELD and that measured experimentally using neutron diffraction. They have used GMAW deposited weld beads on low carbon steel. Their results show that longitudinal component of the residual stress is the most significant and the normal and transverse components are much smaller and comparable to each-other [100].

Joshi et al. have reported computation of weld-induced residual stresses in a prototype dragline cluster using SYSWELD and comparison of the computed values with design codes. They reported that the computed values of the residual stresses in the fused area was higher than the yield stress at some points, however, these were generally not capable of inducing cracks on their own. These solutions provide temporal evolution and spatial distribution of temperature, displacement, strain and residual stresses of the weld joints produced by arc welding and are useful for distortion engineering of welded structures [101].

G. A. Moraitis et al. have reported thermo-mechanical computation of laser welding in high strength steel and an aluminum alloy using ANSYS. They have reported transient temperature field and residual stress profiles across the weld joint and through thickness of the weld joint. However, details of the steel in terms of composition and properties and also if any SSPT has been considered is not reported in this paper [102].

Shanmugam et al. have reported transient thermal computation using SYSWELD for T-joints in austenitic stainless steel (SS304L) made by laser welding. Lack of penetration was reported by them for a beam angle of 30°. For the beam angle of 45° they reported that proper fusion of base material was achieved between the horizontal and vertical sheets, however, lack of fusion could not be ruled out. A very good agreement between the computed and the experimentally measured depth of penetration and width of the fusion zone was reported, with standard errors of 2.78% and 1.9%, respectively [103].

Phase transformation consideration during thermo-mechanical analysis of welding is important, but due to complexity in welding process some researchers ignored it. Y. C. Kim et al. studied the effects of phase transformation on distortion and residual stresses generated by LBW on high-strength steel were investigated. Results of analysis showed that welding distortion and residual stress were largely affected by phase transformation in the cooling process, although the bead width of LBW was extremely narrow (around 5 mm) compared with that of existing arc welding [104]. Author also studied the effects of the phase transformation on the generation of welding distortion and residual stress of LBW and HYBW, on the high strength steel (HT780) Results showed that the phase transformation in the cooling process largely affected and controlled welding distortion. The effects were caused by not only the transformation expansion but also the transformation super-plasticity [105].

From the large number of literatures sited above, it is clear that extensive work has been carried out on both measurement and simulation of residual stress in welded joints. For simulation, different FEM packages like ANSYSIS, ABACUS, SYSWELD etc. software have been used. Literatures reveal that phase transformations that occur during weld thermally cycle have significant effect on the residual stress distribution in the weld joint.

2.7.4. Distortion analysis

In literature it is observed that different researchers employed two basic displacement theories such as large displacement theory and small displacement theory in the distortion analysis. In large displacement theory, the un-deformed and deformed configurations of the continuum are significantly different. It deals with deformations of both rotations and strains. In small deformation theory, the un-deformed and deformed configurations of the body are assumed as identical. It is used in the analysis of deformations in materials exhibiting elastic behaviors.

Dean Deng et al. compared the strain distribution and residual stress results with large deformation and small deformation theories. The distortion predicted using large deformation theory had very close agreement with the experimental measurements, and the inherent strain method effectively predicted the deformation in the thin plate structure [106].

C. Wang et al. developed FE computational procedure to predict the distortion in GMA welded T-joint. Development of weld bead with the welding speed was numerically calculated using element rebirth technique (ERT). The longitudinal bending and angular distortion results of three different models were studied. It was reported that the numerical model with ERT and large deformation theory had been used for the reliable prediction of deflection [107].

J. Wang et al. studied the weld induced buckling distortion in bead on plate welding. A thermal-elastic-plastic FE analysis was carried out to predict weld induced buckling distortion. The buckling performance was studied using large deformation theory employed in elastic FE analysis. It was reported that the large deformation theory had been used for the prediction of buckling [108].

Mahapatra et al. investigated the influence of submerged arc welding (SAW) process parameters on thermal effect and angular distortions in single-pass butt joints with bottom and top reinforcements. The three-dimensional FE analysis was used to simulate the SAW process [109].

S. K. Bate et al. carried out uncouple thermal and mechanical analysis using SYSWELD software code in order to model a single bead on plate specimen. The heat input from welding arc was modelled using double ellipsoidal heat source distributions. Isotropic hardening model and small displacement theory were employed in mechanical analysis [110].

Biswas et al. developed 3D FE model for double sided fillet submerged arc welding process. The heat input from the SAW was given as surface distributed heat flux. For mechanical analysis, the large displacement theory was employed with rate-dependent thermo-elastic-plastic model. The FE analysis was conducted in ANSYS program [135].

M. Seyyedian et al. investigated the effect of weld sequence and direction on angular distortions in single pass butt welded 304 stainless plates and also studied their effect on residual stresses by numerical simulation. Their study showed that welding sequence and direction have a great influence on angular distortions. He has also modeled the effect of plate dimensions on distortion during welding and verified the prediction for each case with results obtained from experimental results. Results revealed that plate thickness, length and width influence the magnitude and mode of distortion [112-113].

M. V. Deo et al. studied welding induced buckling by means of decoupled computational approach, where investigation process was divided into two steps, in first step, determination of residual stress by thermo-mechanical analysis was carried out and in second step the critical buckling stress and buckling mode with Eigen value was obtained [114].

Comparison between experimental and simulated results for distortions is developed by Tsirkas et al. who used the commercial welding simulation software SYSWELD for analysis. However, the results are limited to the temperature contours and displacement contours [115].

Yupiter et al. investigated the influence of sequence in GMA welding on angular distortion. Low manganese carbon steel was selected for their investigations. The SYSWELD code with Multipoint welding adviser (MWA) was employed for the numerical simulation. Goldak's double ellipsoidal heat source model was used for heat input modeling. It was concluded that the outside to inside welding sequence yielded less angular distortion than the inside to outside sequence [116].

2.8. Welding Analysis of Modified 9Cr-1Mo steel

High chromium martensitic steel is generally regarded as being more difficult to weld than austenitic steel because in order to avoid cracking steel are preheated before welding. Phase transformation takes place during heating cooling and cooling. Till now few researchers have been published work on thermo mechanical analysis for Modified 9Cr-1Mo steel welds.

D. Deng et al. have reported computation of welding residual stresses using ABAQUS in multi-pass arc welded modified 9Cr-1Mo steel pipe in butt configuration, considering solid state phase transformation (SSPT) effects. They have also used axisymmetric model and considered the effects of volumetric and/or yield strength change arising out of SSPT of austenite into martensite during welding. It was reported that the volume and yield strength changes associated with SSPT of austenite to martensite during welding have significant effects on residual stress and must be considered for computation of stresses arising out of welding of this material. Because of non-availability of mechanical properties of the low temperature austenite, they have used properties of the base metal itself in this regime. However, it was recommended that phase-dependent mechanical properties of the material should be used for further improvements in the computed results [117].

Yaghi et al. have reported residual stress simulation using ABAQUS in multi-pass arc welded section of P91 pipes. They have used an axisymmetric model of the butt joint between P91 steel pipes for this simulation and have computed through thickness residual stress profiles along weld center line and in the HAZ. They performed the analysis for five joint configurations each for two wall thicknesses 7.1 mm and 40 mm, by varying the inside radius to wall thickness in 1 to 100 range. It was reported that the peak tensile stresses occurred nearer to the inside surface of the pipe in the thin walled joints and nearer to the outside surface of the pipe in the thick-walled joints. The peak compressive stresses, if any, occurred nearer to the outside surface of the thin walled pipe and nearer to the inside surface of the thick-walled pipe. A set of material properties generated for this purpose was used in this study. However, material properties of super-cooled austenite were not considered in these computations. In addition, solid state phase transformation (SSPT) of the austenite into martensite was also not considered in their model [118-120].

Kim et al. have reported numerical computation using ABAQUS and experimental measurements using neutron diffraction of residual stresses for a modified 9Cr-1Mo steel weld joint. They have used material property data from Yaghi et al. [118] and have not used phase-dependent material property data. The weld joints were produced in butt and fillet configurations using arc welding methods. They had not implemented SSPT of austenite into martensite however, based on the experimental results it was recommended that SSPT should be considered for arriving at more reliable results [121].

S Kumar et al. measured residual stress in longitudinal, transverse and normal direction for 9 mm thick plate using neutron diffraction technique for laser welding. Thermo-mechanical analysis of welding analysis is carried out using SYSWELD by combining double ellipsoidal and conical heat source model. The results showed that stress distributions in normal and longitudinal direction are tensile and compressive in nature at FZ and base material [122].

C. Heinze et al. reported the thermo-mechanical analysis of welding of low alloy structural steel and P91 steel. Author studied the austenite grain size effect on residual stress and martensite temperature with fraction. Authors showed the martensite transformation effect on HAZ residual stress [123].

Serizawa et al. reported FEM modelling and simulation of EB welding of RAFMS to assess weldability of 90 mm thick plates this steel under restraint. They considered models of different total lengths (150 mm, 200 mm and 400 mm) with weld lengths of 136 mm and 176mm to examine cracking tendency under the restraint. Their results showed that for assessing weldability study of 90 mm thick plates of this steel by EB welding, the minimum coupon size should be 200 mm long, 400 mm wide and 90 mm thick with ~ 180 mm long weld length [124].

Z. Hu et al. studied the thermo-mechanical analysis of P91 welded joint using ABAQUS software using subroutines. Effect of martensitic transformation (MT) and latent heat on temperature field was considered. Temperature field, the residual stress was calculated by considering the effects of volume expansion, the yield strength change and the transformation plasticity due to martensitic. The results show that the MT latent heat makes the temperature increase. The effects of MT on residual stress can be divided into three types. The volume expansion can counteract the shrinkage of the material during cooling, resulting in a significant reduction in residual stress. The yield strength change can increase the residual stress. The transformation plasticity has the relaxation effect [125].

Abburi et al studied the effect of post weld heat treatment parameters on the relaxation of welding residual stresses in electron beam welded P91 steel plates and validated the predicted residual stress with experimentally measured values. Effect of the different holding temperature and time of PWHT on modified 9Cr-1Mo steel weld made Laser welding was studied. 2D-Thermo-elastic-plastic model was developed considering the effect of phase transformation. Predicted longitudinal residual stresses were compared with experimentally measured values and the results were found to be in good agreement. Also, the result from an analysis without phase transformations is included in the comparison to show the significance of these on the final residual stress distribution. The longitudinal stress without phase transformation shows a peak tensile stress at the weld center whereas the one with phase transformation shows a compressive stress. [126]

2.9 Beneficial Effect of SSPT on Residual Stress Distribution of the Weld Joint

From the literature review presented above it can be seen that solid state transformation of austenite to martensite, which takes place at a relatively low temperatures has a beneficial effect on bringing down the peak tensile residual stress levels in the weld joints. Though not directly related to the scope of the present work, it is interesting to note that this beneficial effect has been exploited in developing welding consumables with low transformation temperatures and producing weld joints and components that which has in fact compressive residual stress at the weld location. This has been demonstrated by Moat et al in a work published recently [127]. The weld joints of 304L austenitic stainless steel were made with low temperature transformation welding consumable Cam-alloy 4. During welding inter-pass dwell temperature was maintained above the martensitic start temperature so the weld metal remained austenitic throughout welding and then transformed martensite when cooled down to room temperature at the end of welding, taking full advantage of the transformation to reverse the tensile residual stresses generated during cooling from solidification temperature range down to transformation start temperature to compressive subsequent to transformation. Residual stresses were measured using neutron diffraction technique. Longitudinal stress profile showed that for weld joints made with non transforming filler wire, residual stress is tensile in nature with peak value 400MPa.while LTT filler wire weld shows compressive stress distribution due to martensitic transformation with peak value -600MPa. [127]

2.10. Research Gap

Based on literature review, it is observed that there is limited literature is available on thermo-mechanical analysis of modified 9Cr-1Mo steel welding and available literature is limited to higher thickness of two-dimensional pipes and plate only. Similarly, very limited work is available on welding analysis using three dimensional models. Further, thermo-mechanical models to that consider solid state phase transformation of austenite to martensite, which has a beneficial effect on the residual stress distribution, are also limited.

It is well known that steels like modified 9Cr-1Mo steel are susceptible to Hydrogen Assistant Cracking. Pre-heating or combined pre heating & post heating are used for reducing the cracking susceptibility. However, studies, both experimental and modeling, to reveal the effect of pre heating and combined pre heating & post heating on residual stress and distortion of welds of this class of steels are missing in literature.

Above mentioned points are identified as the gap in the research work in the available literature on thermo-mechanical analysis of welding of Grade 91 steel.

These research gaps are addressed in the present work as per the activities listed below.

1. The development of numerical models to investigate the thermo-mechanical behavior of thin ferritic-martensitic modified 9Cr-1Mo steel welds.
2. The comparative study with an autogenous and multi-pass GTA welding with and without preheating using numerical models.
3. Thermo-mechanical analysis of effect of phase transformation on residual stress and distortion analysis of modified 9Cr-1Mo steel welding analysis.
4. Experimental study of effect of pre heating and combined pre heating and post heating on residual stress and distortion of autogenous and multi-pass welding of modified 9Cr-1Mo

steel.

5. Thermo-mechanical analysis of welding with combined pre heating & post heating on GTA welding of modified 9Cr-1Mo steel.

2.10. Objective and Scope of the Work

The objective of the present work is to develop a numerical model for autogenous and multi-pass GTA welding of modified 9Cr-1Mo steel that would consider preheating and post heating employed during welding aytnd capable of prediction residual stress and distortion with reasonable accuracy. Hence, objective also includes validation of this model by preparation of autogenous and multi-pass weld joints and experimental estimation of residual stress and distortion. To achieve these objectives, scops of the work includes the following

1. Creation of material database for modified 9Cr-1Mo steel by considering the effect of phase transformation which will be an input for thermo-mechanical analysis.
2. Incorporation of the effect of phase transformation in the thermo-mechanical analysis of modified 9Cr-1Mo steel welding.
3. Validation of the accuracy and consistency of double ellipsoidal model by carrying out bead-on-plate experiments.
4. Thermal analysis of 3 mm thick plate autogenous and 6 mm thick plate multi-pass welding and its validation with experimentally generated thermal cycles from temperatures recorded using K type thermocouples at different locations.
5. Mechanical analysis of 3 mm thick plate autogenous and 6 mm thick plate multi-pass welding and its validation with experimentally estimated residual stress values using X-ray diffraction technique and displacement values measured on the welded plates using electronic height gauge.

6. Thermo-mechanical analysis of welding with pre heat for both autogenous and multi-pass welding and its validations by comparing the predicted weld thermal cycles, residual stress and vertical displacement at different locations with those obtained from experiments.

7. Thermo-mechanical analysis of welding with preheating and post heating for both autogenous and multi-pass welding and its validations by comparing predicted weld thermal cycles, residual stresses and vertical displacement at different locations with those obtained from experiments

8. Study of effect of pre heating and combined pre heating & post heating on residual stress and displacement of both autogenous and multi-pass welding of modified 9Cr-1Mo steel plates.

References

1. J. Pesicka, R. Kuzel, A. Dronhofer, G. Eggeler, "The evolution of dislocation density during heat treatment and creep of tempered martensitic freeitic steels" Acta Material, 2003, Vol. 51, 4847-4862.
2. K. H. Mayar, W. Bendick, R.U. Husemann, T. U. Kern, R. B. Scarlin, "New materials for improving the efficiency of fossil-fired thermal power station" International Joint Power Generation Conference. PWR-Vol.33, 1998, ASME, 831-841.
3. R. Viswanathan, W. T. Bakk er, "Materials for boilers in ultra-super critical power plant". Proceedings of 2000 International Joint Power Generation Conference. Miami Beach, Florida, ASME, 1-22.
4. R. Viswanathan, K. Coleman, U. Rao, "Materials for ultra-supercritical coal-fired power plant boilers", International Journal of Pressure Vessels and Piping, 2006, Vol. 83, 778-78.
5. H. Cerjak, E. Letofsky, "The effect of welding on the microstructure development of advanced 9-12% Cr steels", International Conference on Microstructural Stability of Creep Resistant Alloys for High Temperature Plant Application. London, Institute of Materials, 323-337.
6. F. Masuyama, R. Viswanathan, J. Nutting, "New developments in steels for power generation boilers", Advanced Heat Resistant Steel for Power Generation. London, 1999, IOM Communications Ltd, 33-48.
7. J. Orr, F. R. Beckitt, G. D. Fawkes, "The physical metallurgy of chromium – molybdenum steels for fast breeder reactor boilers", Procedia of conference on ferritic steels for fast reactor steam generators, BNES, London ,91-109, 1978.

8. S. J. S Anderson, “Mechanical properties and metallurgy of 9%Cr1%Mo steel”, proceeding of International Conference on ferritic steels for high temperature applications, Penn USA, 1983, 153-162.

9. D. C. Lundin, P. Liu, Y. Cui, “A literature review on characteristics of high temperature ferritic Cr-Mo steels and weldments”, Welding Research Council Bulletin 2000, 454.

10. R. Viswanathan, W. Bakker, “Materials for ultra-supercritical coal power plants-boiler materials” Part 1 Journal of Materials Engineering and Performance, 2001, Vol. 10, 81-95.

11. K. Haarmann, Y. C. Vaillant, B. Vandenberghe, W. Bendick, A. Arbab, “The T91/P91 Book”, 2002, Vallourec & Mannesmann Tubes.

12. E. L. Bergquist, A. B. Esab “Consumables and welding modified 9Cr-1Mo steel”, 1999, Svetsaren, Sweden,Nos. 1-2, 22-25

13. R. Blume, K. Leich, H. Heuser, F. W. Meyer, “Stainless Steel Europe”, 1995, 49-53.

14. J. F. Lancaster, “Metallurgy of Welding” London, 1993, Chapman & Hall.

15. W. F. Savage, E. F. Nippes, E. S. Szekeres, “Study of weld interface Phenomena in a low-alloy steel”. Welding Journal, 1976, Vol. 55, 260-268.

16. P. A. Agyakwa, “Creep and microstructure development in P91 weldments at Elevated temperature”, Materials and Manufacturing Engineering, 2004, University of Nottingham, PhD thesis.

17. M. Peter, “Evolution of microstructure and mechanical properties of the heat affected zone in B-containing 9% chromium steels”, 2007, University of Graz, Austria, PhD Thesis.

18. R. C. Reed, H. K. D. H. Bhadesia, “A Simple Model for Multipass Steel Welds”, Acta Metallurgy and Materials, 1994, Vol. 42, Issue 11, 3663-3678.

19. S. A. David, J. A. Siefert, Z. Feng, “Welding and weldability of candidate ferritic alloys for future advanced ultrasupercritical fossil power plants”, Science and Technology of Welding and Joining, 2013, Vol. 18, Issue 8, 631-651

20. K. Laha, K. S. Chandravathi, P. Parameshwaran, K. B. S. Rao, S. L. Mannan, “Characterization of Microstructures across the Heat-Affected Zone of the Modified 9Cr-1Mo Weld Joint to Understand Its Role in Promoting Type IV Cracking”, Metallurgical and Materials Transitions A, 2007, Vol. 38, 1, 58-68.

21. R. Mythili, P. V. Thomas, S. Saroja, M. Vijaylakshmi, V. S. Raghunathan, “Microstructural modification due to reheating in multipass manual metal arc welds of 9Cr-1Mo steel”, Journal of Nuclear Materials, 2003, Vol. 312, 199-206.

22. R. K. Shiue, K. C. Lan, C. Chen, “Toughness and austenite stability of modified 9Cr-1Mo welds after tempering”, Material Science and Engineering A, 2000, Vol. 287, 10-16.

23. B. Arivazhagan, S. Sundaresan, M. Kamaraj, “Effect of TIG arc surface melting process on weld-metal toughness of modified 9Cr-1Mo (P91) steel”, Materials letters, 2008, Vol. 62, 2817–2820.

24. P. K. Ghosh, U. Singh, "Influence of pre- and post- weld heating on weldability of modified 9Cr-1Mo (V-Nb) steel pipe under shielded metal arc and tungsten inert gas welding process”, Science and Technology of Welding and Joining, 2004, Vol. 9, Issue 3, 229-236.

25. T. Watanabe, M. Tabuchi, M. Yamazaki, H. Hongo, T. Tanabe, “Creep damage evaluation of 9Cr-1Mo-V-Nb steel welded joints showing Type IV fracture”, International Journal of Pressure Vessels and Piping, 2006, Vol. 83, 63-71.

26. H. Hongo, M. Tabuchi, T. Watanabe, “Type IV Creep Damage Behaviour in Gr.91 Steel Welded Joints”, Metallurgical and Materials Transitions A, 2012, Vol. 43, Issue 4, 1163-1173.

27. P. Kumar, “An Overview of Welding and Fabrication Aspects during Manufacture of Nuclear Reactor Components for 500 MWe Prototype Fast Breeder Reactor”, Proceeding of International Welding Congress 2014 (IWC 2014), New Delhi, India (2014).

28. J. P. Barthoux, “Narrow gap welding of heavy wall thickness materials in nuclear and fossil fuel industries”, Focus on Nuclear Power Generation, November 2008, 36

29. B. Arivazhagan, M. Vasudevan, “A comparative study on the effect of GTAW processes on the microstructure and mechanical properties of P91 steel weld joints”, Journal of Manufacturing Process, 2014, Vol. 16, 305-311.

30. S. Sulaiman, “Structure of properties of the heat affected zone of P91 creep resistant steel”, PhD Thesis, University of Wollongong, Wollongong, Australia (2007) [http://ro.uow.edu.au/theses/777].

31. B. Arivazhagan, S. Sundaresan, M. Kamaraj, “A study on influence of shielding gas composition on toughness of flux-cored arc weld of modified 9Cr–1Mo (P91) steel”, Journal of Materials Processing Technology, 2009, Vol. 209, 5245-5253.

32. S. Paddea, J. A. Francis, A. M. Paradowska, P. J. Bouchard, I. A. Shibli, "Residual stress distribution in a P91 steel-pipe girth weld before and after post weld heat treatment", Material Science and Engineering A, 2012, Vol. 534, 663-672.

33. J. Parker, “Factors affecting type IV creep damage in Grade 91 steel welds”, Material Science and Engineering A, 2013, Vol. 578, 430-437

34. Z. Xu, “Laser welding and post weld heat treatment of modified 9Cr-1VNb steel”, Report No. ANL/NE-12/12, Argonne National Laboratory, Chicago, Illinois (2008).

35. B. Shanmugarajan, G. Padmanabham, H. Kumar, S. K. Albert, A. K. Bhaduri, “Autogenous laser welding investigations on modified 9Cr-1Mo (P91) steel”, Science and Technology of Welding and Joining, 2011, Vol. 16, 6, 528-534.

36. W. H. Lee, R. K. Shiue, d C. Chen, “Mechanical properties of modified 9Cr-1Mo steel welds with notches”, Material Science and Engineering A, 2003, Vol. 356, 153-161.

37. Y. V. Harinath, K. A. Gopal, S. Murugan, S. K. Albert, “Study on laser welding of fuel clad tubes and end plugs made of modified 9Cr-1Mo steel for metallic fuel of Fast Breeder Reactors”, Journal of Nuclear Materials, 2013, Vol. 435, 32-40.

38. W. H. Johnson, Some remarkable changes produced in iron by the action of hydrogen and acids, Proceedings of the Royal Society (London), 1875, Vol. 23, 168-179.

39. P. G. Bastien, “A Study of Cracking in Low-Alloy Steel Welded Joints”, Welding Journal, 1960, Vol.39, 546-557.

40. A. E. Flanigan, J. L. Kaane, "Temperature Dependence of the Rate of Underbead Cracking in an Arc Welded Low-Alloy Steel”, Welding Journal, 1964, 43, 80-85.

41. A. E. Flanigan, M. S. Tucker, "Escape of Dissolved Hydrogen from Weld Metal”, Welding Journal, 1966, Vol. 45, 368-373.

42. S. Yamasaki, Hydrogen trapping in steels, Modelling the precipitation of carbides in martensitic-steels: http://www.msm.cam.ac.uk/phase-trans/2001/shingo/img6.htm

43. G. K. Padhy, V. Ramasubbu, N. Murugesan, C. Ramesh, S. K. Albert, “Hot extraction of diffusible hydrogen and its measurement using a hydrogen sensor”, Welding In the World, 2012, Vol. 56, Issue 7-8, 18-25.

44. G. K. Padhy, V. Ramasubbu, N. Murugesan, C. Ramesh, S.K. Albert, “Effect of preheat and post heating on the diffusible hydrogen content of welds”, Science and Technology of Welding and Joining, 2012, Vol. 17, Issue 5, 408-413.

45. G. K. Padhy, V. Ramasubbu, N. Murugesan, C. Ramesh, S. K. Albert, "Diffusible hydrogen measurement in steel welds using an electrochemical hydrogen sensor", Indian Welding Journal, 2012, Vol.45, Issue 1, 35-46.

46. G. K. Padhy, V. Ramasubbu, N. Murugesan, N. Parvathabarthini, C. Ramesh, S. K. Albert, "Determination of apparent diffusivity of hydrogen in 9Cr-1MoVNbN steel using a hot extraction technique", International Journal of Hydrogen Energy, 2013, Vol. 38, 10683-10693.

47. D. Rosenthal, "the theory of moving sources of heat and its application to metal treatments", Transition ASME, 1946, Vol. 68, 849-865.

48. V. Pavelic, R. Tanbakuchi, O. A. Uyehara, P. S. Myers, "Experimental and computed temperature histories in gas tungsten-arc welding of thin plates", Welding Journal Research Supplement, 1969, Vol. 48, 295-305.

49. D. T. S. Hook, A. E. F. Gick, "Penetration welding with lasers", welding Research Supplement, 1973, Vol. 60, 492-498.

50. J. Dowden, M. Davis, P. Kapadia, "Some aspects of the fluid dynamics of laser welding", Journal of Fluid Mechanics, 1983, Vol. 126, Issue 3, 123-146.

51. J. A. Goldak, A. Chakravarti, M. Bibby, "A new finite-element model for welding heat-sources", Metallurgy Material Transition B, 1984, Vol. 15, Issue 2, 299-305.

52. J. A. Goldak, M. Akhlaghi, "Computational Welding Mechanics" 2005, Springer Publications.

53. W. M. Steen, J. Dowden, M. Davis, P. Kapadia, "A point and line source model of laser keyhole welding" Journal of Physics D: Applied Physics, 1988, Vol. 21, Issue 8, 1255-1260.

54. M. R. Frewin, D. A. Scott, "Finite element model of pulsed laser welding", Welding Research Supplement, 1991, Vol. 78, 15-22.

55. R. Brockmann, K. Dickmann, P. Geshev, K. J. Mathes, “Calculation of temperature field in a thin sheet heated with laser beam”, International Journal of Heat and Mass Transfer, 2003, Vol. 46, 717-723.

56. G. Ravichandran, V. P. Raghupathy, N. Ganesan, “Analysis of Temperature Distribution During Circumferential Welding of Cylindrical and Spherical Components Using the Finite Element Method”, Computers and Structures, 1996, Vol. 59, 225-255.

57. D. H. Bae, C. H. Kim, S. Y. Cho, J. K. Hong, C. L. Tsai, “Numerical Analysis of Welding residual stress using heat source models for the multi-Pass weldment”, KSME International Journal, 2002, Vol. 16, Issue 9, 1054-1064.

58. R. N. S. Fassani, O. V. Trevisan,’ Analytical modeling of multipass welding process with distributed heat source’, Journal of the Brazilian Society of Mechanical Sciences and Engineering, 2003, Vol. 25, 302-305.

59. D. Deng, H. Murakawa, W. Liang, “Numerical simulation of welding distortion in large structures”, Computer Methods in Applied Mechanics and Engineering, 2007, Vol. 196, 4613-4627

60. G. Tsoukantas, G. Chryssolouris, “Theoretical and experimental analysis of the remote welding process on thin, lap-joined AISI 304 sheets”, Journal of Advanced Manufacturing Technology, 2008, Vol. 35, 880-894.

61. K. Kazemi, J. A. Goldak, ‘Numerical simulation of laser full penetration welding’, Computational Materials Science, 2009, Vol. 44, 841-849.

62. H. Zhang, G. Zhang, C. Cai, H. Gao, L. Wu, “Fundamental studies on in-process controlling angular distortion in asymmetrical double-sided double arc welding”, Journal of Materials Processing Technology, 2008, Vol. 205, 214-223.

63. I. Sattari-Far, Y. Javadi, “Influence of welding sequence on welding distortions in

pipes", International Journal of Pressure Vessels and Piping, 2008, Vol. 85, 265-74.

64. H. M. Asl, V. Ali, "Numerical analysis of the burn-through at in-service welding of 316 stainless steel pipeline", International Journal of Pressure Vessels and Piping, 2013, Vol. 105-106, 49-59

65. J. R. Chukan, M. Vasudevan, S. Muthukumaran, R. R. Kumar, N. Chanrasekhar, "Simulation of laser butt welding of AISI 316L stainless steel sheet using various heat sources and experimental validation" Journal of Material Processing Technology, 2015, Vol. 219, 48-59.

66. A. Capriccioli, P. Frosi, "Multipurpose ANSYS FE procedure for welding processes simulation", Fusion Engineering and Design, 2009, Vol. 84, 546-554.

67. P. Mollicone, D. Camilleri, T. Grey, "Procedural influences on non-linear distortion in welded thin plate fabrication", Thin-walled Structures, 2008, Vol. 46, 1021-1034

68. J. J. Del Coz Díaz, P. Menéndez Rodríguez, P. J. García Nieto, D. Castro-Fresno, "Comparative analysis of TIG welding distortions between austenitic and duplex stainless steels by FEM", Applied Thermal Engineering, 2010, Vol. 30, 2448-2459.

69. B. Q. Chen, M. Hashemzadeh, G. C. Soares, "Numerical and experimental studies on temperature and distortion patterns in butt-welded plates", International Journal of Advanced Manufacturing Technology, 2014, Vol. 72, 1121-1131.

70. A. kareem, S. Aloraier, S. Joshi, "Residual stresses in flux cored arc welding process in bead-on-plate specimens", Materials Science and Engineering A, 2012, Vol. 534, 13- 21.

71. M. Peric, Z. Tonkovic, A. Rodic, M. Surjak, I. Garašic, I. Boras, S . Švaic´, "Numerical analysis and experimental investigation of welding residual stresses and distortions in a T-joint fillet weld", Materials and Design, 2014, Vol. 53, 1052-63.

72. M. Hadi, I. Sattari-Far, "Different finite element techniques to predict welding residual

stresses in aluminum alloy plates", Journal of Mechanical Science and Technology, 2014, Vol. 28, Issue 2, 679-689.

73. X. Shan, C. M. Davies, T. Wangsdan, N. P. O'Dowd, K. M. Nikbin, "Thermo-mechanical modelling of a single-bead-on-plate weld using the finite element method', International Journal of Pressure Vessels and Piping, 2009, Vol. 86, 110-121

74. A. Kermanpur, M. Shamanian, E. V. Yeganeh, "Three-dimensional thermal simulation and experimental investigation of GTAW circumferentially butt-welded Incoloy 800 pipes", Journal of Materials Processing Technology, 2008, Vol. 199, 295-303.

75. A. Yaghi, T. H. Hyde, A. A. Becker, W. Sun, J. A. Williams, "Residual stress simulation in thin and thick-walled stainless steel pipe welds including pipe diameter effects", International Journal of Pressure Vessels and Piping, 2006, Vol. 83, 864-874.

76. H. K. Narang, M. M. Mahapatra, P. K. Jha, I. Mukherje, "Modelling and predicting the effects of SAW process parameters on weldment characteristics and shape profile", Proceedings of the Institution of Mechanical Engineers, B, J Engineering Manufacture, 2012, Vol. 226, Issue 7, 1230-1240.

77. N. Yadaiah, S. Bag, "Development of egg-configuration heat source model in numerical simulation of autogenous fusion welding process", International Journal of Thermal Science, 2014, Vol. 86, 125-138.

78. H. Purmohamad, A. Kermanpur, M. Shamanian, "Numerical simulation and experimental investigation of temperature distribution in the circumferentially butt GTAW of Incoloy 800H pipes", International Journal of Pressure Vessels and Piping, 2010, Vol. 7, 424-32.

79. X.Y. Shan, M. J. Tan, N. P. O'Dowd, "Developing a realistic FE analysis method for the welding of a NET single-bead-on-plate test specimen", Journal of Materials

Processing Technology, 2007, Vol. 192-193, 497-503.

80. C. Lee, K. Chang, "Temperature fields and residual stress distributions in dissimilar steel butt welds between carbon and stainless steels", Applied Thermal Engineering, 2012, Vol. 45-46, 33-41.

81. J. J. Xu, P. Gilles, Y. G. Duan, C. Yu, "Temperature and residual stress simulations of the NeT single-bead-on-plate specimen using SYSWELD", International Journal of Pressure Vessels and Piping, 2012, Vol. 99-100, 51-60.

82. C. Heinze, M. Schwenk, Rethmeier, "Numerical calculation of residual stress development of multi-pass gas metal arc welding under high restraint conditions", Materials and Design, 2012, Vol. 35, 201-209.

83. K. H. Chang, C. H. Lee, "Finite element analysis of the residual stresses in T-joint fillet welds made of similar and dissimilar steels", International Journal of Advanced Manufacturing Technology, 2009, Vol. 41, 250-258.

84. M. Adak, S. C. Guedes, "Effects of different restraints on the weld-induced residual deformations and stresses in a steel plate", International Journal of Advanced Manufacturing Technology, 2014, Vol. 71, 699-710.

85. D. Deng, H. Murakawa, "Numerical simulation of temperature field and residual stress in multi-pass welds in stainless steel pipe and comparison with experimental measurements", Computational Materials Science, 2006, Vol. 37, 269-277.

86. D. Deng, H. Murakawa, 'Finite element analysis of temperature field, microstructure and residual stress in multi-pass butt welded 2.25Cr–1Mo steel pipes', Computational Materials Science, 2008, Vol. 43, 681-695.

87. D. Deng, "FEM prediction of welding residual stress and distortion in carbon steel considering phase transformation effects", Materials and Design, 2009, Vol. 30, 359-366.

88. D. Deng, Y. Zhou, T. Bi, X. Liu, "Experimental and numerical investigation of welding distortion induced by CO_2 gas arc welding in thin bead-on-plate joints", Material and Design, 2013, Vol. 52, 720-729.

89. I. Sattari-Far, M. R. Farahani, "Effect of the weld groove shape and pass number on residual stresses in butt-welded pipes", International Journal of Pressure Vessels and Piping, 2009, Vol. 86, 723-31.

90. G. A. Moraitis, G. N. Labeas, "Residual stresses and distortion calculation of laser beam welding for aluminum lap joints", Journal of Materials Processing Technology, 2008, Vol. 198, 260-269.

91. Z. Barsoum, A. Lundbäck, "Simplified FE welding simulation of fillet welds-3D effects on the formation residual stresses", Engineering Failure Analysis, 2009, Vol. 16, 2281-2289.

92. Y. Javadi, M. Hasani, S. Sadeghi, "Investigation of clamping effect on the welding sub-surface residual stress and deformation by using the ultrasonic stress measurement and finite element method", Journal of Non-destructive Evaluation, 2015, Vol.34, 1-11.

93. X. Ficquet, D. J. Smith, C. E. Truman, E. J. Kingston, R. J. Dennis, "Measurement and prediction of residual stress in a bead-on-plate weld benchmark specimen", International Journal of Pressure Vessels and Piping, 2009, Vol. 86, 20-30.

94. G. Hilson, S. Simandjuntak, P. Flewitt, K. R. Hallam, M. J. Pavier D. J. Smith, "Spatial variation of residual stresses in a welded pipe for high temperature applications", International Journal of Pressure Vessels and Piping, 2009, Vol. 86, 748-756.

95. R. Keivani, M. Jahazi, T. Pham, K. R. Khodabandeh, M. R. Afshar, "Predicting residual stresses and distortion during multi sequence welding of large size structures using FEM", International Journal of Advanced Manufacturing Technology, 2014,

Vol. 73, 409-419.

96. S. Singh, N. Yadaiah, S. Bag, S. Pal, “Numerical simulation of welding-induced residual stress in fusion welding process using adaptive volumetric heat source”, Proceeding of the Institution of Mechanical Engineers Part C, Journal of Mechanical Engineering Science, 2014, Vol. 228, 2960-2972.

97. D. Afshari, M. Sedighi, M. R. Karimi, Z. Barsoum, “On Residual Stresses in Resistance Spot-Welded Aluminum Alloy 6061-T6”, Experimental and Numerical Analysis”, Journal of Materials Engineering and Performance, 2013, Vol. 22, Issue 12, 3612-3619.

98. S. A. A. Mousavi, R. Miresmaeili, “Experimental and numerical analyses of residual stress distributions in TIG welding process for 304L stainless steel’, Journal of Materials Processing Technology, 2008, Vol. 208, 383-394.

99. A. A. Bhatti, Z. Barsoum, M. Khurshid, “Development of a finite element simulation framework for the prediction of residual stresses in large welded structures”, Computers & Structures, 2013, Vol. 133, 1-11.

100. J. W. H. Price, A. Z. Paradowska, S. Joshi, T. Finlayson, C. Semetay, H. Nied, “Comparison of experimental and theoretical residual stresses in welds, the issue of gauge volume”, International Journal of Mechanical Science, 2008, Vol. 58, 513-521.

101. S. Joshi, C. Semetay, J. W. H. Price, H. F. Nied, “Weld-induced residual stresses in a prototype dragline cluster and comparison with design codes”, Thin-walled Structure, 2010, Vol. 48, 89-102.

102. G. A. Moraitis, G. N. Labeas, “Prediction of residual stresses and distortions due to laser beam welding of butt joints in pressure vessels”, International Journal of Pressure Vessel and Piping, 2009, Vol. 86, 133-142.

103. N. S. Shanmugam, G. Buvanashekaran, K. Sankaranarayanasamy, S. R. Kumar, "A transient finite element simulation of the temperature and bead profiles of T- joint laser welds", Material and Design, 2010, Vol. 3, 4528-4542.

104. Y. C. Kim, M. Hirohata, K. Inose, "Effects of phase transformation on distortion and residual stress generated by LASER Beam welding on high-strength steel", Welding in the World, 2012, Vol. 56, Issue 3-4, 64-70.

105. Y. C. Kim, M. Hirohata, K. Inose, "FEM Simulation of Distortion and Residual Stress Generated by High Energy Beam Welding with Considering Phase Transformation", Open Journal of Metal, 2014, Vol. 4, 31-39.

106. D. Deng, H. Murakawa, "Prediction of welding distortion and residual stress in a thin plate butt-welded joint", Computational Materials Science, 2007, Vol. 43, 353-365.

107. C. Wang, Y. Kim, J. Kim, "Comparison of FE Models to Predict the Welding Distortion in T-Joint Gas Metal Arc Welding Process", International Journal Of Precision Engineering and Manufacturing, 2014, Vol. 15, Issue 8, 1631-1637.

108. J. Wang, X. Yin, H. Murakawa, "Experimental and computational analysis of residual buckling distortion of bead-on-plate welded joint", Journal of Materials Processing Technology, 2013, Vol. 213, 1447-1458.

109. M. M. Mahapatra, G. L. Datta, B. Pradhan, "Three-dimensional finite element analysis to predict the effects of shielded metal arc welding process parameters on temperature distributions and weldment zones in butt and one-sided fillet welds", Institution of Mechanical Engineers, 2006, Vol. 220, 837-845.

110. S. K. Bate, R. Charles, A. Warren, "Finite element analysis of a single bead-on-plate specimen using SYSWELD", International Journal of Pressure Vessels and Piping, 2009, Vol. 86, 73-78.

111. P. Biswas, M. M. Mahapatra, N. R. Mandal, "Numerical and experimental study on

prediction of thermal history and residual deformation of double-sided fillet welding", Proc. of the Institution of Mechanical Engineers Part B, 2010, Journal of Engineering Manufacture, Vol. 224, pp. 125-134.

112. M. Seyyedian, M. Haghpanahi, M. sedighil, "Investigation of the effect of clamping on residual stresses and distortions in butt welded plates", Transaction B Mechanical Engineering, 2010, Vol. 17, Issue 5, 387-394.

113. M. Seyyedian, "effect of geometrical parameters on distortion in butt welded plates", Journal of strain analysis for engineering design, 2013, Vol. 48, Issue 4, 258-268.

114. M. V. Deo, P. Michaleries, J. Sun, "Prediction of buckling distortion of welded structures", Science and Technology of Welding and Joining, 2003, Vol. 8, Issue 1, 55-61.

115. T. Srikas, P. Papanikos, T. Kermanidis, "Numerical simulation of laser welding process in butt joints joint specimens", Journal of Materials Processing and Technology, 2003, Vol. 134, Issue 1, 59-69.

116. H. P. M. Yupiter R. N. Lidam, M. R. Rahim, Y. Zakaria, M. R. Redza, M. S. Sulaiman, G. Tham, S. K. Abas, "Welding distortion analysis of multipass joint combination with different sequences using 3D FEM and experiment", International Journal of Pressure Vessels and Piping, 2013, Vol. 111-112, 89-98.

117. D. Deng, H. Murakawat, "The Prediction of welding residual stress in multi-pass butt-welded modified 9Cr–1Mo steel pipe considering phase transformation effects", Computational Material Science, 2006, Vol. 37, Issue 3, 209-219.

118. A. Yaghi, T. Hyde, A. Becker, J. William, W. Sun, "Residual stress simulation of welded section of P91 pipes", Journal of Material Processing Technology, 2009, Vol. 209, Issue 8, 3905-3913.

119. A. Yaghi, T. Hyde, A. Becker, J. William, W. Sun, "Measuring and Modeling residual stresses in a butt welded P91 steel pipe", Proceedings of Sustainable Power Generation and Supply, Beijing, April 6-7, 2009.

120. A. Yaghi, T. Hyde, A. Becker, J. William, W. Sun, "Finite element simulation of welding and residual stresses in a P91 steel pipe incorporating solid state phase transformation and post weld heat treatment", Journal of Strain Analysis for Engineering Design, 2008, Vol. 43, Issue 5, 275-293.

121. S. Kim, J. Kim, W. Lee, "Numerical Prediction and neutron diffraction measurement of residual stress for modified 9Cr-1Mo steel", Journal of material Processing Technology, 2005, Vol. 167, Issue 2, 480-487.

122. S. Kumar, R. Awasthi, C. S. Vishwanadham, K. Bhuanumurthy, G. K. Dey, "Thermo-metallurgical and thermo-mechanical computations for laser welded joint in 9Cr–1Mo (V, Nb) ferritic/martensitic steel" Material and Design, 2014, Vol. 59, 211-220.

123. C. Heinze, A. Pitter, M. Rethmeier, S. Babu, "Dependency of martensite start temperature on prior austenite grain size and its influence on welding induced residual stresses", Computational Material Science, 2013, Vol. 69, Issue 1, 251-260.

124. H. Serizawa, S. Nakamura, M. Tanaka, Y. Kawahito, H. Tanigawa, S. Katayama, "Effect of mechanical restraint on weldability of reduced activation ferritic/martensitic steel thick plates", Journal of Nuclear Material, 2011, Vol. 417, 55-58.

125. Z. HU, J. Zhao, "Effects of martensitic transformation on residual stress of P91welded joint", Material research express, 2018, Vol. 5, No. 9, 96528-96529.

126. K. Abburi Venkataa, S. Kumar, H. C. Dey, D. J. Smith, P. J. Bouchard,C. E. Truman,"Study on the Effect of Post Weld Heat Treatment Parameters on the Relaxation of Welding Residual Stresses in Electron Beam Welded P91 Steel Plates", Procedia Engineering,2014, Vol. 86, 223 – 233

CHAPTER-3

RESEARCH METHODOLOGY

3.1. Plan of Research Work

The entire research is for development of a finite element model that can be used to carry out thermo-mechanical analysis of multi-pass GTA welding of modified 9Cr-1Mo steel with filler addition so that this model can be used to predict residual stress and distortion in the weld joint with a reasonable accuracy. This model considered the phase transformation that take place during weld thermal cycle and able to handle pre heating and post heating given to the weld joint. Experimental validation of the model is an important component of this research work. This work is carried out progressively, initially, model is developed for autogenous welds without filler addition and without preheating and post heating; the model is modified progressively so that it can predict residual stress and distortion is multi-pass welds carried out with preheating and post heating. Broadly three stages of development can be identified

Stage I: Numerical and experimental investigation of autogenous and multi-pass GTA welding of 3 mm thick plate with square joint and 6 mm thick plate with V groove joint of modified 9Cr-1Mo steel.

Stage II: Numerical and experimental study of effect of pre heating on autgenous and multi-pass welding of modified 9Cr-1Mo steel of thickness 3 mm and 6 mm respectively.

Stage III: Numerical and experimental study of effect of combined preheating and post heating on autogenous and multi-pass welding of modified 9Cr-1Mo steel of thickness 3 mm and 6 mm respectively.

The key aspects and steps involved in various stages are illustrated as block diagram in Fig. 3.1. In each stage, both thermal and mechanical analyses have been carried out sequentially to evaluate thermal histories, residual stress and distortion. Double ellipsoidal heat source distribution model is used for GTA welding analysis.

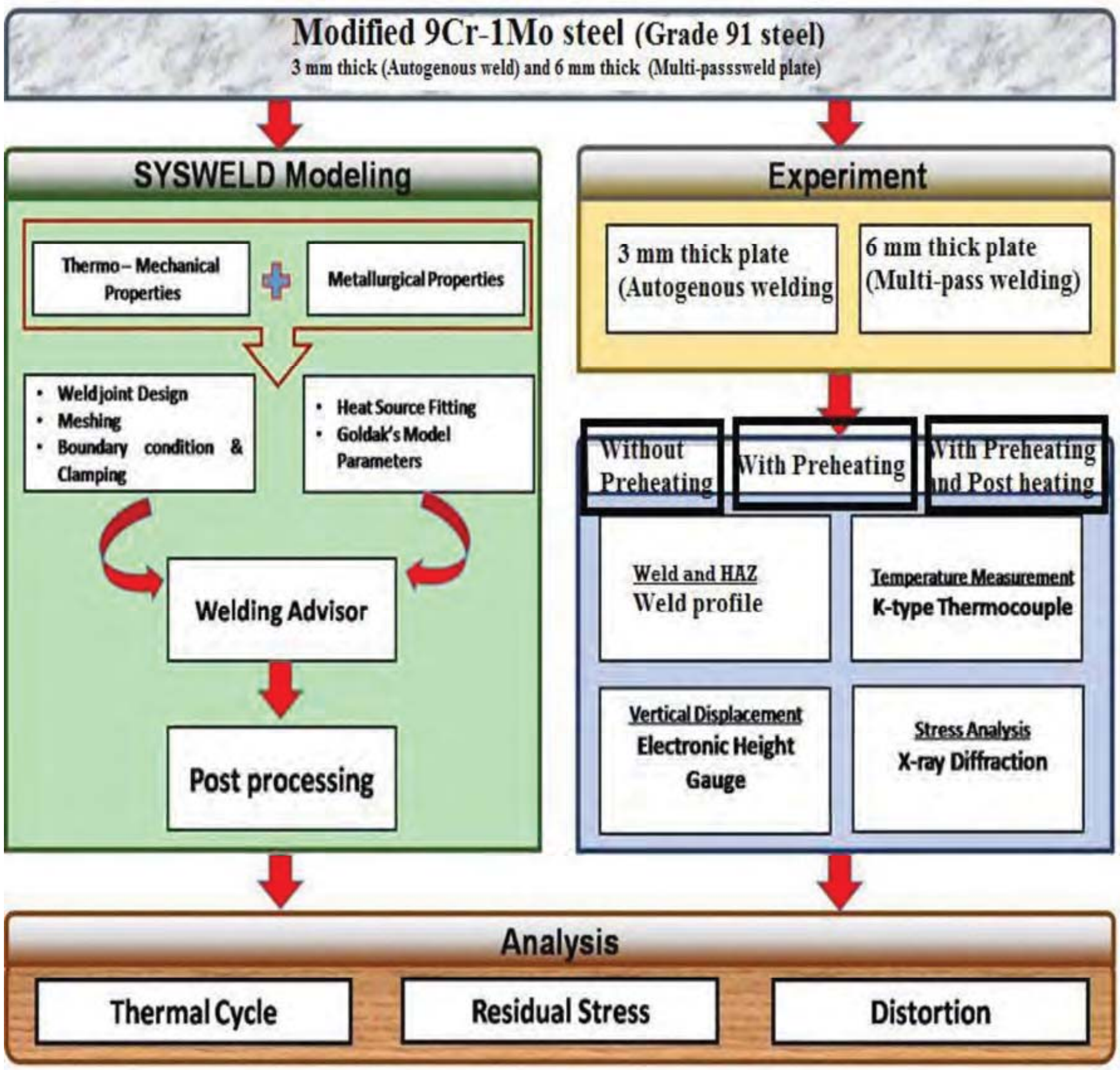

Fig.3.1. Research and numerical Methodology

For pre heating disk shaped combined with double ellipsoidal heat source have been employed to simulate the welding with pre heated plate. Temperature-dependent physical and mechanical properties are used during the simulation study. In order to achieve real-time results, the convection and radiation heat transfer coefficients have been incorporated in the model. Thermo-mechanical analysis of autogenous and multi-pass GTA welding of modified 9Cr-1Mo steel was carried out in two basic steps. First a transient heat transfer analysis taking into account temperature dependent thermo-physical material for different phases was carried out and in second step the generated temperature distribution was used as an input to the mechanical analysis.

3.2. Methodology for numerical simulations

In this work, for thermo-mechanical analysis of GTA welding process, FE modelling program SYSWELD is used on a Dual Intel Xeon E5-2687W @ 3.1 GHz (8 Core, 64 GB RAM, 992GFLOPS) processor PC with a Windows 7 Operating System. The methodology of welding simulation during this research is described as follows.

SYSWELD software involve three phases in welding simulation, these are modeling, analysis using welding advisor and post-processing as shown in Fig. 3.2. Material, geometry and heat source fitting belong to the first phase in weld simulation step [1].

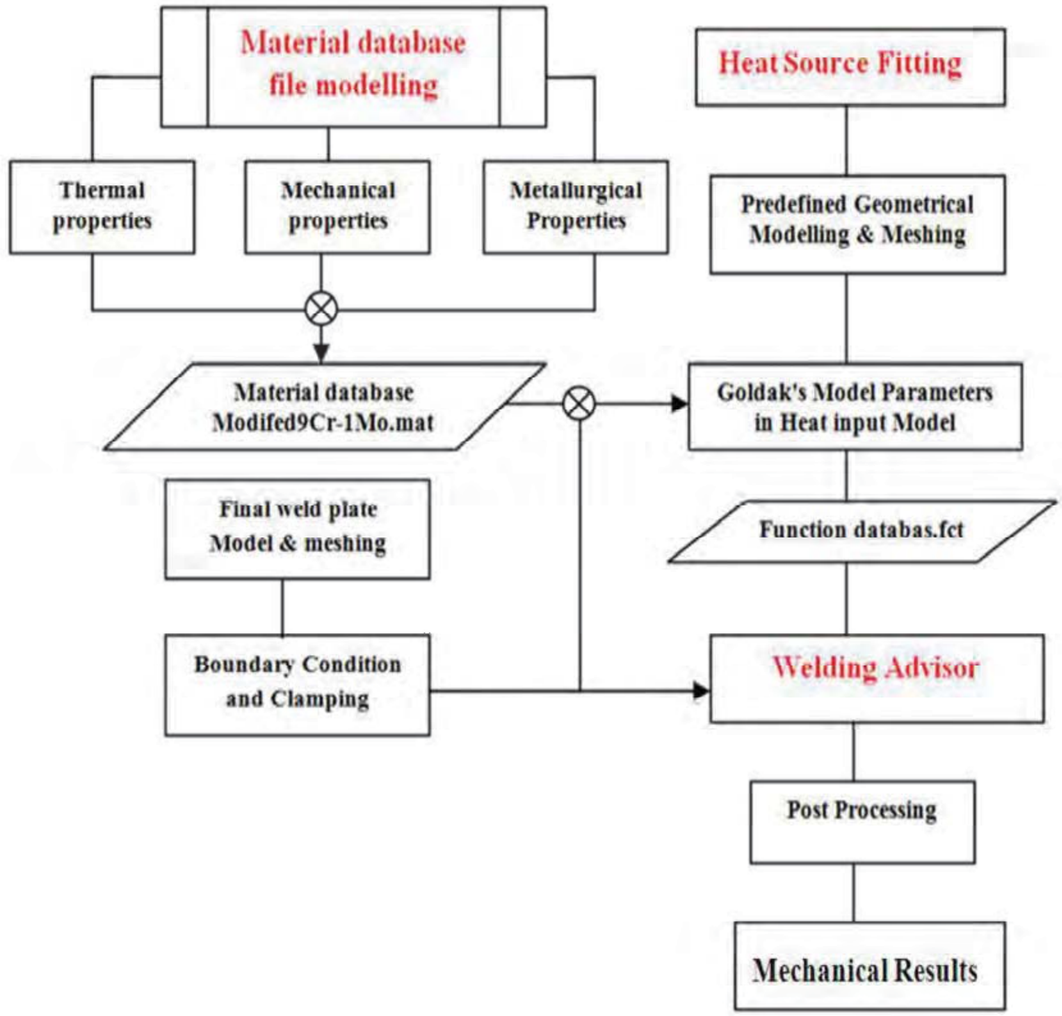

Fig.3.2. Steps in Thermo-mechanical analysis of welding in SYSWELD

Heat source fitting and thermal transient analysis are conducted to obtain heat source distribution and temperature history with heating and cooling rate. Heat source fitting is conducted by bead-on-plate welding to obtain GTA welding heat source distribution and temperature history.

Heat source fitting involve the following procedure.

1) Preparation of bead-on-plate welds of different heat inputs.
2) Measurement of bead parameters like width of the bead and depth of penetration for each of the bead-on-plate weld.

3) Head source fitting (HSF) in which heat source parameters chosen for simulation are adjusted in such a way that molten pool size simulated by the simulated heat source matches with the bead parameters for different heat inputs.
4) Use of fitted heat source for thermo-mechanical simulation of weld.

Meshed model, material properties with boundary condition along with heat source fitting file (.fct file) are the inputs for thermo-metallurgical analysis. Temperature histories and its corresponding phase fractions at each node were employed as the thermal load for subsequent mechanical analysis. Finally, visual viewer is used to display the result obtained from the analysis as shown in Fig. 3.2.

Because of the complex nature of weld pool formation, it is extremely difficult to include each and every phenomenon occurring within the molten zone in the modeling. Some of the phenomena like vaporization, ions formation, molten metal circulation etc. are ignored in this study.

The SYSWELD is a FEM based computational tool for simulation of heat treatment, welding and corresponding welding assembly processes. It has the capability to consider various aspects such as phase transformations, latent heat effects during phase transformation, changes in microstructure, diffusion and precipitation of chemical elements, hardening behavior (i.e. isotropic, kinematic and mixed), visco-plasticity and phase dependent strain hardening etc. Temperature dependent material properties, phase proportions and proportion of chemical composition can be considered. It is also possible to develop a user defined heat source by a volume density of energy which moves along the weld trajectory with a FORTRAN program using graphic user interface. In this work, the numerical simulation procedure was performed by a sequentially coupled thermo-metallurgical-mechanical analysis. The term 'sequentially coupled' implies that initially, temperature histories and phase fractions were computed at each node which is coupled with thermo-metallurgical analysis [2-11].

3.3. Welding heat transfer

The mode of heat transfer in the welded component is mainly through conduction. In order to predict the thermo-mechanical behavior of autogenous and multi-pass weld, the multi-physics aspects were suppressed and the problem was simplified as conduction heat transfer problem. Welding analysis was limited up to thermo-metallurgical-mechanical problem by neglecting fluid flow effect in weld pool, plasma physics, electromagnetism etc. Hence the equilibrium equations left to solve are the heat balance and force equilibrium for the thermal and mechanical analysis.

In heat transfer analysis, the transient is conducted by solving the governing partial differential equation for the transient heat conduction. The governing partial differential equation for the transient heat conduction (temperature field in time) *(t)* and space *(x, y, z)* is by Eq. 3.1.

$$\left[\frac{\partial}{\partial x}(K\frac{\partial T}{\partial x})+\frac{\partial}{\partial y}(K\frac{\partial T}{\partial y})+\frac{\partial}{\partial z}(K\frac{\partial T}{\partial z})\right]+\overset{o}{q}=\rho C\frac{dT}{dt} \tag{3.1}$$

Where x, y, z are the Cartesian coordinates, q^o is the internal heat generation. In addition, ρ refers to the density, K to the thermal conductivity and C_p to the specific heat, which is function of temperature T. Both base and weld metal are isotropic hence thermal conductivity value is same in all directions.

Matrix form of above equation can be written as Eq. 3.2-3.3

$$\rho C\frac{\partial T}{\partial t}=(L)^T\left[|D|\{L\}T\right]+Q \tag{3.2}$$

Where,

$$L = \begin{bmatrix} \frac{\partial}{\partial x} \\ \frac{\partial}{\partial y} \\ \frac{\partial}{\partial z} \end{bmatrix} \text{ and } D = \begin{pmatrix} K & 0 & 0 \\ 0 & K & 0 \\ 0 & 0 & K \end{pmatrix} \tag{3.3}$$

3.4. Welding Arc Efficiency

It is safe to assume that all electric energy of the arc converts into heat energy. But not all the energy is used for the heating of the filler and base metal. A part of this energy goes to heat dissipation (losses through electrode tip heating, radiation to the surroundings, metal spatter etc). So, the effective energy of the welding arc can be expressed in Eq. 3.4.

$$Q = VI\eta \tag{3.4}$$

Where Q is net heat input in Watt, V is voltage, I is current and η is weld efficiency, In general the arc efficiency is very much dependent on the welding processes used, the penetration achieved, the shielding gas and many other factors which make it difficult to be predicted. Groove geometry also affects efficiency. The efficiency value in the range of 0.68-0.75 is considered for the GTA welding process in the present study.

3.5. Heat source distribution model

Residual stresses in welds can vary widely depending on the transient temperature distributions that occur during welding which in turn are related to total heat applied and the type of heat source. Thus, for determination of realistic temperature profile in the target application, a careful and accurate modeling of heat source is required.

Goldak's Double ellipsoidal model is used for thermo-mechanical analysis [12]. This model gives the Gaussian distribution and has excellent features for power and density distribution control in the weld pool and HAZ of base metal as shown in Fig. 3.3. The heat input of the welding forms the basis for governing factors concerned with thermal cycle [7-12].

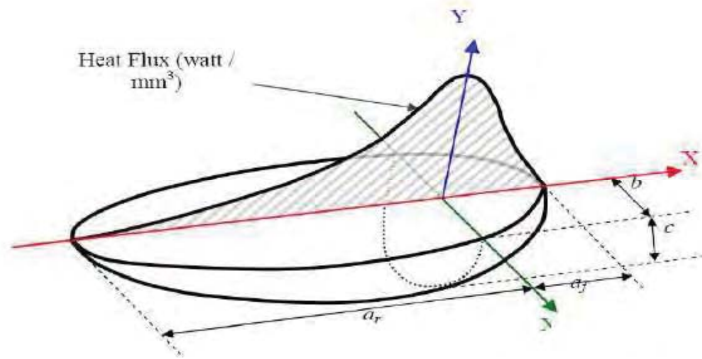

Fig.3.3. Double ellipsoidal heat source distribution model

In this model, the heat distribution is modelled as a double ellipsoidal configuration combines two different ellipses, one in the front quadrant of the heat source and the other in the rear quadrant. It is observed that this 3D power density heat source could overcome the shortcomings of all previous models to predict the temperature for the welded joints with deeper penetration. Calculation experience with the double ellipsoidal heat source distribution revealed that temperature gradient in front of the heat source distribution was not steep as expected. At the trailing edge because of moving heat source trailing edge molten pool is steeper than experimental measurement.

Power densities of double-ellipsoidal heat source model are q_f (x, y, z) and q_r (x, y, z), which describe front and rear quadrant heat flux distributions of the heat source. Heat density q(x, y, z, t) within the front and rear half ellipsoid is Eq. 3.5-3.6.

$$q_f(x,y,z,t) = \frac{6\sqrt{3} f_f Q}{a_f bc\pi\sqrt{\pi}} e^{-3x^2/a_f^2} e^{-3y^2/b^2} e^{-3\left[z+v(\tau-t)\right]^2/c^2} \tag{3.5}$$

$$q_r(x,y,z,t) = \frac{6\sqrt{3} f_r Q}{a_r bc\pi\sqrt{\pi}} e^{-3x^2/a_r^2} e^{-3y^2/b^2} e^{-3\left[z+v(\tau-t)\right]^2/c^2} \tag{3.6}$$

Where a_f, a_r, b, c are the ellipsoidal heat source parameters, a_f is front length of molten pool, a_r is rear length of molten pool, c is depth of penetration in all cases and b is half width. v is the velocity of the heat source, t is the time and τ is a lag factor needed to define the position of the source at time $t = 0$. Q is net heat input, f_f and f_r proportional coefficient at front and rear ellipsoid such that $f_f + f_r = 2$, $6\sqrt{3}$ is heat flux distribution parameter which characterize the concentration level of heat flux distribution.

A double ellipsoidal heat source axes and parameters implemented in SYSWELD are shown in Fig. 3.4.

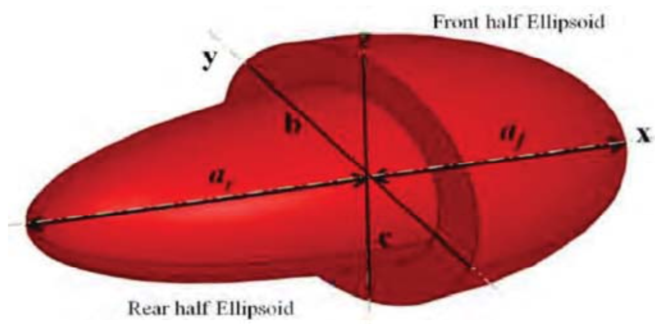

Fig.3.4. Axes and parameters as implemented in SYSWELD.

3.6. Pre heating heat source model

Pavelic et al. (1969) proposed disc shaped heat source model with Gaussian distribution. The Gaussian heat source model is in bell shape as shown in Fig. 3.5. The heat input within the space at a distance 'r' from the centre of the arc is given by Eq. 3.7 [14].

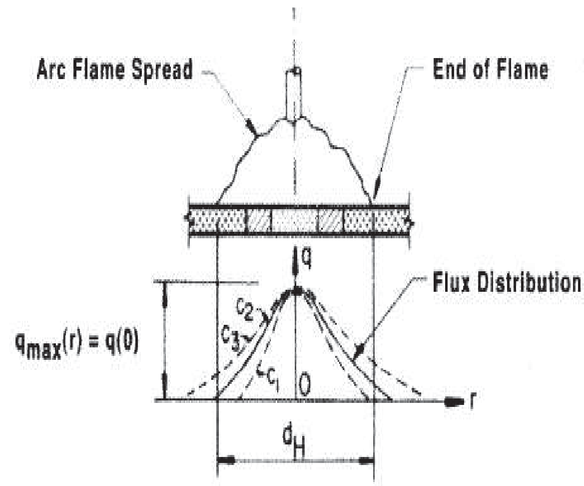

Fig.3.5. Circular heat source distribution

$$q(r) = q(0)e^{-Cr^2} \tag{3.7}$$

Where

q (r) = surface flux at radius *r (w/m²)*

q (0) = Maximum flux at the centre of the heat source *(w/m²)*

C = Distribution width coefficient *(m⁻²)*

r = Radial distant from the centre of heat source *(m)*

Friedman, Krutz and Segerland [15-16] suggested a coordinate system that moves with source for Pavelic disc model with following equation

$$q(x,\xi) = \frac{3Q}{\pi c_r^{\,2}} e^{-3x^2/x^2} e^{-3\xi^2/z^2} \tag{3.8}$$

Q = Energy input rate

C_r = Characteristic radius of heat flux distributions

With *(x,y,z)* system a lag factor τ is needed for defining the positions of source as shown in Fig. 3.6.

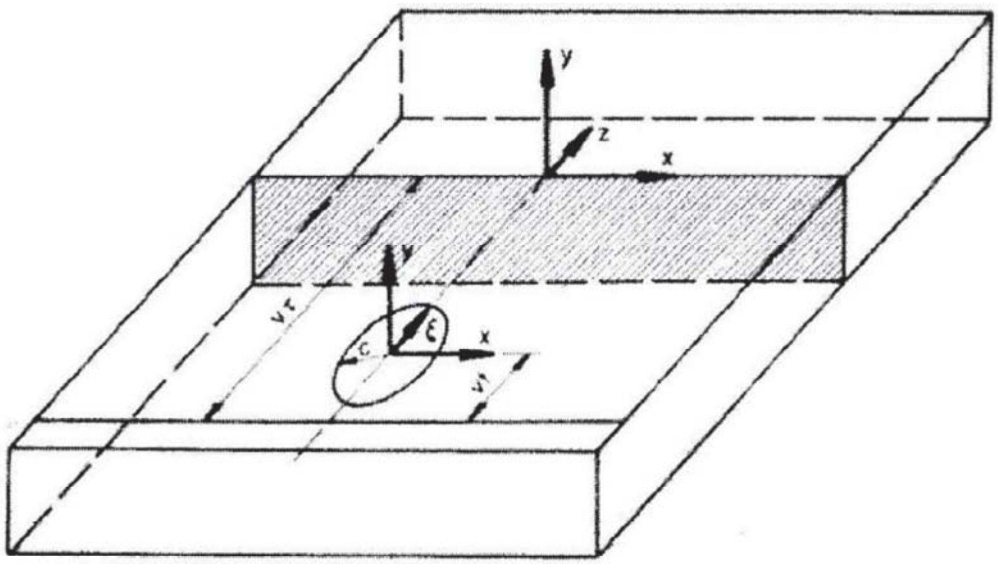

Fig.3.6. Co-ordinate system form used for FEM analysis of Disc model

In this study for modeling the preheating effect, moving co-ordinate disk shaped model as shown in Fig. 3.6 is used. For the purpose of pre heating analysis 7 mm and 14 mm radius are considered for moving co-ordinate disk shaped model for 3 mm and 6 mm thick plates respectively. Disk shaped model combined with doubled ellipsoidal model is used for analysis of welds made with preheating for autogenous and multi-pass welding of modified 9Cr-1Mo steel.

3.7. Metallurgical Transformation

For metallurgical computation, three different phases are considered. First phase of material is ferrite which during heating transforms to austenite and during cooling, the austenite transforms to martensite. Reactions for phase transformation were defined between corresponding transformation temperatures.

Ferrite to austenite transformation occurs between (Ac_1 = 820°C and Ac_3 = 900°C) and this transformation was computed according to Leblond's equation [17].

$$\frac{dP(T)}{dt} = F(\overset{0}{T})\frac{P_{eq}(T) - P(T)}{\tau(T)} \tag{3.9}$$

Where *P (T)* is proportion of phase, *t* is time, *T* is temperature, P_{eq} *(T)* is equilibrium phase fraction and τ is delay time. It should be mentioned that τ is the function of temperature while *F* is the function of heating rate.

Koistinen-Marburger (K-M) equation was used to describe the Austenite-Martensite transformation Martensitic transformation was defined for austenite cooling below Ms Temperature (375°C) and Martensite phase fraction was computed according to Koistinen-Marburger equation [18].

$$P(T) = \left[1 - \exp(-b(M_s - T))\right] \tag{3.10}$$

Where *P (T)* is proportion obtained at an infinitely low temperature (fraction of Martensite at a temperature). Martensite starts temperature (*Ms)* was taken as 375°C, (M_f) Martensite finishing Temperature is 200°C for modified 9Cr-1Mo steel. *b* = 0.011 is a constant which represents the evolution of Martensitic transformation process.

3.8. Boundary conditions

In a welding process, the cooling of the part due to radiation and convection plays a significant role hence for the evaluation of realistic temperature history heat loss to the surroundings has been taken into account by considering radiation and convection losses. During thermal cycle, radiation heat losses dominate in and around the weld pool while the convection losses dominate away from the weld pool. Combined radiation and convection loss from the material to surrounding is given by Eq. 3.11-3.12.

$$q_n = h(T - T_\alpha) + \varepsilon\sigma(T^4 - T_\alpha^4) \tag{3.11}$$

$$q_n = \left[h + \varepsilon\sigma(T^2 + T_\alpha^2)(T + T_\alpha)\right](T - T_\alpha) = h_{eff}(T - T_\alpha) \tag{3.12}$$

Where, the first term is convective heat loss and h=25 $Wm^{-2}K$ the convective heat transfer coefficient. The second term is the heat loss due to radiation where, σ= $5.67\times10^{-8}Wm^{-2}K^{-4}$ Stefan's constant, ε = 0.8 as emissivity of plate [19].

Following assumption are made in the formulation of model during finite element analysis of modified 9Cr-1Mo steel weld.

1- Initial temperature of plate and atmospheric temperature is considered as 26°C. In case of welding with combined pre heating and post heating initial and atmospheric temperature is considered as 200°C.
2- Material properties are homogenous and isotropic and temperature dependent.
3- Welding heat source is moving at a certain predefined speed in the welding direction on weld trajectory only.
4- The convection stirring in the molten pool was balanced in the present analysis by artificially increasing the thermal conductivity of the material after the melting point.

The temperature distributions obtained by solving heat conduction equation from thermal analysis will be further used as input for mechanical analysis in order to obtain stress-strain fields. The mechanical analysis is based on the solution of force equilibrium equations. The elastic strain component is modeled using isotropic Hook's law with temperature dependent Young's modulus and Poisson's ratio. The plastic behavior is employed with Von-Misses criterion, temperature dependant mechanical properties and isotropic hardening model. To calculate the thermo-metallurgical strain, strains that arise due to temperature dependent thermal expansion coefficient and phase change are included. During fusion welding, high temperature thermal cycle period is very short period so creep behavior of material is neglected, finally the total strain will be Eq.3.13.

$$\varepsilon^{Total} = \varepsilon^{elastic} + \varepsilon^{plastic} + \varepsilon^{thermal} + \varepsilon^{Volume} \tag{3.13}$$

3.9. Meshing of bead-on-plate

The accuracy of FEA depends upon the mesh density used. Fig. 3.7 shows the 3 mm thick bead-on-plate meshed model of size 100 × 60 mm used for analysis. During welding, temperature in weld centre line and Fusion Zone (FZ) goes beyond the material melting point, away from weld centre line this peak temperature decreases sharply. Therefore, weld centre line and surrounding zone (HAZ) should be meshed carefully for predicting correct temperature [5-12]. Mesh density affects the thermal analysis and fine meshing predicts more accurate results as compared to coarse meshing. Therefore, in order to predict correct temperature in fusion zone and HAZ, fine meshing is done in those regions and similarly in order to reduce the simulation time coarse meshing is done for the regions away from weld centre line. Total number of nodes and elements used in model are 18602 and 18511 respectively.

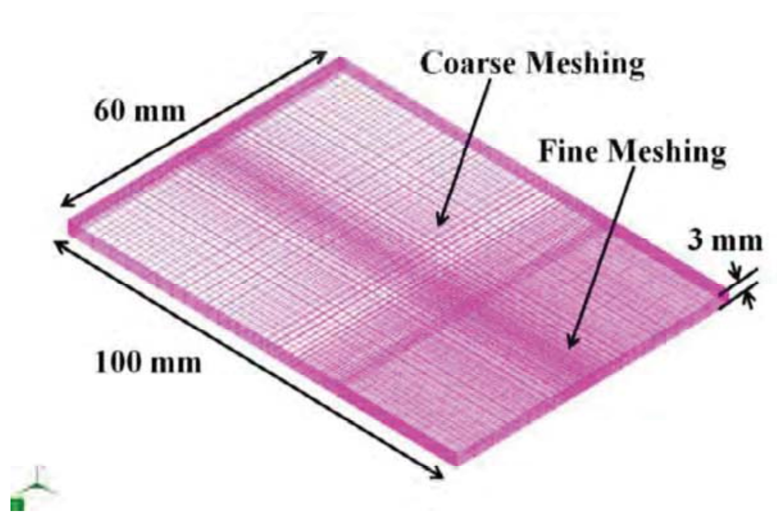

Fig.3.7. Bead-on-plate meshed model

3.10. Meshing of 3 mm thick square joint plate

For square butt joint weld plate, solid modeling technique is used in visual weld mesh tool. In this tool fine meshing can be done as per requirement of complexity of weld plate.

Sensitivity of the model was analyzed using variable mesh size by trial and error approach. Square butt joint, high temperature and flux gradients are anticipated in and around the FZ and HAZ and therefore a relatively fine meshing is used within a distance of 15-30 mm from weld line in 3 mm thick plates of dimension 240 mm × 300 mm × 3 mm as shown in Fig. 3.8. The element size of 0.5 mm was kept constant within 30 mm on each side of weld line in transverse direction (to cover the HAZ on either side). Total number of nodes and elements used in 3 mm thick 3D meshed model are 100307 and 119836. The model was created such that the welding path was parallel to the X axis and it was placed on the XY plane.

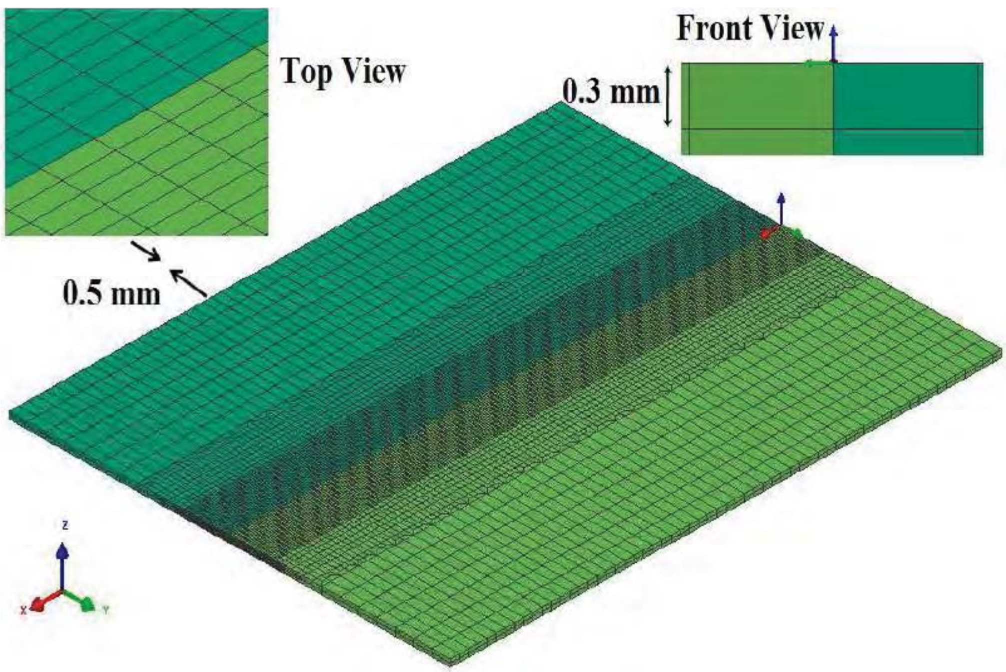

Fig.3.8. 3D meshed model for 3 mm thick plate

3.11. Meshing of 6 mm thick multi-pass weld plate

Multi-pass welding is more challenging than single pass welding because of repeated thermal cycles and deposition of filler material affecting the residual stress and distortion. For studying the effect of meshing on distortion analysis of multi-pass welding, two types of 3D models with coarse and fine mesh were used. Study also includes thermo-mechanical analysis using 2D model for multi-pass welding as shown in Fig. 3.9.

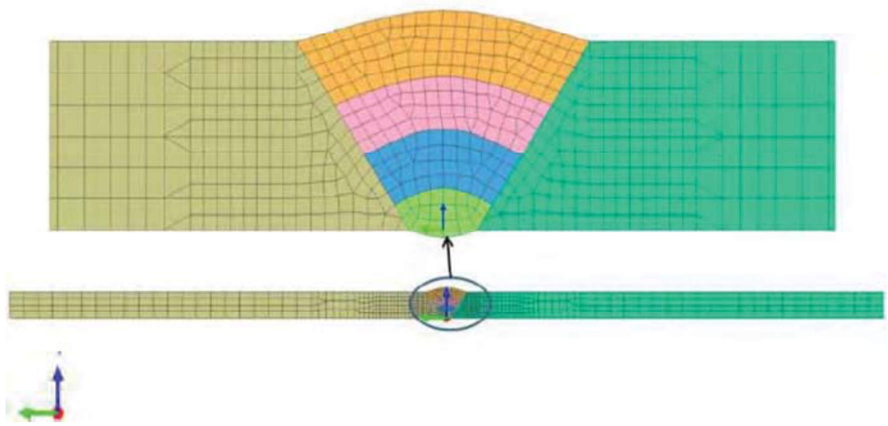

Fig.3.9. 2D meshed model for 6 mm thick multi-pass welding plate

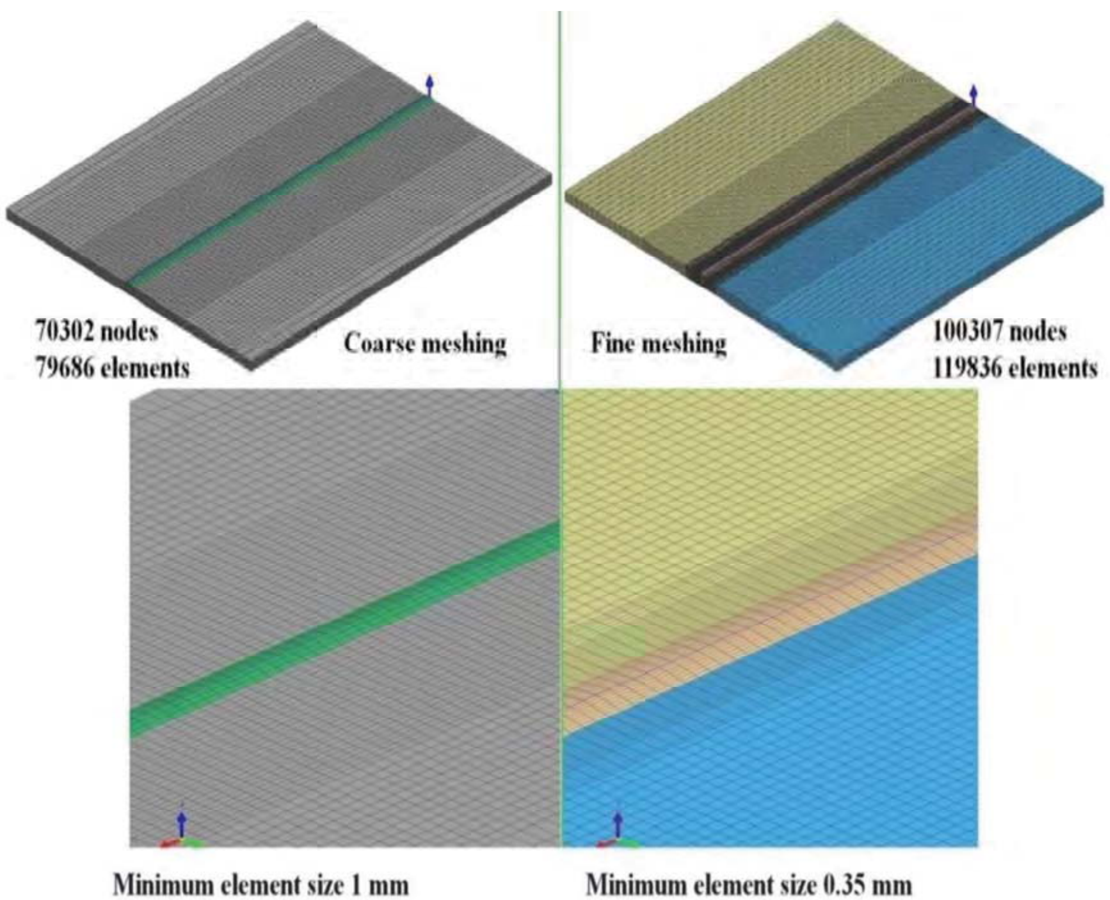

Fig.3.10. Different meshed model of 6 mm thick multi-pass welding plate

2D and 3D models were meshed using Visual mesh (Design and meshing tool) as shown in Fig. 3.10 and saved as an ASC format [1]. In FE analysis of multi-pass welding process, the role of filler material deposition is very important. The FE model of weld joint consists of base metal and filler material in a single mesh.

Filler material activation is achieved by Chewing Gum method by assuming dummy phase material. The chewing gum method is independent of the mesh type, whereas in case of activation method the element activation is limited to solid only, not available for shells elements. Another advantage of the chewing gum method is if the heat source intensity is insufficient, the chewing gum material remains as chewing gum, which is easy to check. For the element activation method, combined with heat sources that do not have enough heat intensity, the solver can struggle to deal with elements that are activated with a significant stiffness. This might lead to numerical oscillations and cause more computation time. During first pass analysis remaining three passes are considered as a dummy so that they do not contribute during first pass analysis. Similarly, for second and third passes the above methodology was followed [8-10]. Dummy material has been assigned low stiffness (1 N/mm^2 for solid elements and 5 N/mm^2 for shell elements) and yield stress equal to that of parent material.

3D elements are used for meshing the weld bead and base plate. In order to reduce computational time, different mesh size elements from weld line to end of weld plate are used. High temperature and flux gradients are anticipated in and around the FZ and HAZ therefore a relatively fine meshing is used within a distance of 30 mm from weld line as shown in Fig. 3.10.1 and 3 mm element size is used within 30 mm on each side of weld line (to cover the HAZ of weld) in transverse direction for fine and coarse meshed model. Away from this, the element size increases with an increase in the distance from weld line as shown in Fig. 3.10. In weld direction, minimum element size is kept constant 0.35 mm in fine meshed model and 1 mm in coarse mesh model. Total number of nodes used in 3D coarse meshed model is 70302 and total number of elements is 79686. Similarly, in case of 3D fine meshed model total number of nodes and elements are 100307 and 119836 respectively.

Three types of elements are used such as 1D linear elements, 2D and 3D quadrilateral elements. 1D linear element used for the weld trajectory and reference lines. Weld heat source moves on weld trajectory on a predefined path. The reference line is parallel to the weld trajectory line and having equal number of elements as shown in Fig. 3.11. The trajectory was chosen to be along the center line of the whole substrate plate, with mesh size control of the weld line to ensure that the nodes coalesced with those on the skin and volume elements.

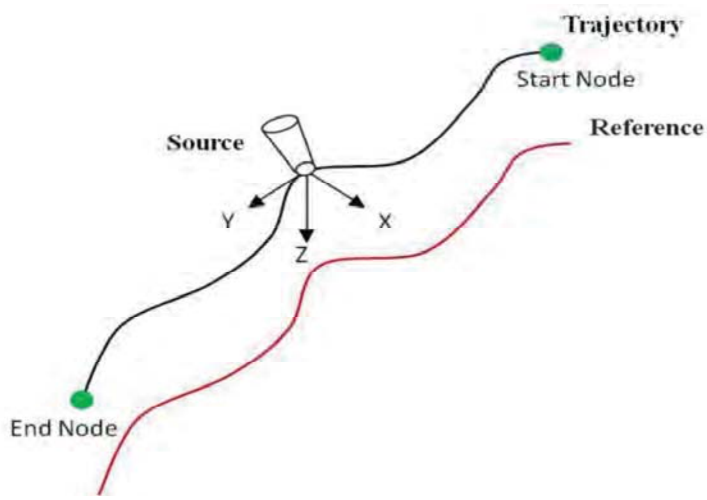

Fig.3.11. Weld trajectory and reference line

3.12. Clamping condition

If a metallic component is heated uniformly and if it has complete freedom toexpand in all directions, it will return to its original form after cooling uniformly. During welding process, heating is not uniform. The heat is concentrated at the joint location, with the arc temperature being very much higher than the base metal temperature. Due to this uneven expansion and contraction between the weld metal and base metal, stresses generate at the welded joint. These stresses are greatly influenced by different factors such as external constraint, material thickness, type of weld process etc. As the extent of external constraint increases, magnitude of internal stresses will increase. If no external constraint is applied during welding, the stresses will cause the component to distort very freely. It can be concluded that the constraint is a measure of structure's ability to develop residual stresses and diminish distortions [20--28]. There are two types of clamping condition introduced in modelling, elastic and rigid. Elastic constraints for elements are the simplest way to simulate real clamping conditions. In this study, to match the experimental boundary condition, minimum clamping was applied as the artificial boundary condition in order to prevent rigid body motion in the numerical simulation**.** The rigid body motion is prevented by fixing the body by constraining three corners and one corner is left free to allow the free expansion of the material. One of the corners is arrested in all the three directions as shown in Fig. 3.12. Another corner is arrested in 'y' and 'z' directions whereas the remaining one is arrested in 'y' direction alone. Elastic clamping applied for elements and nodes with a stiffness of 1000 N/mm^2.

During thermal cycle, radiation heat losses dominate in and around the weld pool while the convection losses dominate away from the weld pool. In order to generate the convection and radiation boundary conditions, skin elements (2D) were constructed on all the exposed domains of the model as shown in Fig. 3.12. As before, the mesh density of the surface mesh was specified such that the skin element nodes were coincident with the volume element nodes lying underneath them. Radiation loss is considered using skin effect with a emission coefficient is 0.8 and 25 w/mm^2 convective heat loss is considered [19].

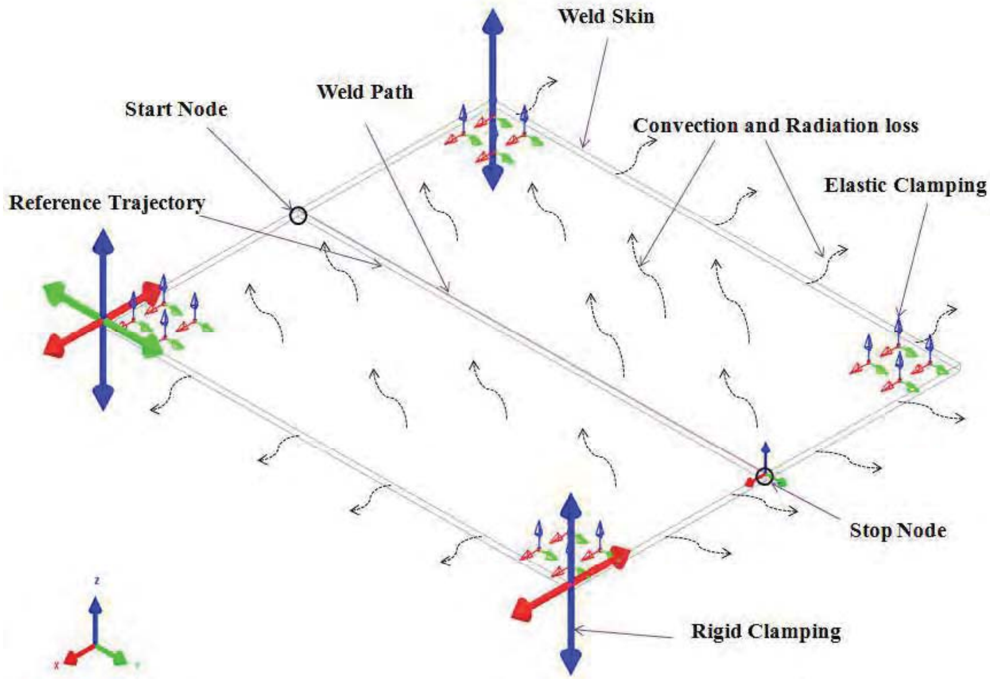

Fig.3.12. Boundary condition in welding analysis

References

1. SYSWELD Tool box (2010).
2. S. Y. P. Manurung, R. N. Lidam, M. R. Rahim, M. Y. Zakaria, M. R. Redza, M. S. Sulaiman, G. Tham, S. K. Abas, "Welding distortion analysis of multipass joint combination with different sequences using 3D FEM and experiment", International Journal of Pressure Vessel and Piping, 2013, Vol. 111-112, 89-98.
3. C. Heinze, C. Schwenk, M. Rethmeier, "Numerical calculation of residual stress development of multi-pass gas metal arc welding", Journal of Constructional steel research, 2012, Vol. 72, 12-19.
4. H. P. M. Yupitar, M. S. Sahar, K. A. Sunhaiji, T. Ghalib, H, Esa, " Investigation on welding distortion of combined butt and T-joints with 9-mm thickness using FEM and experiment", International Journal of Advance Manufacturing and Technology, 2014, Vol. 75, 775–82.
5. K. C. Ganesh, K. R. Balasubramanian, M. Vasudevan, P. Vasantharaja, N. Chandrasekhar, "Effect of Multipass TIG and Activated TIG Welding Process on the Thermo-Mechanical Behavior of 316LN Stainless Steel Weld Joints", 2016, Metallurgical and Materials Transactions B, Vol. 47, 1347-1362.
6. K. C. Ganesh, M. Vasudevan, K. R. Balasubramanian, N. Chandrasekhar, P. Vasantharaja, "Thermo-mechanical Analysis of TIG Welding of AISI 316LN Stainless Steel", Materials and Manufacturing Processes, 2014, 29, 903-909.
7. K. C. Ganesh, M. Vasudevan, K. R. Balasubramanian, N. Chandrasekhar, S. Mahadevan, P. Vasantharaja, T. Jayakumar, "Modeling, Prediction and Validation of Thermal Cycles, Residual Stresses and Distortion in Type 316 LN Stainless Steel Weld Joint made by TIG Welding Process", 2014, Procedia Engineering, 86, 767-774.

8. S. R. Kala, N. S. Prasad, G. Phanikumar, "Studies on multipass welding with trailing heat sink considering phase transformation", Journal of Materials Processing Technology, 2014, Vol. 214, Issue 6, 1228-1235.

9. S. K. Velaga, A. Ravishankar, "Finite element based parametric study on the characterization of weld process moving heat source parameters in austenitic stainless steel", International Journal of Pressure Vessel and Piping, Vol. 157, 2017, 63-73.

10. S. K. Velaga, R. Gaurav, S. Murugan, A. Ravishankar, S. Venugopal, "Comparison of weld characteristics between longitudinal seam and circumferential butt weld joints of cylindrical components", Journal of Manufacturing Process, 2015, Vol. 18, 1-11.

11. S. K. Velaga, G. Rajput, T. Selvaraj, B. M. Anandarao, A. Ravishankar, "A study on the effect of weld induced residual stresses and the influence of weld sequencing of centrifugal extract rotating bowl using numerical simulation and experimental validation", Ciência & Tecnologia dos Materiais, 2015, Vol. 27, 84-91.

12. A. Ravishankar, S. K. Velaga, G. Rajput, S. Venugopal, "Influence of welding speed and power on residual stress during Gas Tungsten Arc Welding (GTAW) of thin section with constant heat input: A study using numerical simulation and experimental validation", Journal of Manufacturing Processes, 2014, Vol. 16, 200-211.

13. J. Goldak, A. Chakravati, M. Bibly, "A new finite element model for welding heat sources", Metallurgical Transitions B, 1984, Vol. 15, Issue. 2, 299-305.

14. V. Pavelic, R. Tanbakuchi, O. A. Uyehara, P. S. Myers, "Experimental and computed temperature histories in gas tungsten-arc welding of thin plates", Welding Journal Research supplement, 1969, Vol. 48, 295-305.

15. E. Friedman, "Thermo-mechanical Analysis of the Welding Process Using the Finite Element Method", International Journal of Pressure Vessel and Piping, 1975, Vol. 97, Issue 3, 206-213.

16. G. W. Krutz, L. J. Segerlind, “Finite element analysis of welded structures”, Welding Research Supplement, 1978, Vol. 57, 211-216.

17. J. B. Leblond, J. Devaux, “A new kinetic model for isothermal metallurgical transformations in steels including effect of austenite grain size”, Acta Metallurgica, 1984, Vol. 32, 137– 146.

18. D. P. Koistinen, R. E. Marburger, “A general equation prescribing the extent of the austenite-martensite transformation in pure iron–carbon alloys and plain carbon steels”, Acta Metallurgica 1959, Vol. 7, 59–60.

19. S. Kumar, R. Awasthi, C. S. Vishwanadham, K. Bhuanumurthy, G. K. Dey, “Thermo-metallurgical and thermo-mechanical computations for laser welded joint in 9Cr-1Mo (V, Nb) ferritic/martensitic steel” Material and Design, 2014, Vol. 59, 211-220.

20. D. Deng, H. Murakawa, “Prediction of welding distortion and residual stress in a thin plate butt-welded joint” Computational Material Science, 2008, Vol.43, 353-365.

21. J. Wang J, “Investigation of buckling distortion of ship structure due to welding assembly using inherent deformation theory”. Doctoral thesis. Osaka University; 2012.

22. S. Okano, M. Morchizuki, “Transient distortion behavior during TIG welding of thin steel plate”, Journal of Material Processing technology, 2017, Vol. 241, 103-111.

23. P. Michaleris, L. Zhang, S. R. Bhide, P. Marugabandhu, “Evaluation of 2D, 3D and applied plastic strain methods for predicting buckling welding distortion and residual stress”, Science and Technology of Welding and Joining, 2013, Vol. 11, Issue 6, 707-716.

24. G. Fu, M. Lourenco, M. Duan, S. F. Estefan, “Influence of the welding sequence on residual stress and distortion of fillet welded structures” Marine Structure, 2016, Vol. 46, 30-55.

25. J. Wang, N. Ma, H. Murakawa, “An efficient FE computation for predicting welding induced buckling in production of ship panel structure”, Marine Structure, 2015, Vol. 41, 20-52.

26. J. Wang, W. Yin, H. Murakawa, “Experimental and computational analysis of residual buckling distortion of bead-on-plate welded joint”, Journal of Material Processing Technology, 2013, Vol. 213, Issue 8, 1447-1458.

27. J. Sun, X. Liu, Y. Tong, D. Deng, “A comparative study on welding temperature fields, residual stress distributions and deformations induced by laser beam welding and CO_2 gas arc welding”, Material and Design, 2014, Vol. 63, 519-530.

28. Y. C. Kim, M. Hirohata, K. Inose, “FEM Simulation of distortion and residual stress generated by high energy beam welding with considering phase transformation”, Open Journal of Metal, 2014, Vol.4, Issue 2, 31-39.

CHAPTER-4

EXPERIMENTAL WORK

In this chapter, details about the experimental works carried out to validate finite element modeling prediction on the thermal cycles, residual stresses and distortion are given. The welding experiments were carried out in the welding laboratory of Advanced Welding Processes and Modeling Section, Material Technology Division, IGCAR, Kalpakkam, India. Weld thermal cycles experienced by the plate at different distances from the weld fusion line was acquired while welding is in progress. Weld bead profiles, residual stress, distortion (vertical displacement), and hardness of the weld metal and HAZ were measured using appropriate experimental tools. Microstructure of the weld joint was also examined under optical microscope.

Complete details about the thermocouple locations on the weld joints and data acquisition system for temperature recording and procedures for the residual stress measurement using X-ray diffraction technique and distortion measurements by height gauge are also given. Autogenous and multi-pass GTA welding parameters employed for carrying out welding of 3 mm and 6 mm thick modified 9Cr-1Mo steel plates are discussed. Hardness measurements details are also provided.

Modified 9Cr-1Mo steel plates used in current study were normalized at 1080°C and tempered at 760°C for 2 hours. The chemical composition of modified 9Cr-1Mo steel plates provided by manufacturer is presented in Table. 4.1.

Table.4.1. Chemical Composition of modified 9Cr-1Mo steel

C	Si	Mn	P	S	Cr	Ni	Mo	N	V	Nb
0.10	0.43	0.40	0.015	0.06	8.5	0.10	0.88	0.045	0.23	0.018

Bead-on-plate experiments were carried on the modified 9Cr-1Mo steel plates for heat source fitting at various heat input values and for verifying the accuracy of material data base. Three set of plate welds of thicknesses 3 mm and 6 mm were fabricated employing Autogenous and multi-pass GTA welding process respectively. Autogenous welding technique was used for 3 mm thick square butt joint plate using Semi-Automatic GTA welding machine as shown in Fig. 4.1. Multi-pass welding process is used for 6 mm thick plate with V groove joint (70°). Four passes were required for completing the joint using matching composition filler wire (ER 90S-B9) of 1.4 mm diameter size by manual GTA welding process. The first set of weld joints were made without pre heating, the second set with pre heating of 200°C and the third set with combined pre heating and post heating at 200°C. The experimental setup of different welding processes is discuused in detail below.

4.1. Bead-on-plate weld

For heat source fitting and checking the accuarcy or suitability of material datbase, bead-on-plate experiments were carried out on 3 mm thick plate at a different heat inputs. Bead on plate welding carried out on 3 mm thick plates using Semi-Automatic GTA welding machine.

Fig.4.1. Autogenous welding of 3 mm thick plate using Semi-Automatic weld machine

Sixteen numbers of bead-on-plates were made at 60, 100, 120 and 150 mm/min speed for 90, 95, 100 and 110 A current with an arc length of 1.5 mm. Pure Argon is used as a shielding and purging gas with flow rate of 10 lit/min. Square butt joint of 3 mm thick plate was made using optimized welding parameters of 90 A at 100 mm/min weld speed. Fig. 4.2 (a-e) shows different bead-on-plates at different heat inputs. After welding, weld samples were cut, metallographically polished and etched using Villella's reagent to examine the weld bead profile as shown in Fig. 4.3.

(a) 100 A at 120 mm/min

(b) 100 A at 150 mm/min

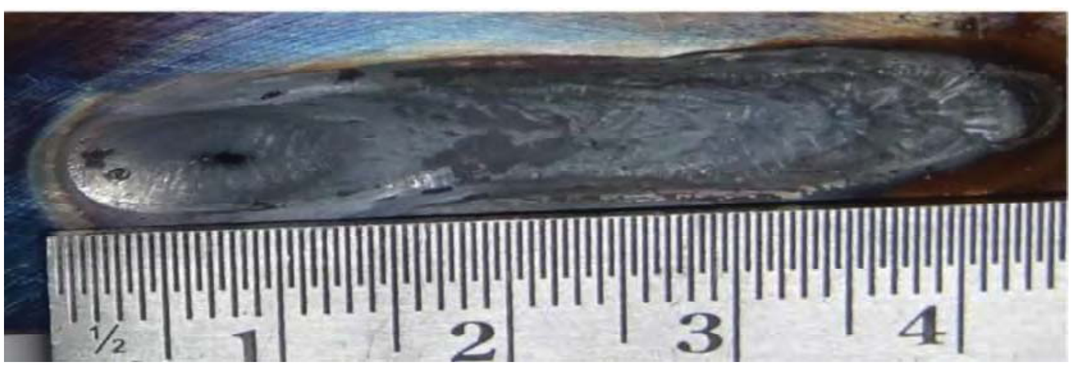

(c) 110 A at 150 mm/min

(d) 90 A at 120 mm/min

(e) 90 A at 60 mm/min

Fig.4.2. Bead-on-plates at different heat inputs

Fig.4.3. Weld sample

4.2. Autogenous welding

In GTA welding, the electric arc is produced between non-consumable electrode and the work piece. An autogenous welding process is employed for the study, in which the arc moves over the substrate material and joining of plate is performed without any addition of filler material. The argon gas shielding is used to prevent oxidation at the fusion zone. Fig. 4.4 shows weld bead produced during autogenous welding.

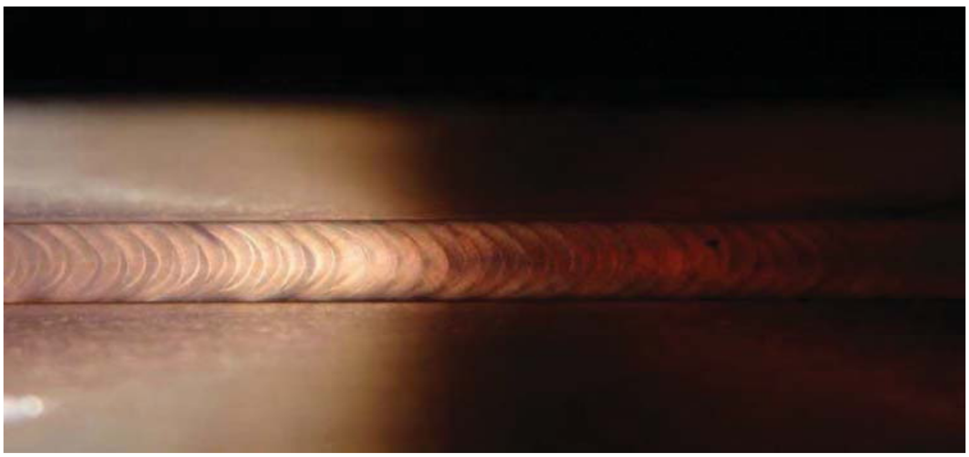

Fig.4.4. Weld bead using Autogenous weld

Fig. 4.5 shows the location of thermocouples, used for measuring temperature history at 10, 15 and 18 mm. K type thermocouples are used for recording thermal cycles at a sampling time 1 second. Sampling time is duration between two consequence recording temperatures, in this case for duration of every one second temperature has been recorded. The thermal cycles have been recorded down to room temperature. The temperature histories are recorded during the entire period of heat source movement and the cooling period. A data logger interfaced with computer is used for storing and analysis of thermal histories. The other end of the thermocouple is connected to a multichannel temperature measuring system. Thermal history has been recorded by thermocouple in terms of voltage, which converts to temperature by data logger and entire data is recorded in laptop. The experimental setup of the temperature measurement with data logger and thermocouples is shown in Fig. 4.6.

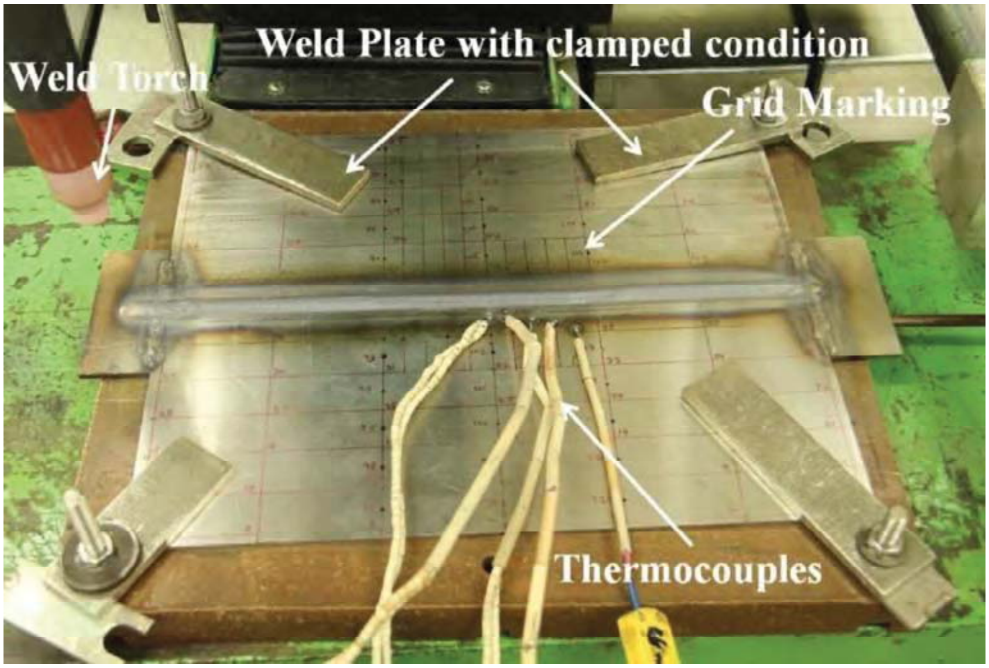

Fig.4.5. Autogenous weld plate

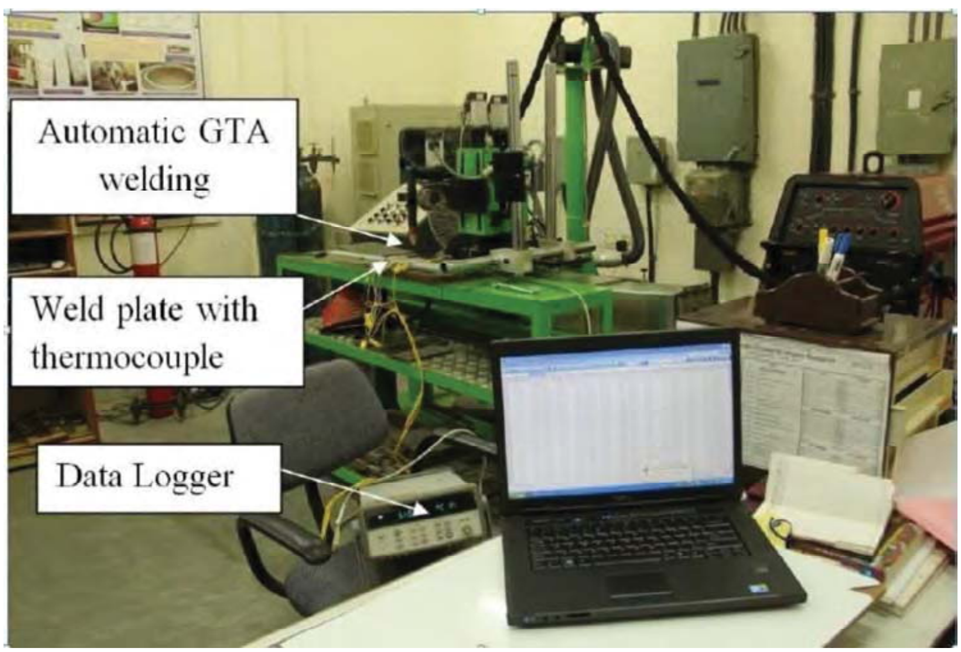

Fig.4.6. Experimental setup for thermal cycle measurement

4.3. Multi-pass welding

Manual multi-pass GTA welding was performed with V-groove edge configuration as shown in Fig. 4.7 (a). Run-in and run-out plates were tack welded to the weld joint. Stiffeners were provided during experiment to avoid excess distortion of weld joint as shown in Fig. 4.7 (b). Plates with V groove joint preparation at 70° angle of dimension 240 mm ×300 mm × 6 mm welded using matching filler wire of 1.4 mm diameter by manual welding process and the electrode tip angle of 30° was used. Pure Argon is used for shielding and purging while the gas flow rate was kept at 10 lit/min. Thermal cycle during welding was recorded using K type thermocouple. After welding, weld sample was prepared by metallographic techniques. FZ and HAZ size of each sample is measured using optical microscope. Average heat input paramters used during welding of multi-pass welding for different cases is given in Table 4.2.

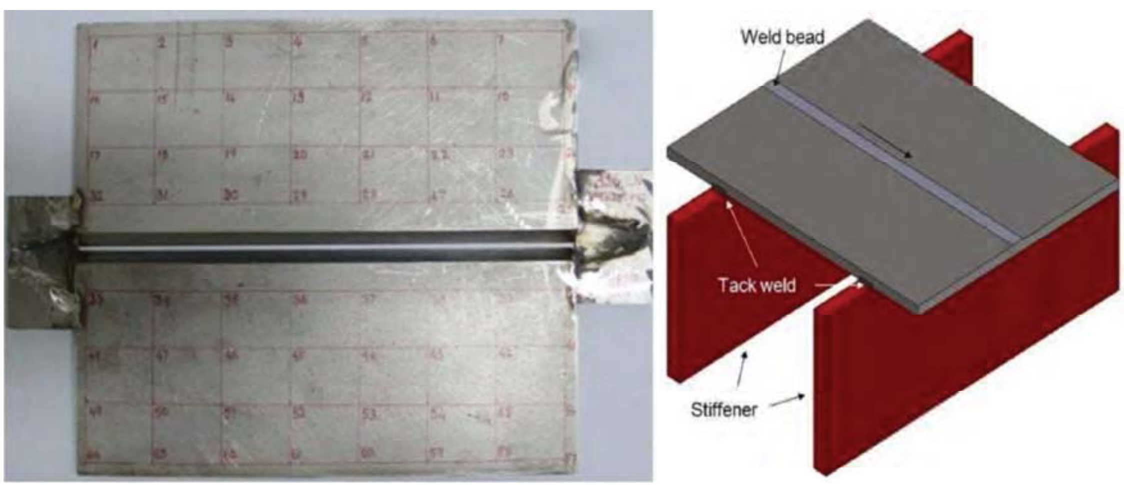

(a) V Groove weld joint (b) Schematic diagramme of welding

Fig.4.7. Multi-pass welding of modified 9Cr-1Mo steel

Table.4.2. Heat input for multi-pass welding

Pass No	Current (I)	Voltage (V)	Average weld speed (mm/sec)	Heat input (KJ/mm)
1	105	14.5	1	1.522
2	120	15	1.5	1.2
3	140	15.8	1.5	1.47
4	140	16	1.5	1.49

4.4. Pre-heating and Post-heating

In case of welding with pre heating, base metal is pre heated to 200°C using Oxy-acetylene flame. The heated material is checked, whether it has attained the required temperature by using thermal chalk "THERMELTIK" by striking on the surface of the plate. During welding with pre heat, the joint area comprising fusion zone and the adjacent area of 7 mm (for 3 mm thick plate) and 14 mm (for 6 mm thick plate) wide on each side from the weld centre line was heated up to 200°C using oxy-acetylene flame heating. During welding with post heating, first tacked plates were pre heated up to 200°C and then welding was carried out. After the weld joint cooled down to 200°C, the temperature of 200°C was maintained for next 0.5 hr by heating with Oxy-acetylene flame for studying the effect of post heating. During multi-pass welding, inter-pass temperature of 200°C was maintained in between each pass.

4.5. Distortion /Vertical Displacement Measurement

The distortion of the weld joint was measured before and after welding process using a digital electronic height gauge. Grids were marked on the weld joint surface prior to welding to measure the vertical displacement as shown in Fig. 4.5. Vertical displacement at each grid points were measured and plotted to understand the variations over a surface [1-5].

Displacement in a weld joint was measured on grid marked position at 50 × 20 mm locations using electronic vertical height gauge (least count 0.001 mm) as shown in Fig. 4.8. Difference in reading before and after welding was plotted as a vertical displacement in weld joint.

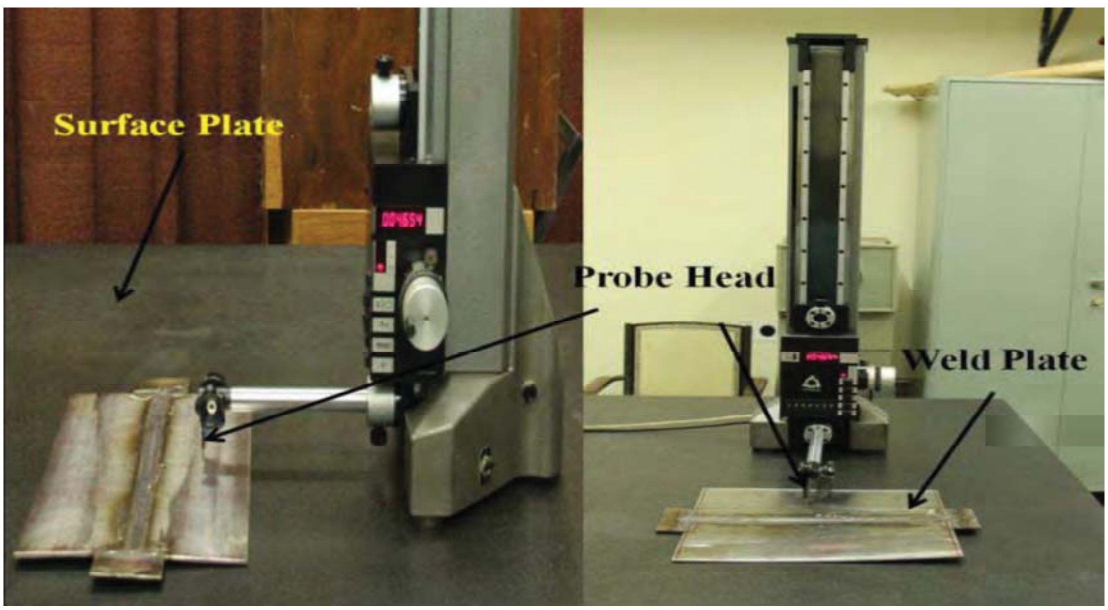

Fig.4.8. Vertical Displacement measurement using vertical height gauge

4.6. Residual Stress Measurement using X-Ray Diffraction Technique

Residual stress measurements are made using X-ray diffraction technique at an interval of 5-10 mm from weld center line. This technique uses the distance between the crystallographic planes as a strain gauge. If tensile stresses were present, the lattice spacing will increase for planes perpendicular to the stress direction and decreases for planes parallel to stress direction. The elastic strain and change in the value of lattice spacing is proportional to magnitude of residual stress. Diffraction from the grains satisfy the Bragg's law.

Fig. 4.9 shows the equipment used for the XRD based residual stress measurements in the present study and it is a portable X-ray stress analyzer (Rigaku Strain flex MSF-2M) having a back-reflection type goniometer with Chromium Kα radiation. The locations of measurements were polished before the measurements to minimize/avoid errors due to surface defects. The complete method of measuring the shift in the peak position of diffracted X-rays of a selected set of planes and thereby calculating the residual stresses is discussed in detail in the literature [7-10].

Fig.4.9. X-ray Diffraction equipment

In this technique, strain in the surface layers of a material is estimated by measuring the shift in the position of the diffraction peak of a set of parallel planes. These strains are then converted into stresses analytically using various assumptions. The description of fundamental relation between lattice spacing and stress in the specimen surface is given below. Fig. 4.10 depicts the pictorial representation of the angles and principal stresses for plane stress elastic model.

XRD based stress measurement is confined to the surface of the sample. In the exposed surface layer, a condition of plane stress is assumed to exist. That is, distribution of stresses described by principal stresses σ_1 and σ_2 in the plane of the surface, and no stress is assumed perpendicular to the surface, $\sigma_3 = 0$. However, a strain component perpendicular to the surface ε exists as a result of the poison's ratio (μ), contractions caused by the two principal stresses. The expression of strain in terms of orientation angles is given below [10].

$$\varepsilon_{\phi\psi} = \left[(1+\mu)/E\left(\sigma_1 Cos^2\phi + \sigma_2 Sin^2\phi\right)Sin^2\psi\right] - \left[(\mu/E)(\sigma_1+\sigma_2)\right] \quad (4.1)$$

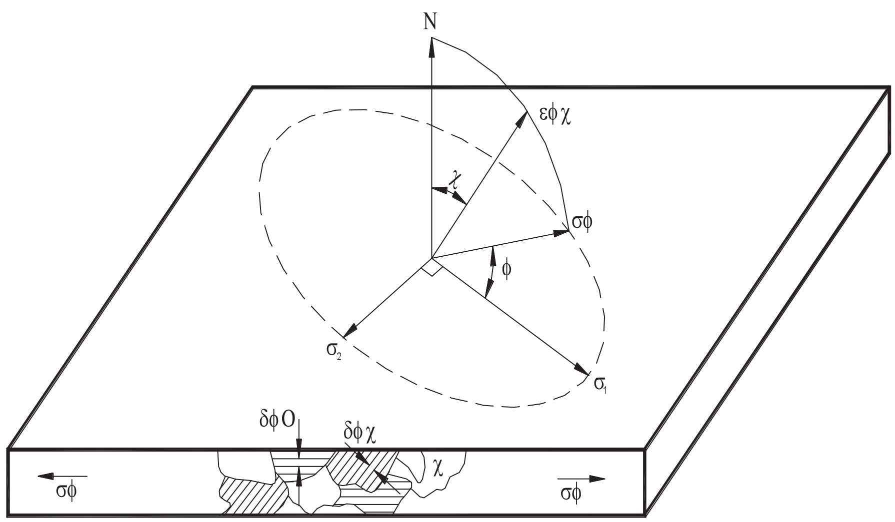

Fig.4.10. Plane Stress Elastic Model

Angle ϕ denotes the angle between one of the principal stress axes and the projection of the measured strain direction on the specimen surface. Angle ψ is the angle between specimen normal and direction of strain measurement. E is Young's modulus, μ is Poisson's ratio.

The lattice spacing for any direction is:

$$d_{\phi\psi} = \left[\left((1+\mu)/E\right)_{hkl} \sigma_\phi d_o Sin^2\psi\right] - \left[(\mu/E)_{hkl} d_o (\sigma_1 + \sigma_2) + d_o\right] \tag{4.2}$$

Eq. 4.2 describes the fundamental relation between lattice spacing and the biaxial stresses on the surface of the sample. The lattice spacing is a linear function of the $\sin^2\psi$. Schematic representation of this variation is shown in Fig. 4.11. The intercept of the plot (*d vs. $sin^2\psi$*) at $sin^2\psi = 0$ is:

$$d_{\phi\psi} = d_o - (\mu/E)_{hkl} d_o (\sigma_1 + \sigma_2) \tag{4.3}$$

The slope of the plot (*d vs. $sin^2\psi$*) given in Fig. 4.11 is

$$\partial d_{\phi\psi} / dSin^2\psi = \left((1+\mu)/E\right)_{hkl} \sigma_\phi d_o \tag{4.4}$$

$$\sigma\phi = (E/1+\mu)_{(hkl)} 1/d_0 (\partial d_\psi / \partial \sin^2\psi) \tag{4.5}$$

Negative and positive slopes correspond to compressive and tensile stress and the slope gives the value of σ_ϕ. This instrument has a back-reflection type goniometer with a *2Ø* scan range from 140° to 170° having parallel beam geometry.

A multiple ψ method (*$Sin^2\psi$*) was used for the stress measurement. In this method, diffraction measurements are made at several tilt angles ψ. The residual stresses are measured within the top layer of about 20 to 50 μm in thickness after electrochemically polishing at the selected measurement locations. The X-ray tube is operated at 30 kV with a target current of 8 mA. The peak shift at various ψ angles defined as the angle between sample normal and diffraction vector (ranging from 0° to 45° in steps of 9°) is related to the change in the d-spacing of the (211) plane and is used for estimating the residual stresses. Scanning in steps of 0.2° with a dwell time of 3 sec at each step was employed to obtain good statistics of the measurements. The scanning was carried out within the angular range of 148° to 164°. At all the locations on the surface two sets of measurements were carried out and the values reported are averaged stress values based on the combined analysis of the change in the peak location with varying ψ . All the peaks were corrected for background and for absorption by fitting a parabola to the 20% of the corrected peak and the peak of the parabola were taken as the peak top. The conditions used for XRD measurements are given in Table 4.3.

In the present work only XRD technique has been used for residual stress measurements and the results have not been verified with those obtained from another complimentary techniques. However, it may be noted that the equipment and the procedure employed for residual stress measurements using XRD technique is same as those used for results of residual stress measurements carried out by XRD technique and those reported by Javadi et. al. In that work results of residual stress values obtained by XRD technique on dissimilar welds between P91 steel and 316LN stainless steel have been compared with those obtained by hold drilling and neutron diffraction techniques. Residual stress estimated at distance of 4.6 mm distance from weld line on P91 plate side is 221 MPa using hole drilling technique and the corresponding value estimated using XRD techniques is 218 MPa. This confirms the reliability of the technique and procedure adopted for the residual stress measurement and hence, only this technique was employed for the residual stress measurement.

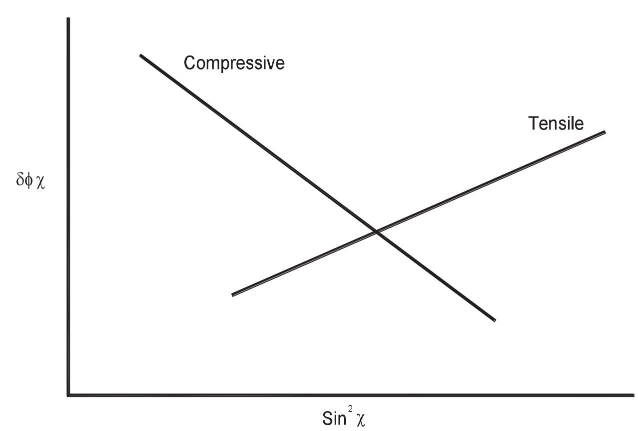

Fig.4.11. Slope of the Plot Provides Information about Nature of the Stress

4.7. Hardness Measurement

For measuring hardness values across weld joint and microstructure of modified 9Cr-1Mo steel, a metallography specimen was cut from 3 mm thick plate welds with weld at the center of the specimens. The cross section of weld specimen was polished and etched using Villella's reagent (1 gm of picric acid, 100 ml ethanol and 5 ml of hydrochloric acid) [11]. Micro-hardness measurements (Vickers Hardness) were made at specified intervals (every 2-5 mm) from the weld centerline of as weld using 100 gm load with SHIMADZU, HMV-2000 Micro-hardness tester. The hardness profiles and microstructure were taken across the weld joint.

Table.4.3. X-Ray diffraction Conditions

Characteristic X-ray	Cr K_α	ψ Range	0° - 45°
Diffraction plane	{211}	Step width	0.2°
Diffraction angle (degrees)	156.5	Wave length	2.2896 A°
Filter	Vanadium	Spolier slit	1°
Tube voltage	30 kV	Aperture	2 x 4 mm
Tube current	7 mA	Dwell time	3 sec

References

1. R. Pamnani, M Vasudevan, T Jayakumar, K C Ganesh, P Vasantharaja, "Numerical Simulation and Experimental Validation of Arc Welding of DMR-249A Steel", Defense Technology, 2016, Vol. 12, 305–315.
2. K. C. Ganesh, K. R. Balasubramanian, M. Vasudevan, P. Vasantharaja, N. Chandrasekhar, "Effect of Multipass TIG and Activated TIG Welding Process on the Thermo-Mechanical Behavior of 316LN Stainless Steel Weld Joints", 2016, Metallurgical and Materials Transactions B, Vol. 47, 1347-1362.
3. K. C. Ganesh, M. Vasudevan, K. R. Balasubramanian, N. Chandrasekhar, P. Vasantharaja, "Thermo-mechanical Analysis of TIG Welding of AISI 316LN Stainless Steel", Materials and Manufacturing Processes, 2014, 29, 903-909.
4. K. C. Ganesh, M. Vasudevan, K. R. Balasubramanian, N. Chandrasekhar, S. Mahadevan, P. Vasantharaja, T. Jayakumar, "Modeling, Prediction and Validation of Thermal Cycles, Residual Stresses and Distortion in Type 316 LN Stainless Steel Weld Joint made by TIG Welding Process", 2014, Procedia Engineering, 86, 767-774.
5. P. Vasantharaja, V. Maduarimuthu, M. Vasudevan, P. Palanichamy, "Assessment of Residual Stresses and Distortion in Stainless Steel Weld Joints" Materials and Manufacturing Processes, 2012, Vol. 27, Issue 12, 1376-1381.
6. Y. Javadi, M.C. Smith, K. Abburi Venkata, N. Naveed, A.N. Forsey, J.A. Francis, R.A. Ainsworth, C.E. Truman, D.J. Smith, F. Hosseinzadeh, S. Gungor, P.J. Bouchard, H.C. Dey, A.K. Bhaduri, S. Mahadevan, "Residual stress measurement round robin on an electron beam welded joint between austenitic stainless steel 316L(N) and ferritic steel P91" 2017, International Journal of Pressure Vessels and Piping, 154, 41-57.

7. I. C. Noyan, J. B. Cohen, “Residual stress Measurement by Diffraction and Interpretation”, First Ed. Springer-Verlag, New York, 1987.

8. B. D. Cullity, S. R. Stock, “Elements of X-ray diffraction”, Fist Ed. Prentice Hall, New Jersey, 2001.

9. B. Raj, T. Jaykumar, S. Mahadevan, S. K. Rai, “X-ray diffraction based residual stress measurement for assessment of fatigue damage and rejuvenation process for undercarriages of aircraft”, Journal of Non-destructive Evaluation, 2009, Vol. 28, Issue 3-4, 157-162.

10. A. Joseph, G. K. Sharma, T. Jayakumar, N. Murugan, “Evaluation of residual stresses in weld joints of pipes using X-Ray Diffraction techniques”, Journal of Non-Destructive Testing & Evaluation, 2005, Vol. 4, Issue 1, 31-38

11. A. K. Bhaduri, C. R. Das, S. K. Albert, A. Klenk, B. S. Murty, “Study of deformation behavior of simulated inter-critical heat-affected zones of modified 9Cr-1Mo steel”, Materials and Manufacturing Processes, 2011, Vol. 26, Issue, 1, 62–65.

CHAPTER-5

RESULTS AND DISCUSSION

This chapter is divided in to six different sections. In first section, creation of material properties data base is presented and heat source fitting analysis for 16 bead-on-plates is discussed in detail. Predicted weld profile and HAZ profile is compared with experimental measured profile for different heat input. In second section thermo-mechanical analysis of autogenous welding of 3 mm thick modified 9Cr-1Mo steel plate welding and its experimental validation is presented. The results clearly bring out the effect of phase transformation during weld thermal cycles on the residual stresses generated as well as distortion. In third section thermo-mechanical analysis of multi-pass welding process for 6 mm thick plate of modified 9Cr-1Mo steel is discussed.

Thermo-mechanical analyses of welding made with pre heating are presented in the fourth section. Disk shaped heat source distribution model is proposed for modelling the effect of preheat. In the fifth section thermo-mechanical analysis of welding with both pre heating and post heating are carried out. Different assumptions and boundary conditions considered while modeling welding with post heating for autogenous and multi-pass welding is also discussed. In each of these sections predicted residual stress and distortion in weld plates are verified with experimental measured values.

In last six section comparison of results presented in the sections 2-5 are made to bring out the role of pre heating and post heating in altering the residual stress distribution and distortion in the weld and also to demonstrate the validity of the thermo-mechanical analysis for autogenous and multi-pass welding and welding without preheating, with preheating and with both preheating and post heating.

5.1. *Material data base creation and Bead-on-plate weld*

Material data base for modified 9Cr-1Mo steel was not available in default SYSWELD libraray. Hence two types of material data base considering with and without phase transformation effect were created from the material property data collected from literature. Using this data thermal analysis of bead-on-plate weld was carried out. Heat source fitting of bead-on-plate was done using double ellipsoidal heat source model. Degree of accuracy of heat source fitting and suitability of material datbase are checked using autogenous bead-on-plate welds made on 3 mm thick plate at a different heat input.

5.1.1 Material data base of Modified 9Cr-1Mo steel

Material database is not available for modified 9Cr-1Mo steel in default database of SYSWELD library, so material properties data base of modified 9Cr-1Mo steel is created using data base tool. During heating part of the weld thermal cycles, ferrite phase with Body-Centered-Cubic (BCC) structure transforms to austenite phase with Face-Centered-Cubic (FCC) structure resulting in decrease in volume [1-4]. In the cooling part of weld thermal cycles, austenite transforms in to martensite with Body-Centered-Tetragonal (BCT) structure with a corresponding expansion in the volume. These phase transformations are considered in material properties database. For modeling strain hardening behavior of ferrite and austenite phases of this steel, properties provided for X20Cr13 steel are considered. For martensite phase properties of modified 9Cr-1Mo steel, properties of martensite given for DP 600 steel (Dual Phase steel) are considered. Composition of X20Cr13 steel is similar to that of the modified 9Cr-1Mo steel, but carbon content in this steel is high. Because of this, properties of ferrite and austenite phases are similar for both the steels; but for martensite phase of X20Cr13 steel is harder than that of modified 9Cr-1Mo steel. It is found that variation of yield strength with temperature for martensitic phase in DP 600 steel is similar to that of modified 9Cr-1Mo steel and hence properties of this martensitic phase is taken for generating data base for modified 9Cr-1Mo steel [5]. Fig. 5.1.1-5.1.2 shows the different phase dependent thermo-physical and mechanical material properties taken from literature [1]. During computation of the phase fraction as a function of temperature. The effect of martensitic phase transformation is calculated based on the Koistinen and Marburger model with coefficient is 0.0268 [6]. Martensite start temperature (M_s) and Martensite finishing (M_f) temperature are 375°C and 200°C considered. Ferrite to austenite transformation was defined between (Ac_1 = 820°C and Ac_3 = 900°C) and this transformation was computed according to Leblond's equation [7-10].

Accuracy of FEA is depends upon the accuracy of material property data base. While making the material data base as recommended in literature, curve fitting and sharp changes in values are avoided [11-15].

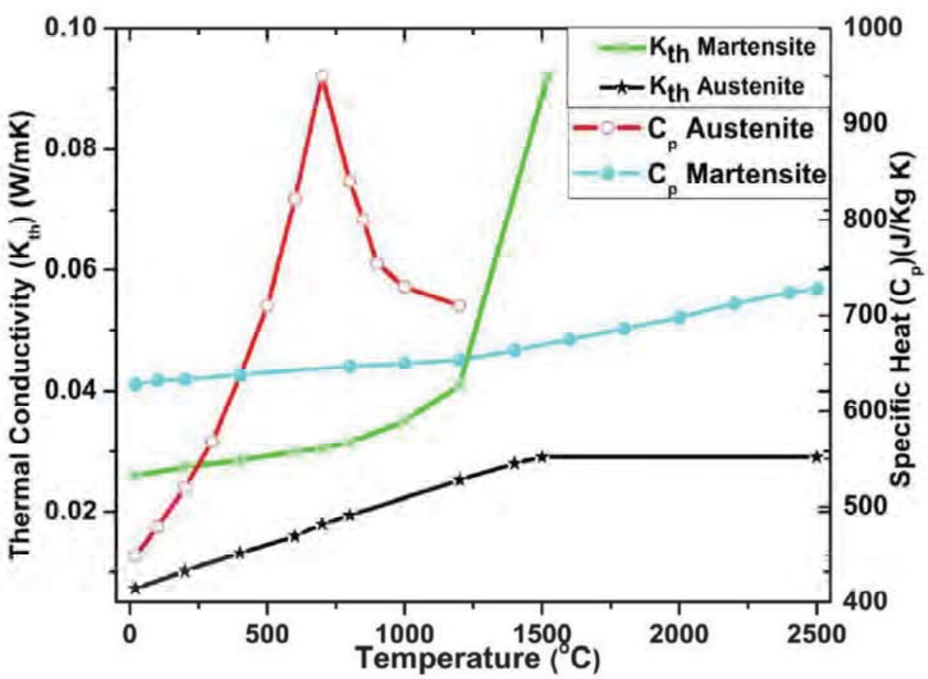

(a) Thermal conductivity and specific heat

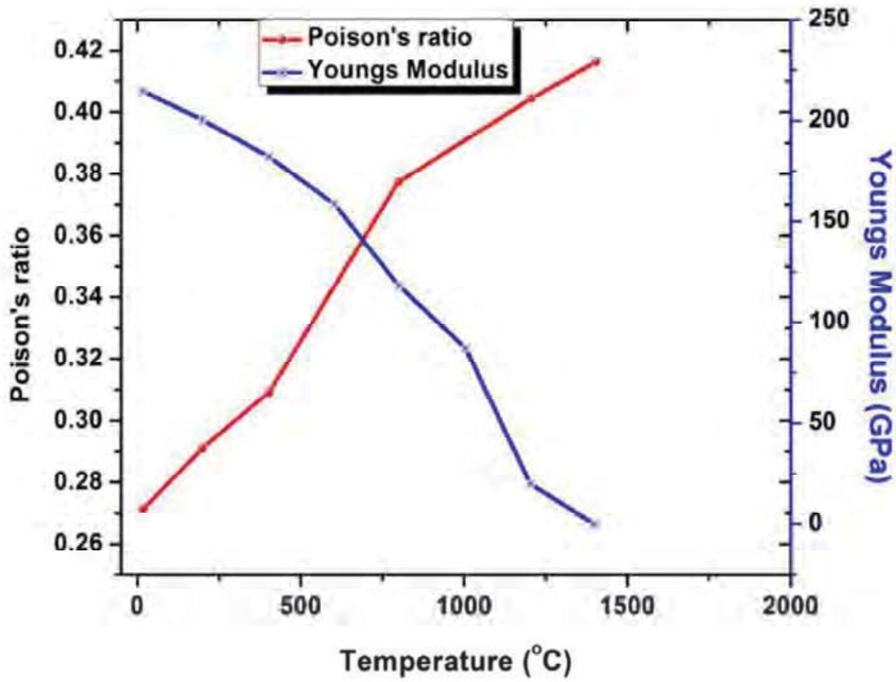

(b) Poison’s ratio and Young’s modulus

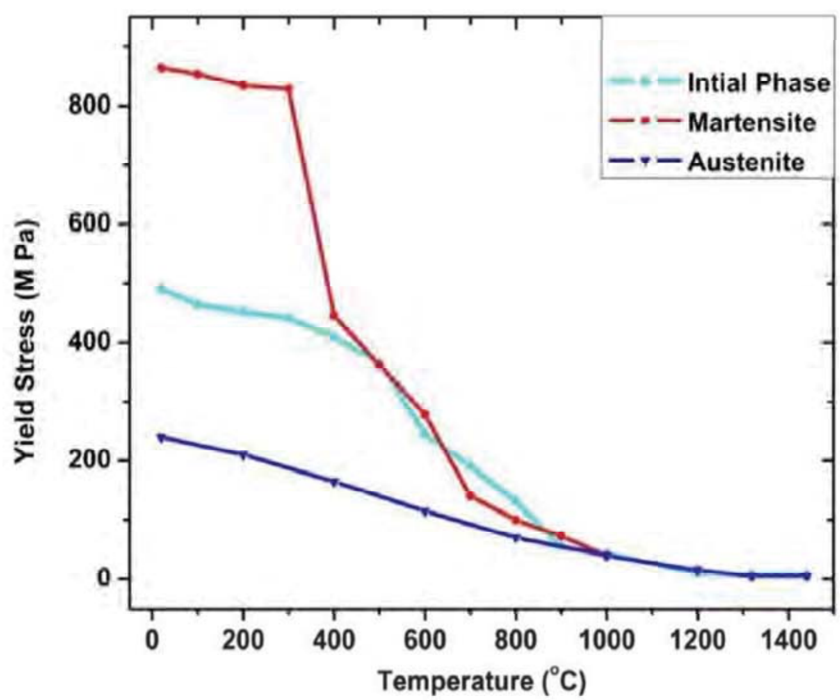

(c) Yield stress

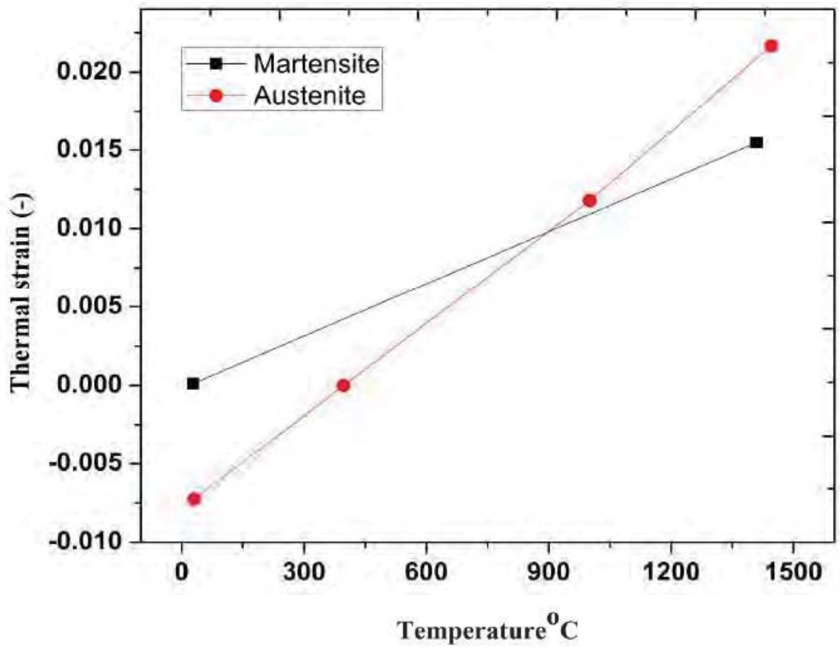

(d) Thermal strain

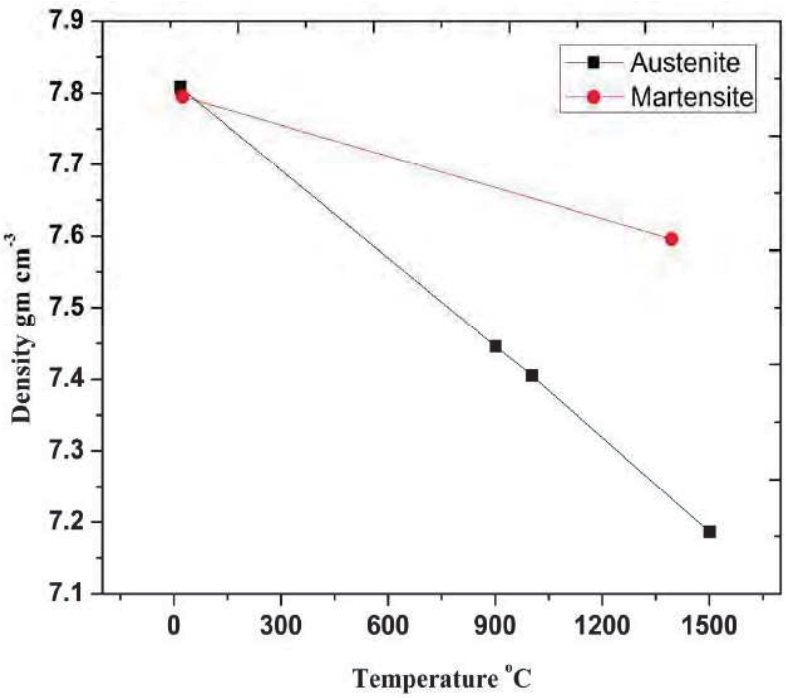

(e) Density

Fig.5.1.1. Thermo-physical properities [5]

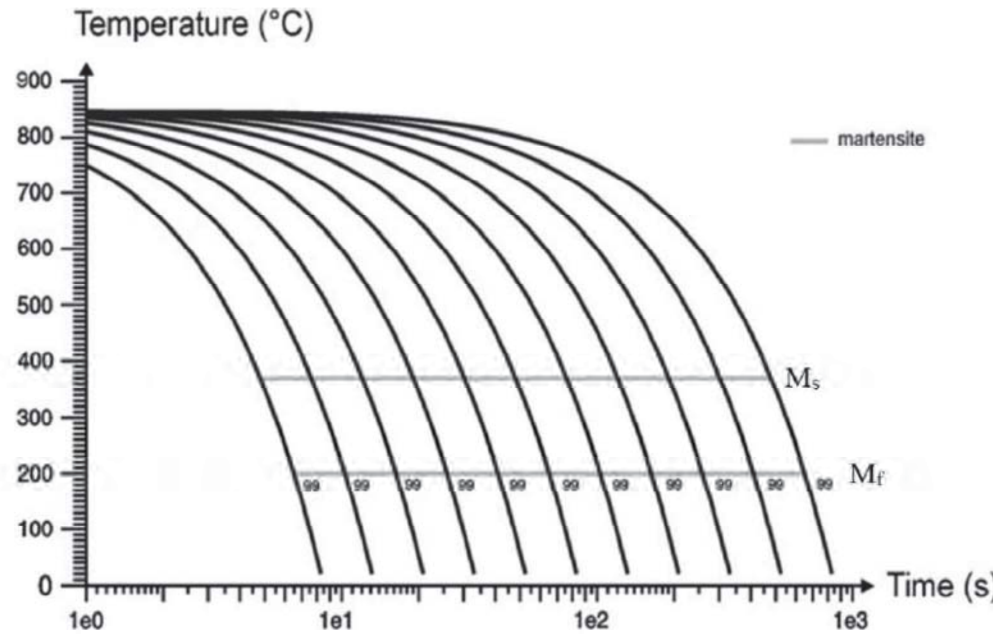

Fig.5.1.2. CCT diagramme of modified 9Cr-1Mo steel [5]

5.1.2. Heat Source Fitting of Bead-On-Plate Welding

Bead-on-plate welds of 3 mm thick plate were prepared using Semi-Automatic GTA welding machine at a different heat inputs Fig.5.1.3 shows the Weld profile and HAZ profile of weld plate measured vertically downward at each 0.3 mm distance.

Fig. 5.1.4 shows the top surface of bead-on-plate where sum of a_f and a_r is weld length and b are weld width parameters used for heat source fitting. Heat input parameters and experimentally obtained weld length and width for all sixteen bead-on-plates are given in Table. 5.1.1.

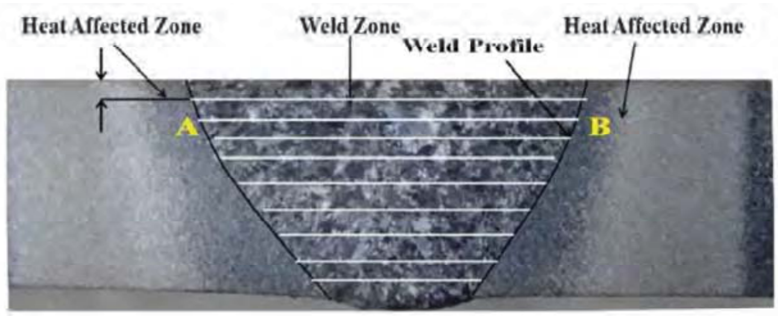

Fig.5.1.3. FZ profile and HAZ measurment

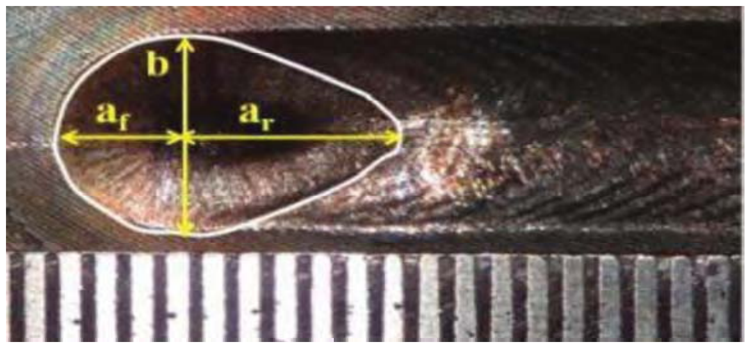

Fig.5.1.4. Double ellipsoidal heat source parameters

During heat source calibration step the weld bead profile was calibrated with respect to experimentally observed weld bead profile as shown in Fig. 5.1.5 (a). In this Figure the red zone indicates the melting point of the material as 1510°C. FZ profile obtained by FEA is validated with experimental profile measured by optical microscope; this comparison of results shows a good matching weld profile. Final predicted weld profile is compared with experimental results shown in Fig. 5.1.5 (b), it shows comparison of isotherms on the cross section of the weld bead by FEA (left side of weld center line) with respect to fusion and HAZ boundaries revealed in the cross section of experimental weld bead (right side of weld center line) after etching. Heat affected zone and fusion zone width of all bead-on-plate welds were measured using optical microscope and further compared with predicted values as given in Table. 5.1.1.

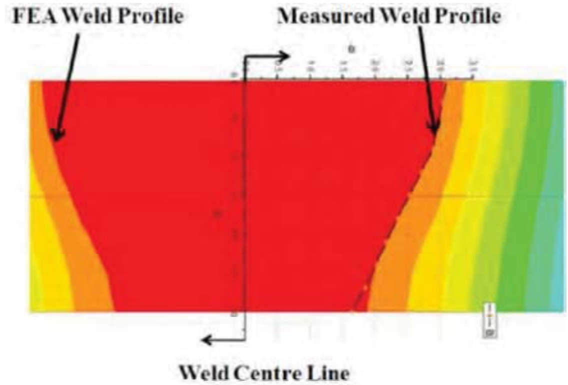

(a) Measured weld profile with simulated results

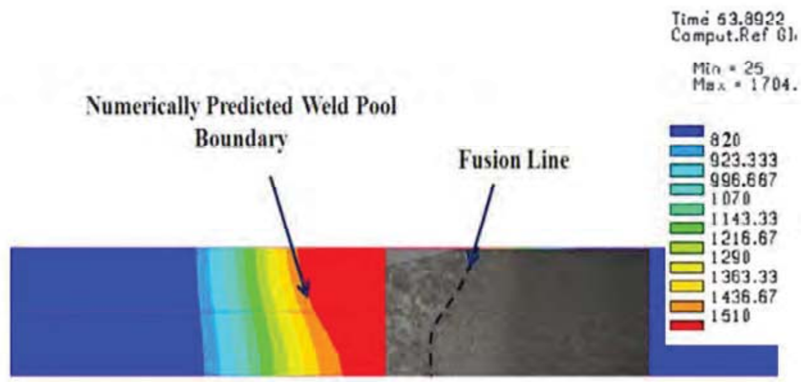

(b) Experiment and predicted weld profile

Fig.5.1.5. Heat source fitting of bead-on-plate

For all 16 bead-on-plate welds same procedure is repeated. Fig. 5.1.6 (a-d) shows comparison of the predicted and experimental profiles of cross section of bead-on-plate weld made with currents in the range of 90-110 A, voltage of 10.2-14.4 V and welding speed at 100 mm/min with arc length maintained at 1.3 mm. Variation of current changes the heat source distributions and its magnitude, this influences the input of heat flux applied in weld regions, consequently it affects the temperature distributions in FZ and HAZ. Comparison of experimental and simulated results shows good agreement, overall error of 5-9% is observed, which is because of difference in heat losses consideration in FEA and actual heat losses in experiment.

Fig. 5.1.6 (e) shows the finite element analysis of all bead-on-plates for different heat input. Maximum weld width of 8.9 mm is obtained for 110 A current and 60 mm/min (heat input=1.04 kJ/mm) weld speed while minimum weld width of 5.2 mm is obtained for 90 A current at 150 mm/min weld speed (heat input=0.3 kJ/mm). For same heat input predicted results are 9.4 mm and 5.9 mm respectively, which are nearer to measured values. For higher welding speed the FZ profile are not wide because of short heat interaction time with weld material, it transforms the FZ profile into conical shape, this type of conical fusion zone profile is predicted as shown in Fig. 5.1.6 (c) for 90 A current at 150 mm/sec weld speed. Based on all 16 bead-on-plates experiment, FZ profile is optimum for 90 A current at 100 mm/min weld speed, selected for square butt joint weld plate. All bead-on-plate welds are fully penetration welds for different heat input as shown in Fig. 5.1.6 (e).

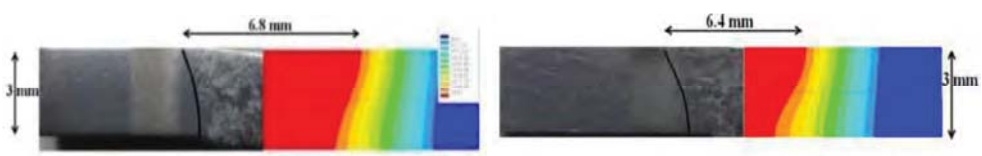

(a) 110A (b) 100A

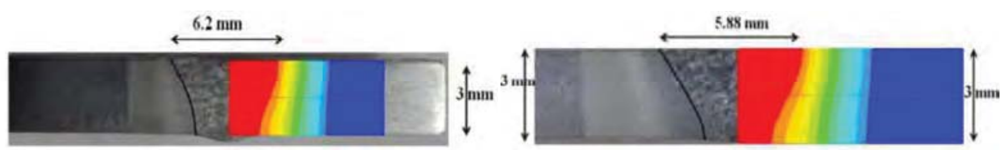

(c) 95A (d) 90A

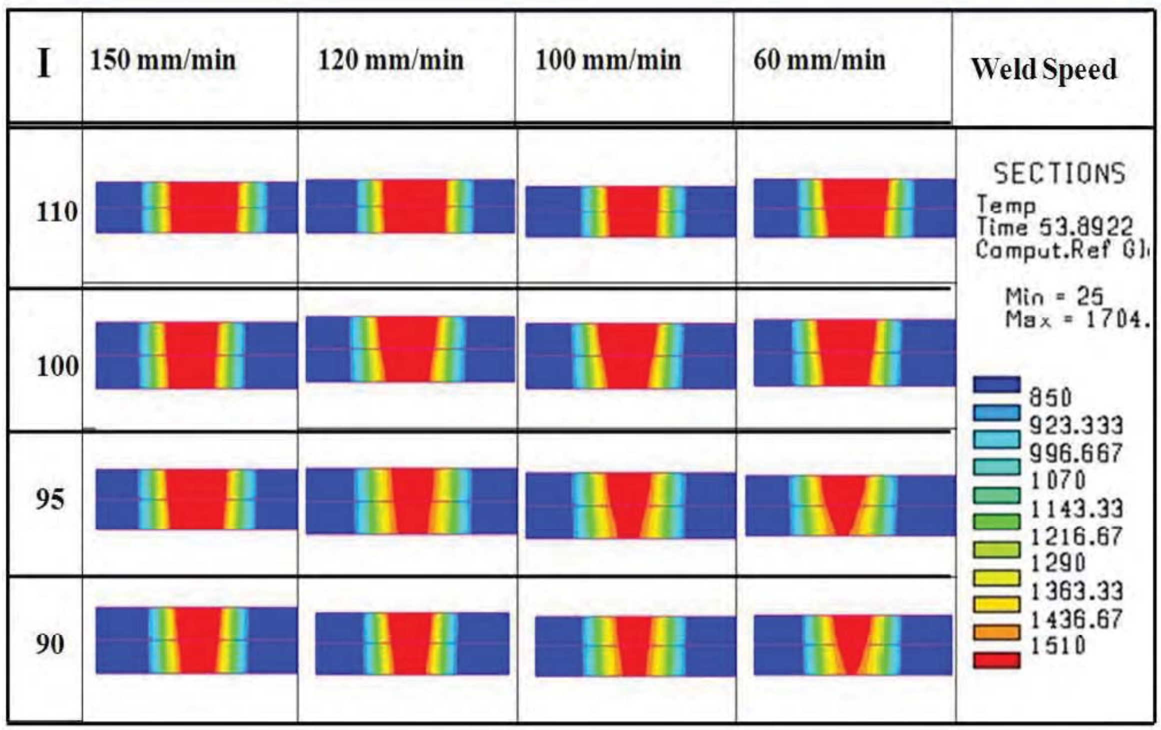

(e) Thermal Analysis of all bead-on-plates

Fig.5.1.6. FZ and HAZ profile comparison

Measured FZ and HAZ compared with predicted results are as given in Table. 5.1.1. Maximum HAZ width obtained for 110 A current at 60 mm/min weld speed is 4.08 mm, based on heat source fitting it is 4.5 mm with 9% error. Similarly, minimum HAZ width is 1.8 mm experimentally and 2.3 mm from heat source fitting analysis at 90 A for 150 mm/min weld speed.

For all sixteen bead-on-plates experimental measured HAZ and FZ width are plotted against finite element heat source fitting results as shown in Fig. 5.1.8. Heat source fitting analysis results of FZ and HAZ are closer to experimental measured results, with an accuracy of 97% as shown in Fig. 5.1.7. Root mean square error value for FZ width is 0.0946 and for HAZ width is 0.083.

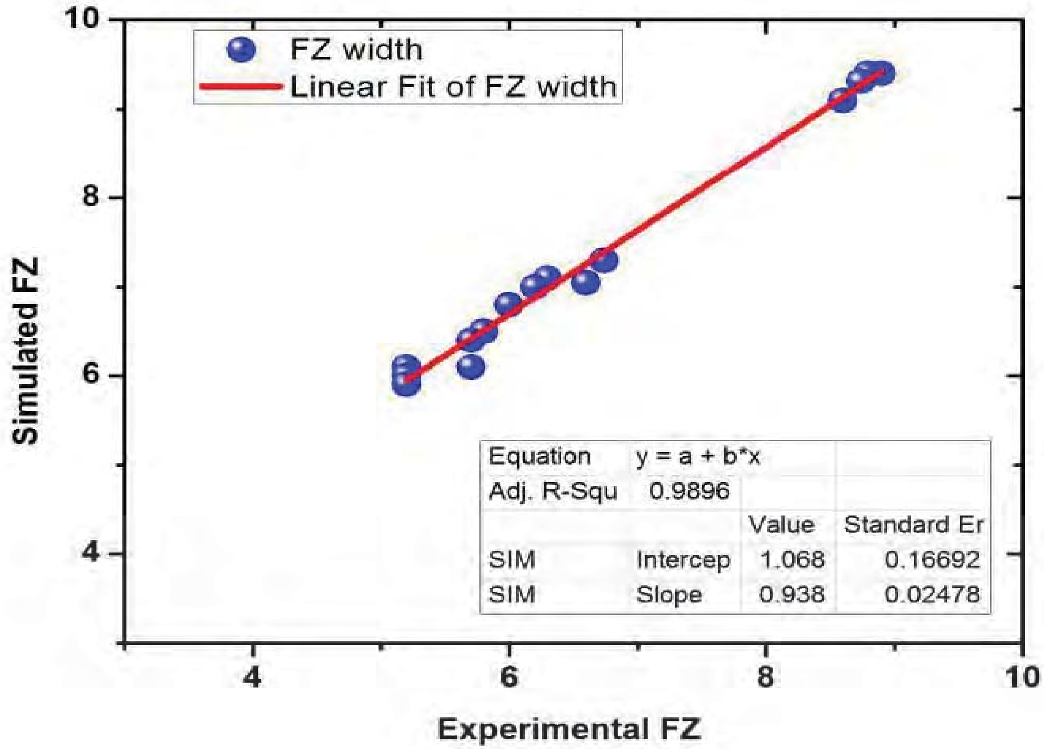

(a) FZ comparison

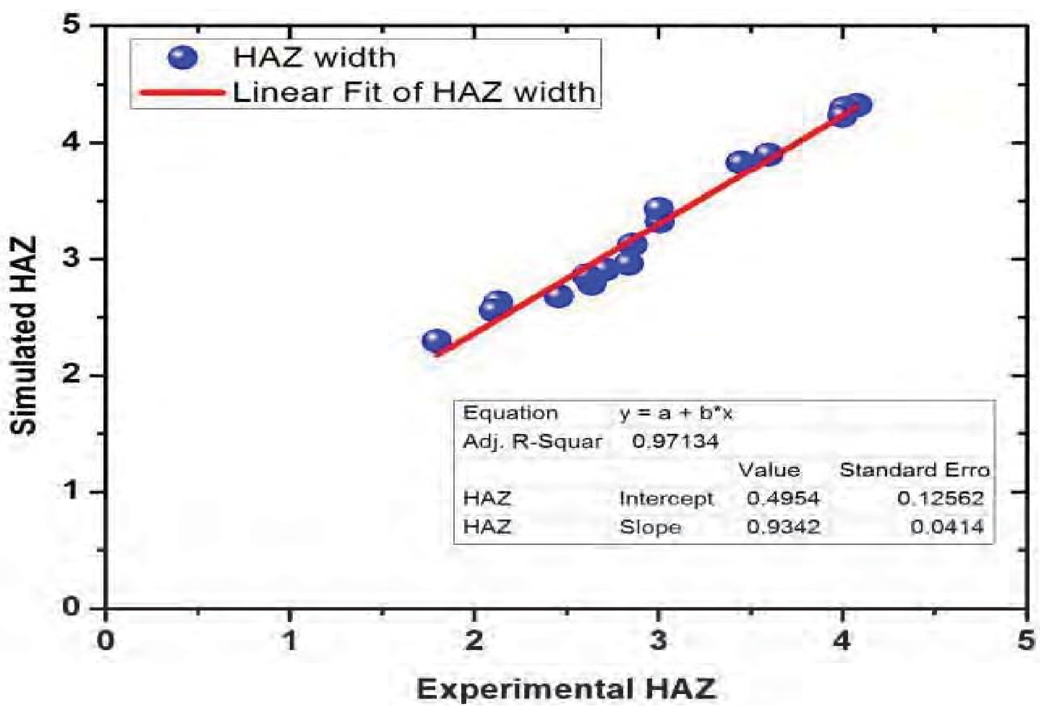

(b) HAZ comparison

Fig.5.1.7. Predicted and experimental FZ and HAZ width fitting

5.1.3 Heat Power Density

Heat power density by FEA using Goldak's heat distribution model is compared with analytical results for 90 A current at 100 mm/min weld speed. Heat power density is the amount of heat concentrated on welded plate for a particular heat input. Fig. 5.1.8 shows the heat power density calculated using MATLAB.

Fig. 5.1.9 shows the heat power density profile comparison, in terms of weld nugget profile obtained by SYSWELD, MATLAB (analytical) and experimental results. It is calculated by MATLAB code, based on simple heat input calculations using double ellipsoidal heat source distribution, which are 33 W/mm^3 by MATLAB and 35 W/mm^3 by SYSWELD simulation.

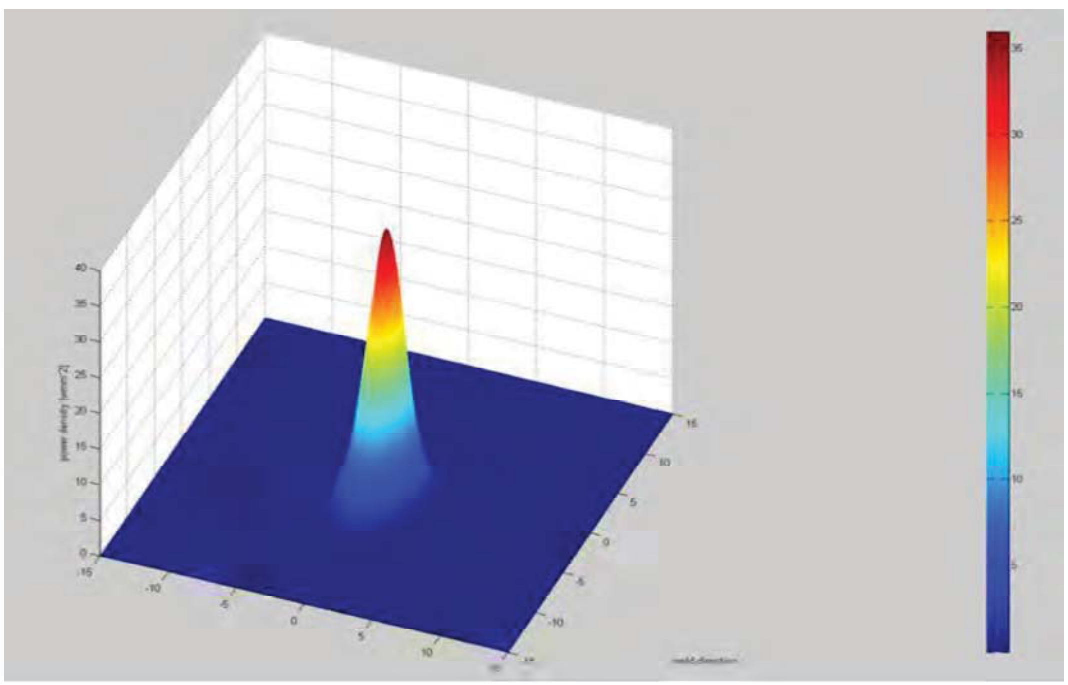

Fig.5.1.8. Heat source distribution calculation using MATLAB

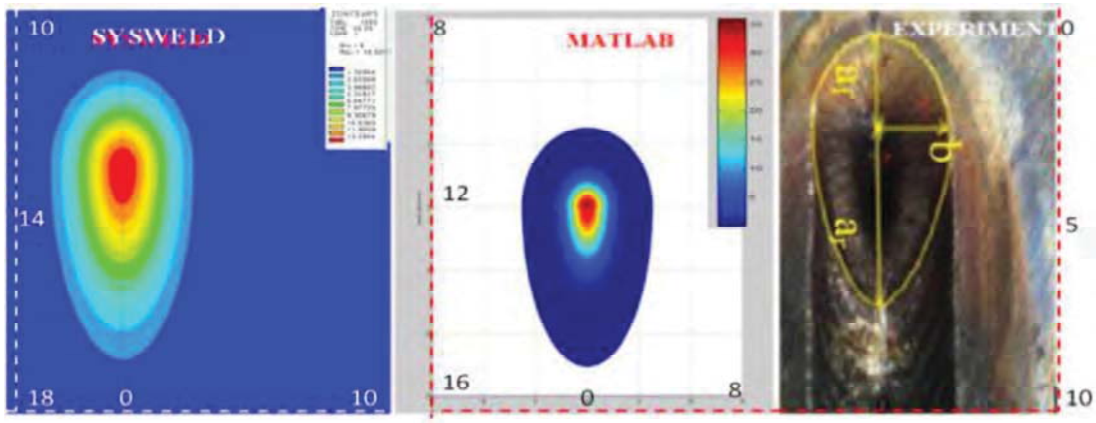

Fig.5.1.9. Heat power density comparison for autogenous weld

Table 5.1.1 Heat affected zone and fusion zone width of bead-on-plates

S. No	Current (A)	Voltage (V)	Weld speed (mm/min)	Weld length (mm)	Exp. FZ Width (mm)	Simulated FZ Width (mm)	Heat Input (J/mm)	Experimental HAZ (mm)	Predicted HAZ (mm)
1	110	12.6	60	15.6	8.9	9.4	1039	4.08	4.5
2	100	12	60	15	8.8	9.4	900	4.01	4.48
3	95	12	60	14.6	8.74	9.31	855	4.002	4.23
4	90	11.4	60	14.5	8.6	9.1	769	3.6	3.9
5	110	14.4	100	7.5	6.3	7.1	711	3.45	3.83
6	100	11.4	100	7	6.6	7.05	511	3.01	3.42
7	95	11.3	100	8	5.7	6.1	482	2.86	3.12
8	**90**	**10.6**	**100**	**6.8**	**5.2**	**6.1**	**428**	**2.61**	**2.86**
9	110	12.8	120	7.9	6	6.8	528	3.002	3.43
10	100	12.6	120	8.54	6.74	7.3	472	2.84	2.96
11	95	12	120	8	6	6.8	427	2.71	2.91

12	90	11.9	120	7.6	6.2	7.0	401	2.64	2.87
13	110	11.5	150	7.8	5.8	6.5	379	2.46	2.68
14	100	11	150	7.5	5.7	6.4	330	2.13	2.63
15	95	11.5	150	7.6	5.2	6.0	328	2.11	2.56
16	90	11	150	7.3	5.2	5.9	297	1.8	2.3

5.2. Thermo-Mechanical Analysis of Autogenous Weld

In this section, a detailed numerical study and its experimental validation of autogenous welding of modified 9Cr-1Mo steel is presented. Square butt joint of modified 9Cr-1Mo steel 3 mm thick plate of dimension 240 mm × 300 mm × 3 mm was prepared using autogenous welding process as shown in Fig. 5.2.1.

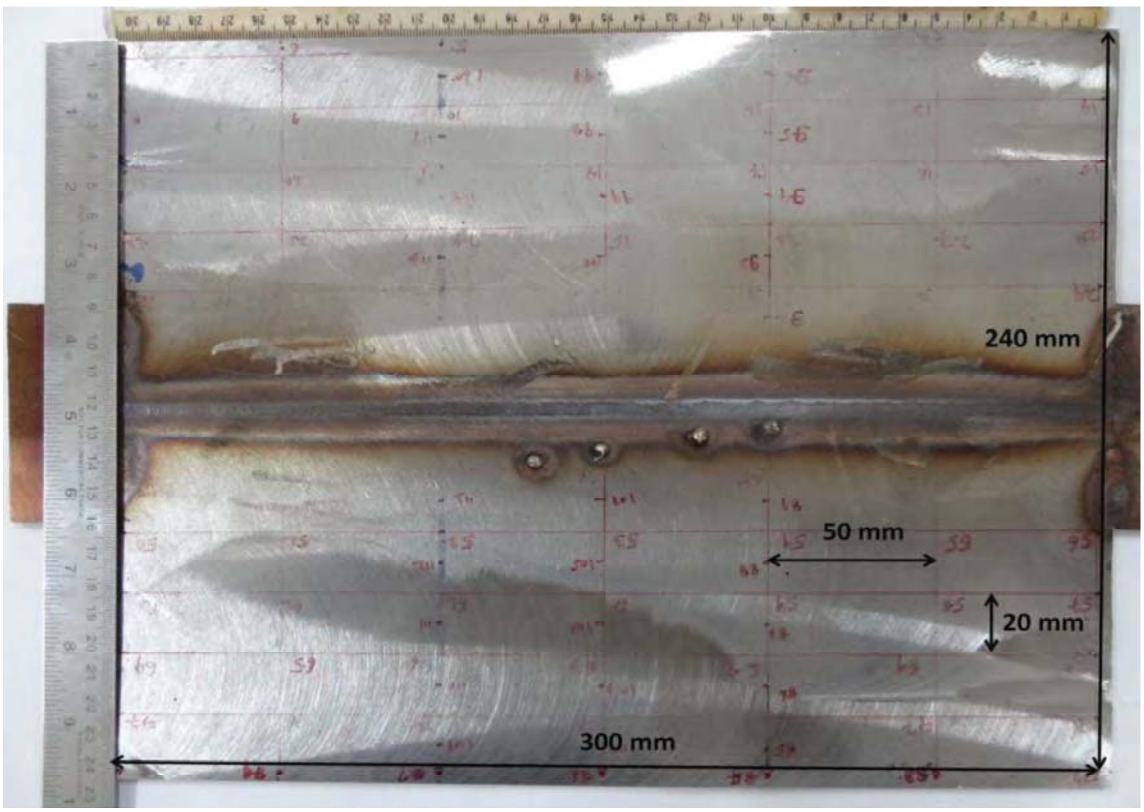

Fig.5.2.1. 3 mm thick square joint weld plate

In the developed computational approach coupled thermal, metallurgical and mechanical behavior was considered using SYSWELD software. SYSWELD is a welding and heat treatment computational software used for predicting thermal history, residual stress and distortion in weld plate using suitable heat source.

5.2.1. Heat Source Fitting

Heat source fitting is carried out based on experimentally measured double ellipsoidal parameters. Fig. 5.2.2 shows the comparison of weld and HAZ profile of predicted and experimental measurement at 90 A and 100 mm/min welding speed. As the predicted bead profile is close to the experimentally observed weld bead profile, this heat source fitting was employed in the thermo-mechanical analysis of weld joint.

Double ellipsoidal heat source parameters used for thermo-mechanical analysis for autogenous welding are given in Table. 5.2.1. Heat source fitting is carried out based on experimentally measured double ellipsoidal parameters as shown in Fig.5.1.2.

Table.5.2.1. Double ellipsoidal parameters for Autogenous welding

a_f	a_r	b	c	Weld efficiency in terms of %
3.8	5.7	2.8	3	75

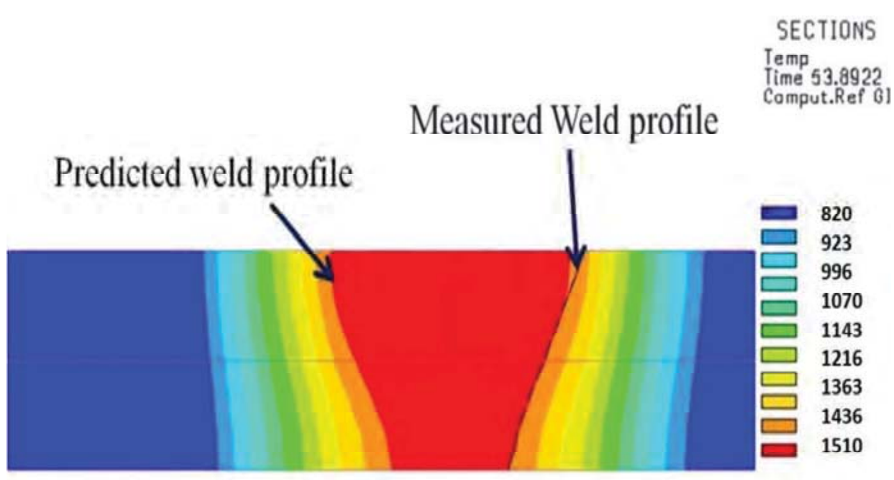

Fig.5.2.2. Heat Source Fitting of 3 mm thick plate autogenous weld

5.2.2. Thermal Analysis of Autogenous Welding

Thermal analysis is carried out using heat source fitting as an input. Fig. 5.2.3 shows the transient temperature distribution during the welding process. The welding was started at the run-in plate and completed in the run-out plate. A moving heat source model is applied to the top surface of weld center line by setting up a heat flux distribution which varies with time. The weld pad was allowed to cool down to room temperature after the completion of welding. Maximum predicted temperature reached during welding is 1613°C, which is higher than melting point of modified 9Cr-1Mo steel.

Double ellipsoidal heat source distribution is clearly visible in thermal analysis of welding as shown in Fig. 5.2.4, liquidous temperature is kept as 1510°C (pink color).

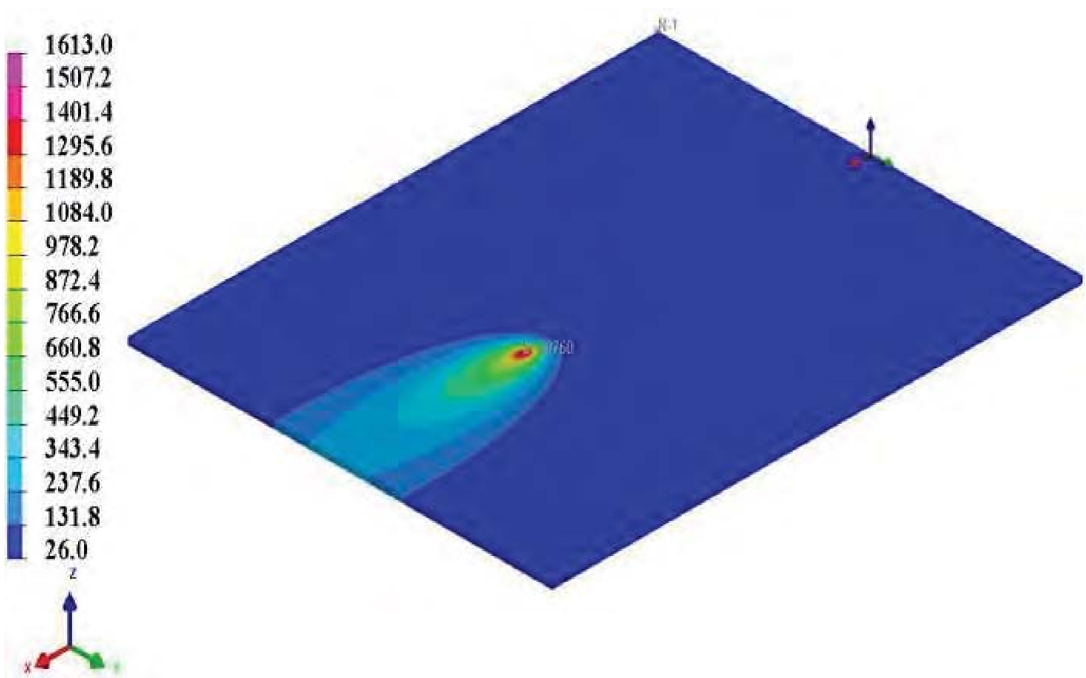

Fig.5.2.3. Thermal Analysis of 3 mm thick plate autogenous weld

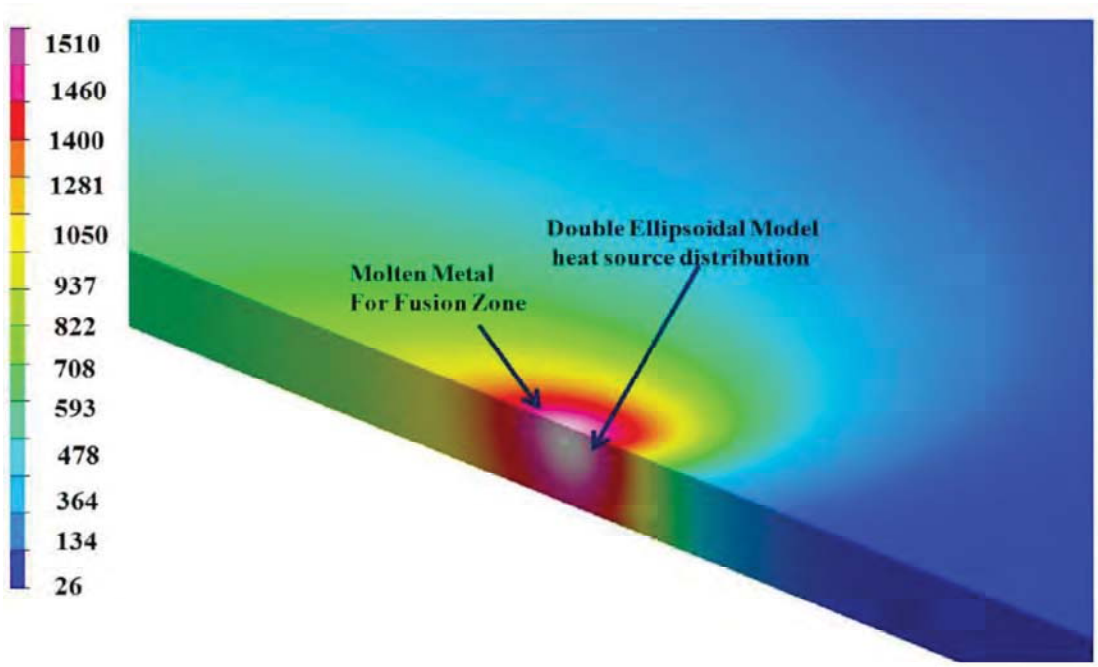

Fig.5.2.4. Thermal Analysis showing temperature distribution for 3 mm thick plate autogenous weld

Fig. 5.2.5 shows the temperature distribution on the top of weld plate at different locations along the weld line is plotted for different locations. When heat source comes in its contact node along the weld line it is heated to its peak temperature up to 1613°C, it starts cooling once heat source moves further and during welding the peak temperature remains same for each node along the weld line. The quasi-steady state condition produces almost same peak temperature at different location along the center line of the weld in the plate during welding as shown in Fig. 5.2.5. It is noticed that the heating rate is higher than the cooling rate because of the accumulation of heat in front of heat source.

Fig. 5.2.6 shows temperature distribution on top surface of weld plate in transverse direction. There is nonlinear variation in temperature at different locations from weld line because of local heating by welding torch and non-linear variation of thermal properties of weld plate. As shown in Fig. 5.2.6 the temperature was distributed and decreased towards room temperature.

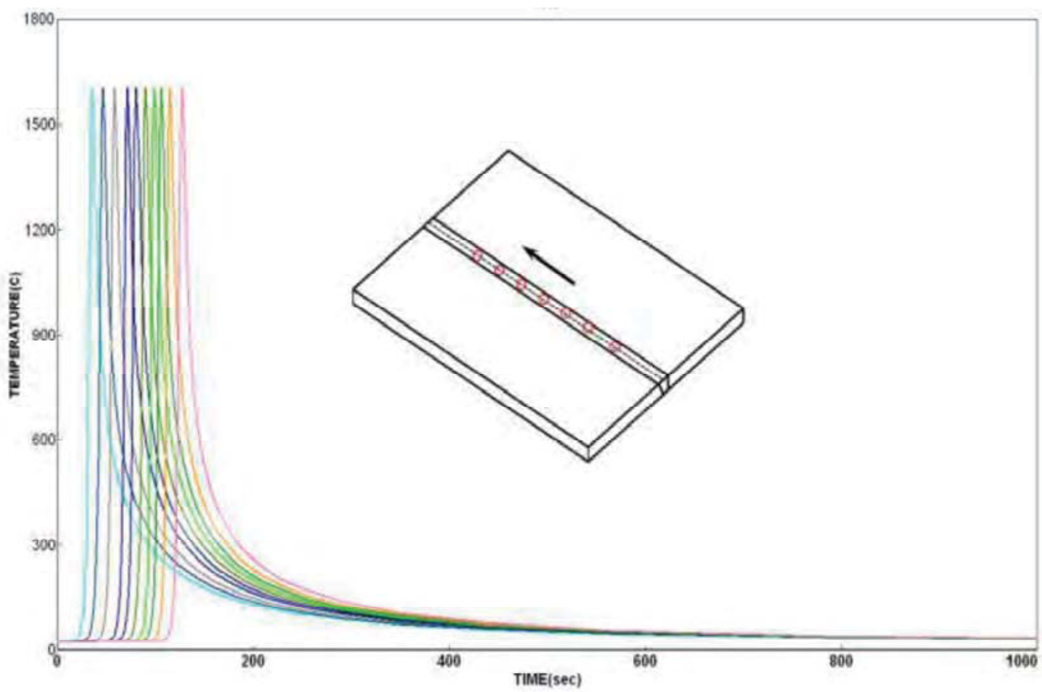

Fig.5.2.5. Predicted thermal cycle at different locations along weld center line for 3 mm thick plate autogenous weld

Comparison of predicted thermal cycles and recorded by the thermocouple at three different locations from the weld center line are shown graphically in Fig. 5.2.7 (a-c). Each thermocouple has attained its peak temperature when the arc has passed over the thermocouple line. The peak temperature for 10 mm distance from weld center line measured by thermocouple is 620°C and by FEA is 630°C, only 10°C difference is observed. Similarly, for 12 and15 mm distance temperatures are 493°C and 412°C by thermocouple and corresponding temperature predicted from FEA are 518°C and 434°C respectively with 5.9% and 4.5% difference between the measured and predicted values. Thus, the results of FE analysis closely follow the experimental measurements. It is also seen that the heating and cooling periods of test data are in very close agreement with double ellipsoidal heat source model.

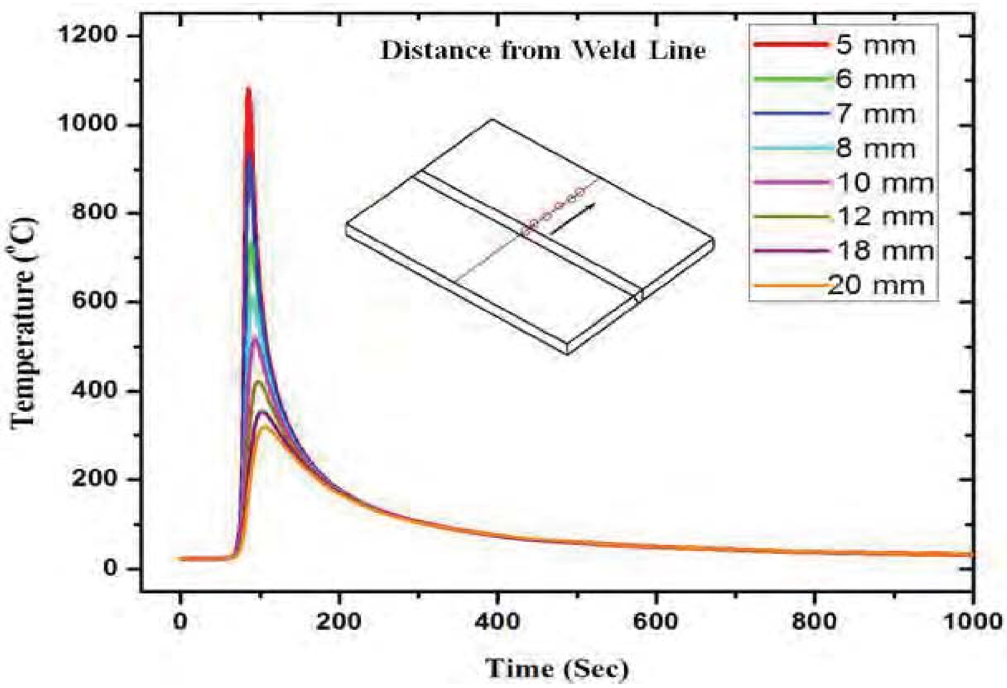

Fig.5.2.6. Predicted thermal cycle at different locations in transverse direction for 3 mm thick plate autogenous weld

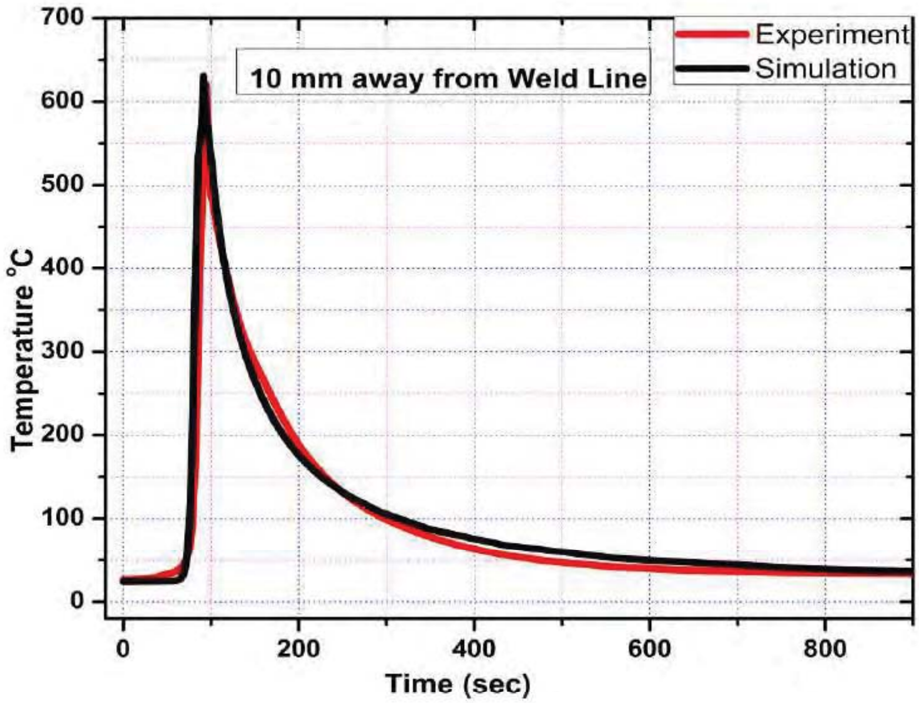

(a) At 10 mm location from weld center line

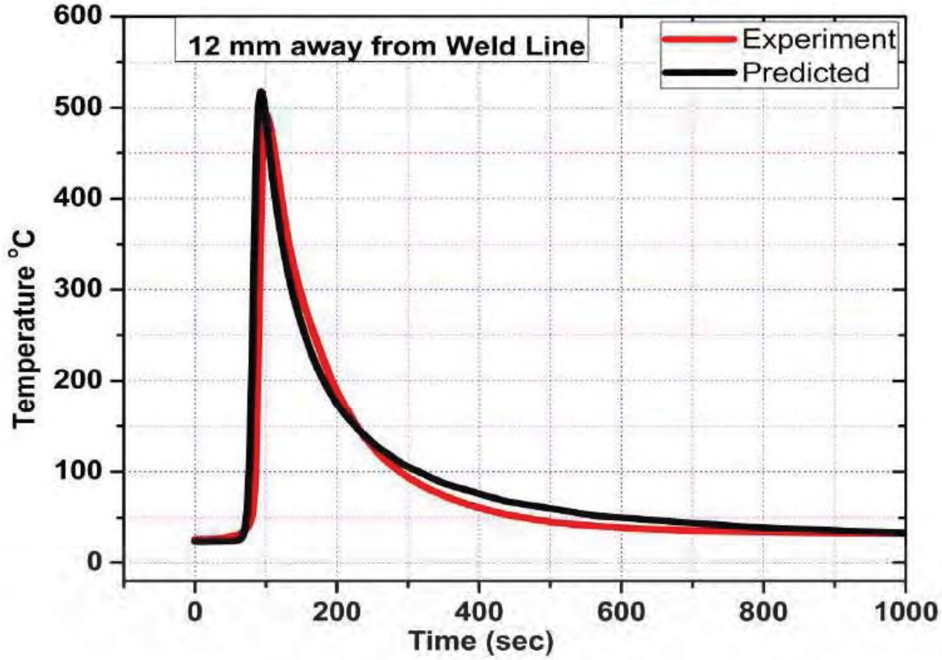

(b) At 12 mm location from weld center line

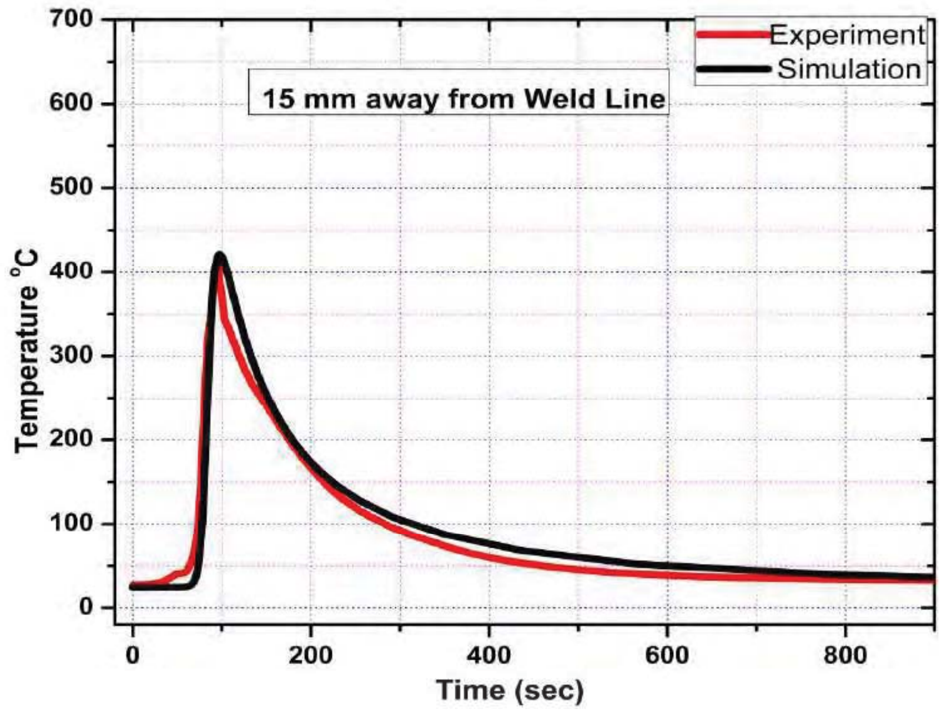

(c) At 15 mm location from weld center line

Fig.5.2.7. Thermal cycle comparison for 3 mm thick plate autogenous weld

5.2.3. Residual Stress Analysis of Autogenous welding

The validated temperature distribution is given as an input thermal load for mechanical analysis for prediction of residual stress and distortion. Modelling for 3 mm thick autogenous weld was carried out using two different material data-base, with and without considering the phase transformation. For prediction made with phase transformation, properties of austenite, ferrite and martensite and the transformation temperatures for these phases were considered separately. For the case of without phase transformation only initial phase ferrite is considered.

Fig. 5.2.8-5.2.9 shows the predicted longitudinal stress in 3 mm thick plate considering without and with phase transformation effect respectively. It can be seen that the tensile stresses are present in the weld zone when plate is cooled to atmospheric temperature. Residual stress profile across weld joints exhibited tensile nature at the region close to weld line and compressive stress away from weld line. During heating the central region expands, but this expansion is resisted by adjacent zone. During cooling weld region contracts, and it experience more restraint due to joining of the two plates and being at high temperature, the weld zone often deforms plastically. Away from the weld zone, residual stresses would be compressive to balance the tensile stresses present in the weld zone. This is typically the distribution of residual stress, if phase transformation is not considered, which is shown in Fig. 5.2.8. The peak value of tensile residual stress appears at the region of fusion zone and HAZ. In contrast, if phase transformation is considered, peak residual stress is not in the fusion zone, but in HAZ as shown in Fig. 5.2.9. Peak value of longitudinal residual stress is tensile in nature and value is 560 MPa and 635 MPa for the case with and without considering phase transformation respectively.

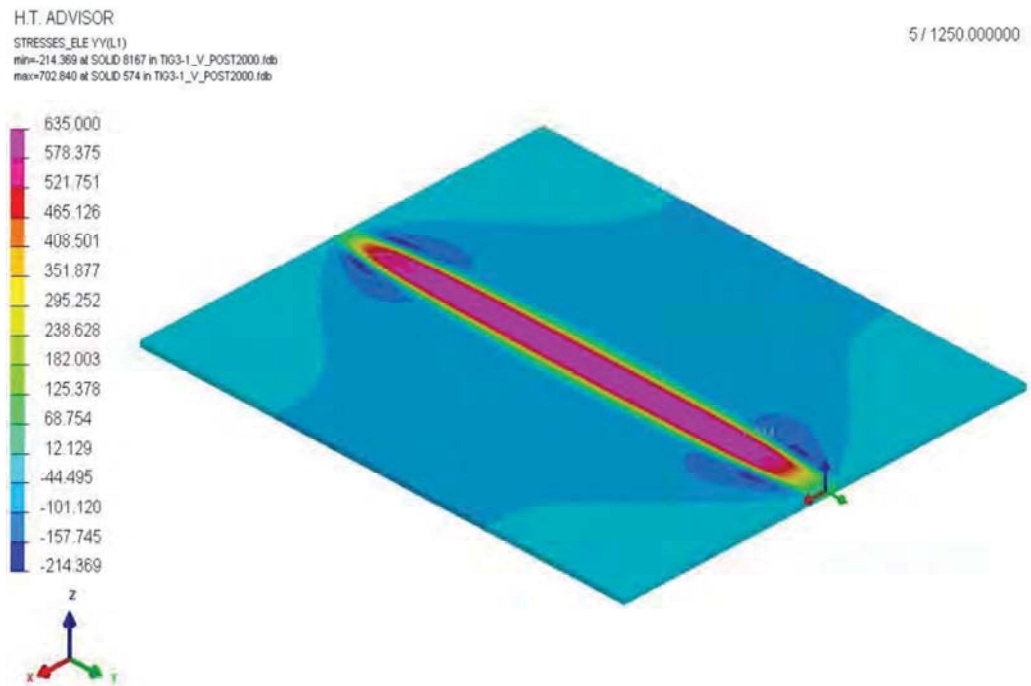

Fig.5.2.8. Residual stress analysis without considering phase transformation for 3 mm thick plate autogenous weld

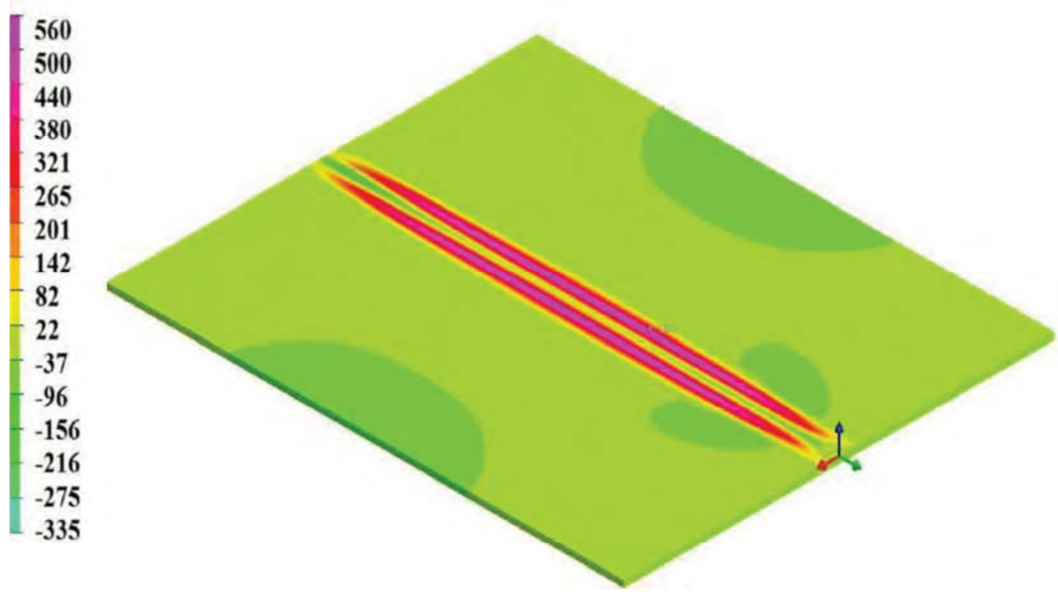

Fig.5.2.9. Residual stress analysis considering phase transformation for 3 mm thick plate autogenous weld

Finite element analysis results of longitudinal stress distribution in transverse direction (with and without phase transformation) are compared with experimentally measured results of residual stress Fig. 5.2.10. The solid symbols are the average of the multiple values of residual stresses measured at one point and scatter in the measurements is shown separately as scatter bands. The residual stress distribution predicted after considering phase transformation is in good agreement with the experimental results obtained.

Residual stress profile is of typical 'M' shape. This is in agreement with the results reported in the literature for welds of this steel produced by EB [25], laser [18] and GTA [2] processes. The 'M' shaped profile is the result of compressive residual stresses generated during phase transformation (martensite) dominating the shrinkage residual stresses generated during cooling cycle. For different welding process of modified 9Cr-1Mo steel, similar type of longitudinal residual stress profile is reported in literature [1-5, 16-19]. The measured maximum tensile stress value is observed at 10 mm from weld center line 542 MPa while predicted residual stress value for same location is 560 MPa and this stress value is decreased rapidly to 220 MPa at weld center line, where as in case of without phase transformation it predicted to be 635 MPa.

It is clear that martensitic transformation shall be considered in the modelling for a reasonable prediction of the residual stress distribution across the weld joint. Measured residual stress at weld line is 269 MPa, which is less than that obtained for HAZ. This change in stress profile is due to austenite to martensitic transformation which takes place at low temperature range (375-200°C) which is accompanied by expansion in contrast to contraction that take place for the weld while cooling after welding.

Numerically predicted longitudinal stress considering without phase transformation are larger than the one predicted considering phase transformation and then that measured experimentally. This shows that the phase transformation from austenite to martensite, especially the volume changes associated with it has a significant influence on residual stress distribution at the end of cooling. Volume changes associated with transformation can largely nullify the accumulated tensile stresses caused by contraction that accompany cooling of the weld. It is concluded based on this simulation, that thermo-mechanical analysis without considering phase transformation gives higher stress value, which significantly differs from actual stress present in the weld joint Nature of residual stress predicted by simulation carried out with and without considering phase transformations is matching with experimentally measured value in HAZ, but in fusion zone there is large difference observed for the values predicted with and without considering phase transformation. Hence for accurate simulation of modified 9Cr-1Mo steel welding, phase transformation effects should be considered in material data base properties.

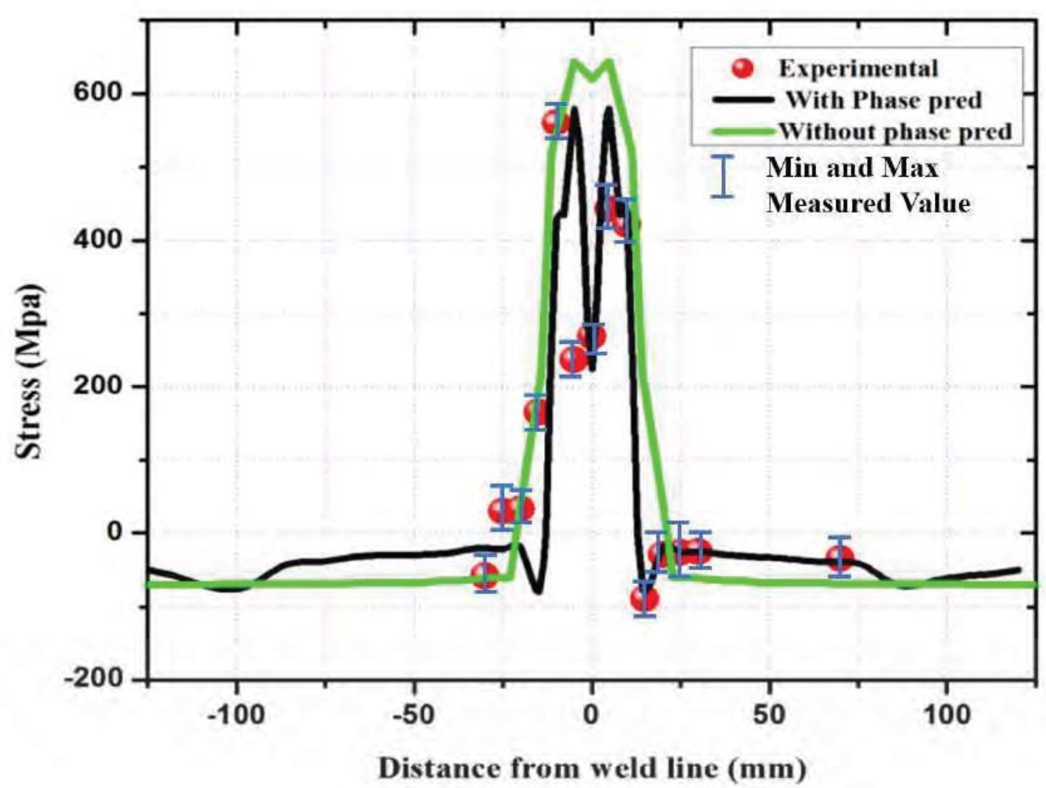

Fig.5.2.10. Residual stress comparison for 3 mm thick plate autogenous weld

5.2.4. Hardness Measurement

Typical microstructures of weld metal, HAZ and base metal of 3 mm thick square butt joint plate weld made with a current of 90 A are shown in Fig. 5.2.11 (a). The grain size in weld zone and HAZ zone changes during welding, because of heat input and thermal cycles and transformation.

Fig.5.2.11 (b) shows the measured Vickers's hardness plotted at 7 different locations for both sides of weld at 2.5 to 10 mm distance from weld line. Large variation in hardness is noticed from weld metal (503 Hv) to HAZ (447 Hv) and to base metal (283 Hv). The hardness value in HAZ and weld metal is higher than that of the base metal due to martensitic structure of weld metal and HAZ formed during weld thermal cycles experienced by these zones.

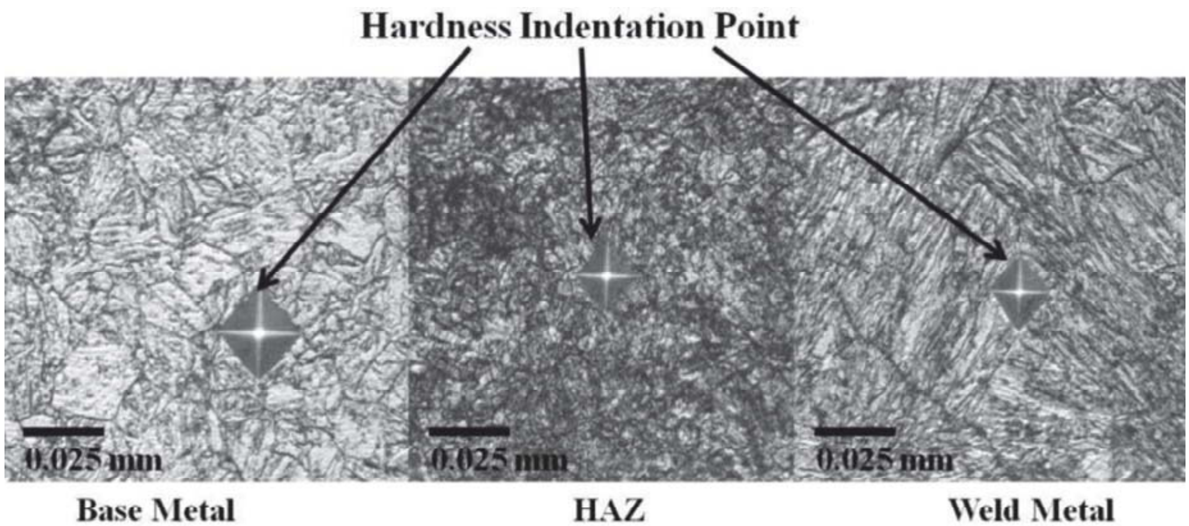

(a) Microstructure at different location

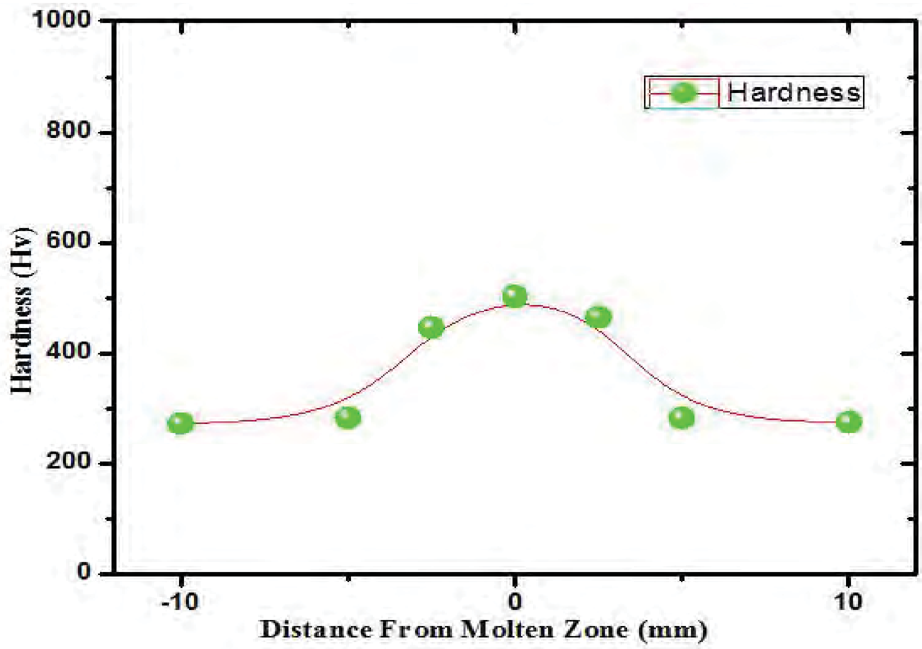

(b) Micro-Vickers's Hardness

Fig.5.2.11. Hardness measurement for 3 mm thick plate autogenous weld

5.2.5. Distortion Analysis of Autogenous welding

Distortion (vertical displacement) of a thin plate is predicted in the present analysis by applying both small and large displacement theory with non-linear geometry also taken in to account. According to large displacement theory equations related to strain and displacements are essential to describe the buckling behavior and this kind of nonlinear response is considered as a stability problem. If small displacement is assumed, then strains are given as a linear function of displacement. In large displacement theory non-linear relationship between strain and displacement is considered, Green-Lagrange strain which is second order function of the displacement is given by Eq. (5.2.1). The first order term represents the linear response behavior; second order term is essential to nonlinear behavior utilizing the large distortion theory as given in Eq. (5.2.1-5.2.2). [20-23]

$$\varepsilon_x = \frac{\partial u}{\partial x} + \frac{1}{2}\left\{\left(\frac{\partial u}{\partial x}\right)^2 + \left(\frac{\partial v}{\partial x}\right)^2 + \left(\frac{\partial w}{\partial x}\right)^2\right\}$$

$$\varepsilon_y = \frac{\partial u}{\partial y} + \frac{1}{2}\left\{\left(\frac{\partial u}{\partial y}\right)^2 + \left(\frac{\partial v}{\partial y}\right)^2 + \left(\frac{\partial w}{\partial y}\right)^2\right\} \tag{5.2.1}$$

$$\varepsilon_z = \frac{\partial u}{\partial z} + \frac{1}{2}\left\{\left(\frac{\partial u}{\partial z}\right)^2 + \left(\frac{\partial v}{\partial z}\right)^2 + \left(\frac{\partial w}{\partial z}\right)^2\right\}$$

$$\gamma_{xy} = \frac{\partial u}{\partial y} + \frac{\partial v}{\partial x} + \left\{\left(\frac{\partial u}{\partial x}\right)\left(\frac{\partial u}{\partial y}\right) + \left(\frac{\partial v}{\partial x}\right)\left(\frac{\partial v}{\partial y}\right) + \left(\frac{\partial w}{\partial x}\right)\left(\frac{\partial w}{\partial y}\right)\right\}$$

$$\gamma_{yz} = \frac{\partial v}{\partial z} + \frac{\partial w}{\partial y} + \left\{\left(\frac{\partial u}{\partial y}\right)\left(\frac{\partial u}{\partial z}\right) + \left(\frac{\partial v}{\partial y}\right)\left(\frac{\partial v}{\partial z}\right) + \left(\frac{\partial w}{\partial y}\right)\left(\frac{\partial w}{\partial z}\right)\right\}$$

$$\gamma_{xz} = \frac{\partial u}{\partial z} + \frac{\partial w}{\partial x} + \left\{\left(\frac{\partial u}{\partial x}\right)\left(\frac{\partial u}{\partial z}\right) + \left(\frac{\partial v}{\partial x}\right)\left(\frac{\partial v}{\partial z}\right) + \left(\frac{\partial w}{\partial x}\right)\left(\frac{\partial w}{\partial z}\right)\right\} \tag{5.2.2}$$

Where $\mathcal{E}_x$, $\mathcal{E}_y$ and $\mathcal{E}_z$ are normal Green Lagrange strain in *x, y* and *z* directions respectively γ_{xy}, γ_{yz} and γ_{xz} are shear Green-Lagrange strain on the *x-y, y-z* and *z-x* plane. *u, v* and *w* are the displacement in the *x*, *y* and *z* direction respectively.

Fig. 5.2.12 shows the predicted distortion in weld plate using finite element analysis. In order to present distortion profile similar to experimental measured weld plate, meshing of run-in-plate and run-out-plate was added. At the end of weld maximum displacement produced is 0.6 mm as shown in Fig. 5.2.12 (a), at this stage plates are in clamped condition. Similarly, just after removal of clamping it increased to 2.1 mm as shown in Fig. 5.2.12 (b). After removal of clamp and plate temperature came down to room temperature after 7200 s, maximum displacement in longitudinal direction is enhanced to 3.88 mm as shown in Fig. 5.2.12 (c).

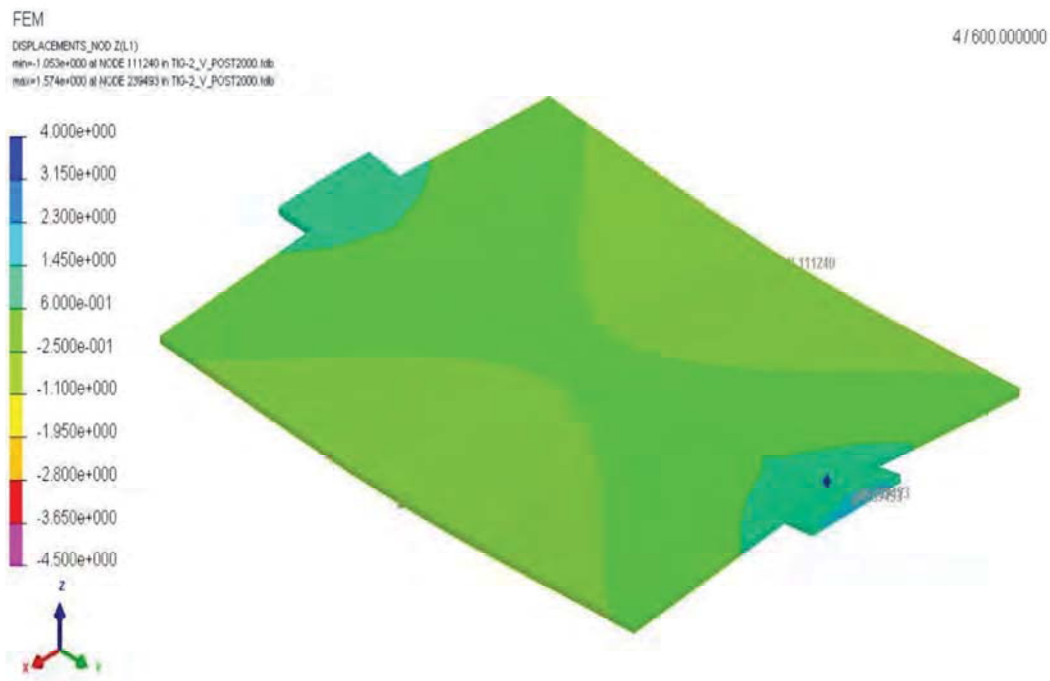

(a) Just at the end of welding

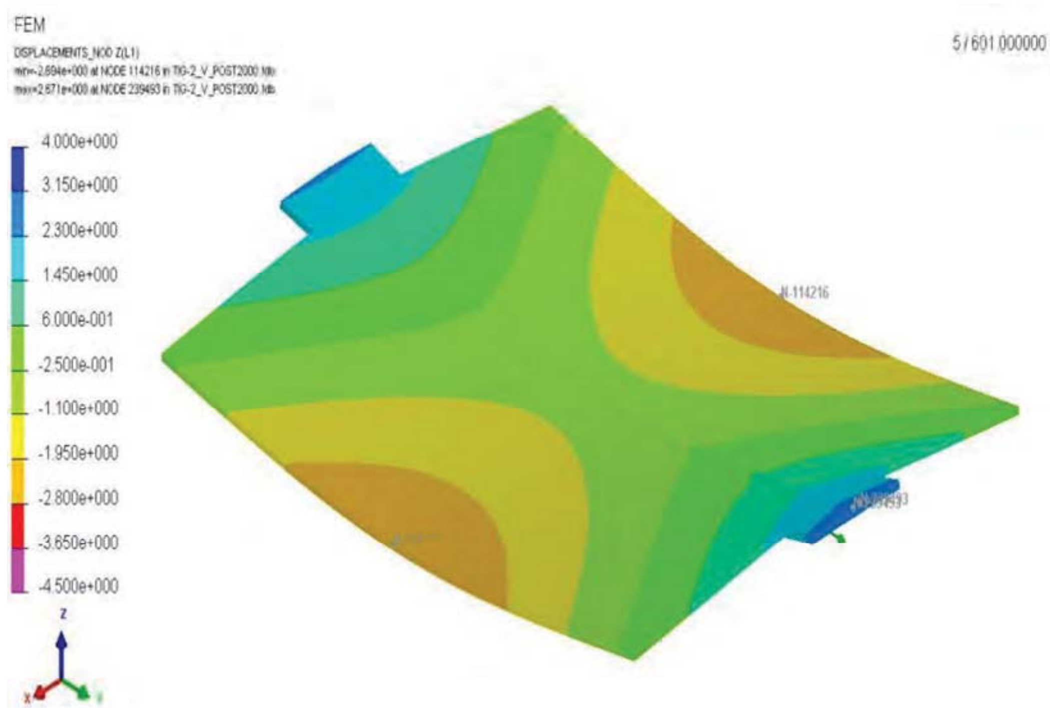

(b) At the removal of clamp

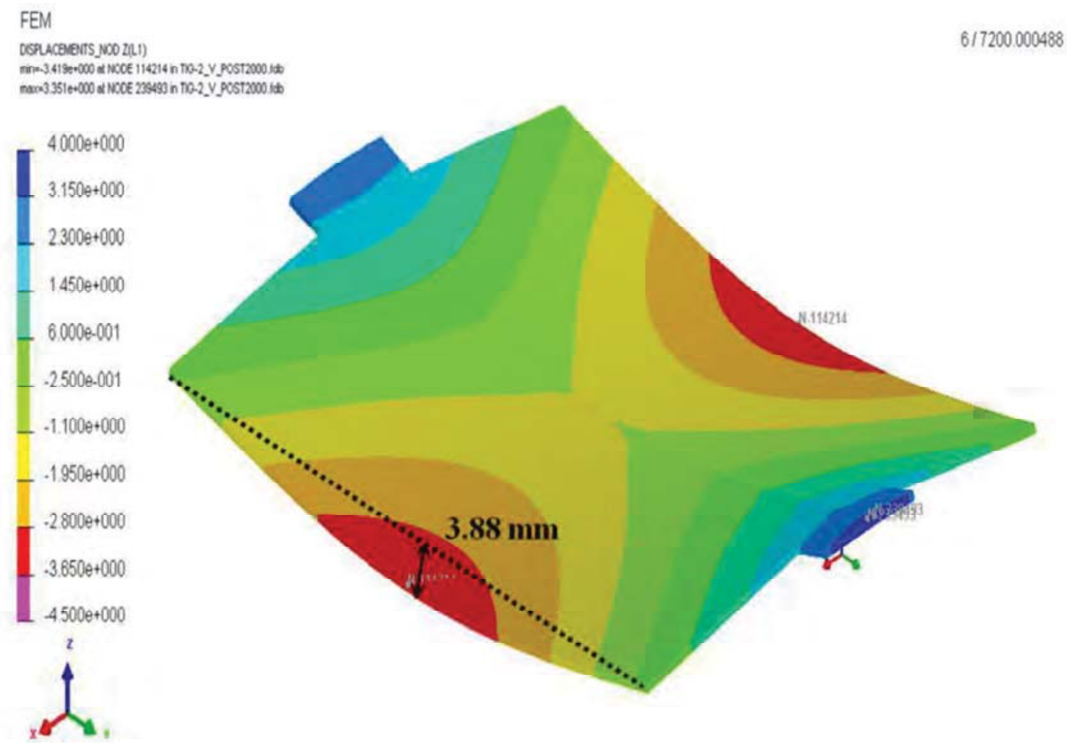

(c) After cooled down to room temperature

Fig.5.2.12. Predicted distortion for 3 mm thick plate autogenous welds

During welding of thin plate, temperature gradient across the thickness is negligible, so out of plane distortion in weld plate is not produced. But at the end of welding and after removal of clamp with plate cooled down to room temperature, peak displacement occurs in weld plate as shown in Fig. 5.2.12 (c). For transverse direction simulated distortion result is showing out of plane distortion at the end of welding and after plate cooled up to room temperature, this type of distortion is produced because of compressive residual stress trying to balance tensile stresses around weld line.

Vertical displacement induced in autogenous weld plate after cooling down to room temperature in different direction is shown in Fig. 5.2.13. Vertical displacement is measured using electronic height gauge over grids and plotted as a three-dimensional distortion profile using origin software as shown in Fig. 5.2.14.

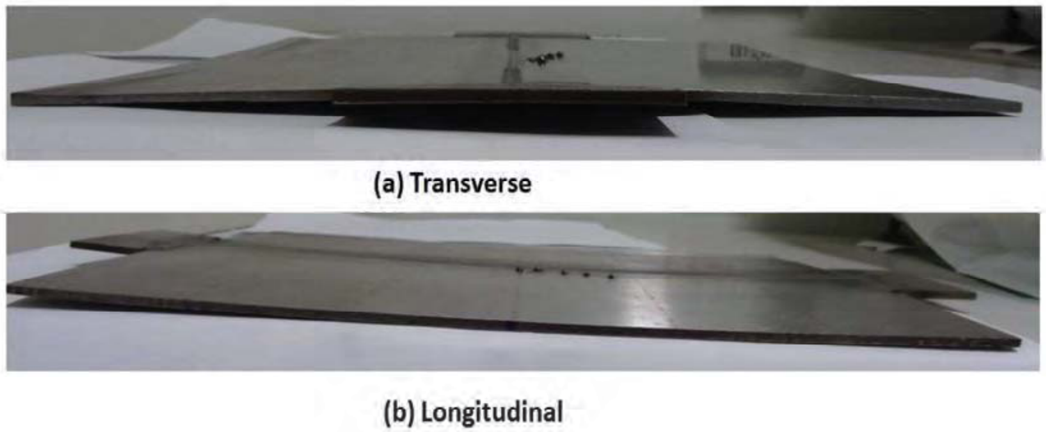

Fig.5.2.13. Vertical displacement in different direction for 3 mm thick plate autogenous weld

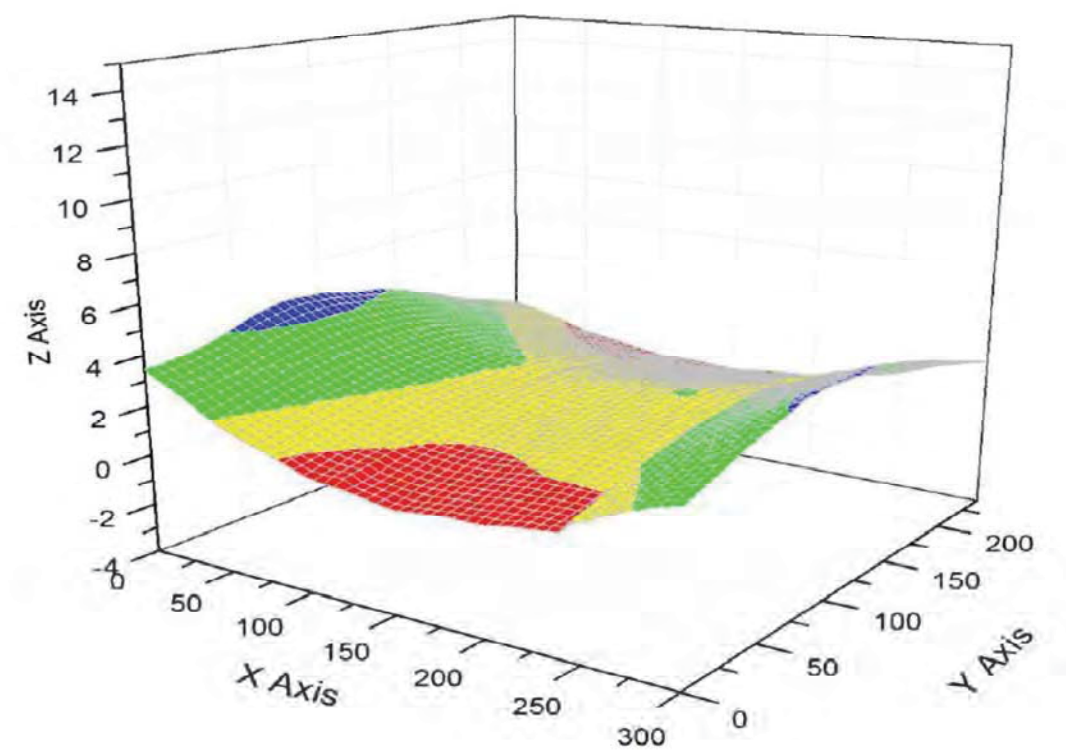

Fig.5.2.14. 3D experimental measured displacement in 3 mm thick plate autogenous weld

In finite element analysis, if large displacement theory is not employed, the buckling type distortion produced by compressive stress can't be predicted [21-23]. Fig. 5.2.15 shows the negligible out of plane distortion produced around the weld using small displacement theory by accumulation of in-plane shrinkage. For the same heat input and Gaussian distribution parameters (Fig. 5.2.12 (c)) shows the distortion produced in welded plate considering large displacement theory, maximum vertical displacement produced at centre of weld plate is 3.88 mm for same location 0.26 mm distortion obtained using small displacement theory in FEA. Simulated distortion result is showing out of welding distortion at the end of welding and plate cooled up to room temperature, this type of distortion is produced because of compressive residual stress trying to balance tensile stresses around weld line.

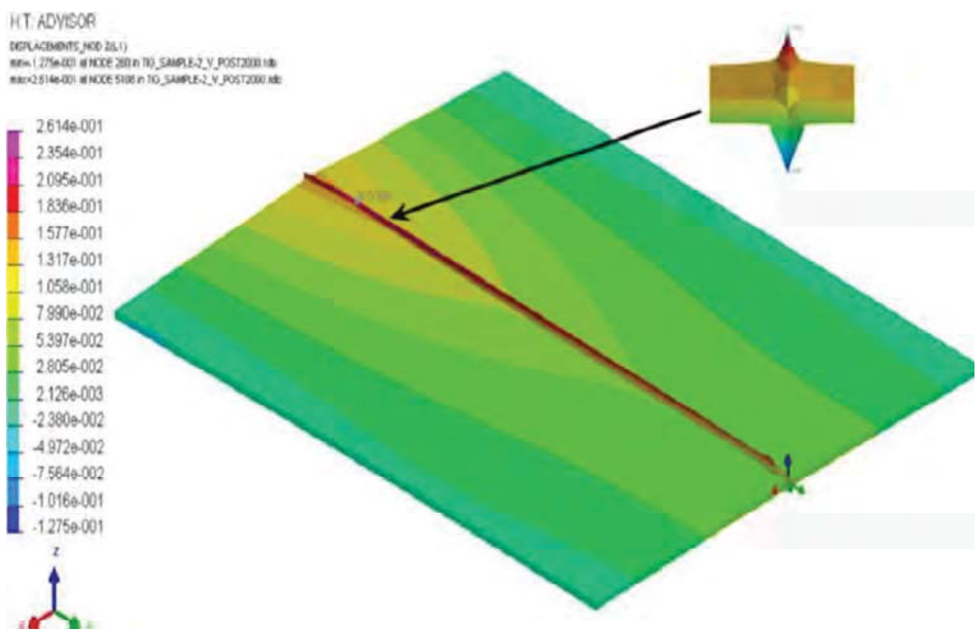

Fig.5.2.15. Predicted distortion using small displacement theory

Predicted distortion (vertical displacement) is further compared with experimental distortion in longitudinal and transverse direction as shown in Fig. 5.2.16. Displacement measured at corner of weld plate line is in longitudinal direction (parallel to weld line) and in transverse direction (perpendicular to weld line). Displacement in weld plate is plotted in such a way that, bottom of weld plate is considered as a reference point. Fig. 5.2.16 (a-b) shows deflection (in Z direction) of weld plate after cooling down to room temperature, by considering large displacement theory (nonlinear geometry) and small displacement theory (linear geometry) at two different locations. Results shows maximum vertical displacement occurs at the weld clamped location (corner of plate), whereas minimum occurs at mid length of weld plate. The numerical results predicted by large displacement theory matches with experimental results, whereas the vertical displacement result predicted using small displacement theory is significantly lower than the experimental results. The trend of deflection curve is similar as in experimental and simulation results.

Fig. 5.2.16 (a) shows vertical displacement results comparison in longitudinal direction at corner of weld plate. Maximum vertical displacement obtained experimentally is 3.5 mm, while vertical displacement obtained by large displacement theory is 3.88 mm which is nearer to experimental values. Whereas numerically obtained maximum vertical displacement using small displacement theory is 0.3 mm, which is 10 times smaller than former one. Maximum vertical displacement produced at weld line in transverse direction is 5.2 mm and predicted using large displacement theory is 4.9 mm, whereas small displacement theory it is 0.4 mm, which is 12 times smaller than former one as shown in Fig. 5.2.16 (b).

It may be noted that for prediction of distortion of weld joints presented above, material data base that considers phase transformation is used. Prediction was also done using data base that does not consider phase transformation. However, not much difference is found in the distortion of the autogenous welds of 3 mm thickness with both the predictions. Hence, results obtained with the use of material data base that considers phase transformation alone is presented here.

Based on above results, it is clear that prediction of thermal cycles, residual stress and distortion of autogenous GTA welds of 3 mm thick modified 9Cr-1Mo steel using the FEM model are reasonably accurate. Results also confirm that data base which considers phase transformation should be used for accurate prediction of residual stress for the weld joints. It is also shown that distortion of the weld joints is predicted more accurately with the model considering large displacement theory than that considers small displacement theory.

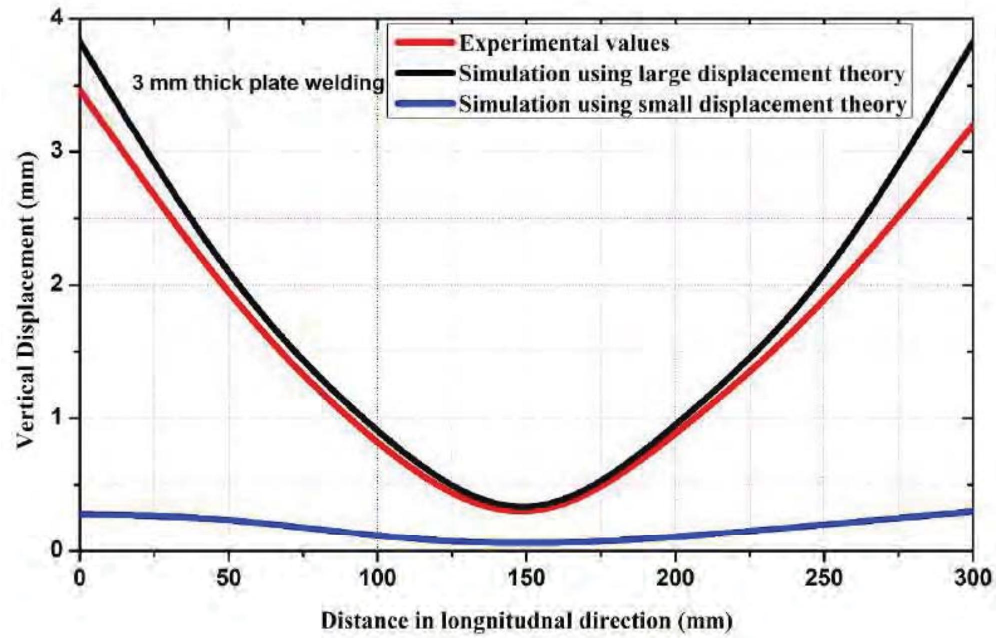

(a) Longitudinal direction

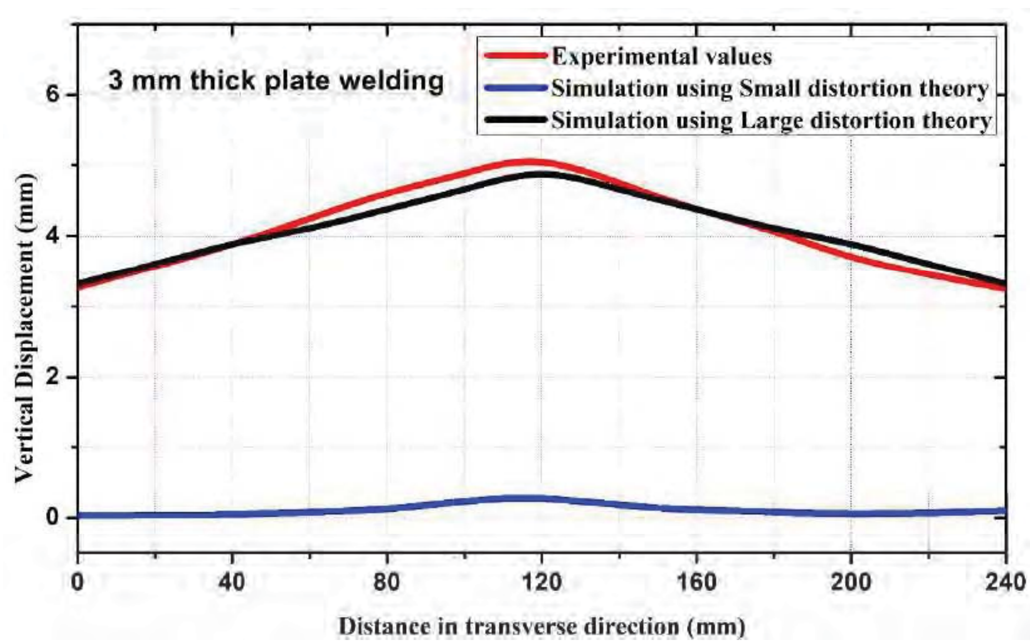

(b) Transverse direction

Fig.5.2.16. Vertical displacement comparison for 3 mm thick plate autogenous weld

5.3. Thermo-Mechanical Analysis of Multi-pass Welding

In this section, a detailed numerical study and its experimental validation of multi-pass welding of modified 9Cr-1Mo steel is presented. For distortion analysis, numerical modelling of multi-pass welding is carried out using 2D and 3D (coarse and fine) mesh models. The weld joints were prepared using 6 mm thick modified 9Cr-1Mo steel plates of dimension 240 mm × 300 mm × 6 mm was prepared using manual GTA welding process as shown in Fig. 5.3.1

Fig. 5.3.2 shows the weld cross section of the multi-pass welds of modified 9Cr-1Mo steel. In order to obtain the welding heat input (the ratio of welding power to the welding speed) and weld bead profile, the experimental trials were conducted before numerical modelling. Heat input values obtained from the experimental trials and actual weld bead profile were used as inputs for simulation. Then simulation was performed in two steps, the heat source parameters were calibrated initially, followed by the thermo-mechanical welding simulation.

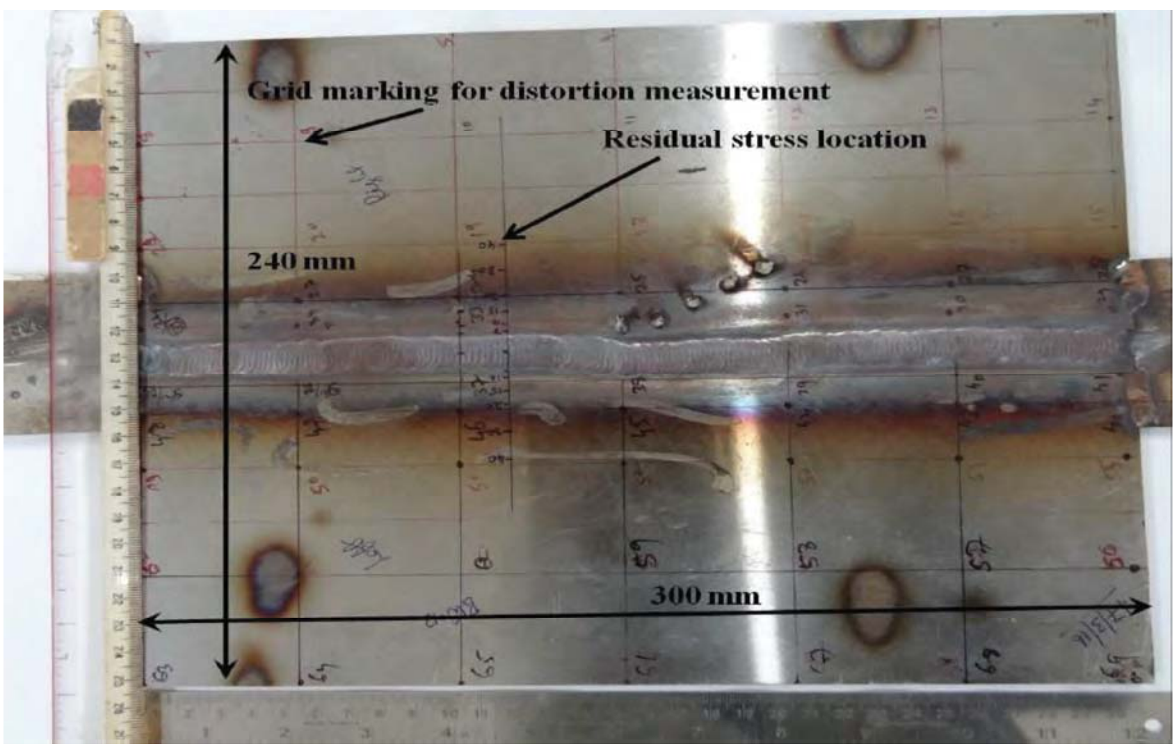

Fig.5.3.1. Multi-pass weld plate

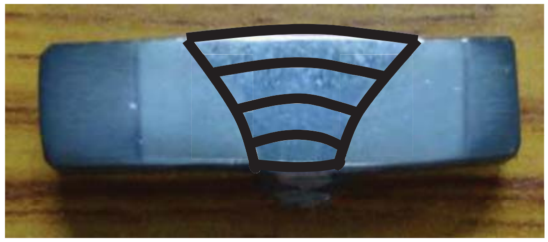

Fig.5.3.2. Weld profile of multi-pass weld

5.3.1. Heat Source Fitting of Multi-pass welding

Weld pool was represented using double ellipsoidal heat source model. The heat source parameters were calibrated such that the simulated macrograph matches the experimentally obtained weld bead profile as discussed in autogenous weld plate case. Finally, using the calibrated heat source parameters, the thermo-mechanical analysis of welding was carried out.

The heat source model parameters adjusted as per experimental weld profile. Fusion boundary weld profile was an output of heat source fitting analysis. During this analysis, the initial temperature of the component was considered at 26°C. The double ellipsoid heat source parameters as given in Table 5.3.1 and the arc efficiency parameter for heat input estimated from the welding parameters was iteratively adjusted till the fusion zone shape was similar to actual weld profile. Fig. 5.3.3 shows the results of heat source fitting carried out for each pass of multi-pass welding.

Table.5.3.1. Double ellipsoidal parameters for multi-pass welding

Plate	a_f	a_r	b	c	Weld efficiency in terms of %
6 mm	3.8	5.5	4	3	68

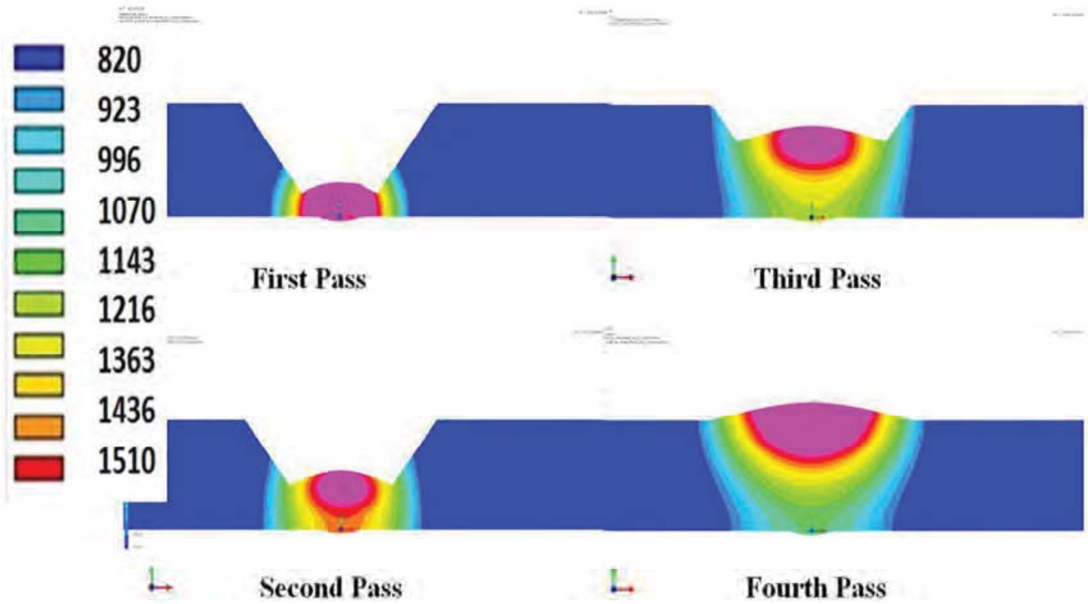

Fig.5.3.3. Heat source fitting for each pass of multi-pass welding

Weld profile and width of HAZ was measured using optical microscope. Predicted weld profile based on heat source fitting is compared with experimental measured profile as shown in Fig. 5.3.4. An experimentally measured value for weld width at the top side is 18 mm and combined width of fusion zone with HAZ on either side is 28 mm. The corresponding values predicted from HSF are 16.5 mm and 26.8 mm respectively. Based on this result it is concluded that the heat source model is reasonably accurate.

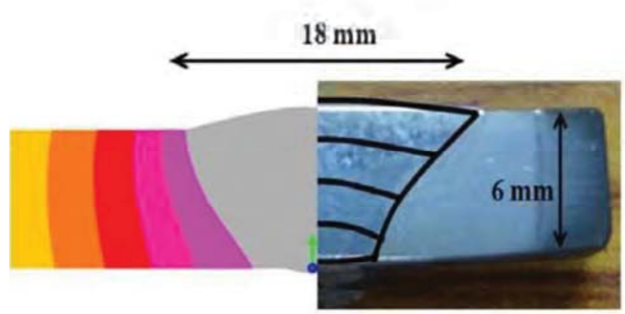

Fig.5.3.4. Heat source fitting comparison for multi-pass welding

5.3.2. Thermal Analysis of Multi-pass welding

Based on heat source analysis, thermal analysis of multi-pass welding is carried out. Fig. 5.3.5 shows the thermal analysis of final pass of modified 9Cr-1Mo steel multi-pass GTA welding analysis for fine meshed model. Peak temperature reached in thermal analysis is 1860°C, which is above melting point of modified 9Cr-1Mo steel.

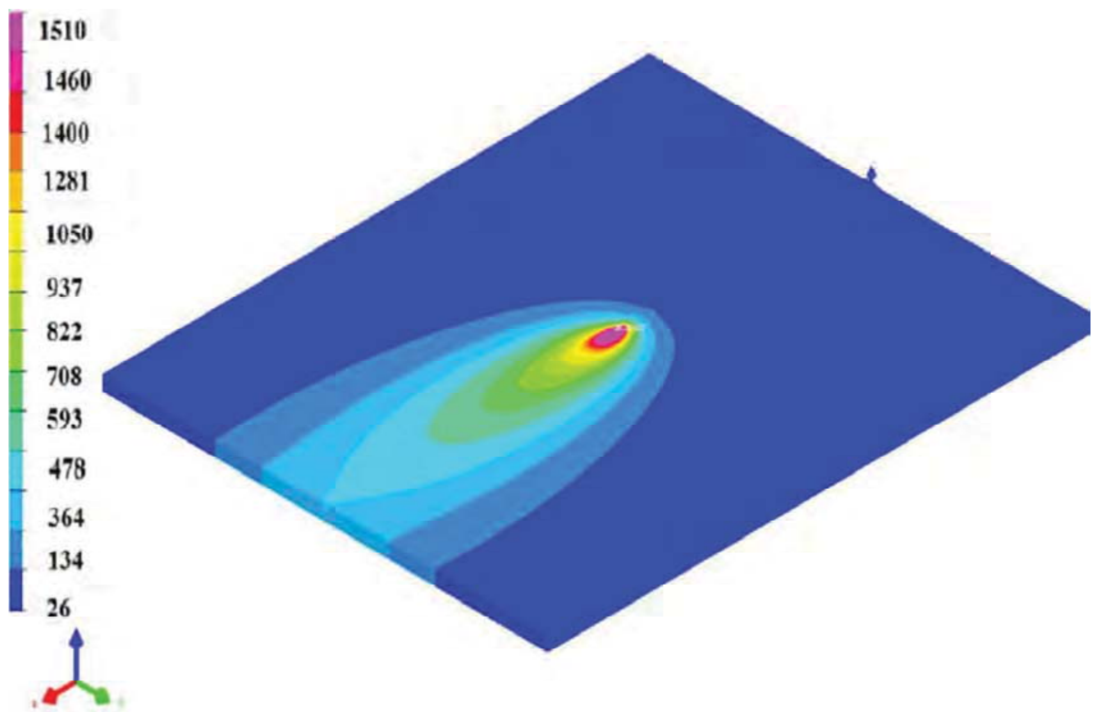

Fig.5.3.5. Thermal analysis of 6 mm thick weld plate

Predicted thermal cycles at 10 mm away from weld line is compared with thermal cycles measured using K type thermo-couple as shown in Fig. 5.3.6. This comparison shows that there is good agreement in peak temperature values for all the four passes for both the 3D fine and coarse meshed models. Fast cooling rate is observed in case of coarse meshed model as compared to fine meshed model. Peak value for first and second pass is deviated within 16°C and 18°C due to difficulties in modeling the complex weld shape. Corresponding deviations in the peak temperatures for third and fourth passes are only 5°C and 8°C respectively.

Consequently, the validated thermal cycles were given as an input thermal load for further mechanical analysis for prediction of residual stress and distortion in weld plates.

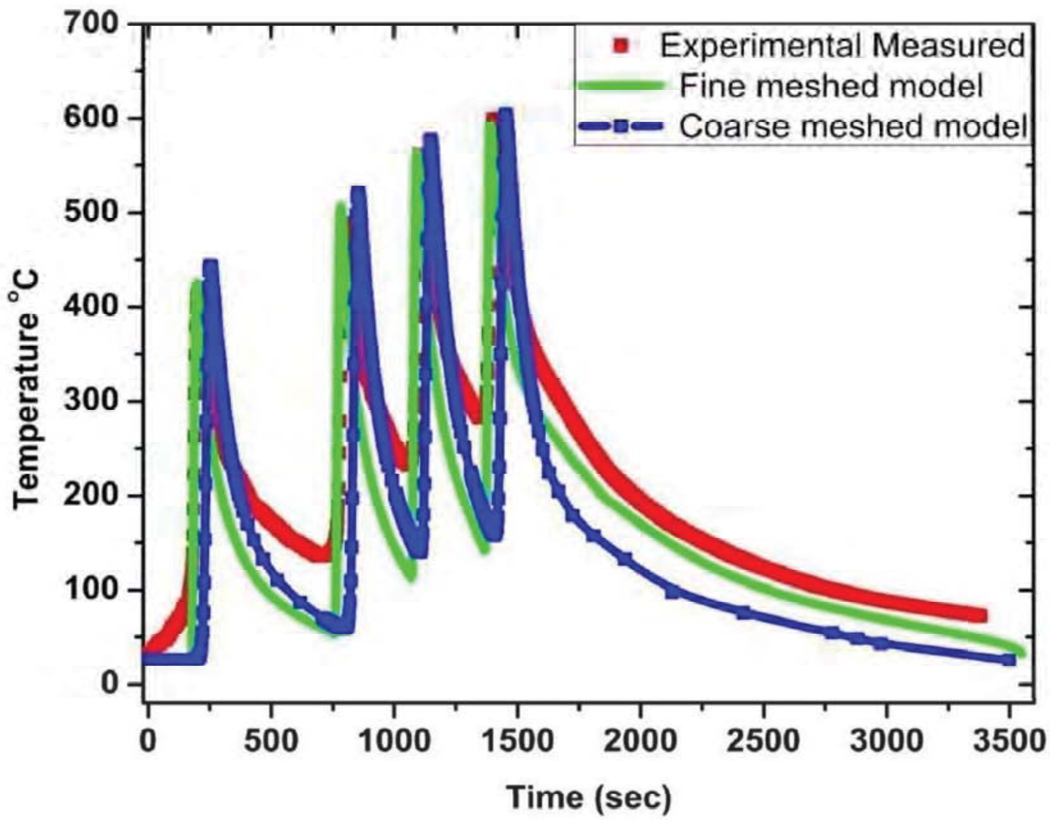

Fig.5.3.6. Thermal cycle comparison for 6 mm thick weld plate

5.3.3. Residual Stress Analysis of Multi-pass welding

The longitudinal residual stress profile was predicted in the transverse direction at the center line of the welded plate (same line at which residual stress measurements were carried out) by taking average value of 4 nodes around the point in 0.35-1 mm depth from top surface of meshed model. Fig. 5.3.7 shows the residual stress comparison between experimental and simulated results. Effect of phase transformation on residual stress profile is exhibited with 'M' shape profile in the weld and HAZ, which is similar to experimental measured values. Maximum residual stress measured at a location 15-17 mm right and left side of weld line was 400 MPa. Predicted residual stress value at same location is 428 MPa. Simulation considering without phase transformation shows maximum tensile stress 485 MPa nearer to weld line. At weld line, 196 MPa stress is observed experimentally where as predicted value considering phase transformation is 230 MPa. At the end of HAZ higher residual stresses exhibited in both cases. The difference between predicted residual stress and measured values is small as shown in Fig. 5.3.7.

In case of 3 mm thick plate autogenous welding, maximum predicted longitudinal stress is observed at 10 mm location next to HAZ as 560 MPa. Where as in 6 mm thick multi-pass welding maximum predicted longitudinal stress is 428 MPa at 17 mm location. This reduction in stress is observed due to repeated thermal cycles and increase in the volume fraction of molten metal multi-pass welding.

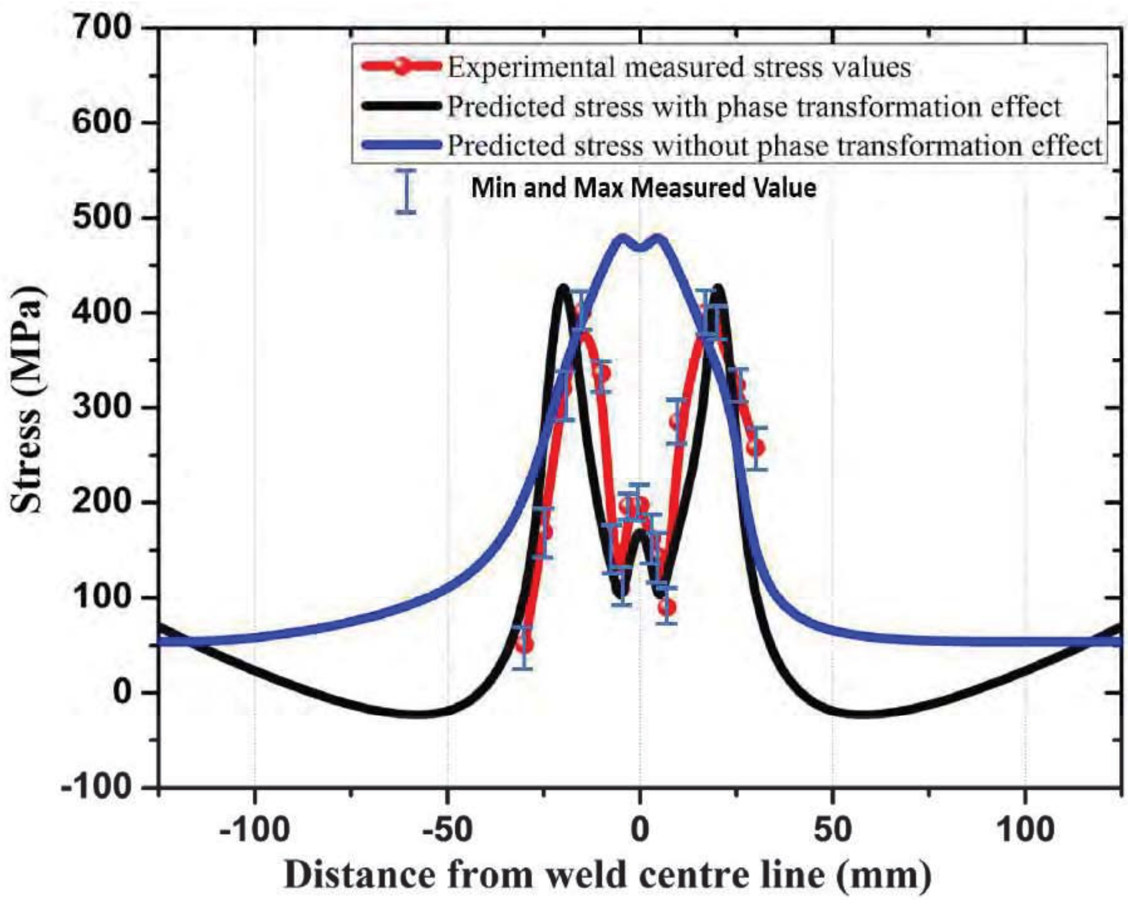

Fig.5.3.7. Residual stress comparison of 6 mm thick multi-pass weld

5.3.4. Distortion Analysis of Multi-pass welding

During welding, thermal cycle is very steep and during cooling it is highly non-uniform along weld line. This effect cannot be modelled accurately using a standard 2D meshed model. Hence it is necessary for actual prediction of weld plate displacement profile a 3D meshed model should be used because out of plane displacement in transverse direction can be studied using 3D model only. In this study, vertical displacements were predicted using both 2D and 3D meshed models and the predicted displacements values are compared with actual measurements. Fig. 5.3.8-5.3.9 shows the 2D meshed model and 3D coarse-fine meshed model distortion analysis. Maximum vertical displacement observed in 2D meshed model is 2.9 mm as shown in Fig. 5.3.8. Similarly, maximum vertical displacement observed in 3D coarse and fine meshed model is 4.85 mm and 5.6 mm respectively as shown in Fig. 5.3.9 (a-b).

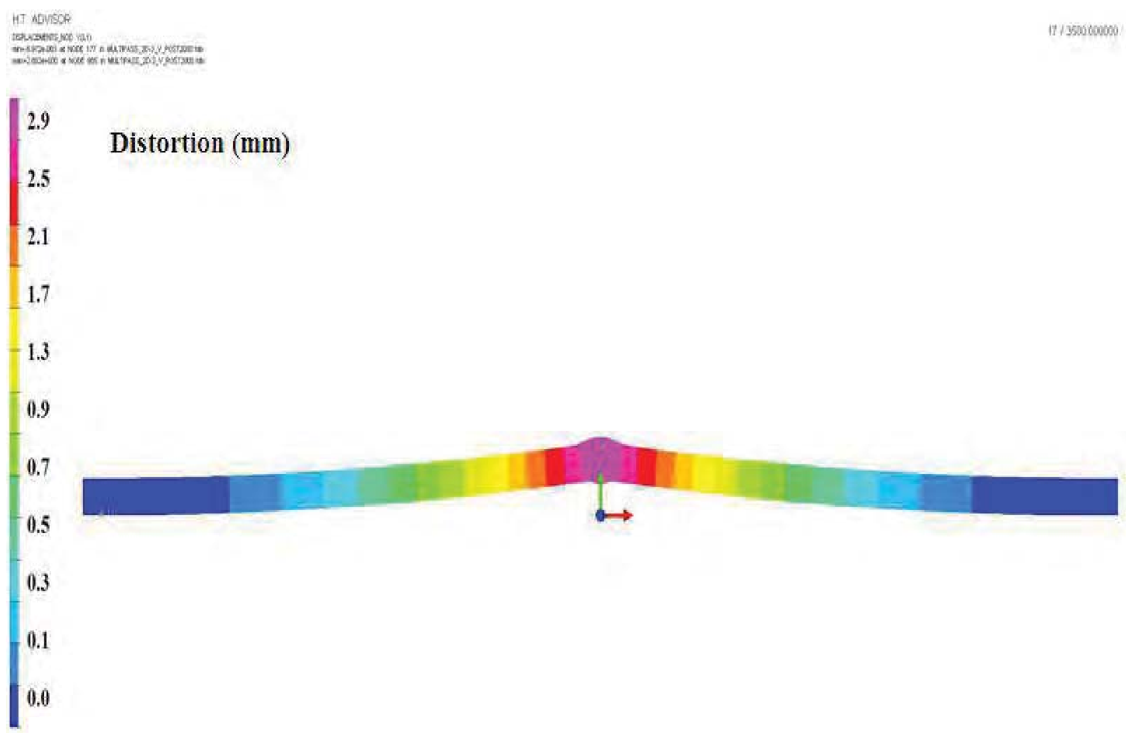

Fig.5.3.8. 2D distortion analysis of 6 mm thick weld plate

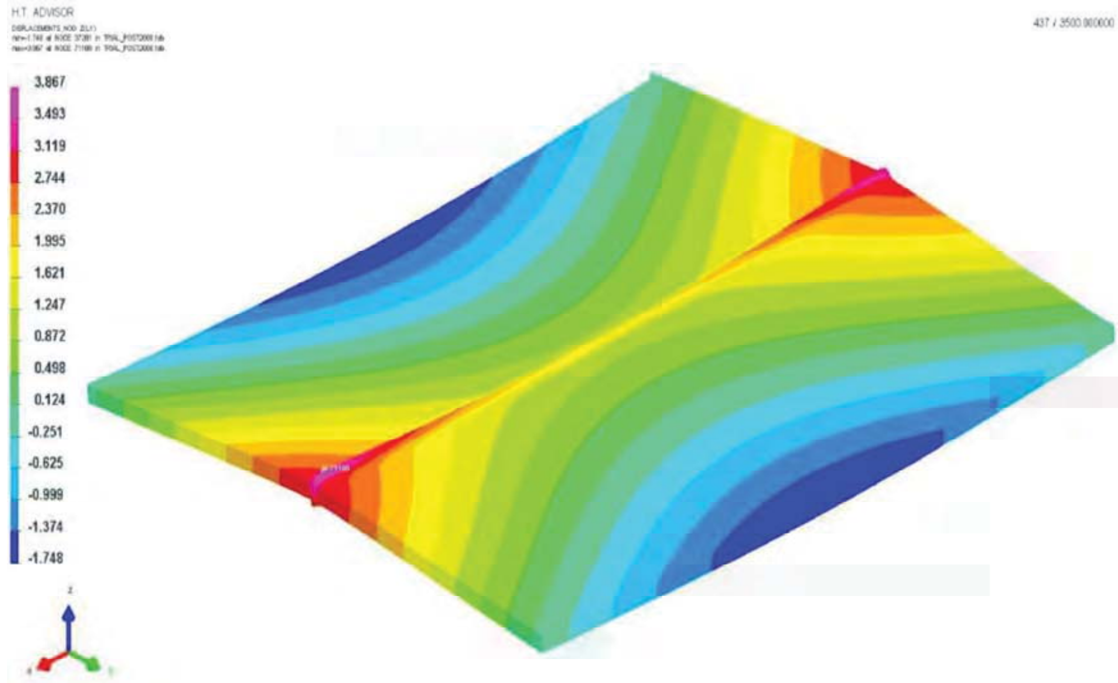

(a) Fine meshed model

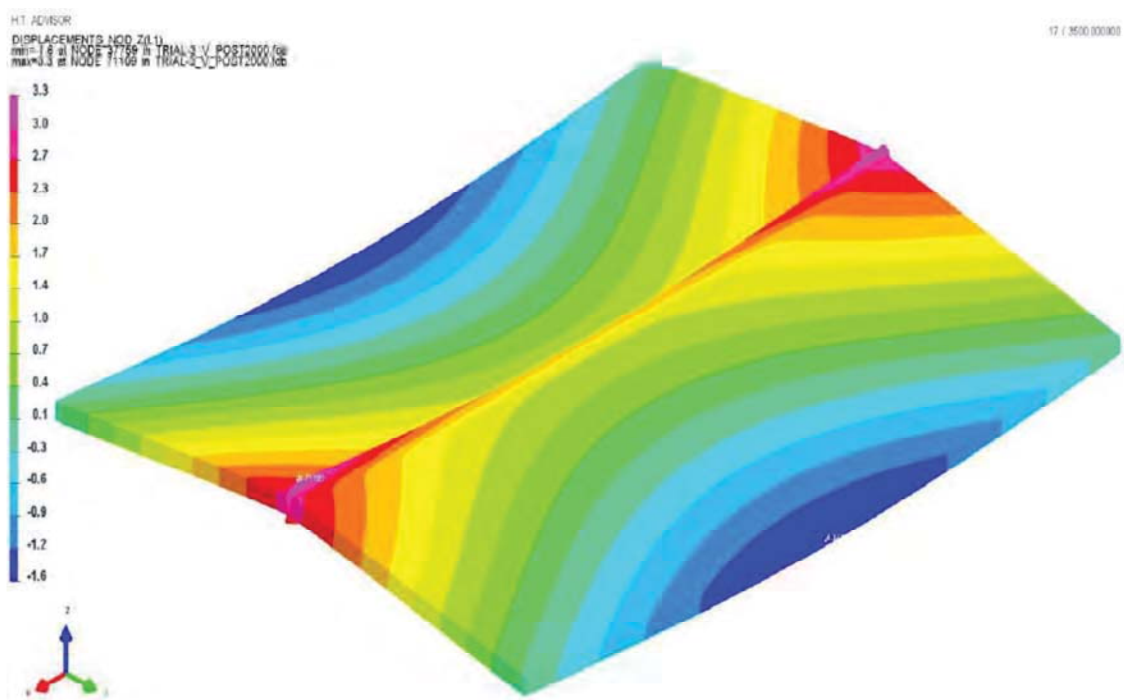

(b) Coarse meshed model

Fig.5.3.9. 3D Distortion analysis of 6 mm thick multi-pass weld

Table.5.3.2. Vertical displacement comparison for multi-pass weld in different directions

vertical displacement	Experimental	2D Model	3D Coarse model	3D Fine model
Longitudinal direction	2.8	NA	1.9	2.5
Transverse direction	6.2	2.9	4.85	5.6

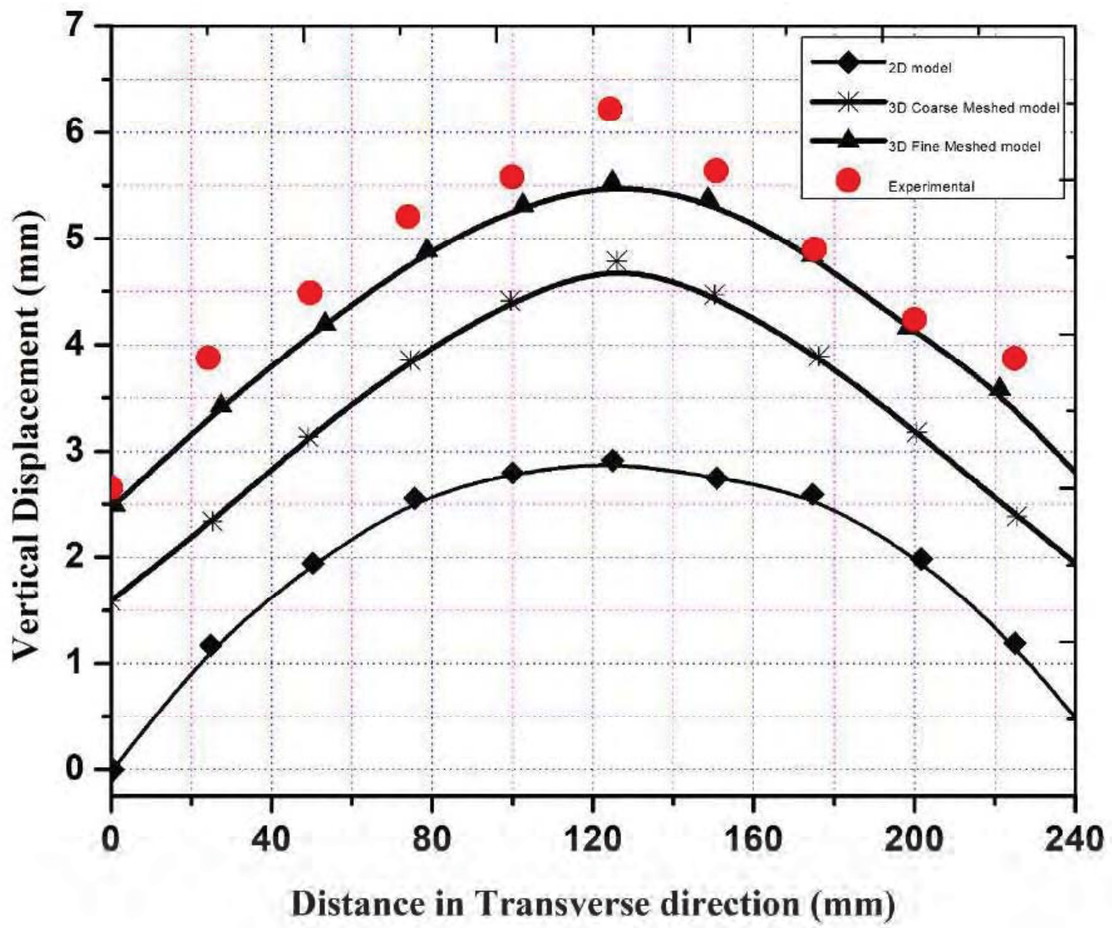

Fig.5.3.10. Comparison of displacement in transverse direction for 6 mm thick multi-pass welding

Fig.5.3.10 shows the comparison of transverse vertical displacement predicted using 2D meshed model and 3D coarse and fine meshed model with experimental measured values.

Though the displacement profiles are similar for all the three models, only the displacement predicted with 3D fine mesh model matched reasonably well with the measured displacements. Maximum predicted vertical displacement using 2D meshed model is 2.9 mm, where as predicted vertical displacement using coarse 3D meshed model is 4.85 mm at same location. Fine meshed model predicts 5.6 mm vertical displacement at weld line, which is nearer to experimental value. 2D meshed model gives 53% error (Experimental measured value 6.2) in vertical displacement prediction, whereas coarse and fine meshed model exhibit 21% and 9% error respectively in distortion prediction.

Table.5.3.2 shows the vertical displacement comparison using all three meshed model and experimental measured values in different direction. Maximum vertical displacement produced in weld plate in longitudinal direction is 2.8 mm, similarly in transverse direction is 6.2 mm. Displacement comparison results confirm that distortion analysis using 3D fine meshed model is fairly accurate with experimental values. Accordingly, all subsequent analyses are carried out with 3D fine meshing model.

5.3.5. Effect of Phase Transformation in Distortion Analysis

Based on literature survey it is observed that the effect of phase transformation in modified 9Cr-1Mo steel on distortion analysis is not available [1-5, 16-18, 24-26]. Hence, a separate study is undertaken to find out the effect of phase transformation on distortion analysis of multi-pass welding of modified 9Cr-1Mo steel. Fig. 5.3.11 shows the distortion analysis considering without phase transformation in material database using 3D fine mesh model. In case of 3 mm thick plate (thin plate) displacements predicted using model that consider phase transformation and the model that does not consider phase transformation were not much different. However, this is not the case for multi-pass weld of 6 mm thick plate weld.

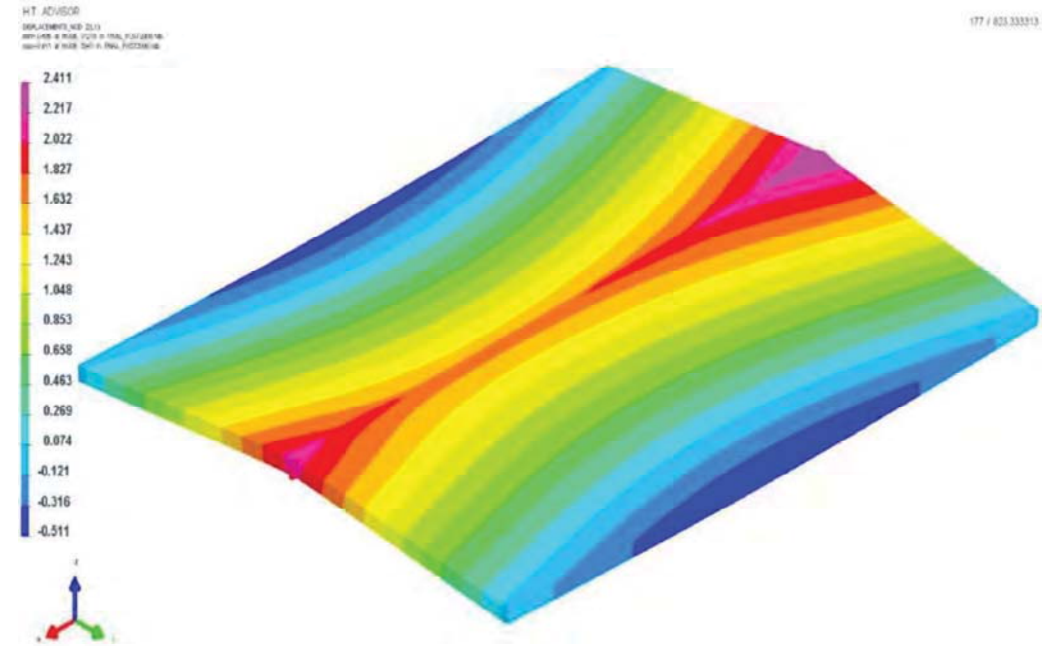

Fig.5.3.11. Distortion analysis without phase transformation for 6 mm thick multi pass weld

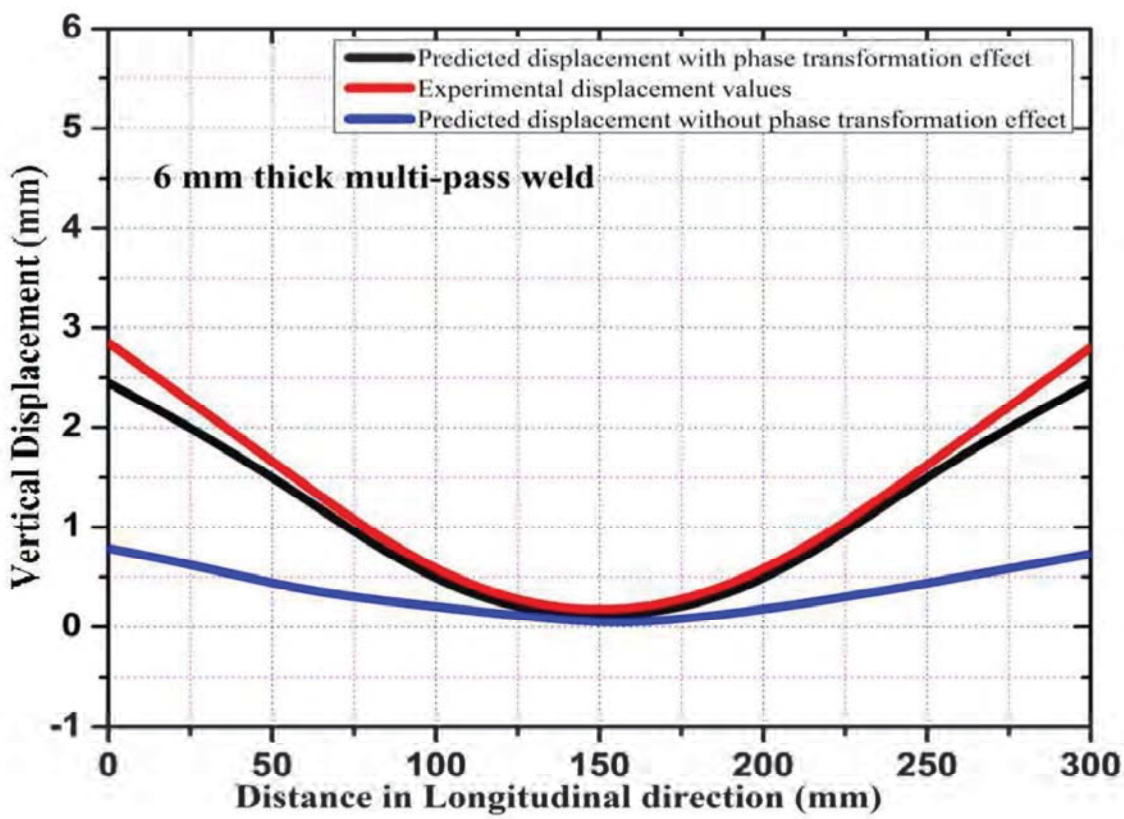

Fig.5.3.12. Effect of phase transformation on displacement

Comparison between predicted and measured vertical displacement along the longitudinal direction at the edge of the plate (considering with and without phase transformation) is shown in Fig. 5.3.12. Predicted vertical displacement without considering phase transformation exhibited larger deviation from actual measured values, while the predicted displacement considering phase transformation are in good agreement with the experimental values. Maximum vertical displacement produced in longitudinal direction is 2.8 mm (at the corner of weld plate). FEM based distortion analysis without phase transformation predicted the maximum vertical displacement value is 0.8 mm, where as in the case with phase transformation is 2.5 mm as shown in Fig. 5.3.12. Thus, it is proved that not only residual stresses but also the displacement is affected by the phase transformation that the weld undergoes during welding. Effect of this transformation on distortion is only marginal in the autogenous weld but significant in the multi-pass welds.

Results from multi-pass weld of 6 mm thick plate show that the FEM model also predicts the thermal cycles, residual stress and distortion for multi-pass welds with a ‘V’ groove geometry and filler metal additions. For accurate results 3D fine meshing should be used for FEM analysis.

5.4. Thermo-Mechanical Analysis of Modified 9Cr-1Mo steel GTA welding with Preheating

In this section thermo-mechanical analysis of welding with preheating is carried out for autogenous and multi-pass welding of modified 9Cr-1Mo steel using GTA welding process. Disk shaped heat source model is used first time for FEM analysis of the effect of preheating during autogenous and multi-pass welding of GTA welding process.

Preheating analysis is carried out using weld heat treatment tool in SYSWELD software. Combined disk-shaped heat source model with double ellipsoidal model is used for preheating with GTA welding FE analysis. Double ellipsoidal parameters used for heat source modeling are given in table 5.4.1.

Table.5.4.1. Double ellipsoidal parameters for welding with pre heating

Plate	a_f	a_r	b	c	Weld efficiency in terms of %
3 mm	3	5	2.8	3	75
6 mm	4	6	5	3	68

5.4.1. Thermal Analysis of Autogenous welding

During welding with pre heating, the joint area comprising fusion zone and the adjacent area of 8 mm wide on each side from the weld center line was heated up to 200°C using oxy-acetylene flame heating. Fig. 5.4.1 shows the transient thermal analysis of pre heating of 3 mm thick modified 9Cr-1Mo steel plate at 200°C. The GTA welding parameters are 90 A current 11 V at 100 mm/min weld speed. Thermal analysis of welding with pre heating of modified

9Cr-1Mo steel autogenous welding is shown in Fig. 5.4.2. The peak temperature reached during welding is 1642°C.

Fig. 5.4.3 (a-c) shows the comparison of thermal cycles for predicted and experimentally measured values for welding with pre heating of 3 mm thick plate. Maximum temperature reached at 10 mm from weld line is in case of welding with pre heating is 590°C only as shown in Fig. 5.4.3 (a). Comparison of predicted cycles with experimental measurement shows a good agreement for all three locations. Experimentally measured peak temperature is 382°C at 15 mm away from weld line and 312°C at 18 mm location from weld line. Difference between predicted and experimental measured peak temperature for the 10 mm, 15 mm and 18 mm locations from weld center was 13°C, 12°C and 28°C respectively observed.

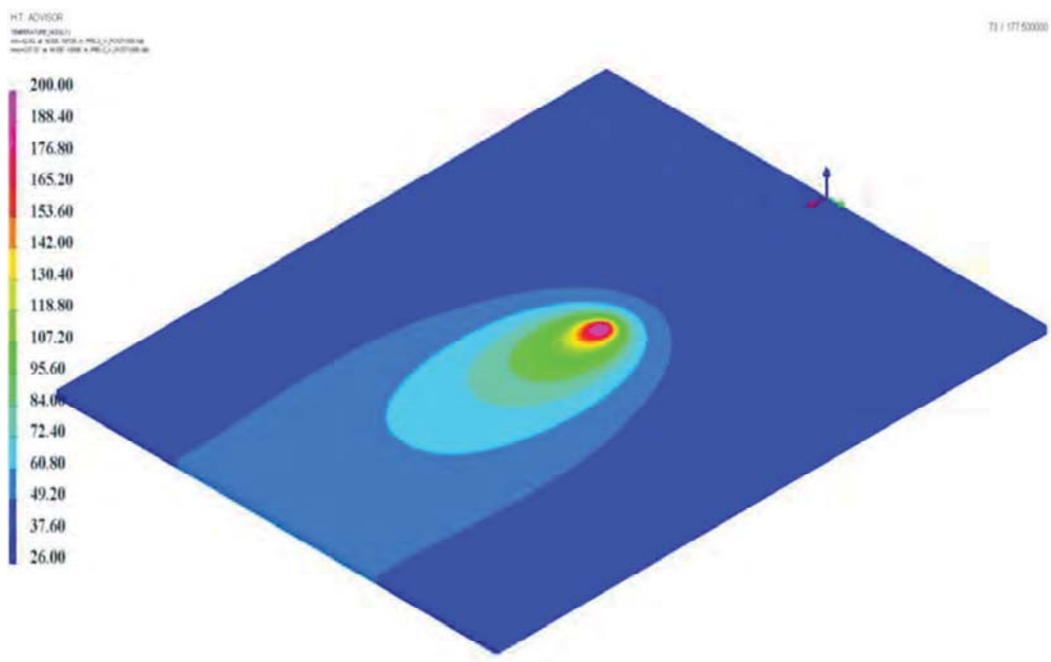

Fig.5.4.1. Thermal analysis of effect of preheating for 3 mm thick plate

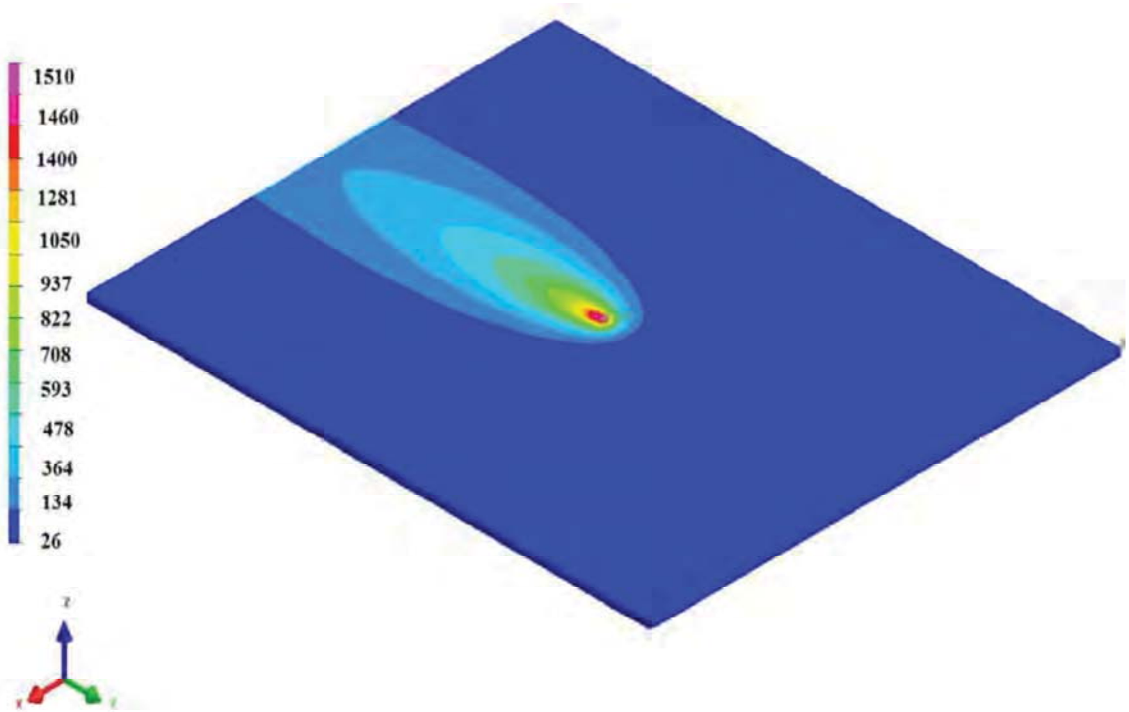

Fig.5.4.2. Thermal Analysis of autogenous welding with preheating

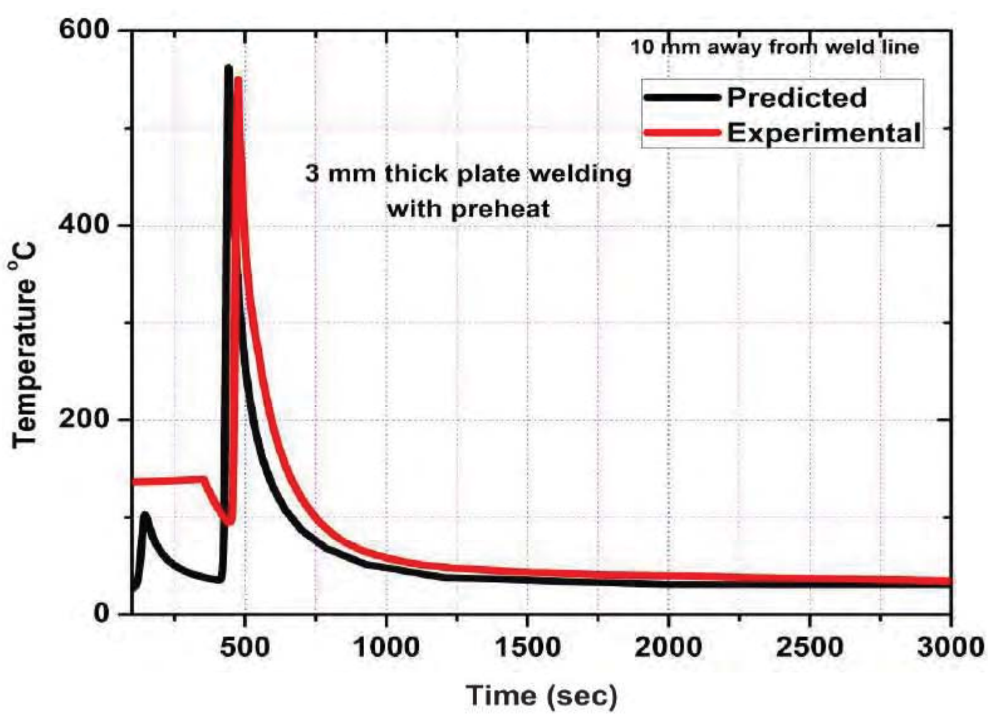

(a) At 10 mm distance from weld line

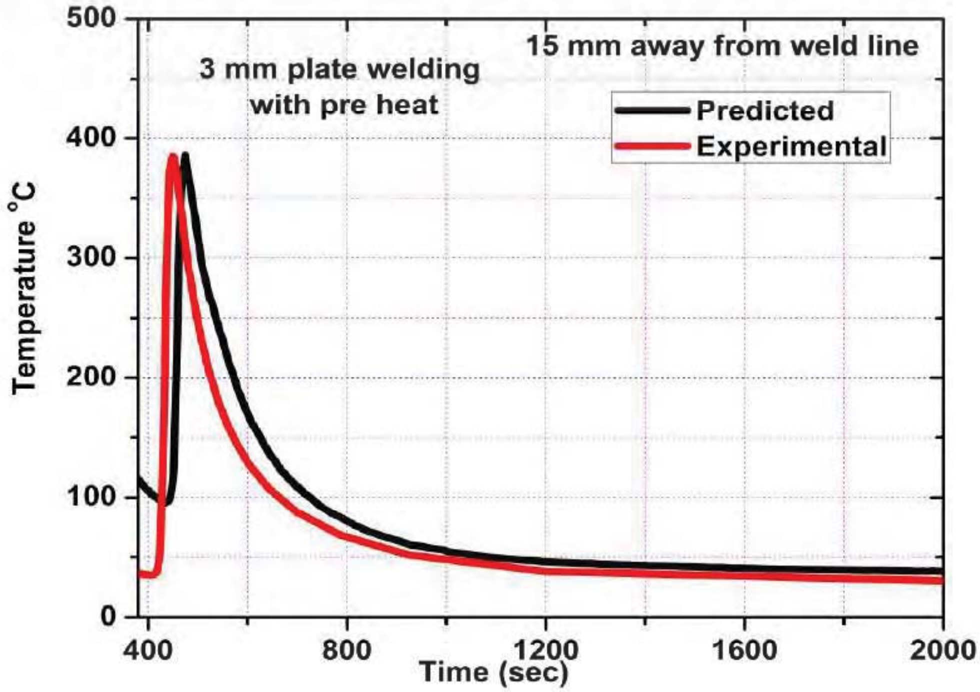

(b) At 15 mm distance from weld line

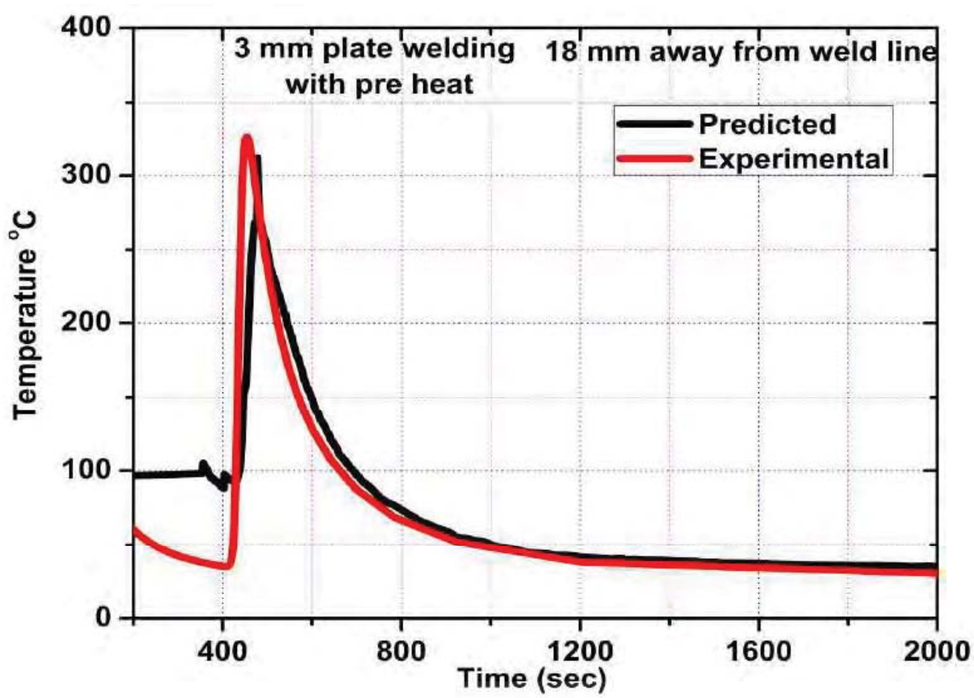

(c) At 18 mm distance from weld line

Fig.5.4.3. Thermal cycle comparison in autogenous welding with pre heating

5.4.2. Residual Stress Analysis of Autogenous welding

Fig. 5.4.4 shows predicted and measured residual stress profile for 3 mm pre heated weld plates. As expected, 'M' shaped residual stress distribution representing the phase transformation affect is obtained. Predicted peak tensile residual stresses are found to occur at 10 mm away from the weld center line. There was a good agreement between predicted and experimental measured longitudinal residual stress with error of 4% at peak tensile stress value, the predicted peak tensile stress values is 492 MPa and experimentally measured is 512 MPa measured at 10 mm distance from weld center line as shown in Fig. 5.4.5. At weld line in case of welding with pre heating, the predicted residual stress value is 179 MPa with an error of 13% (measured value is 208MPa). The predicted and experimental stress profile shows clearly phase transformation effect by reduction in stress at the weld center.

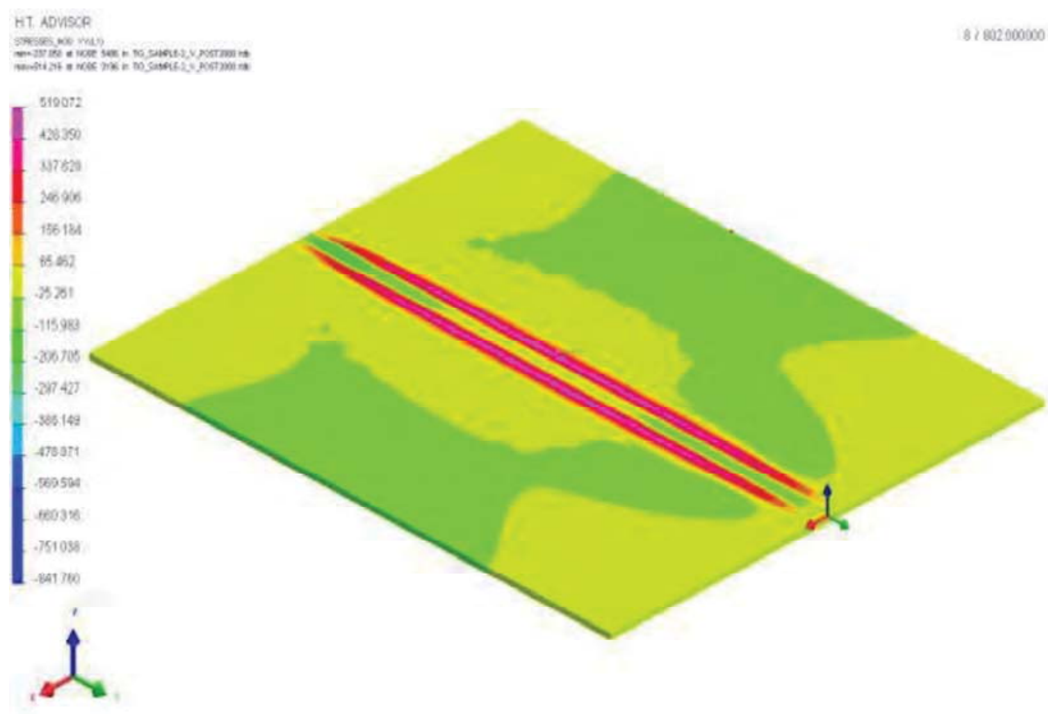

Fig.5.4.4. Residual stress analysis of autogenous welding with pre heating

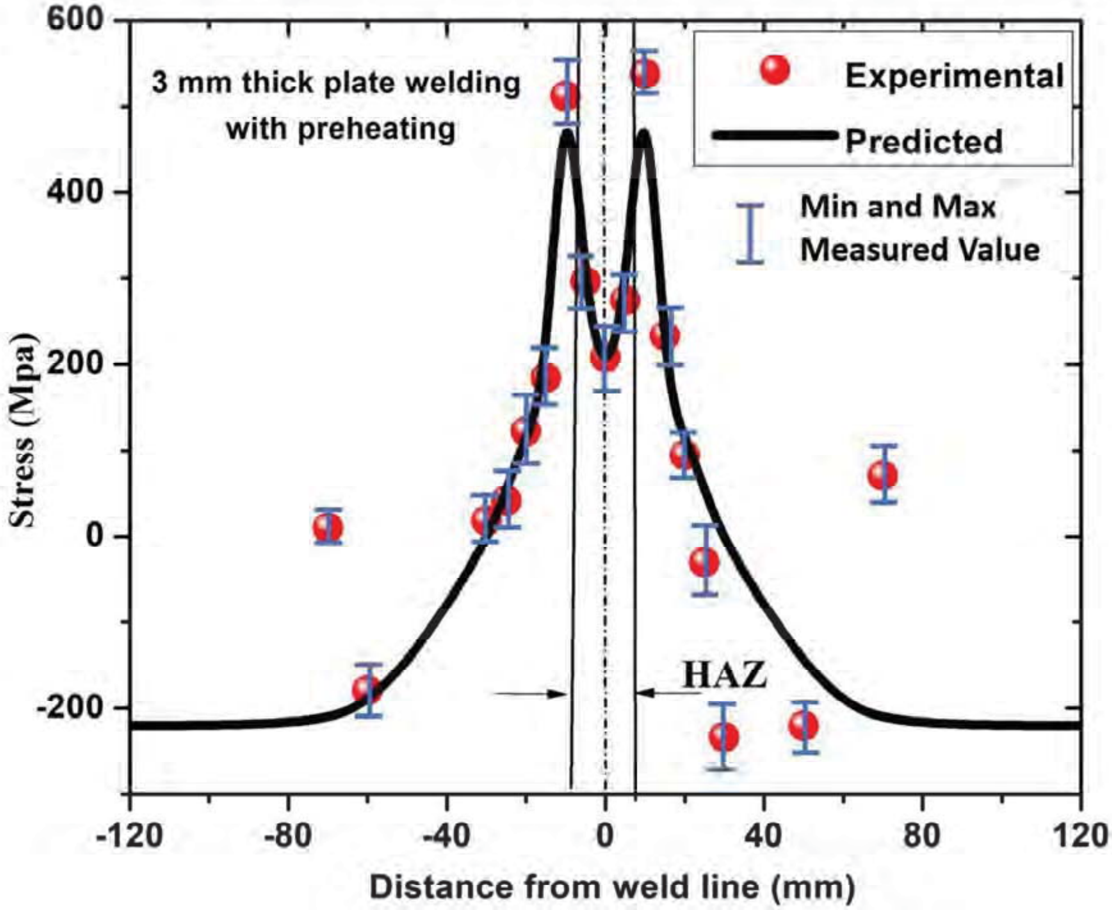

Fig.5.4.5. Residual stress comparison of autogenous welding with pre heating

5.4.3. Distortion Analysis of Autogenous welding

Distortion analysis of welding with pre heating for autogenous welding is shown in Fig. 5.4.5. Maximum displacement is observed at the corner of weld plate after releasing of clamps. The weld joint undergoes distortion due to the release of induced residual stresses beyond the yield point. Maximum verticle displacement oberved in Fig. 5.4.5 is 4.2 mm. Predicted displacements at different locations are validated with experimental measured values.

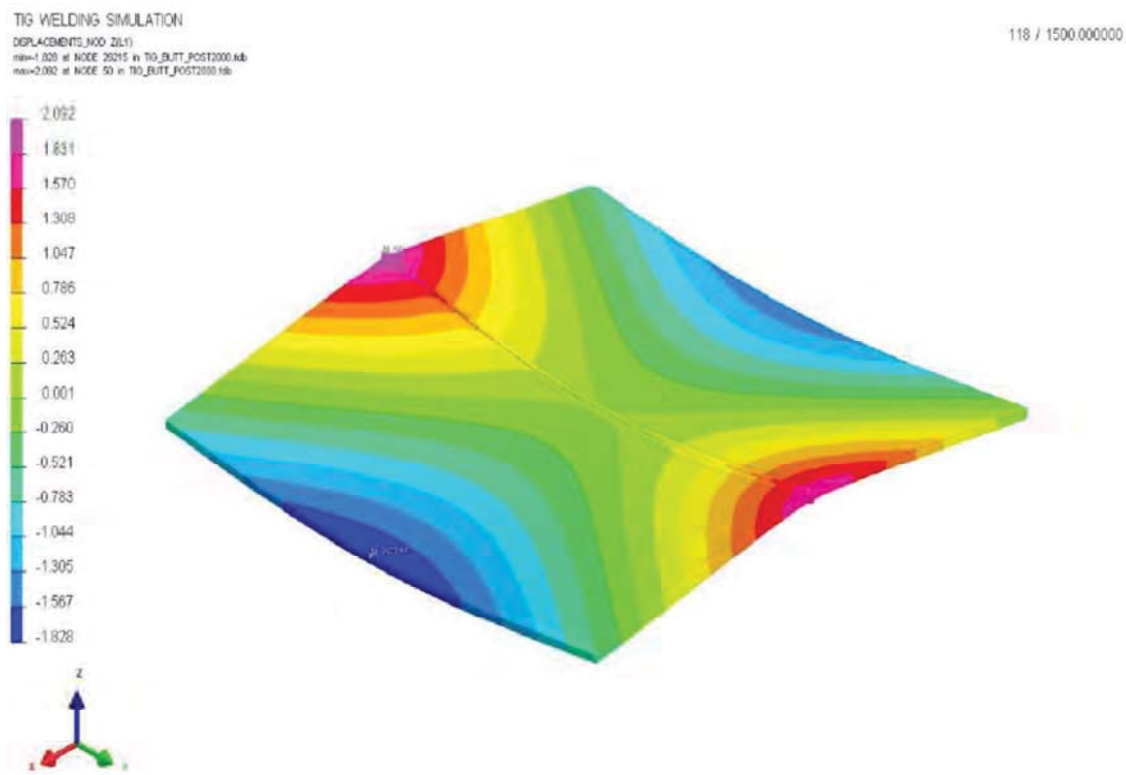

Fig.5.4.6. Distortion analysis of autogenous welding with pre heating

Fig.5.4.7 (a-b) shows the predicted displacement in longitudinal and transverse direction compared with experimentally measured values. Verticle displacement comparison shows a good agreement between the predicted and measured values. Maximum vertical displacement predicted at the corner of plate (in longitudinal direction) is 2.3 mm with an error of 4% (experimental measured value 2.2 mm). Peak vertical displacement in transverse direction is observed at the weld line 3.9 mm, predicted vertical displacements values for same locations is 4.3 mm respectively. Predicted vertical displacements values of welding with pre heating were successfully validated with experimental values.

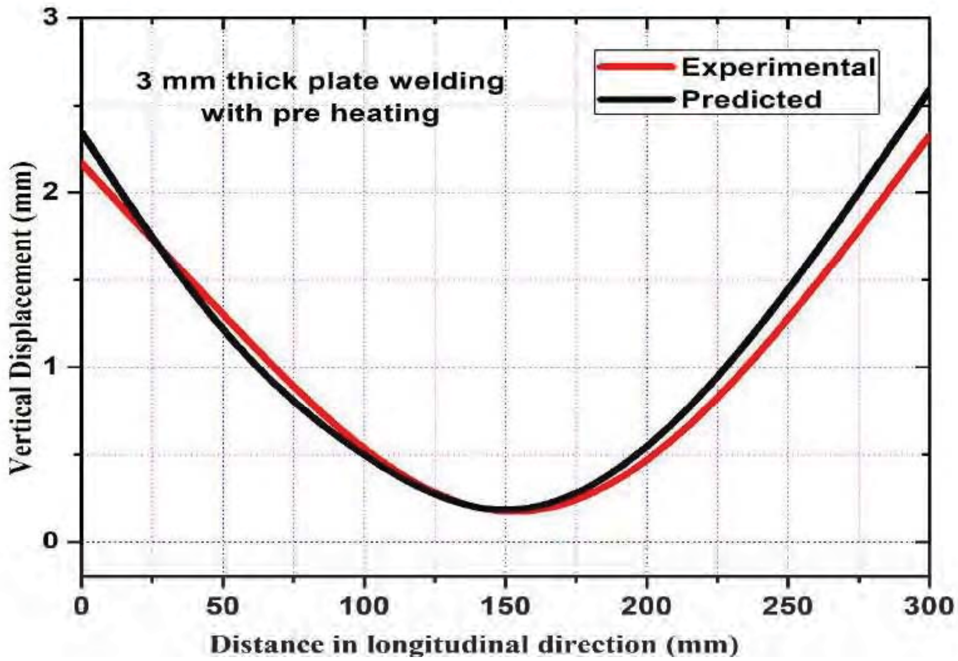

(a) Longitudinal direction

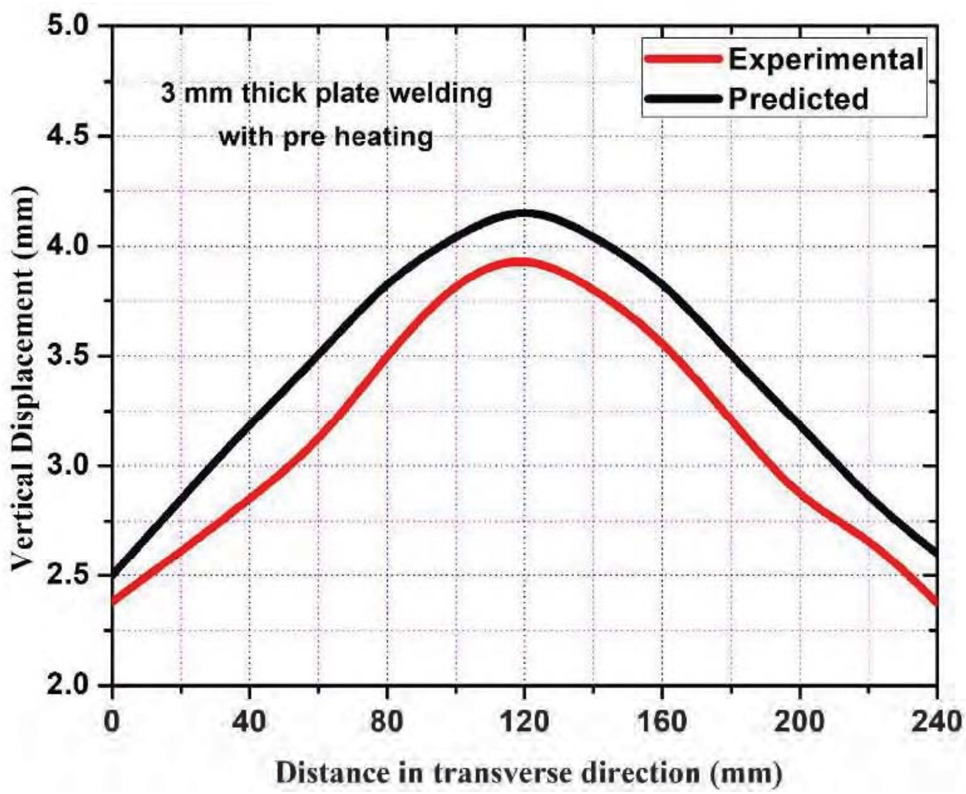

(b) Transverse direction

Fig.5.4.7. Vertical displacement comparison in autogenous welding with pre heating

5.4.4. Thermal analysis of Multi-pass welding

Fig. 5.4.8 shows the thermal analysis of pre heating on multi-pass weld plate before root pass weld. Thermal cycle shows that plate was heated up to 200°C before start of welding and after each pass 200°C is maintained for corresponding next passes. Thermal analysis of last pass weld is shown in Fig. 5.4.9. Maximum temperature reached during welding is 1945°C, which is above melting point of modified 9Cr-1Mo steel.

Fig. 5.4.8 shows the predicted thermal cycles for preheat welding of modified 9Cr-1Mo steel. Predicted peak temperature at 10 mm from the centre line of the weld for root pass was 600°C and experimentally measured peak value was 592°C. Similarly predicted peak temperature for second and third pass 638°C and 646°C and the corresponding measured values were 631°C and 659°C. Predicted peak temperature value for final pass is 655°C at 10 mm location away from weld centre line, while measured value for same location is 662°C.

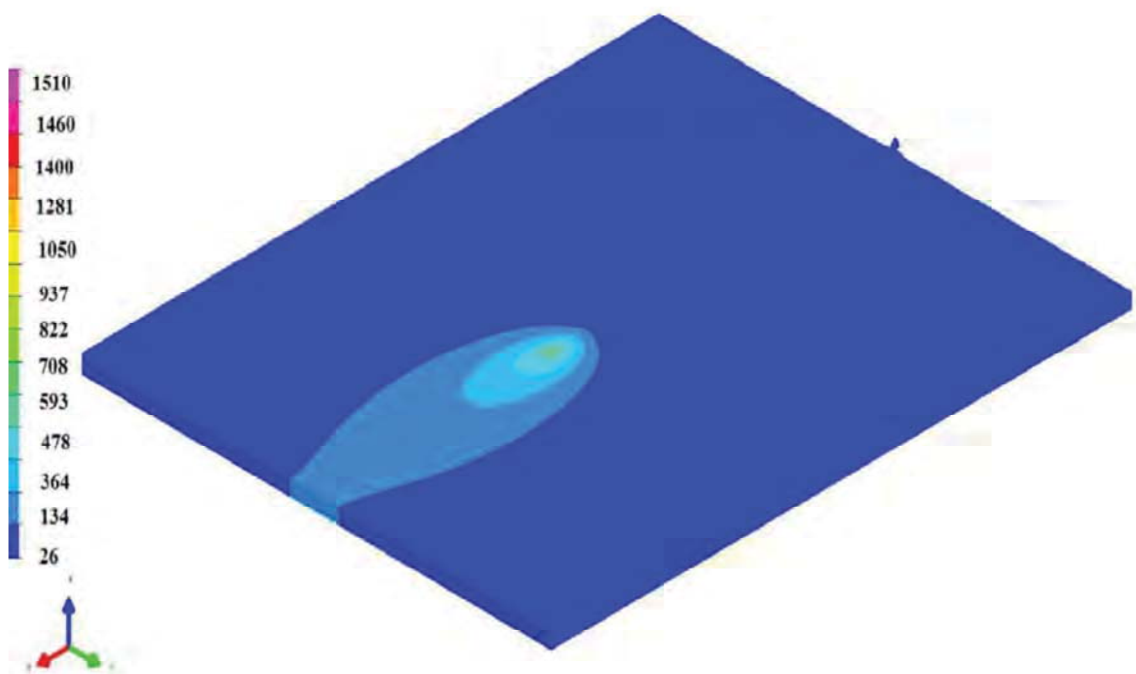

Fig.5.4.8. Thermal analysis for effect of pre heating of multi-pass weld

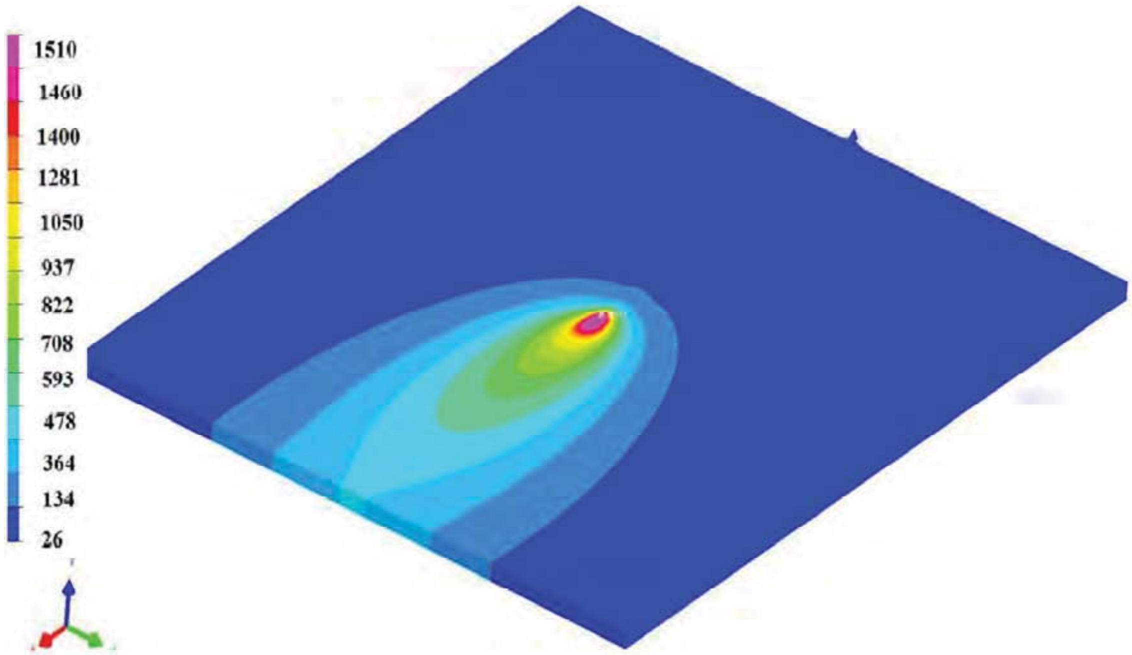

Fig.5.4.9. Thermal analysis of welding of multi-pass welding with pre heating

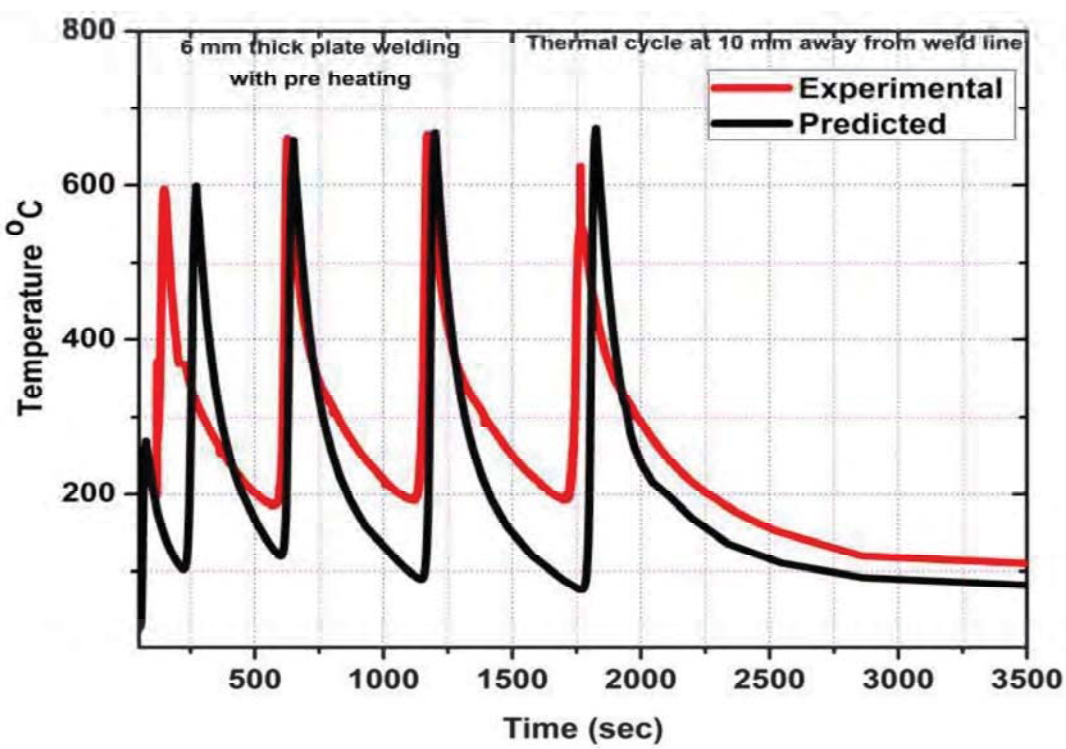

Fig.5.4.10. Thermal cycle comparison in multi-pass welding with pre heating

5.4.5. Residual Stress Analysis of Multi-pass welding

Fig. 5.4.11 shows the comparison of longitudinal residual stress for 6 mm thick plate welding with pre heat. Peak value of predicted longitudinal stress is 405 MPa at 20 mm away from weld line. Experimentally measured value for same location is 322 MPa on right side of weld line and on left side of plate is 385 MPa at 15 mm. Predicted value at weld line is 165MPa with 12.5% error with experimental value.

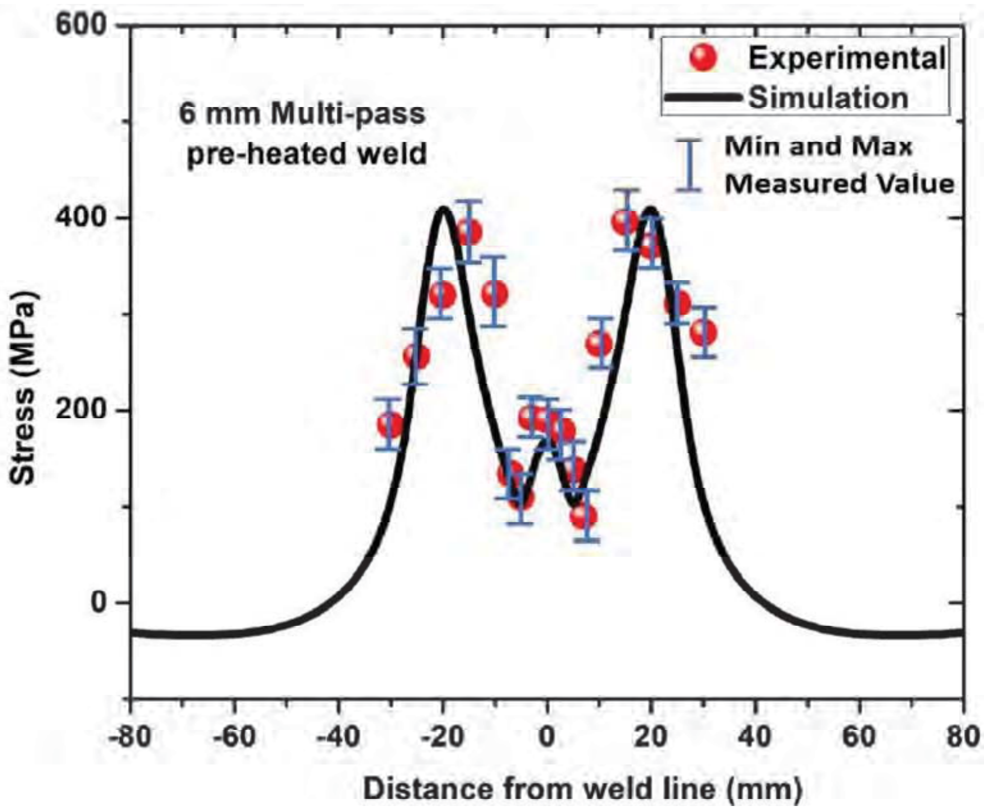

Fig.5.4.11. Residual stress comparison in multi-pass welding with pre heating

5.4.6. Distortion Analysis of Multi-pass welding

Fig. 5.4.12 shows the predicted distortion profile of multi-pass welding with pre heating. Predicted longitudinal verticle displacement at the corners of weld plates are plotted and compared with experimentally measured values for the same locations in Fig. 5.4.13.

Predicted displacement is plotted by taking midpoint of weld line in transverse direction (perpendicular to weld line) as a reference point.

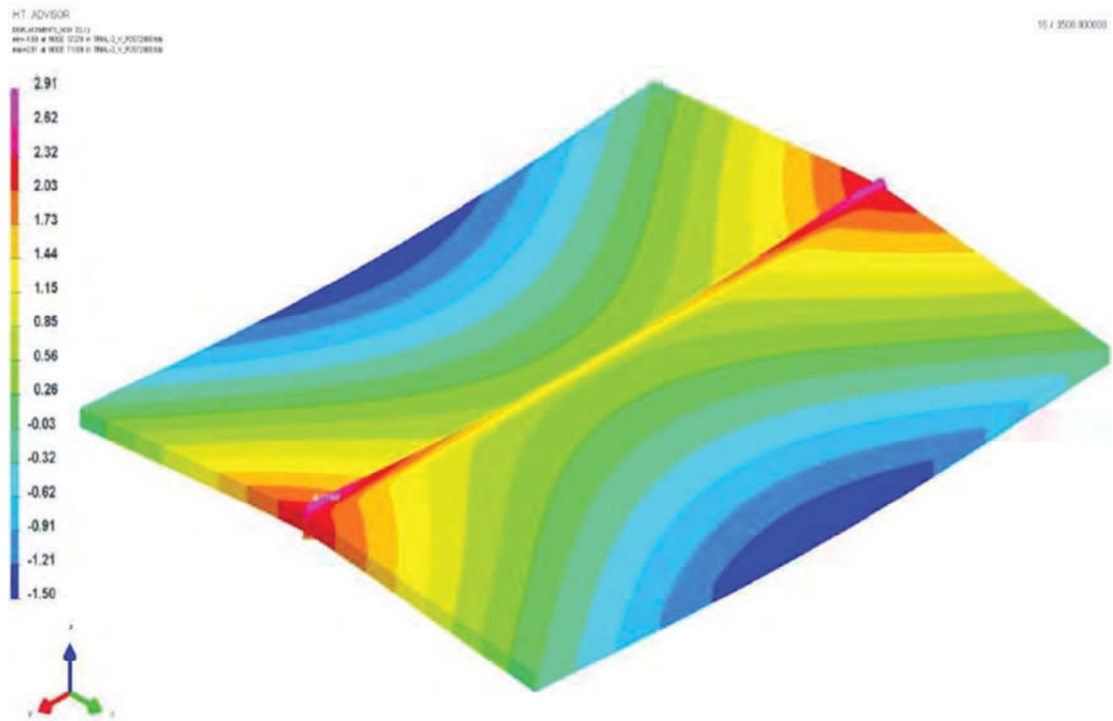

Fig.5.4.12. Predicted distortion in multi-pass welding with pre heating

Fig. 5.4.13 shows that maximum vertical displacements (in longitudinal direction) measured are 2.35 mm and 2.2 mm at the left and right corners of weld joint (at clamping locations) and the corresponding predicted verticle displacement at these locations is 1.94 mm. Maximum verticle displacement observed at weld line in transverse direction is 4.6 mm, where predicted value is 4.3 mm with 0.3 mm difference only. Comparison of predicted and measured verticle displacement shows a good agreement.

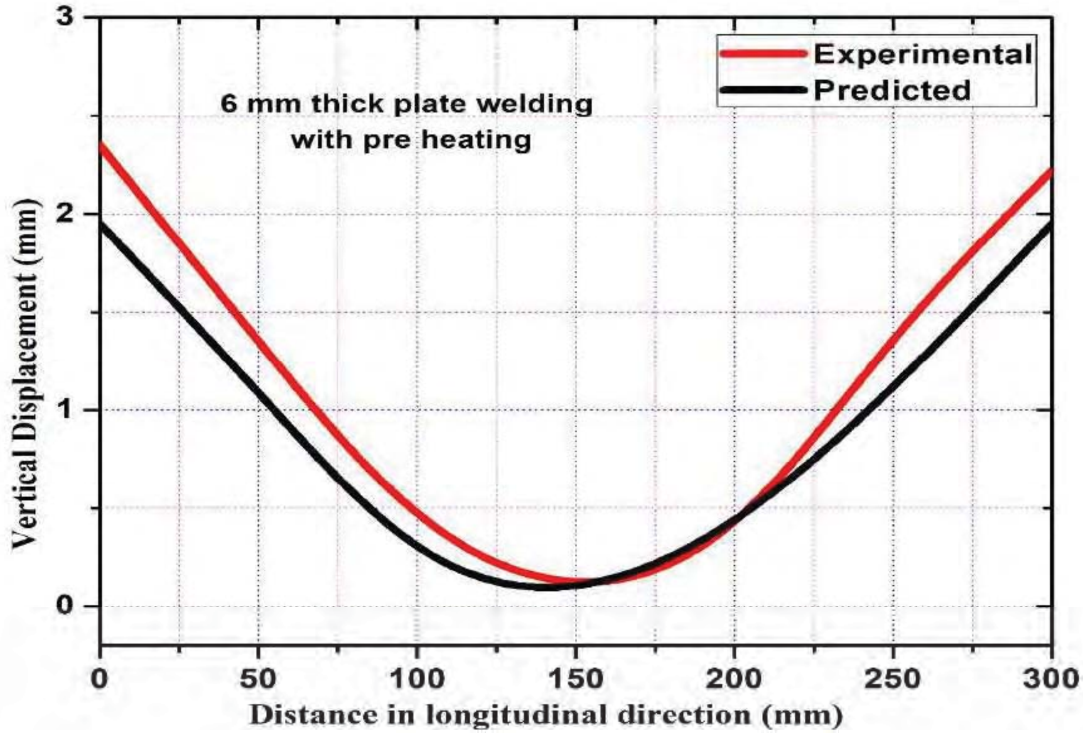

(a) Longitudinal direction

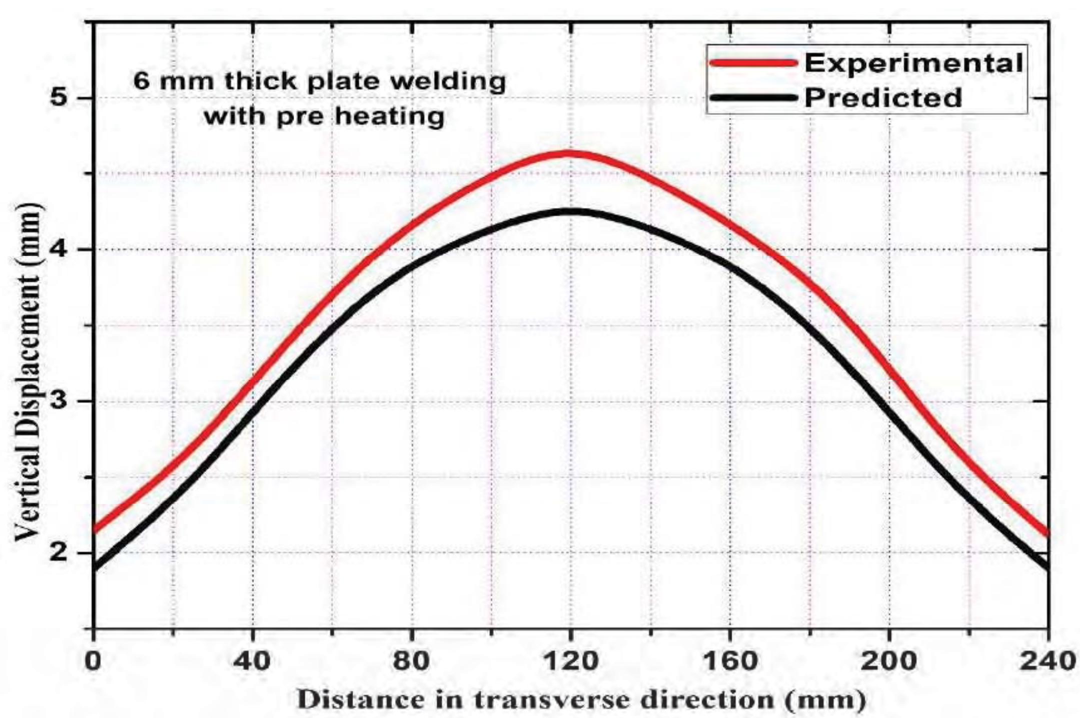

(b) Transverse direction

Fig.5.4.13. Vertical displacement comparison in multi-pass welding with pre heating

The results clearly show that FEM model modified with disk shaped heat source for preheating along with double ellipsoid heat source for welding is able to predict the weld thermal cycle residual stress and distortion in both autogenous and multipass welds with reasonable accuracy. It may also be noted that accuracy of prediction for welds made without preheating and for welds made with preheating are comparable for both residual stress and distortion.

5.5. Thermo-mechanical Analysis of GTA Welding of Modified 9Cr-1Mo steel with combined effect of Pre-heating and Post-heating

In this section, combined effect of pre heating and post heating on the residual stresses and distortion for modified 9Cr-1Mo steel weld joints is presented. Meshing model for both thickness of weld plates is same as in previous cases of with and without pre heating welding cases. Thermo-mechanical analysis of welding with combined pre heating and post heating for both autogenous and multi-pass welding is validated with experimentally measured thermal cycles, tensile residual stress and vertical displacement. Double ellipsoidal parameters used for thermo-mechanical analysis are given in Table 5.5.1.

During thermo-mechanical analysis, the effect of pre heating was considered by assuming initial temperature of weld plate as 200°C. Similarly, after welding for the post heating analysis when weld joint was cooled down to 200°C, same temperature was maintained up to next 0.5 hr. However, cooling down from 200°C to ambient temperature has not been considered

Table.5.5.1. Double ellipsoidal parameters for welding with combined pre heating and post heating

Plate	a_f	a_r	b	c	Weld efficiency in terms of %
3 mm	3	5	2.8	3	75
6 mm	4	6	5	3	68

5.5.1. Thermal Analysis of Autogenous welding

Thermal history was calculated in thermal analysis and results were used as an input file for mechanical analysis. Fig. 5.5.1 shows the thermal analysis of GTA welding. Maximum temperature reached during welding is 1647°C. FEM based calculated thermal cycles at 5 mm and 10 mm away from weld line are compared with measured cycles for autogneous welding of 3 mm thick plate as shown in Fig. 5.5.2. Predicted thermal cycle shows the initial temperature of weld joint as 200°C, which is due to pre heating of weld plate. Thermal cycle comparison at 5 mm away from weld line shows that during welding, maximum temperature reached is up to 852°C while the experimentally measured temperature is 828°C.

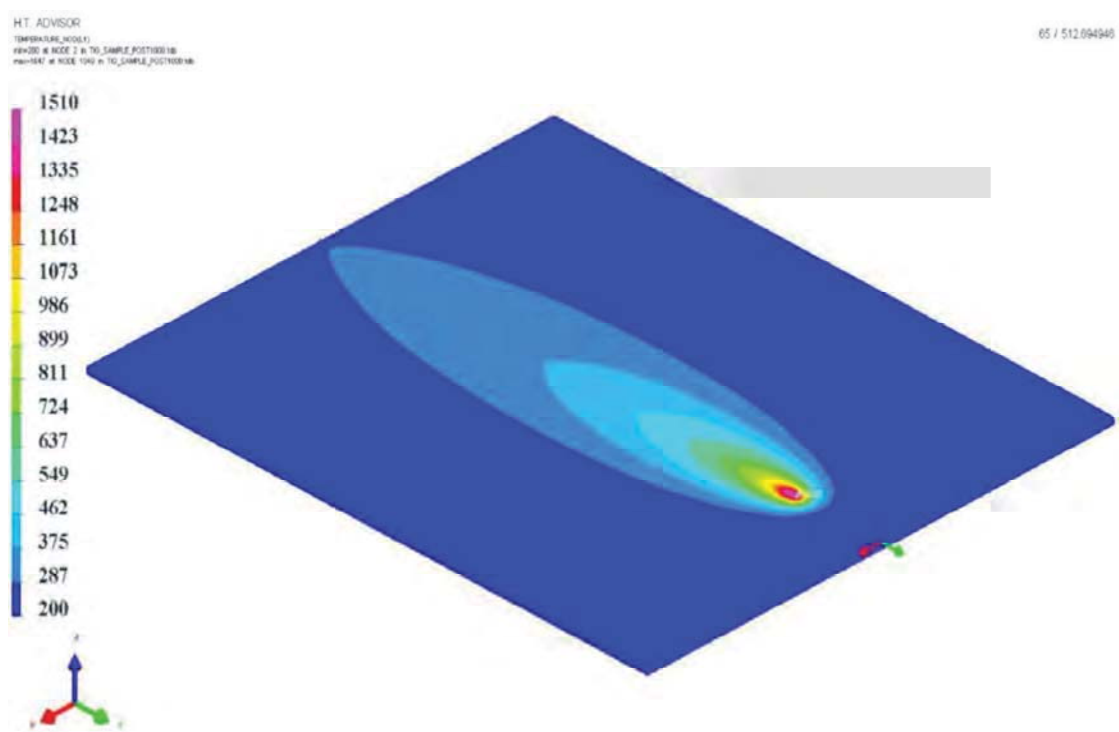

Fig.5.5.1. Thermal analysis of autogenous welding with post heating

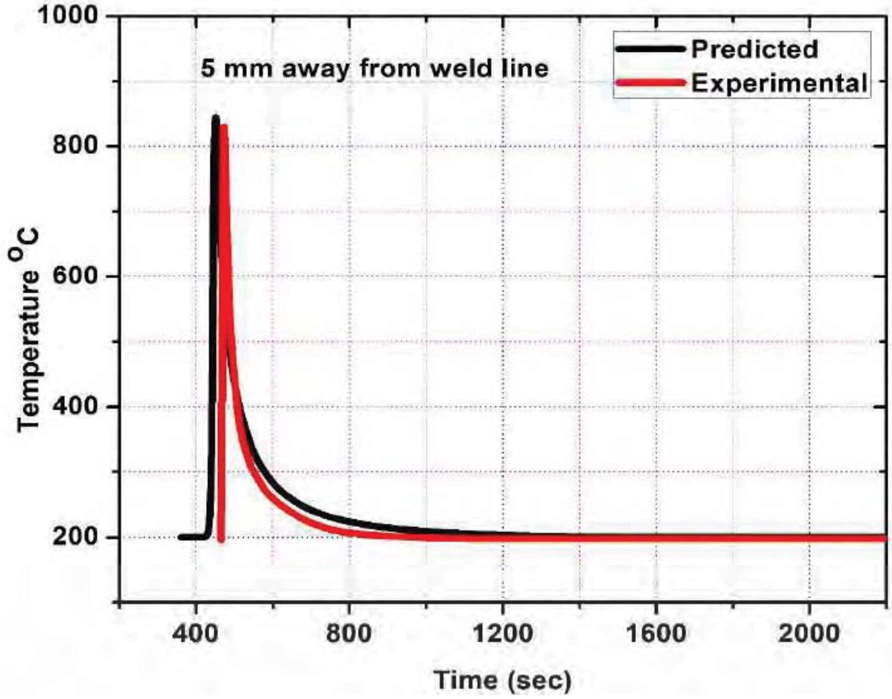

(a) At 5 mm distance from weld centre line

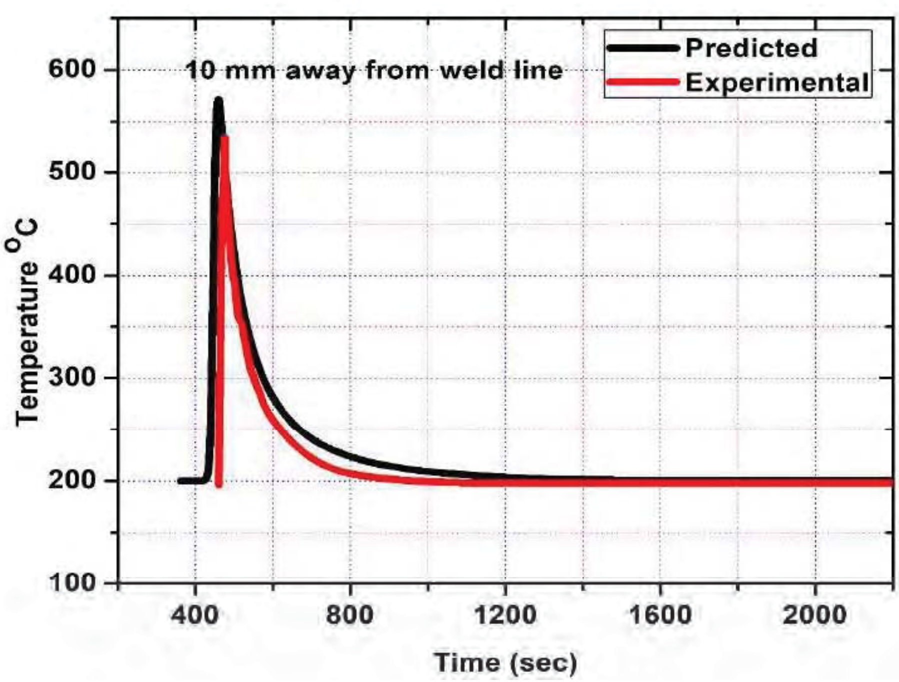

(b) At 10 mm distance from weld center line

Fig.5.5.2. Comparison of predicted thermal cycles in autogenous welding with post heating

At 10 mm distance location predicted peak temperature value is 573°C whereas experimental value is 525°C. There was good agreement between the predicted and measured thermal cycles and the peak temperatures at various locations. During cooling when the weld joint reached 200°C temperature near to the fusion zone, weld joint was post heated at same temperature for next 0.5 hr as shown in both predicted and experimental thermal cycles.

5.5.2 Residual Stress Analysis of Autogenous welding

Fig. 5.5.3 shows the comparison of predicted and experimental measured residual stress at 11 different locations for 3 mm thick plate welded with combined pre and post heating GTA welding. Stress comparison shows clearly the phase transformation effect by shifting the peak stress position from weld line to HAZ. "M" shaped residual stress profile is observed. Residual stress distribution is looking wider than that obtained for welds made with preheating and without pre heating (previous two autogenous weld cases). This could be due to wide HAZ (not marked in figure 5.5.3) produced by combined effect of preheating and post heating.

Maximum predicted longitudinal stress of 405 MPa which is tensile in nature is found next to HAZ with the maximum error is 6% (experimentally measured value at 381 MPa). Predicted residual stress value at 15 mm left side of weld line is 196 MPa with error of only 1%. Experimentally measured stress value at the weld line is 221 MPa, for the same location the predicted stress value is 98 MPa only.

The reason for the deviation of predicted residual stress value at weld line could be due to the fact that for prediction 200°C is taken as ambient temperature; i.e. after 30 minutes of post heating decrease in temperature from the post heating temperature to the actual ambient temperature is not considered in the model. It should be noted that martensitic finish temperature is also close to this post heating temperature. Hence, model does not estimate contribution to residual stress resulting from this cooling. In fact, martensitic transformation is complete at ~200°C, subsequent cooling only results in contraction and hence would contribute to generation of tensile residual stresses. As this contribution is not added in the result from modeling, it gives lower residual stresses in the weld center line, where complete weld metal transforms to martensite, than the values measured at room temperature.

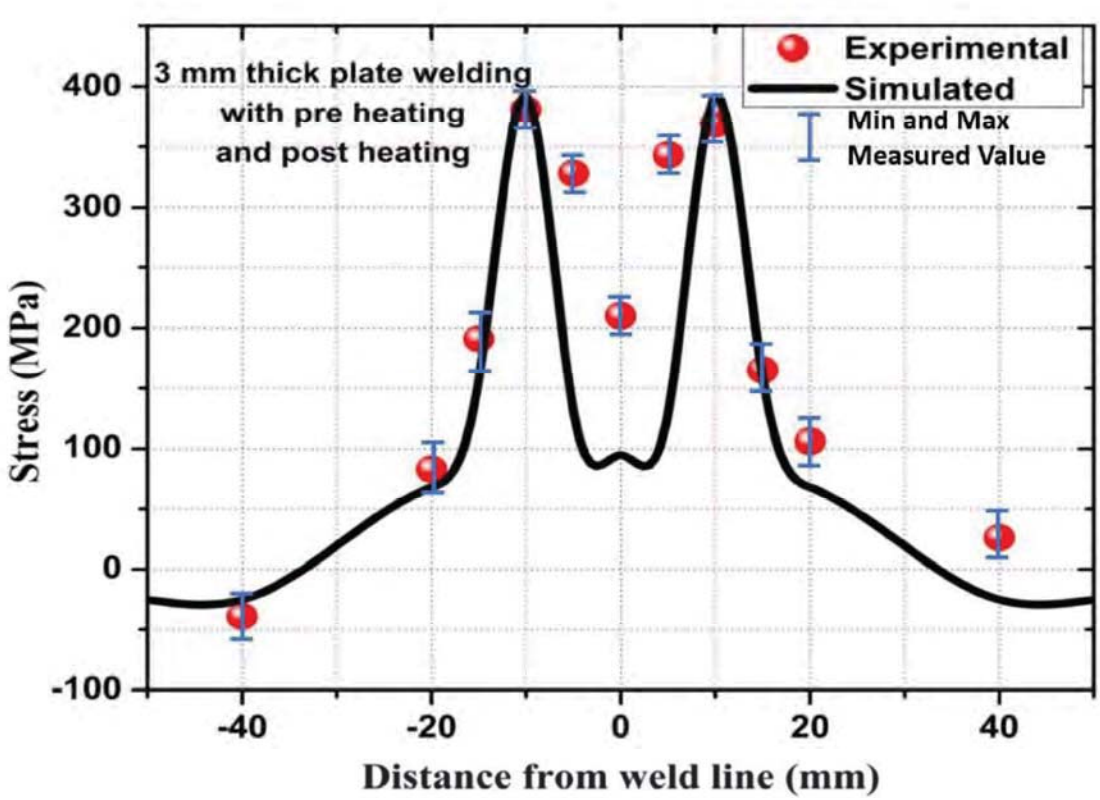

Fig.5.5.3 Residual stress comparison in autogenous welding with post heating

5.5.3. Distortion Analysis of Autogenous welding

Distortion analysis is carried out using 3D meshed model by employing large displacement theory (non-linear geometry). Fig. 5.5.4 shows the predicted vertical displacement profile in longitudinal and transverse direction of weld joint which is similar to that of the experimentally measured profile.

Predicted longitudinal vertical displacement at the corner of weld plate is plotted and compared with experimentally measured values for the same locations as shown in Fig. 5.5.5. Predicted vertical displacement is plotted by assuming midpoint of weld line in transverse direction (perpendicular to weld line) as a reference point. Displacement profile is similar in predicted and experimentally measured profiles.

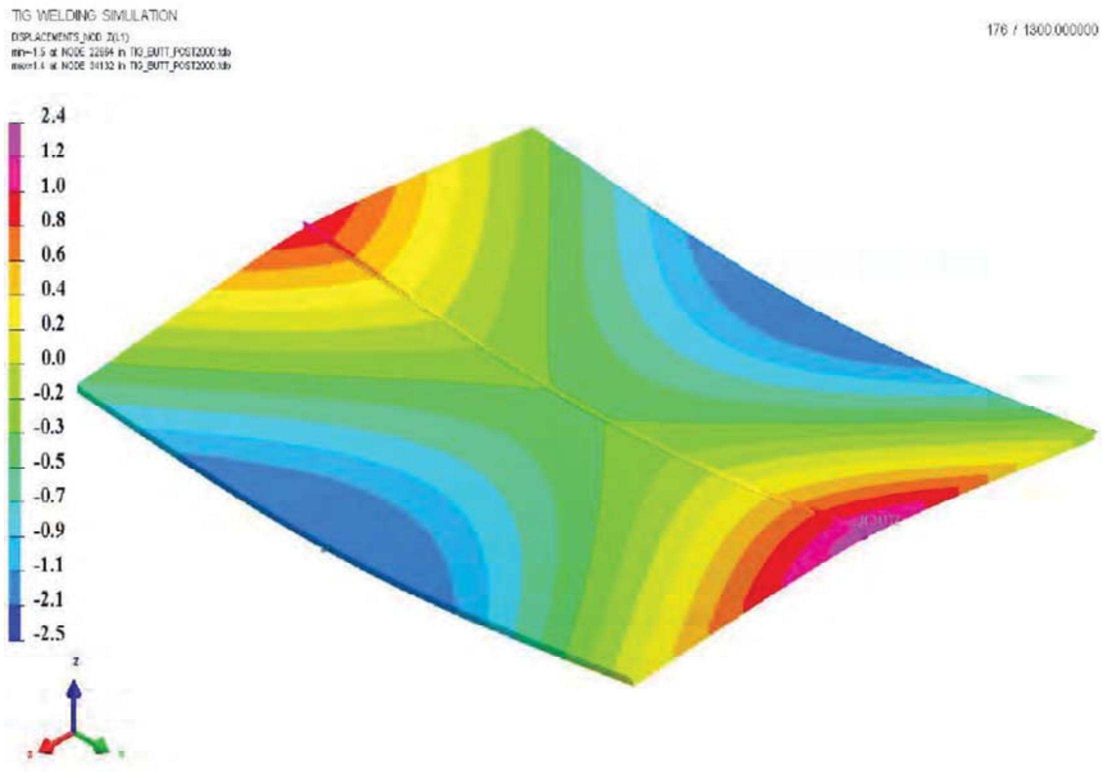

Fig.5.5.4. Predicted distortion of autogenous welding with post heating

Fig. 5.5.5 shows the comparison of predicted and experimentally measured vertical displacement produced in two different directions. The maximum predicted vertical displacement observed at the corner of weld plate in longitudinal direction is 2.1 mm. Experimentally measured vertical displacement value in same locations is 1.9 mm and 2 mm at the left and right corners of weld joint respectively (at the clamping locations). In transverse direction peak value of predicted vertical displacement is 3.35 mm which is same as experimentally measured value as 3.4 mm as shown in Fig. 5.5.5 (b).

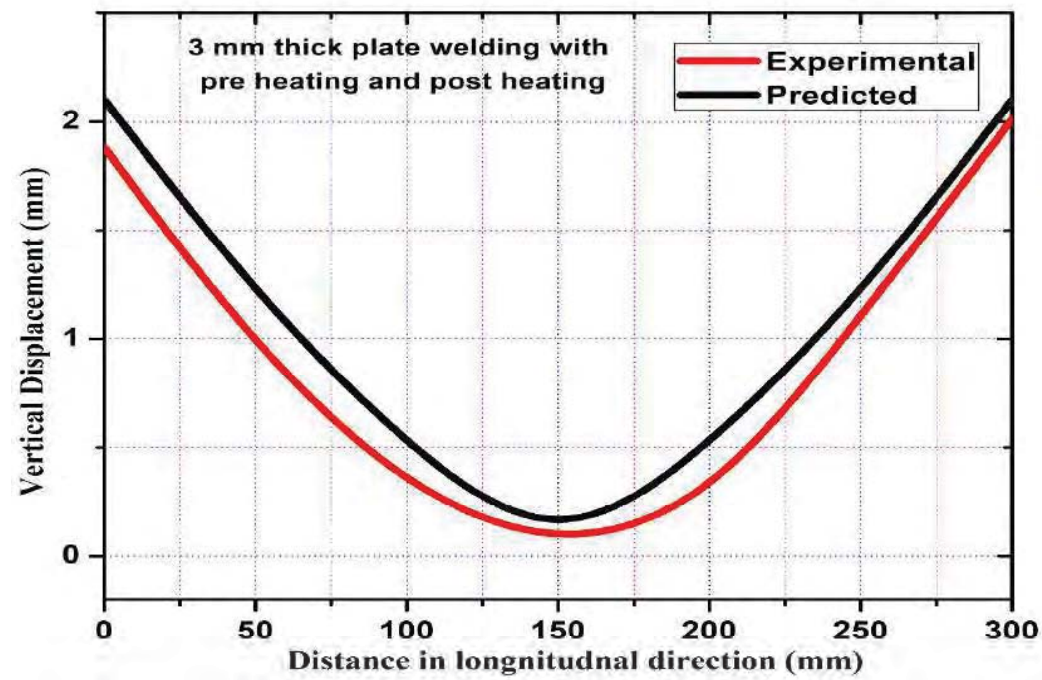

(a) Longitudinal direction

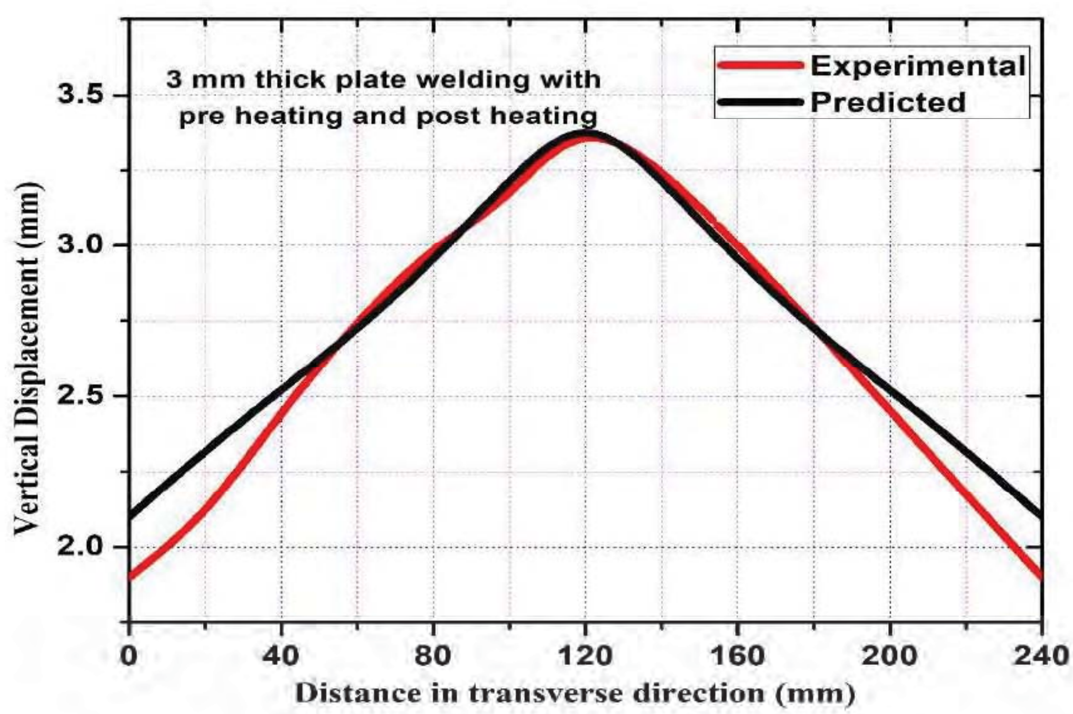

(a) Transverse direction

Fig.5.5.5. Comparison of vertical displacement in autogenous welding with post heating

5.5.4. Thermal Analysis of Multi-pass welding

FEM based calculated thermal cycles at 10 mm distance away from weld centre line is compared with experimentally measured cycles for multi-pass welding of 6 mm thick V groove joint as shown in Fig. 5.5.6. In case of 6 mm thick plate thermal analysis, the initial temperature of weld joint is mainatined 200°C before start of welding and after each pass 200°C is maintained as interpass temperature for sucessive passes. Finally post-heating was carried out by maintaining 200°C temperature for next 0.5 hr. Predicted peak temperature for root pass was 580°C while experimentally measured peak value was 600°C. Similarly predicted peak temperature for second and third passes are 630°C and 670°C and experimentally values ar 645°C and 678°C respectively. There was a good agreement between 2 and 3 passes. After completion of welding 200°C was maintained constant for next 0.5 hr for post-heating purpose as shown in Fig. 5.5.6.

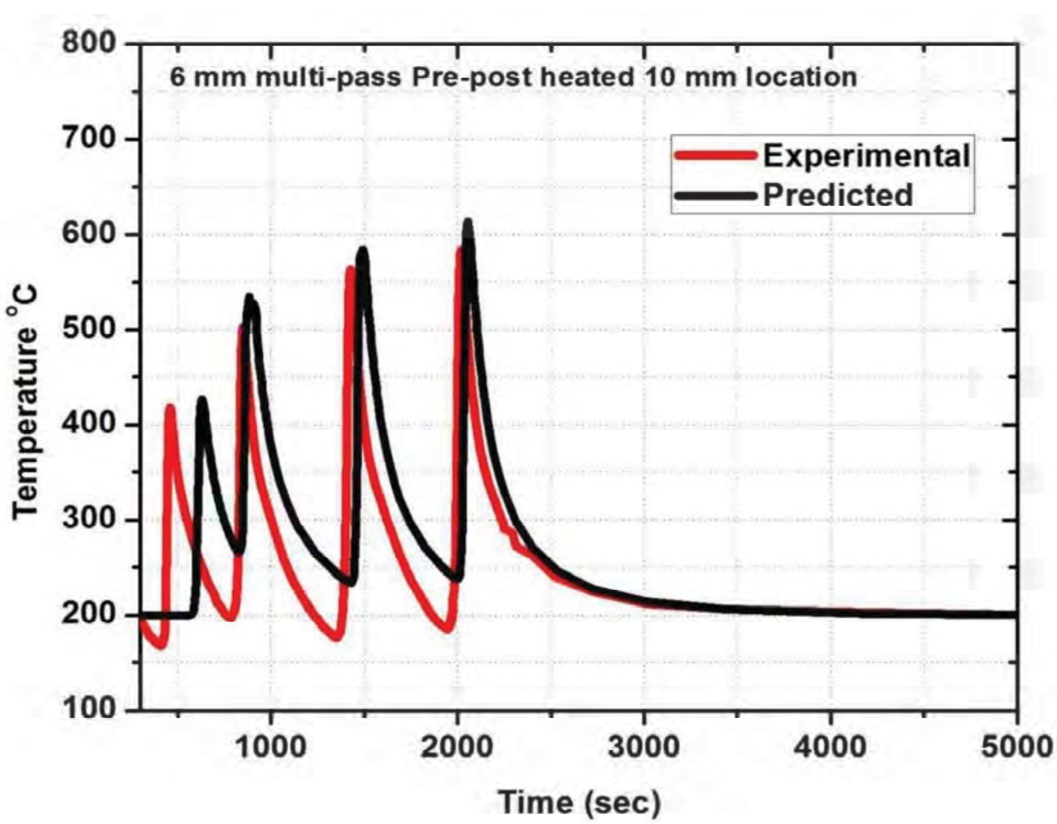

Fig.5.5.6. Thermal cycle comparison in multi-pass welding with post heating

5.5.5. Residual Stress Analysis of Multi-pass welding

Predicted longitudinal residual stresses for welding with combined pre heating and post heating for 6 mm thick multi-pass weld joint are compared with experimentally measured residual stress at 10 diferent locations using X-Ray diffraction technique as shown in Fig. 5.5.7. Maximum predited longitudinal stress of 245 MPa which is tensile in nature is found next to HAZ (at 15 mm left side of weld line) as shown in Fig. 5.5.7. For the same location, exeprimentally measured stress value is 190 MPa. Experimental measured residual stress value at 10 mm left side of weld line is 186 MPa and 142 Mpa on right side of weld line. Experimentally measured stress value at the weld line is 108 MPa, for the same location the predicted stress value is 153 MPa only.

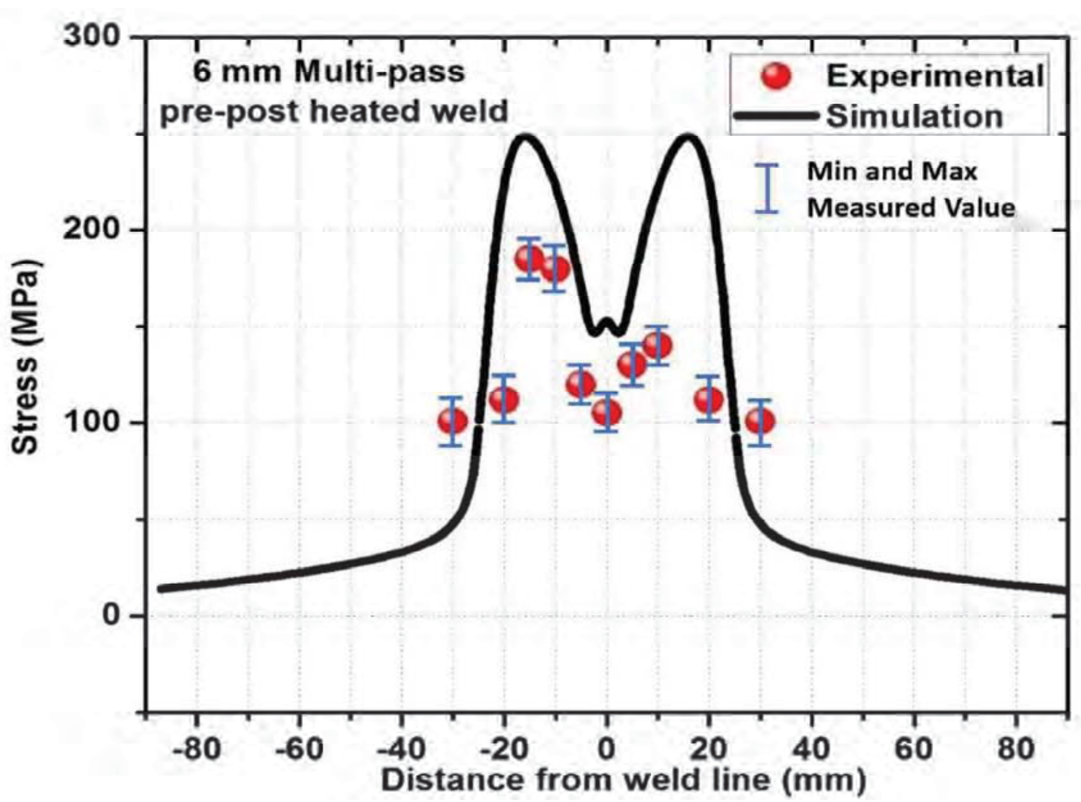

Fig.5.5.7. Residual stress comparison in multi-pass welding with post heating

A comparison of the residual stress prediction for autogensous weld with that of the multipass weld shows that in the case of autogenous weld, residual stress predicted at the weld centre line is lower than actually measured. In contrast in the case of multipass weld, predicted values are slightly more than actually measured. Exact reasons for this difference is not known at present. It could be that multiple weld thermal cycles and associated phase transformation should be altering the residual stress distribution bringing down the tensile residual stress at the weld centreline from that present in the single pass autogenous welds. This is supported by the fact that in all the previous cases also (without preheating and with preheating alone) residual stress at the weld centre line is more for autogenous weld than for the multipass weld.

5.5.6. Distortion Analysis of Multi-pass welding

Fig. 5.5.8 shows the predicted distortion in 6 mm thick multi-pass weld joint. Predicted verticle displacement in longitudinal and transvserse direction measured is compared with experimental measured values shown in Fig. 5.5.9.

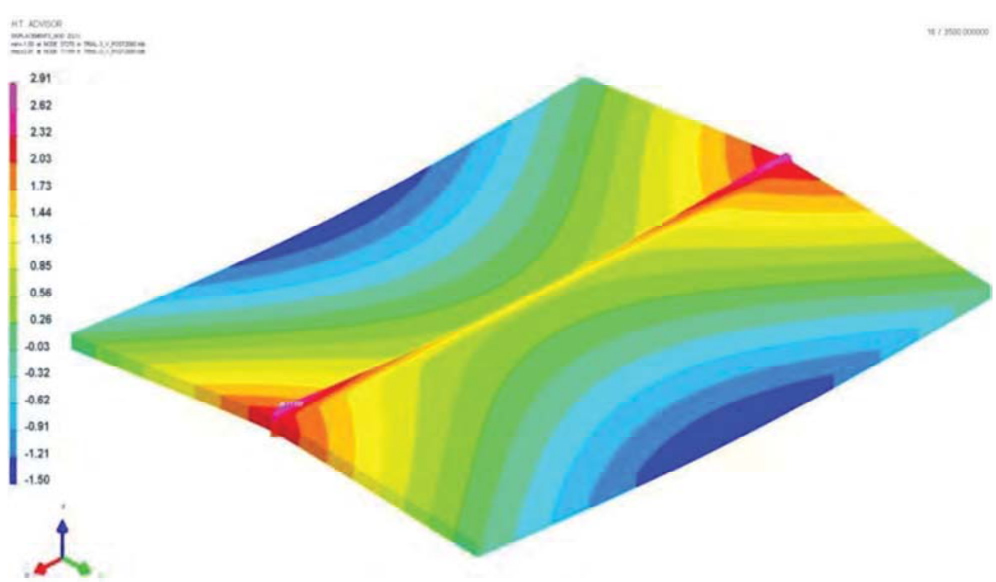

Fig. 5.5.8. Predicted distortion for multi-pass welding with post heating

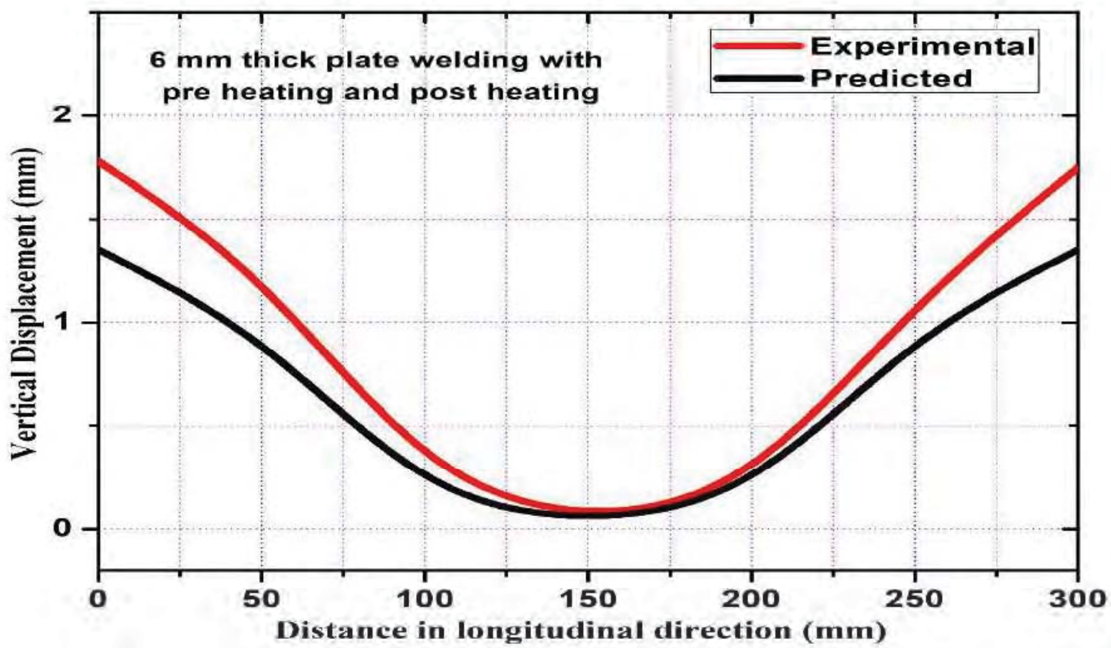

(a) Longitudinal direction

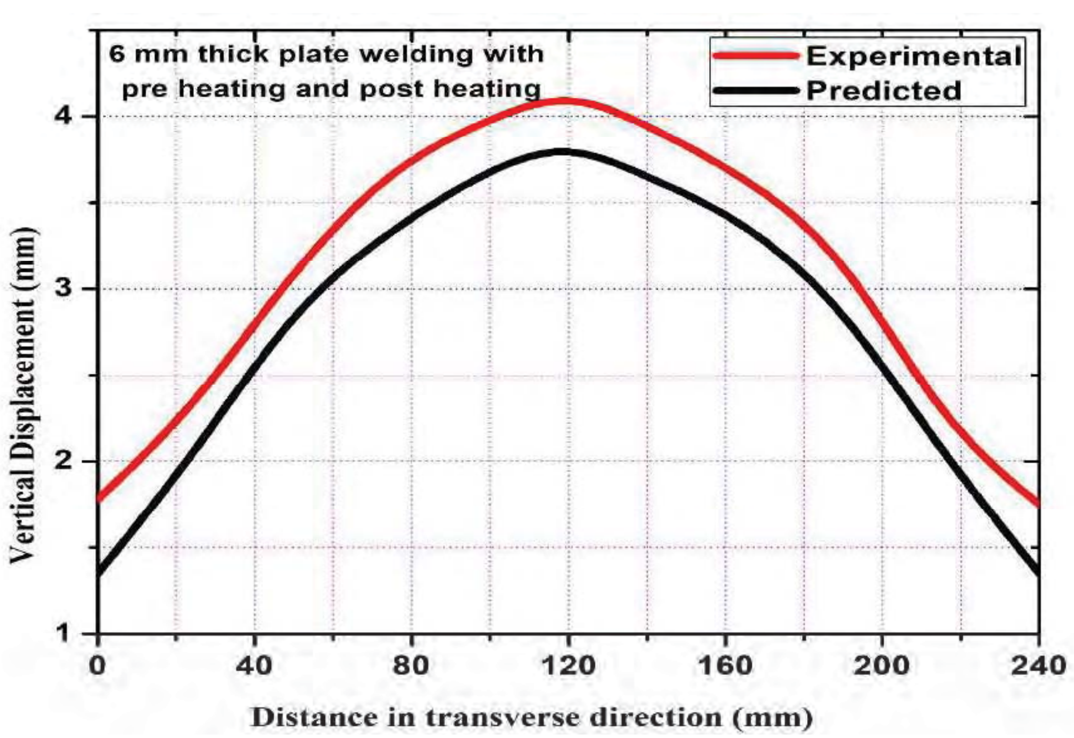

(b) Transverse direction

Fig.5.5.9. Comparison of vertical displacement in multi-pass welding with post heating

Maximum experimentally measured verticle displacement value observed in longitudinal direction is 1.7 mm and 1.62 mm at the left and right corners of weld joint (at clamping locations). Predicted verticle displacement observed for same locations is 1.48 mm in longitudinal direction. Peak verticle displacement in transverse direction observed is 4.12 mm and predicted values for same locations is 3.85 mm with 7% error only.

In summary, FEM model that consider preheating effect has been modified to incorporate effect of post heating in residual stress and distortion. Limitation in this model is in modelling of the cooling down of the weld to the ambient temperature from post heating temperature. Apparently, this limitation has led to some variaion in the predicted residual stress values in the weld centreline from the measured values. Howver, prediction of the peak tensile residual stresses and its location in the weld joints are reasonably accurate.

5.6. Effect of Pre-heating and combined Pre-heating and Post-heating on Residual Stress and Distortion of Modified 9Cr-1Mo steel GTA welding

From the above results it is clear that there is reasonable agreement with predicted and measured residual stress and displacement of the autogenous and multi-pass welds of modified 9Cr-1Mo steel welds produced without preheating, with preheating and with preheating and post heating combined. Hence, by comparing these results one can find out what is the effect of preheating and preheating + post heating on residual stress and distortion of the weld joints of this steel. In this section this comparison is attempted and significance of the results in the context of weldability of modified 9Cr-1Mo steel is discussed.

Fig. 5.6.1 shows comparison of the longitudinal residual stress in the transverse direction of both autogenous and multi-pass welds produced without preheating, with preheating alone and with combined preheating and post heating. Results show that residual stresses are lower in the weld zone for multi-pass welds than for the autogenous weld. Further, peak residual stress decreased, when preheating or preheating + post heating are employed. Reduction is significant for preheating and post heating is combined.

In the case of autogenous welds, only preheating reduces the peak stress value down to 6% from 542 MPa to 512 MPa where as in case of combined pre heating and post heating, it is decreased 30% from 542 MPa to 381 MPa. Similarly, for multi-pass welds of 6 mm thick plate stress is reduced 52% from 400 MPa obtained for weld without preheating to 190 MPa for the welds prepared with preheating and post heating. At the weld center, combined pre and post heating reduces the residual stress value 18% from 269 MPa to 221 MPa for 3 mm thick plate, where as in case 6 mm thick plate it is reduced 45% from 196 MPa to 108 MPa.

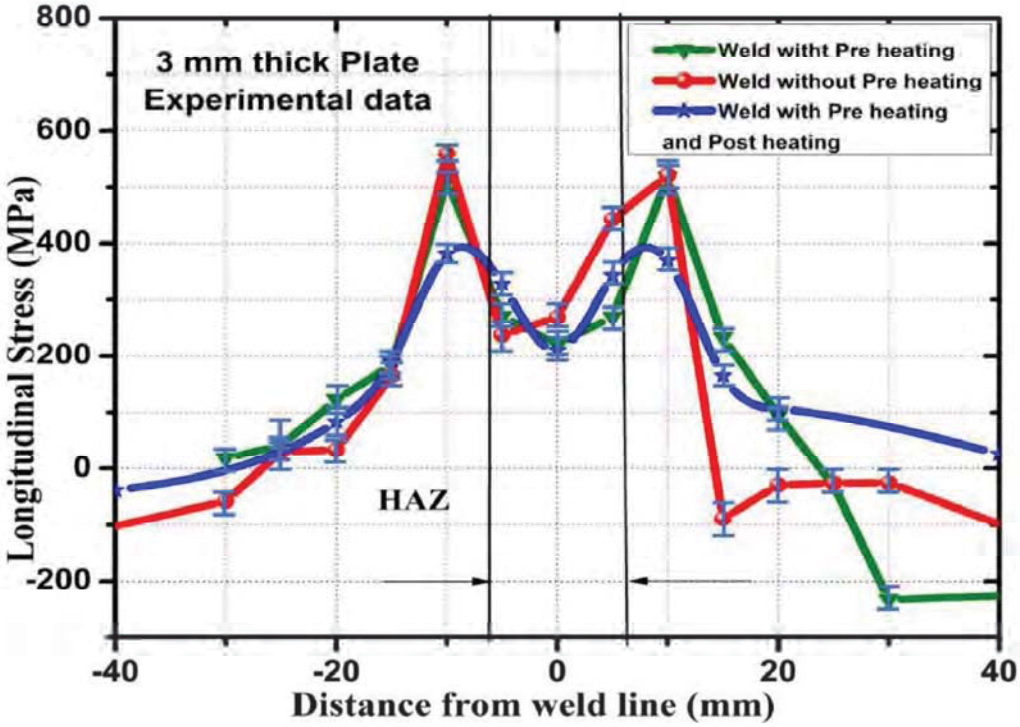

(a) Autogenous weld plate

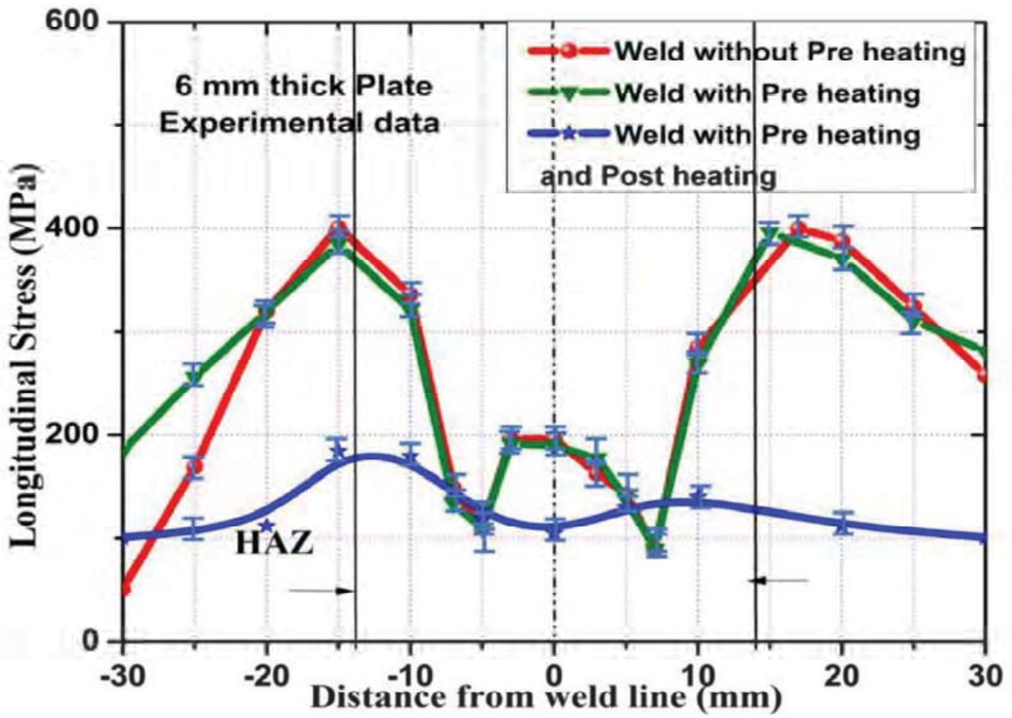

(b) Multi-pass weld plate

Fig.5.6.1. Experimental measured residual stresses for different cases

These results are important in the context of weldability of modified 9Cr-1Mo steels. It is known that, being highly alloyed, this steel is known for hydrogen assisted cracking (HAC) and the most common practice employed to minimize the risk of HAC is to employ preheating and post heating. For steels like modified 9Cr-1Mo steel, the purpose of preheating and post heating is to reduce the hydrogen levels in the weld joints. Along with hydrogen, a susceptible microstructure (martensite) and high tensile residual stress are also prerequisite for HAC to occur. Due to high hardenability of this class of steels, irrespective of preheating and post heating, the microstructure of the weld metal and HAZ would be martensitic. However, the present result shows the preheating and post heating can bring down the peak residual stresses considerably and thus reduce the susceptibility. Results also confirm that combining preheating with post heating is more effective in bringing down residual stress than preheating alone. Hence, the present study proves that preheating and post heating reduced the susceptibility of modified 9Cr-1Mo steel welds to HAC not only by reducing the diffusible hydrogen content but also reducing the peak tensile residual stresses in the joint.

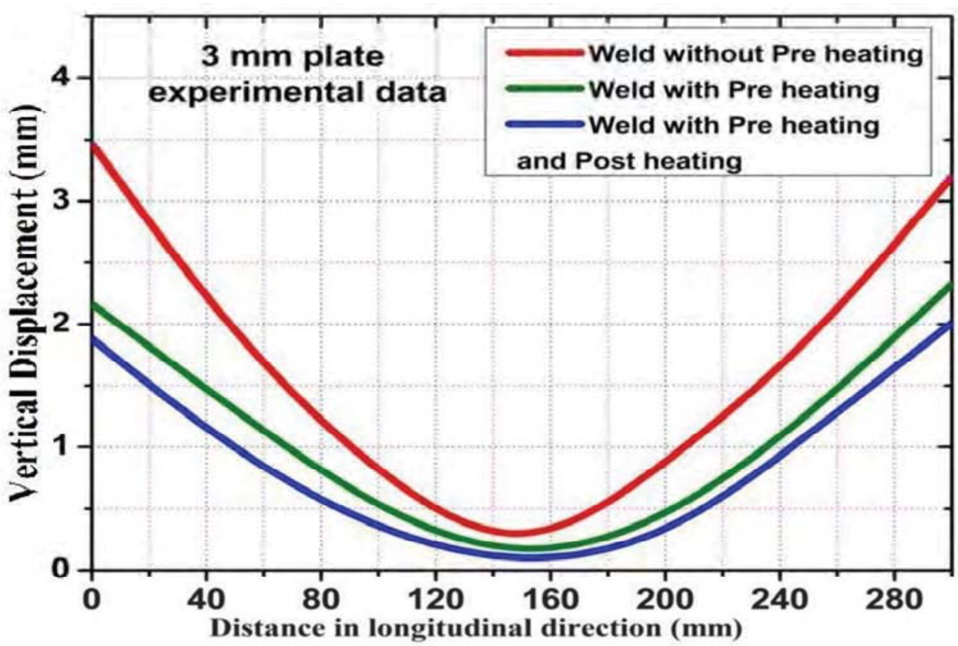

(a) Longitudinal direction

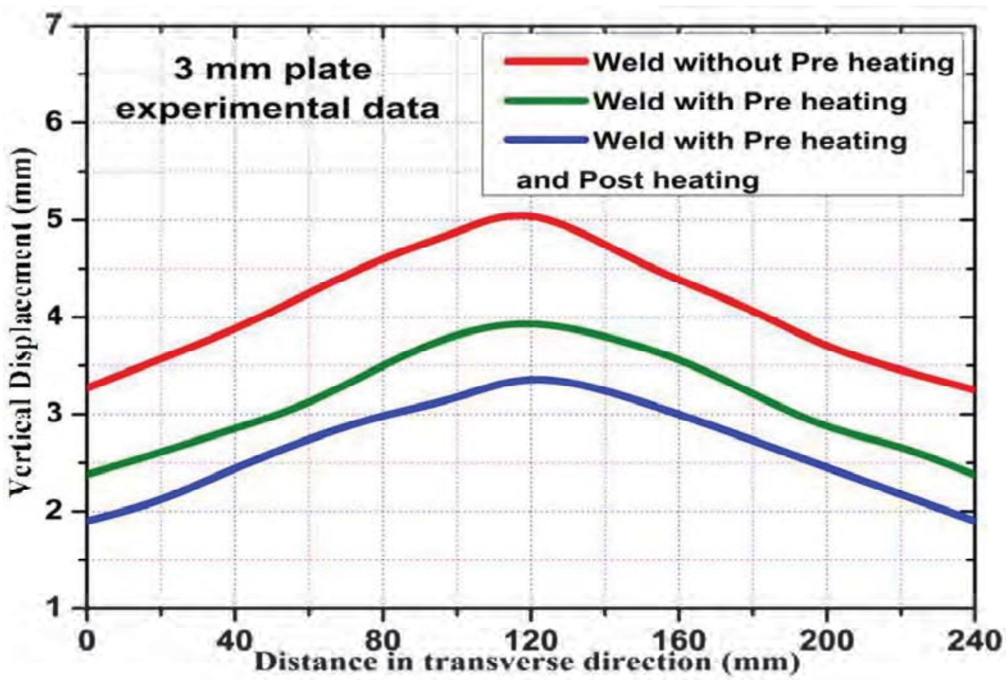

(b) Transverse direction

Fig.5.6.2. Distortion in 3 mm thick plate for all three cases

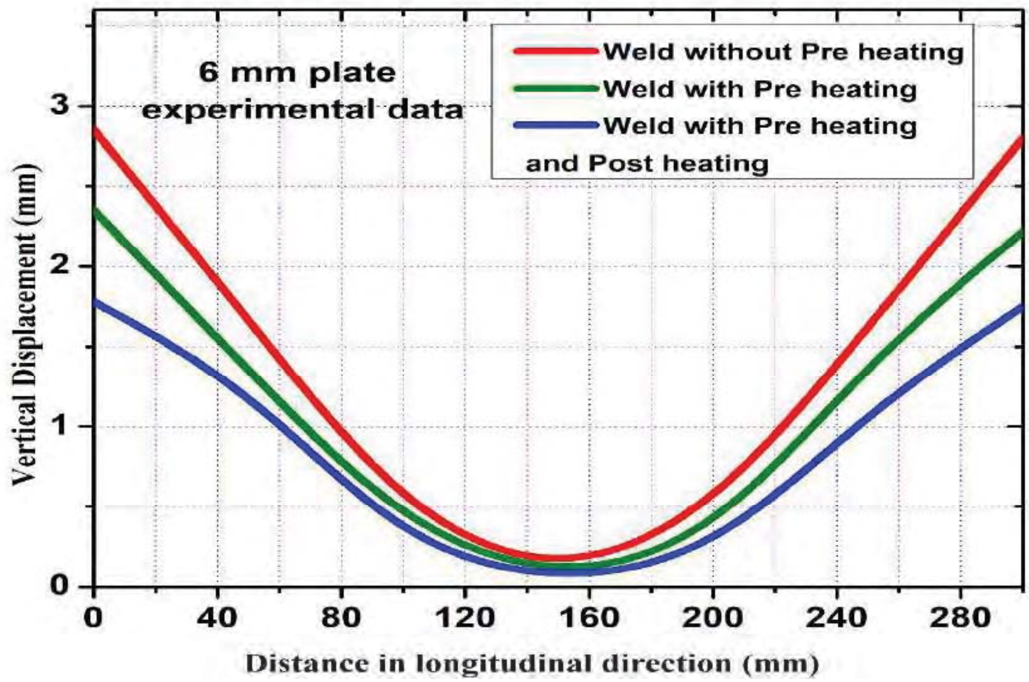

(a) Longitudinal direction

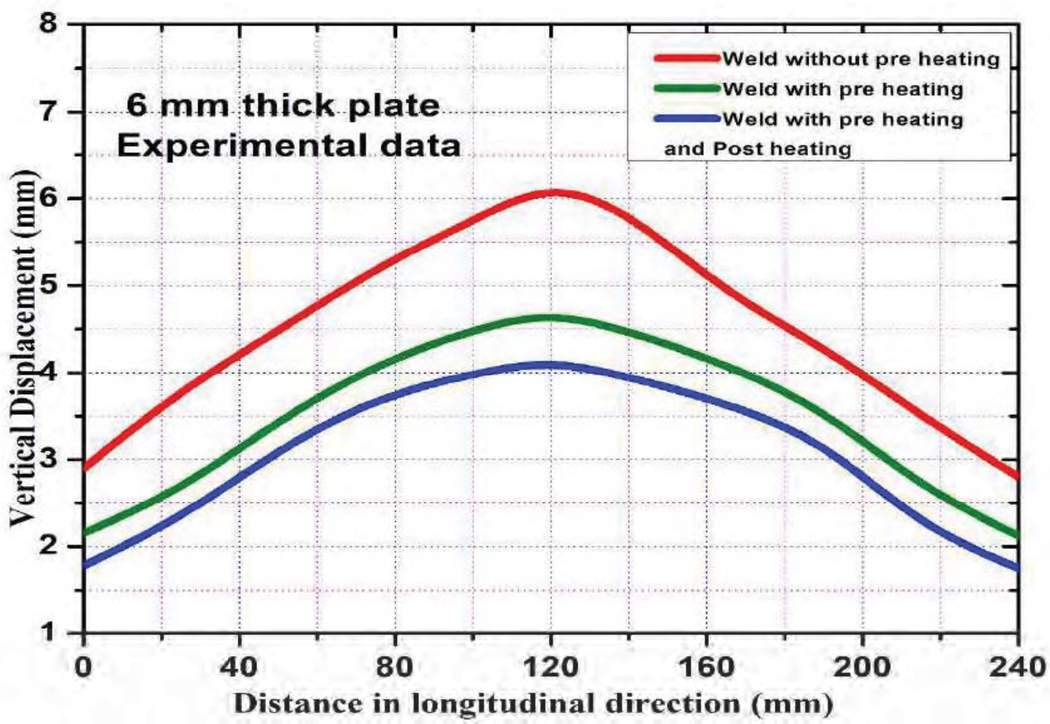

(b) Transverse displacement

Fig.5.6.3. Distortion in 6 mm thick plate for all three cases

Preheating and post heating also helps to reduce the distortion of the weld joints. Effect of preheating and combined effect of preheating and post heating on the displacements measured for the weld joints are given in Fig. 5.6.2-5.6.3. For 3 mm thick plate welded by autogenous welding process, peak value of longitudinal vertical displacement is reduced from 3.5 mm to 1.9 mm due to combined effect of pre heating and post heating as shown in Table.5.6.1. Peak value of verticle displacement in longitudinal direction is reduced up to 34% in second case (pre heating alone) where as combined effect of pre heating and post heating peak verticle displacement value reduced down to 45%. In case of 6 mm thick plate longitudinal verticle displcaement is reduced 39% from 2.8 mm to 1.7 mm due to combined effect of pre heating and post heating. Based on verticle displacement comparison as shown in Fig. 5.6.3 (a) it is observed that effect of pre heating reduces verticle displacement 16% from 2.8 mm to 2.35 mm in longitudinal direction.

Similarly in case of transverse directions, due to combined effect of pre heating and post heating verticle displacement is reduced 38% from 5.2 to 3.54 mm and 34% from 6.2 mm to 4.12 mm, whereas in case of only preheating verticle displacement is reduced up to 25% from 5.2 mm to 3.9 mm and 26% from 6.2 mm to 4.6 mm in 3 mm and 6 mm thick weld joints respectively. Hence welding with preheating is not reducing verticle displacement much. However,results of the the current study.indicate that combined preheating and post heating is significantly reducing verticle displacement

Thus, outcome of the present work is not just providing a FE model for predicting thermal cycle, residual stress and distortion with reasonable accuracy during welding of modified 9C-1Mo steels but also revealing the beneficial effects of preheating and post heating in reducing peak tensile residual stresses and distortion of the joints. This is significant, because reduction in residual stresses can bring down the risk of HAC during welding of this class of steels.

Table.5.6.1. Experimental measured vertical displacement in 3 mm and 6 mm thick plate

Verticle displacement in different direction (mm)	3 mm thick plate			6 mm thick plate		
	Without Preheat welding	With Preheating welding	With Preheating and Postheating welding	Without Preheat welding	With Preheating welding	With Preheating and Postheating welding
Longitudinal	3.5	2.24	1.9	2.8	2.35	1.7
Transverse	5.2	3.9	3.4	6.2	4.6	4.12

Though the present study does not explore the reasons for the beneficial effect of post heating in reducing both tensile residual stresses levels and distortion in the welds, it is not difficult to see that they are linked to the reduction in the temperature gradient across the weld as a result of the post heating. This in turn bring down the differential thermal expansion and the stresses and distortion arising out of this. Use of preheat alone is not as effective as use of preheating + post heating because in the former case, after welding, both the weld zone and the preheated part of the joint cool down together to room temperature, unlike in the case of preheating and post healing in which this zone is held at the post heating temperature. Accordingly, effect of differential expansion on residual stress and distortions would be higher in the case of preheating alone than in the case of combined preheating and post heating.

Similarly, in the case of multi-pass welding, repeated deposition of weld metal maintaining inter-pass temperature of ~200°C keeps the weld zone at a higher temperature than that of an autogenous weld. This also effectively brings down the cooling rate and the differential thermal expansion aiding in bringing down the residual stress level and distortion.

References

1. D. Deng, H. Murakawat, “The Prediction of welding residual stress in multi-pass butt-welded modified 9Cr-1Mo steel pipe considering phase transformation effects”, Computational Material science, 2006, Vol. 37, Issue 3, 209-219.
2. A. Yaghi, T. Hyde, A. Becker, J. William, W. Sun, “Residual stress simulation of welded section of P91 pipes”, Journal of material Processing Technology, 2009, Vol. 209, Issue 8, 3905-3913.
3. A. Yaghi, T. Hyde, A. Becker, J. William, W. Sun, “Measuring and Modeling residual stresses in a butt welded P91 steel pipe”, Proceedings of Sustainable Power Generation and Supply, Beijing, April 6–7, 2009.
4. A. Yaghi, T. Hyde, A. Becker, J. William, W. Sun, “Finite element simulation of welding and residual stresses in a P91 steel pipe incorporating solid state phase transformation and post weld heat treatment”, Journal of Strain Analysis for Engineering Design, 2008, Vol. 43, Issue 5, 275-293.
5. C. Heinze, A. Pitter, M. Rethmeier, S. Babu, “Dependency of martensite start temperature on prior austenite grain size and its influence on welding induced residual stresses”, Computational material science, 2013, Vol. 69, Issue 1, 251-260.
6. D. P. Koistinen, R. E. Marburger, “A general equation prescribing the extent of the austenite–martensite transformation in pure iron–carbon alloys and plain carbon steels”, Acta Metallurgica 1959, Vol. 7, 59–60.
7. J. B. Leblond, J. Devaux, “A new kinetic model for anisothermal metallurgical transformations in steels including effect of austenite grain size” Acta Metallurgica, 1984, Vol. 32, Issue 1, 137-146.

8. J. B. Leblond, G. Mottet, J. Devaux, “A theoretical and numerical approach to the plastic behaviour of steels during phase transformations-I. Derivation of general relations”, Journal of Mechanics and physics of solids, 1986, Vol. 34, Issue 4, 395-410.

9. J. B. Leblond, G. Mottet, J. Devaux, “A theoretical and numerical approach to the plastic behavior of steels during phase transformations-II. Study of classical plasticity for ideal-plastic phases”, Journal of Mechanics and physics of solids, 1986, Vol. 34, Issue 4, 411-432.

10. J. B. Leblond, G. Mottet, J. Devaux, “Mathematical modeling of transformation plasticity in steel I. Case of ideal-plastic phases”, International Journal of plasticity, 1989, Vol. 5, Issue 6, 551-572.

11. SYSWELD Tool box (2010).

12. S. K. Velaga, R. Gaurav, S. Murugan, A. Ravishankar, S. Venugopal, “Comparison of weld characteristics between longitudinal seam and circumferential butt weld joints of cylindrical components”, Journal of Manufacturing Process, 2015, Vol. 18, 1-11.

13. S. K. Velaga, G. Rajput, T. Selvaraj, B. M. Anandarao, A. Ravishankar, “A study on the effect of weld induced residual stresses and the influence of weld sequencing of centrifugal extract rotating bowl using numerical simulation and experimental validation”, Ciencia and Technology dos Mateiais, 2015, Vol. 27, 84-91.

14. A. Ravishankar, S. K. Velaga, G. Rajput, S. Venugopal, “Influence of welding speed and power on residual stress during Gas Tungsten Arc Welding (GTAW) of thin section with constant heat input: A study using numerical simulation and experimental validation” Journal of Manufacturing Processes, 2014, Vol. 16, 200-211.

15. K. C. Ganesh, K. R. Balasubramanian, M. Vasudevan, P. Vasantharaja, N. Chandrasekhar, “Effect of Multipass TIG and Activated TIG Welding Process on the Thermo-Mechanical Behavior of 316LN Stainless Steel Weld Joints”, 2016,

Metallurgical and Materials Transactions B, Vol. 47, 1347-1362.

16. S. Kim, J. Kim, W. Lee, "Numerical Prediction and neutron diffraction measurement of residual stress for modified 9Cr-1Mo steel", Journal of material Processing Technology, 2005, Vol. 167, Issue 2, 480-487.

17. S. Paddea, J. A. Francis, A. M. Paradowska, P. J. Bouchard, I. A. Shibli, "Residual stress distribution in a P91 steel-pipe girth weld before and after post weld heat treatment", Material Science and Engineering, A, 2012, Vol.534, 663-672.

18. S. Kumar, R. Awasthi, C. K. Vishwanadham, K. Bhuanumurthy, G. K. Dey, "Thermo-metallurgical and thermo-mechanical computations for laser welded joint in 9Cr–1Mo (V, Nb) Ferritic-martensitic steel", Materials and Design, 2014, Vol. 59, 211-220.

19. Z. HU, J. Zhao, "Effects of martensitic transformation on residual stress of P91welded joint", Material research express, 2018, Vol. 5, No. 9, 96528-96529.

20. J. Wang, W. Yin, H. Murakawa, "Experimental and computational analysis of residual buckling distortion of bead-on-plate welded joint", Journal of Material Processing Technology, 2013, Vol. 13, Issue 8, 1447-1458.

21. D. Deng, H. Murakawa, "Prediction of welding distortion and residual stress in a thin plate butt-welded joint", Computational Materials Science, 2007, Vol. 43, 353-365.

22. H. P. Yupiter, M. S. Sulaiman, S. K. Abas, G. Tham, E. Haruman, "Investigation on welding distortion of combined butt and T-joints with 9-mm thickness using FEM and experiment", Journal of Advanced Manufacturing Technology, 2015, Vol. 77, 775-782.

23. C. Wang, Y. Kim, J. Kim, "Comparison of FE Models to Predict the Welding Distortion in T-Joint Gas Metal Arc Welding Process", International Journal of Precision Engineering and Manufacturing, 2014, Vol. 15, Issue 8, 1631-1637.

24. Y. C. Kim, M. Hirohata, K. Inose, "Effects of phase transformation on distortion and

residual stress generated by LASER Beam welding on high-strength steel", Welding in the World, 2012, Vol. 56, Issue 3-4, 64-70.

25. Y. C. Kim, M. Hirohata, K. Inose, "FEM Simulation of Distortion and Residual Stress Generated by High Energy Beam Welding with Considering Phase Transformation", Open Journal of Metal, 2014, Vol. 4, 31-39.

26. D. Deng, "FEM prediction of welding residual stress and distortion in carbon steel considering phase transformation effects", 2009, Material and Design, Vol. 30, 359-366.

CHAPTER 6

SUMMARY AND CONCLUSIONS

Summary of the results and major conclusions derived from these results are given in this chapter. It is given separately for each of the sections identified in Chapter 5: (1) Heat source fitting and material property data generation, (2) thermo-mechanical analysis of the autogenous welds of 3 mm thick plate welds, (3) thermo-mechanical analysis of 6 mm thick plate multi-pass welds, (4) thermo-mechanical analysis of welds prepared with preheating, (5) thermo-mechanical analysis of welds prepared with both preheating and post heating and (6) effect of preheating and post heating and residual stress and distortion of the weld joints

6.1. Material data base creation and Bead-on-plate weld

1. Using the weld bead dimensions obtained from bead-on-plate welds made with different heat input, heat source fitting for double ellipsoidal model was successfully carried out
2. Material data base for modified 9Cr-1Mo steel, which considers phase transformation in the steel was generated and provided as material data input file for SYSWELD for thermo-mechnical analysis.

6.2. Thermo-Mechanical Analysis of Autogenous welding

1. A numerical model which can predict weld thermal cycles, residual stress and distortion in the autogeneous welds of modified 9Cr-1Mo steel plate was developed. Material data base generated for this steel and double ellipsoid heat source model with its parameters adjusted to match the experimentally measured bead parameters were used as input for this model.
2. Results of prediction from this model was compared with weld thermal cycles

experienced, residual stress present and distortion that took place in actual weld and it is demonstrated that the predictions are reasonably accurate.

3. For accurate prediction of residual stress distribution, phase-transformation that takes place in the material during weld thermal cycle should be considered in the material data base. It is shown that 'M' shaped distribution of the longitudinal residual stress in the transverse direction of the weld is a direct consequence of solid-state phase transformations (ferrite to austenite during heating part and austenite to martensite during cooling part) that occur during weld thermal cycle.

4. Distortion analysis using two different theories (large and small displacement) showed that distortion is predicted correctly only for models that considers large displacement theory.

6.3. Thermo-Mechanical Analysis of Multi-pass welding

1. The numerical model developed to simulate the thermo-mechanical behavior of autogenous weld was suitably modified for multi-pass welding involving V groove geometry and filler addition. Heat source fitting was also modified to match the multi-pass weld based on bead-geometries.

2. Predictions of weld thermal cycles, residual stress distribution and distortion made using this model matched reasonably well with those obtained from experiments.

3. It is shown that prediction of residual stress and distortion that match the experimental results is obtained only when 3D model with fine mesh is employed. Deviations for the results obtained for the predictions based on 2D model from that measured experimentally is high; 2D model predicts lower displacements than actually measured values.

4. Results of the distortion estimation both from modeling and measurements on multi-pass welds reveal that solid state phase transformations that occur during

weld thermal cycle influences not only the residual stress distribution but also the distortion of the weld joint. This was not revealed in the study carried out on autogenous welds.

6.4. Thermo-Mechanical Analysis of Modified 9Cr-1Mo steel GTA welding with pre heating

1. The numerical models developed for autogenous welds and multi-pass welds were modified by incorporating preheating of the joint prior to welding. A disk shaped heat source with gaussian distribution was used for simulating the effect of preheating.
2. The developed models were able to predict the effect of pre heating on residual stress and distortion with reasonable accuracy. The analysis showed that pre heating before welding reduced the peak tensile residual stress value, caused wider distribution of residual stresses as compared to those without pre heating weld plate in both cases. There was good agreement between the simulated and measured values.
3. Predicted vertical displacements in both transverse and longitudinal direction were validated with experimental measured values. There was a good agreement between predicted and experimental measured displacement values. In case of autogenous welds maximum vertical displacement reduced to 12% from that obtained for weld without preheating. Similarly, in case of longitudinal direction peak value of vertical displacement was reduced by 41%.
4. In case of 6 mm thick multi-pass welding of modified 9Cr-1Mo steel peak value of predicted verticle displcament in transverse direction was redcued 23%, where as in longitudinal direction this reduction was 24%.

6.5. Thermo-Mechanical Analysis of Modified 9Cr-1Mo steel GTA welding with combined pre heating and post heating

1. The numerical models for autogenous and multi-pass welds with preheating was further modified to incorporate post heating of the weld joint after welding. However, this model does not cover cooling of the weld from post heating temperature to ambient temperature i.e. model considers post heating temperature as ambient temperature during cooling part of the weld thermal cycle.
2. Predicted longitudinal residual stress at the weld centerline using this model for autogenous weld is slightly lower than actually measured, though in other location the values are comparable. Similarly, for multi-pass welds, predicted residual stress values are slightly higher than actually measured in most of the cases. These differences are attributed to limitation of the model to consider cooling down of the weld joint down to ambient temperatures.

6.6. Effect of pre heating and combined pre heating & post heating on residual stress and distortion

Residual stresses in a weld plate generated due to localized heating and fast cooling causing generation of differential expansion and contraction at different location of weld joint. Due to pre and post heating, the heating becomes more distributed, it reduces the temperature gradient and it decreases the cooling rate this indirectly reduces thermal expansion and contraction, which reduces the residual stresses. A comparison of both the predicted and experimentally estimated values of residual stress and distortion in the welds made without any preheating, with preheating and with combined preheating and post heating reveals that preheating + post heating significantly bring down residual stress levels in the weld joints as well as distortion from those reported for welds made without any preheating or post heating. In the case of autogenous welds, the reduction in the peak residual stresses is ~30% while in the case of multi-pass welds it is ~50%. Reduction in peak vertical displacement for the weld joints of autogenous and multi-pass welds made with both preheating and post heating are 45 and 39 % respectively from that of the weld made without any preheating and post heating. Corresponding reduction for the welds made only with preheating are 35 and 16% only. Based on this study it can be concluded pre heating and post heating is more beneficial than only pre heating to bring down residual and distortion for modified 9Cr-1Mo steel welds.

Overall, the results from the present study offer a FE based numerical model for predicting residual stress and distortion in the plate butt welds of modified 9Cr-1Mo steels. This model incorporates the material data base for this steel, uses heat source parameters optimized from experimental trials, considers solid state transformations that material undergoes during welding, chooses large displacement theory for prediction of displacement, select 3D fine meshing for multi-pass weld joints and proposes disk shaped heat source for modeling preheating.

6.7. Scope for future work

1. At present the numerical model developed is validated up to 6 mm thick weld joint with 'V' groove weld geometry with single pass for each layer of weld deposition. Model can be validated for large thickness plates and multi-pass welds with multiples passes for the same layer.
2. Numerical model can be developed for tube and pipe weld joints. It may be noted that modified 9Cr-1Mo steels are used extensively in these product forms.
3. The present model can be modified to cover different arc (SMAW, GMAW, SAW etc.) and beam (laser and electron) welding processes. Similar modifications can be attempted for Narrow Gap-Tungsten Inert Gas (NG-TIG) process for which modification in heat source may be required.

4. In the present model that considers post heating, it is not possible to incorporate cooling of the weld joint from the post heat temperature to ambient. This seems to affect the accuracy of the predictions from the model. Hence, modification is needed in the model to overcome this limitation.

5. The present model considers only conductive heat transfer; convective and radiation losses from the molten pool have been neglected. Similarly effect of electromagnetic, buoyancy forces on molten pool is also neglected. Hence, the present model can be modified to include these aspects so that accuracy of prediction can be improved.

Abstract

Name of the Student: Mohammed Zubairuddin
Name of the CI/OCC: Institute for Plasma Research, Gandhinagar
Enrolment No.: ENGG06201104002
Thesis Title: Thermo-mechanical analysis of GTA welding of Mod. 9Cr-1Mo steel considering the effect of phase transformation, Pre-heating and Post-heating
Discipline: Engineering Science **Date of viva voce:** 16January, 2021

The objective of PhD work is to develop numerical models capable of predicting thermal cycles, residual stress and distortion in both Autogenous and multi-pass GTA welding of mod. 9Cr-1Mo steel plates of 3 and 6 mm thicknesses taking into account the effects of phase transforamtion, pre and post heating during welding and experimental validation of the predicted results. In the present work, it is proposed to develop numerical models for predicting residual stress and distortion in modified 9Cr-1Mo steel plate weld joints by considering phase transformation effects for autogenous and multi-pass GTA welding. The beneficial effects of combined preheating and post heating on the residual stresses and distortion need to be quantified. Hence the effect of preheating before welding and the combined effect of pre heating and post heating on the residual stresses and displacements is proposed to be studied in detail using simulation. Validation of the simulated results on the residual stresses and displacements employing suitable experimental tools such as XRD technique and height gauge respectively is envisaged. Two different thicknesses of plates 3 mm and 6 mm were preheated at 200°C and after welding; the joint was post heated at 200°C for 30 minutes. Thermo-mechanical analysis of GTA welding was carried out using SYSWELD software. Predicted and measured values are compared for the joints fabricated employing combined pre heating and post heating.

Thesis Highlight

Name of the Student: MOHAMMED ZUBAIRUDDIN

Name of the CI/OCC: Institute for Plasma Research **Enrolment No.:** ENGG06201104002

Thesis Title: Thermo-mechanical analysis of GTA weldingof Mod. 9Cr-1Mo steel considering theeffects of phase transformation, Pre heatingand Post heating

Discipline: Engineering Science **Sub-Area of Discipline:** Welding analysis

Date of viva voce: 16Jan2021

Keywords: Grade 91 steel, Residual stress, SYSWELD, Distortion, Phase transformation, Pre-post heating.

- Grade 91 (Modified 9Cr-1Mo) steel is ferritic-martensitic steel which undergoes phase transformation during welding. Phase transformation significantly influences the residual stresses of the weld joint. Grade 91 steel is extensively used in fabrication of high temperature components of nuclear industries. In the present work, it is proposed to develop numerical models for predicting residual stress and distortion in modified 9Cr-1Mo steel plate weld joints by considering phase transformation effects for autogenous and multi-pass GTA welding. The beneficial effects of combined preheating and post heating on the residual stresses and distortion need to be quantified. Hence the effect of preheating before welding and the combined effect of pre heating and post heating on the residual stresses and displacements is proposed to be studied in detail using simulation. Validation of the simulated results on the residual stresses and displacements employing suitable experimental tools such as XRD technique and height gauge respectively is envisaged. To study the effect of pre heating and post heating at 200°C on residual stress and distortion in Grade 91 steel fabricated by GTA welding. Two different thicknesses of plates 3 mm and 6 mm were preheated at 200°C and after welding; the joint was post heated at 200°C for 30 minutes. Thermo-mechanical analysis of GTA welding was carried out using SYSWELD software. Predicted and measured values are compared for the joints fabricated employing combined pre heating and post heating. Combined Pre and Post heating reduced the residual stress 32% for 3 mm plate and 54% in 6 mm plate. Effect of phase transformation is manifested as "M" distribution of residual stress across the weld with peak value of tensile residual stress in the base metal close to HAZ. For predicting the effect of preheating disc shape heat source model can be used. For predicting displacement in thin plate welds, large displacement theory should be used Combined Pre and post heating reduces distortion more as compared to preheating alone.FEM model developed in this study is able to predict residual stress and displacement in both autogenous and multi-pass welds of modified 9Cr-1Mo steel with reasonably good accuracy.

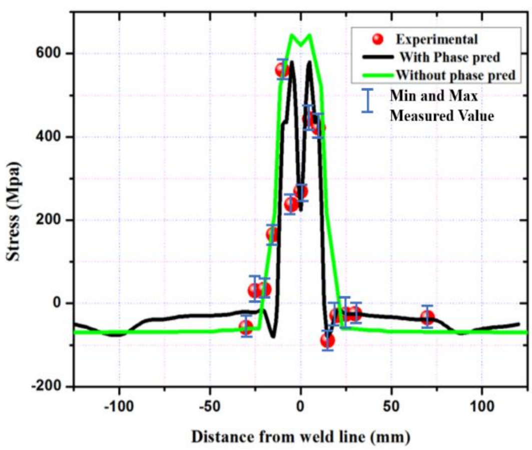

Fig. Effect of Phase transformation on stress

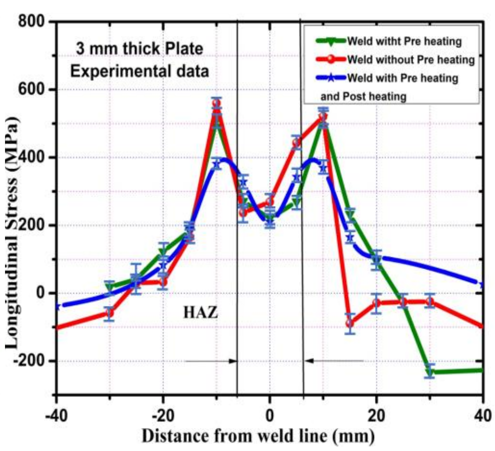

Fig. Effect of Pre and post heating on residual stress